

Technische Universität München

Fakultät für Chemie

Lehrstuhl für Analytische Chemie und Wasserchemie



Insights from isotope fractionation on limitations of micropollutant biodegradation—evaluating mass-transfer limitation and biodegradation in a bench-scale aquifer

Fengchao Sun

Vollständiger Abdruck der von der Fakultät für Chemie der Technischen Universität München zur Erlangung des akademischen Grades eines Doktors der Naturwissenschaften genehmigten Dissertation.

Vorsitzende(r): apl. Prof. Dr. Wolfgang Eisenreich
Prüfer der Dissertation: 1. Prof. Dr. Martin Elsner
2. Prof. Dr. Florian Einsiedl
3. Prof. Dr. Olaf A. Cirpka

Die Dissertation wurde am 07. 07. 2021 bei der Technischen Universität München eingereicht und durch die Fakultät für Chemie am 29. 09. 2021 angenommen.

Abstract

Anthropogenic organic micropollutants threaten groundwater quality worldwide. Identifying the bottlenecks of biodegradation and finding solutions to eliminate organic micropollutants in groundwater is a daunting task. Two possible limiting factors have been hypothesized as the bottlenecks for biodegradations under oligotrophic conditions: (1) Mass-transfer limitation from the bulk phase to the bioavailable phase, particularly the mass-transfer process through the bacterial cell membrane, and (2) physiological limitation (e.g., downregulation of functional genes). Compound-specific isotope analysis (CSIA) creates new windows to glimpse mass-transfer limitation and physiological limitation during biodegradation. Decreased isotope fractionation due to mass-transfer limitation through the bacterial cell membrane during organic contaminant biodegradation by suspended bacteria has been observed in chemostats at low concentrations ($< \text{Monod constant}$). However, there is a lack of studies mimicking a realistic aquifer setting where bacteria attached to sediments are exposed to oligotrophic environments. This thesis evaluates the limitations of micropollutant biodegradation by applying CSIA in a bench-scale aquifer in three sequential experiments. Firstly, isotope effects during aqueous diffusion/dispersion were investigated to address a potentially confounding factor in data interpretations (section 2.1). Secondly, in order to identify mass-transfer limitations at low concentrations, distributions of isotope fractionations, concentrations, and biomass along a concentration cross gradient were verified by reactive-transport simulations (section 2.2). Finally, to explore the remediation strategies for biodegradation enhancement and pinpoint the potential limiting factors in the degradation-stimulated system, the response of the contaminant-degradation activity to a priming strategy (a transient inlet supply of elevated contaminant concentration) and temporal flow fluctuation were characterized by applying CSIA and concentration analysis.

Whether aqueous phase diffusion and dispersion induce isotope fractionation and interfere with the observable isotope values during (bio)chemical reactions has been a long-standing debate. Experiments with Stokes diaphragm diffusion cells and a two-dimensional flow-through sediment tank showed that potential isotopic interferences from diffusion and transverse dispersion in the aqueous phase are negligible for most organic compounds at natural isotopic abundance (e.g., BTEX, 2,6-dichlorobenzamide [BAM]), with changes in carbon and nitrogen isotope values within $\pm 0.5\%$, and $\pm 1\%$, respectively. The observed weak to negligible isotope fractionations did not show a clear mass dependence on isotopologue masses.

Hence, this study proposes that adding a maximum additional $\pm 1\%$ to current instrumental uncertainties on carbon or nitrogen isotope analysis is sufficient to account for potential effects of aqueous diffusion or dispersion in field data evaluation.

After excluding the potential isotopic interference from diffusion and dispersion, CSIA was applied to investigate limitations on biodegradation of the organic contaminant BAM in a two-dimensional flow-through sediment tank system homogeneously inoculated with BAM degrader *Aminobacter* sp. MSH1. By injecting an anoxic BAM solution through the center port of the tank and oxic medium through the rest, a concentration cross gradient from high to low developed and yielded low concentration zones in the top and bottom regions of the tank, mimicking oligotrophic conditions. Decreased isotope fractionation at low concentrations indicated a transition to mass-transfer limitation. Using a reactive transport model that considers mass-transfer limitation into the cells, a threshold concentration of 600 $\mu\text{g/L}$ was identified, below which the apparent isotope enrichment factor ϵ strongly decreased ($< 0.5\%$). Therefore, the mass-transfer limitation was identified as a bottleneck for biodegradation of organic micropollutants, and my results suggest it should be considered when interpreting isotope values at field sites.

Furthermore, I explored priming strategies for increasing degradation capacity and efficiency, especially at low concentrations. When implementing a priming strategy (a transient inlet supply of elevated contaminant concentration) and temporal flow fluctuations, more homogeneous biomass distribution and higher degradation capacity indicated that intermediate elevated concentrations or flow disturbances might be instrumental in increasing *in-situ* or *ex-situ* biodegradation capacity. In addition, analysis of isotope fractionation across the vertical profile under different concentration conditions suggested that mass-transfer limitation became dominant when concentrations approached a threshold level, while limitation by physiological adaptation followed when concentrations were even lower. In sum, an evaluation of isotope fractionation in combination with calculations of remaining substrate fractions may identify limiting factors during biodegradation in the lab and field cases and may, therefore, serve as a performance indicator of bioremediation approaches.

Zusammenfassung

Anthropogene organische Mikroschadstoffe bedrohen weltweit die Grundwasserqualität. Es ist eine große Aufgabe, die Engpässe des biologischen Abbaus zu identifizieren und Lösungen zu finden, wie organische Mikroschadstoffe aus dem Grundwasser eliminiert werden können. Zwei mögliche limitierende Faktoren wurden als Engpässe für den biologischen Abbau unter oligotrophen Bedingungen angenommen: (1) die Begrenzung des Stofftransports von der Hauptphase in die bioverfügbare Phase, insbesondere der Prozess des Stoff-Transfers durch die Bakterienzellmembran, und (2) die physiologische Begrenzung (z.B. Herunterregulierung von funktionellen Genen). Die verbindungsspezifische Isotopenanalyse (CSIA) schafft neue Möglichkeiten, die Begrenzung des Stofftransports und die physiologische Begrenzung während des biologischen Abbaus zu erkennen. In Chemostaten wurde beobachtet, dass bei niedrigen Konzentrationen ($<$ Monod-Konstante) die Isotopenfraktionierung während des biologischen Abbaus organischer Schadstoffe durch suspendierte Bakterien aufgrund des begrenzten Stofftransfers durch die Bakterienzellmembran gedämpft ist. Es fehlen jedoch Studien, die realistisch die Umgebung eines Grundwasserleiters abbilden, in dem die Sediment-gebundenen Bakterien einem oligotrophen Milieu ausgesetzt sind. Diese Arbeit untersucht in drei aufeinanderfolgenden Experimenten die Grenzen des biologischen Abbaus von Mikroschadstoffen unter Anwendung von CSIA in einem Grundwasserleiter im Labormaßstab. Zunächst wurden Isotopeneffekte während der wässrigen Diffusion/Dispersion untersucht, um einen potenziellen Störfaktor bei der Dateninterpretation zu beheben (Abschnitt 2.1). Zweitens wurden Verteilungen von Isotopenfraktionierungen, Konzentrationen und Biomasse entlang eines Konzentrationsquergradienten durch Simulationen des reaktiven Transports (Abschnitt 2.2) verifiziert, um Stofftransferbeschränkungen bei niedrigen Konzentrationen zu identifizieren. Um schließlich Sanierungsstrategien zur Verbesserung des biologischen Abbaus zu untersuchen und die potenziellen limitierenden Faktoren im abbaustimulierten System zu bestimmen, wurden die Reaktion auf eine Priming-Strategie (eine vorübergehende Zufuhr erhöhter Schadstoffkonzentrationen) sowie die zeitliche Fluktuation des Flusses durch Anwendung von CSIA und durch Analyse der Konzentrationen charakterisiert

Seit langem wird diskutiert, ob Diffusion und Dispersion der wässrigen Phase eine Isotopenfraktionierung induzieren und die beobachtbaren Isotopenwerte während (bio)chemischer Reaktionen beeinträchtigen. Experimente mit Stokes' Diaphragma-

Diffusionszellen und einem zweidimensionalen Durchfluss-Sedimenttank zeigten, dass potentielle Isotopeninterferenzen durch Diffusion und transversale Dispersion in der wässrigen Phase für die meisten organischen Verbindungen bei natürlicher Isotopenhäufigkeit (z. B. BTEX, 2,6-Dichlorbenzamid) vernachlässigbar sind [BAM]), mit Änderungen der Kohlenstoff- und Stickstoffisotopenwerte innerhalb von $\pm 0.5\%$ bzw. $\pm 1\%$. Die beobachteten schwachen bis vernachlässigbaren Isotopenfraktionierungen zeigten keine eindeutige Massenabhängigkeit von Isotopologenmassen. Diese Studie schlägt daher vor, dass die Zugabe von maximal $\pm 1\%$ Unsicherheiten zusätzlich zu den aktuellen instrumentellen Unsicherheiten bei der Kohlenstoff- oder Stickstoffisotopenanalyse ausreicht, um potenzielle Auswirkungen der wässrigen Diffusion oder Dispersion bei der Auswertung der Felddaten zu berücksichtigen.

Nach Ausschluss möglicher Isotopeninterferenzen durch Diffusion und Dispersion wurde CSIA angewendet, um die Grenzen des biologischen Abbaus des organischen Schadstoffs BAM in einem zweidimensionalen Durchfluss-Sedimenttanksystem zu untersuchen, das zuvor homogen mit dem BAM-Degrader *Aminobacter* sp. MSH1 geimpft wurde. Durch Injektion einer anoxischen BAM-Lösung durch die zentrale Öffnung des Tanks und eines oxischen Mediums durch den Rest entwickelte sich ein Quergradient von hohen zu niedrigen Konzentrationen und ergab in den oberen und unteren Bereichen des Tanks, die oligotrophe Bedingungen nachahmen, Zonen mit niedriger Konzentration. Eine verringerte Isotopenfraktionierung bei niedrigen Konzentrationen deutete auf einen Übergang zur Stofftransportlimitierung hin. Unter Verwendung eines reaktiven Transportmodells, das die Stofftransportlimitierung in die Zellen berücksichtigt, wurde eine Schwellenkonzentration von $600 \mu\text{g/L}$ identifiziert, unterhalb derer der scheinbare Isotopen-Anreicherungsfaktor ϵ stark abnahm ($<0.5\%$). Der eingeschränkte Stofftransfer konnte somit als limitierender Faktor für den biologischen Abbau organischer Mikroschadstoffe identifiziert werden, und meine Ergebnisse legen nahe, dass dies bei der Interpretation der Isotopenwerte in Feldversuchen berücksichtigt werden sollte.

Darüber hinaus untersuchte ich Priming-Strategien zur Erhöhung der Abbaukapazität und -effizienz, insbesondere bei niedrigen Konzentrationen. Bei der Umsetzung einer Priming-Strategie (einer vorübergehenden Zufuhr erhöhter Schadstoffkonzentrationen am Einlass) und zeitlichen Flussschwankungen deuteten eine homogenere Biomasseverteilung und eine höhere Abbaukapazität darauf hin, dass zwischenzeitlich erhöhte Konzentrationen oder

Flusstörungen bei der Erhöhung der In-situ- oder Ex-situ-Bioabbaukapazität hilfreich sein könnten. Darüber hinaus weist die Analyse der Isotopenfraktionierung über das vertikale Profil unter verschiedenen Konzentrationsbedingungen darauf hin, dass die Stofftransportlimitierung dominant wurde, wenn sich die Konzentrationen einem Schwellenwert näherten, während eine Begrenzung durch physiologische Anpassung folgte, wenn die Konzentrationen noch niedriger waren. Zusammenfassend lässt sich sagen, dass eine Bewertung der Isotopenfraktionierung in Kombination mit Berechnungen der verbleibenden Substratfraktionen die limitierenden Faktoren während des biologischen Abbaus in Labor- und Feldversuchen identifizieren und daher als Leistungsindikator für Bioremediationsansätze dienen kann.

Parts of this thesis have been published in peer-reviewed journals as listed below:

Sun, F.; Peters, J.; Thullner, M.; Cirpka, O. A.; Elsner, M. Magnitude of Diffusion- and Transverse Dispersion—Induced Isotope Fractionation of Organic Compounds in Aqueous Systems. *Environ. Sci. Technol.* **2021, *55* (8), 4772–4782.**

Sun, F.; Mellage, A.; Gharasoo, M.; Melsbach, A.; Cao, X.; Zimmermann, R.; Griebler, C.; Thullner, M.; Cirpka, O. A.; Elsner, M. Mass-Transfer-Limited Biodegradation at Low Concentrations—Evidence from Reactive Transport Modeling of Isotope Profiles in a Bench-Scale Aquifer. *Environ. Sci. Technol.* **2021, *55* (11), 7386–7397.**

Table of Contents

1. Introduction	1
1.1 Groundwater—invisible, invaluable, and vulnerable	1
1.2 Groundwater organic pollution and remediation	1
1.2.1 Groundwater organic pollution.....	1
1.2.2 Remediation of contaminated groundwater	4
1.2.3 Mass-transfer limitation	5
1.2.4 Physiological limitation	6
1.2.5 Challenges in BAM biodegradation.....	7
1.3 Compound-specific stable isotope analysis for evaluating biodegradation of organic contaminants in groundwater	10
1.3.1 Theoretical and analytical basics of CSIA	11
1.3.2 Does diffusion and hydraulic dispersion induce isotope fractionation of organic compounds at natural isotopic abundance in aqueous systems?	12
1.3.3 Can we use CSIA to identify mass-transfer limitation as the bottleneck of biodegradation of organic micropollutants and follow the changing degradation activity in a groundwater system?.....	16
1.4 Transport and degradation mechanisms of contaminants in groundwater.....	20
1.4.1 General solute transport equations.....	20
1.4.2 Michaelis–Menten kinetics.....	21
1.4.3 Monod microbial growth kinetics.....	22
1.5 Outline and objectives.....	23
References	27

2. Research	34
2.1 Magnitude of diffusion- and transverse-dispersion-induced isotope fractionation of organic compounds in the aqueous systems	34
2.2 Mass-transfer limitation of biodegradation at low concentrations- Evidence from reactive transport modeling of isotope profiles in a bench-scale aquifer	62
2.3 Response of BAM-degradation activity to concentration and flow changes in a bench-scale sediment tank.....	92
3. Conclusions and Outlook	123
Acknowledgements	129
List of prior publications	131
Curriculum Vitae.....	132

1. Introduction

1.1 Groundwater—invisible, invaluable, and vulnerable

Groundwater, the invisible subsurface water in the pores of soil and fractures of rocks, is the source of one-third of all freshwater withdrawals and more than 40% of the irrigation water for food production, supplying potable water for more than two billion people worldwide.¹ As an essential component in the ecosystem, groundwater is critical for buffering the impacts of droughts and floods.^{2,3}

Unfortunately, unlike the more visible environmental problems, such as surface water (e.g., rivers and lakes) contamination or air pollution, groundwater problems (e.g., contamination from industry and agriculture⁴⁻⁶ and depletion due to over pumping⁷) are the out-of-sight issues, requiring careful monitoring in order not to be overlooked. Excessive pumping of groundwater, especially nonrenewable groundwater (deep or fossil groundwater), may cause water depletion, subsidence, landslides, etc.⁸⁻¹⁰ Furthermore, groundwater contaminations from industry and agriculture threaten groundwater quality.⁴⁻⁶ With increasing chemical usage, groundwater contamination further endangers water and food supply,¹¹ human health,^{12,13} and ecosystem functioning.¹⁴ It also further aggravates environmental injustice for low-income populations and people in regions that lack access to clean potable water, which is a fundamental human right.¹⁵

1.2 Groundwater organic pollution and remediation

1.2.1 Groundwater organic pollution

Groundwater can be polluted with organic chemicals from industrial discharge, urban and agricultural activities, landfill leachate, domestic and hospital wastewaters, improper hazardous waste disposal, and leakages or spills from inappropriate storage of chemicals and petroleum products. This anthropogenic pollution threatens the safety of potable water supplies and human health.⁵

One prominent group of organic pollutants are volatile organic compounds (VOCs), organic chemicals with high vapor pressure (with low boiling point) at room temperature,

which have been extensively used in domestic activities, industry, and agriculture. Although VOCs easily vaporize into the air, they can dissolve in and be transported with groundwater. Gasoline VOC compounds – benzene, toluene, ethylbenzene, and xylenes (BTEX) – are frequently detected at high abundance in groundwater.¹⁶ BTEX compounds are monocyclic aromatic hydrocarbons, attracting more research focus due to their high toxicities, water solubility, and mobility. BTEX compounds usually access groundwater from storage tank leakage, migrating through the unsaturated soil zone and reaching the groundwater table. Due to their limited solubility and low density (Table 1.1), an individual liquid phase known as LNAPL (light non-aqueous phase liquid) usually accumulates on top of the groundwater table.¹⁷ The BTEX compounds are transported with the groundwater flow, continuously dissolving and developing into a larger contaminant plume through dispersion and diffusion.

Another ubiquitous class of groundwater pollutants are pesticides (e.g., herbicides, insecticides, fungicides) and their metabolites that are transported from land fields to groundwater through infiltration. Every year, millions of tons of pesticides are utilized worldwide, and almost 75% of the global agricultural land is exposed to pesticide pollution.⁴ Even though groundwater seems to be less polluted from pesticides due to low aquifer net recharge,⁴ the concentrations of the pollutants in many wells are higher than the maximum contaminant levels or health advisory levels.⁵

For example, metolachlor (2-chloro-N-(2-ethyl-6-methylphenyl)-N-(1-methoxypropan-2-yl) acetamide), a broad-spectrum pre-emergent herbicide for general weed control,¹⁸ is an aromatic amide, an organochlorine compound, and a possible human carcinogen.¹⁹ It is slightly soluble in water and denser than water (Table 1.1). It is applied as a racemate (1:1 mixture of the (S)- and (R)- stereoisomers). Since the S enantiomer, S-metolachlor, is more effective than the racemic metolachlor for weed control, more S-metolachlor has been applied to replace racemate metolachlor.¹⁸ Among the ten most commonly used herbicides, tons of metolachlor have been used in the European Union and the US every year.¹⁸ Due to leaching of the sorbed metolachlor from the soil, it has been frequently detected in groundwater, with high persistency and mobility.²⁰

Degradation products of pesticides also threaten groundwater quality. Herbicide dichlobenil and fungicide fluopicolide are transformed into 2,6-dichlorobenzamide (BAM) via microbial metabolism or abiotic degradation. BAM has been frequently detected at low concentrations in groundwater, exceeding drinking water guidelines (0.1 µg/L) and causing

problems for drinking-water production in many European countries.²¹⁻²⁴ Dichlobenil, fluopicolide, and BAM can leach into groundwater from the soil (especially soil with low organic matter content) via infiltration or surface water runoff. Due to its low octanol/water partition coefficient ($\log K_{ow} = 0.77$)²⁵, BAM is extremely mobile in groundwater and hardly sorbs onto sediment surfaces ($K_d = 0.1-0.93$ L/kg).²⁵ In addition, it is very persistent, especially under anaerobic conditions.²¹

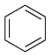
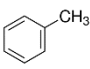
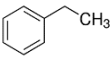
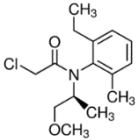
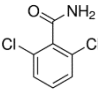
The maximum concentration for pesticides and their degradation products in drinking water set by the European Union regulations is 0.1 µg/L,²⁶ while the United States Environmental Protection Agency's limits are set for individual organic micropollutants (e.g., 2 µg/L for Alachlor and 3 µg/L for atrazine). Although most organic micropollutants are present at very low concentrations in groundwater, many of them are frequently detected above the maximum contaminant levels or health advisory levels for drinking water and exert toxic effects and carcinogenic risks.⁵

According to the contamination source geometry, contamination sources can be classified as point sources and non-point sources (or diffuse sources).¹⁷ Point source is defined as a small areal extent relative to the underground domain under consideration, such as septic tanks, storage tanks, and landfills, etc.¹⁷ BTEX compounds from gasoline spills or leakage are a common example of point source contamination in groundwater. Non-point source is any source of water pollution that does not belong to point source, extending over a large horizontal area relative to the contaminated subsurface area.¹⁷ One typical example of a non-point source pollution is the infiltration of contaminants into groundwater from agricultural land treated with pesticides and herbicides.⁴

Due to the limited solubility, contaminants that are immiscible in water can form an individual liquid phase which is known as NAPL (non-aqueous phase liquid).^{17, 27} When the NAPL quantity is small, it can occupy parts of the pores of the unsaturated porous media and sorb onto the sediments, or slowly vaporize or dissolve in water from infiltration. If the quantity of NAPL is relatively large, this oil phase would expand further horizontally and/or vertically; the DNAPLs (denser than water, e.g., tar) can penetrate the aquifer and cumulate on the aquifer base, while the LNAPLs (less dense than water, e.g., light gas oils) tend to accumulate at the groundwater table.^{17, 27} Even though NAPLs are practically immiscible in water, they can still slowly diffuse into groundwater, and further spread/migrate with groundwater flow.

Table 1.1 lists the properties of the target contaminants discussed in this thesis. I investigated the diffusion- and transverse-dispersion induced isotope fractionation of benzene, toluene, ethylbenzene, S-metolachlor, and BAM at natural isotopic abundance in the aqueous phase (section 2.1) and explored the potential limitations (e.g., mass-transfer limitation) of biodegradation of BAM at low concentrations in a bench-scale aquifer mimicking the natural aquifer (section 2.2, and section 2.3).

Table 1.1: Properties of the target chemicals in this thesis

Compound	Molecular formula	Molecular weight [g mol ⁻¹]	Density [g mL ⁻¹]*	Water solubility [mg L ⁻¹]*	log K _{ow} [-]*	Health concern
Benzene		78.12	0.8756 ^[28]	1780 ^[28]	2.13 ^[29]	Confirmed human carcinogen ³⁰
Toluene		92.15	0.8669 ^[28]	500 ^[28]	2.73 ^[29]	Nervous system ³¹ disturbances
Ethylbenzene		106.18	0.8670 ^[28]	150 ^[28]	3.15 ^[29]	Nervous system disturbances ³²
S-metolachlor		283.79	1.12 ^[33]	488–530 ^[33]	3.13 ^[29]	Possible human carcinogen ¹⁹
BAM		190.02	–	2730 ^[34]	0.77 ^[25]	Slightly toxic by oral route ³⁴

*Properties at temperature 20–25°C.

1.2.2 Remediation of contaminated groundwater

Multiple remediation strategies have been developed to remove contamination or reduce the contaminant concentration in groundwater below the maximum allowable concentrations. These include biological (e.g., bioaugmentation, biostimulation, and phytoremediation), chemical (e.g., *in-situ* chemical oxidation and reduction, permeable reactive barrier), and physical (e.g., pump and treat, activated carbon adsorption, air sparging) approaches.³⁵ Remediation technologies can also be divided into *in-situ* remediation and *ex-situ* remediation based on the location of the treatment.³⁶

Microorganism-based bioremediation technologies, such as monitored natural attenuation, biostimulation, and bioaugmentation have been widely applied because of their advantages of cost efficiency, less secondary contamination, and long-term sustainability.^{35, 37} For example,

bioaugmentation (the addition of pre-grown microbial cultures to enhance microbial populations at a site) is a typical technique for groundwater treatment.^{37,38} It is usually pursued when degrader strains are not abundant within the natural microbial community or treatment facilities. To date, many aerobic and anaerobic bacteria that show strong degradation ability for certain organic contaminants have been isolated from the environment and applied for *in-situ* and *ex-situ* bioremediation.³⁹ For example, *Aminobacter* sp. MSH1 is a well-known microorganism for mineralizing and degrading BAM such that it is of great interest for remediation applications.

However, traditional remediation technologies (e.g., those applied in wastewater plants) have difficulty eliminating organic micropollutants to zero concentration; even under nutrient-rich and bacteria-abundant conditions (e.g., field sites or specially designed bioaugmented sand filters), biodegradation of organic micropollutants is observed to stall below a threshold low concentration. Finding solutions, or even reasons for the bottleneck of organic micropollutants degradation, is a challenging task. To address this knowledge gap, most studies have focused on two dominate hypotheses: mass-transfer limitation and physiological limitation.

1.2.3 Mass-transfer limitation

Mass-transfer of substrate molecules from bulk solution into the bioavailable phase can be limited by several factors, such as dissolution, sorption, diffusion, mass transfer from flowing to immobile water, and the uptake of molecules through the cell membrane. Studies on mass-transfer limitation either focus on the various transport processes from the bulk solution to the bacterial cell surface (assuming the bioavailable concentration is the concentration on the cell surface or at the pore wall),⁴⁰⁻⁴² or mainly discuss the uptake from the bulk solution to the degradation-functional enzyme location (assuming the bioavailable concentration is the concentration that the enzyme experiences).⁴³⁻⁴⁵ In both assumptions, mass transfer from bulk solution to bioavailable solution follows the first-order mass-transfer kinetics,^{41,44}

$$r_{MT}^i = k_{tr} \cdot (c_i^{bulk} - c_i^{bioavailable}) \quad (1.1)$$

in which r_{MT}^i [umol L⁻¹ s⁻¹] is the rate of mass-transfer (i is the target substrate) between the bulk solution and the bioavailable phase, c_i^{bulk} [umol L_{bulk}⁻¹] and $c_i^{bioavailable}$ [umol L_{bio}⁻¹] represent the substrate concentration in the bulk solution and in the bioavailable solution, and k_{tr} [s⁻¹] is mass-transfer rate coefficient.

In this thesis, I focus on the mass-transfer process through the cellular membrane into the intracellular phase. Transport through the cellular membrane is usually classified as either an active transport process or a passive transport process (passive diffusion). For the active transfer, transporters and porins play a crucial role in enhancing diffusion. The transporters can speed up the movement of a solute across a membrane by facilitating diffusion. Thus, the rate of substrate uptake increases with the number of transporters.⁴⁶ Porins serving as channels for diffusion of small solutes into the periplasm may influence the diffusion of solutes and be the rate-limiting step of the enzymatic reaction in cells.⁴⁷ Passive diffusion transfer through the cell membrane is generally driven by a concentration gradient between the intracellular and bulk phases. The transfer rate depends on physiochemical properties of the substrate (e.g., K_{ow}) and the thickness of the membrane.^{48, 49} The mass transfer process of substrates through the cellular membrane in this thesis is assumed to be passive diffusion (Figure 1.1).

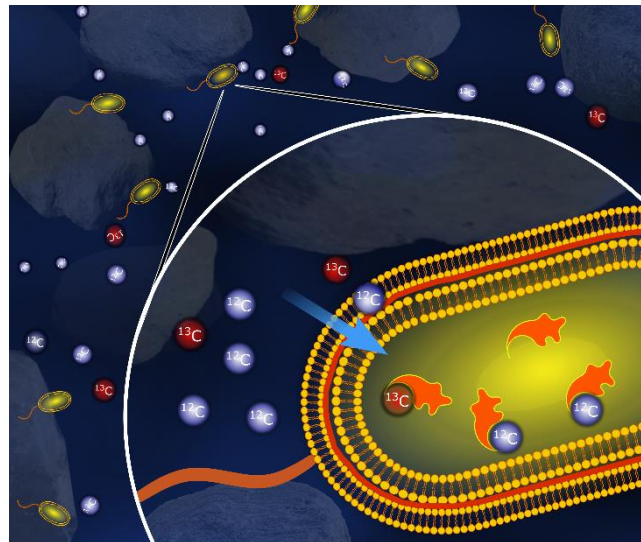


Figure 1.1. Illustration of mass-transfer limitation through the bacterial cell membrane in groundwater

1.2.4 Physiological limitation

Another limiting factor is bacterial physiological limitation under oligotrophic conditions.^{50, 51} To adapt to low substrate concentrations, bacteria developed multiple strategies. For example, bacteria can downregulate the functional genes or reduce the production of functional enzymes. Sekhar et al.⁵¹ observed reduced BAM degrading ability in *Aminobacter* sp. MSH1 at low BAM concentration, which was explained by the reduced production of the amidase BbdA converting BAM to 2,6-DCBA. In addition, bacteria may also reduce their cell size and DNA

content to keep a lower maintenance energy.^{45, 50} In the atrazine biodegradation process with *Atrabacter aureescens* TC1 in a chemostat experiment, cell morphology changed from rod shape under the high-growth-rate, high-atrazine-concentration condition to coccus-like shape at low atrazine concentrations.⁴⁵ This is assumed to be an energy-saving strategy by minimizing the bacterial surface-to-volume ratio.⁴⁵

1.2.5 Challenges in BAM biodegradation

In order to identify the limitation factors during biodegradation of organic micropollutant, I chose BAM, a frequently detected micropollutant in groundwater, as a target compound. The most prominently studied BAM degrader is *Aminobacter* sp. MSH1 which is an aerobic, Gram-negative, rod-shaped, motile, but potentially non-chemotactic⁵² soil bacteria that was firstly isolated from soils frequently treated with dichlobenil in Denmark.^{22, 53} Using BAM as the sole source of carbon, nitrogen, and energy, it mineralizes BAM into CO₂, NH⁴⁺, and chloride ions.^{21, 22, 53, 54} In this thesis, the growth of *Aminobacter* sp. MSH1 is assumed to follow dual-Monod equation (eq 1.16) that takes the extracellular concentrations of electron acceptor and electron donors as input.

Understanding the degradation pathway of BAM is important for the application of *Aminobacter* sp. MSH1 for *in-situ* or *ex-situ* groundwater bioremediation. The first well-known step in this biodegradation pathway is hydrolysis by amidase—BbdA encoded on plasmid pBAM1 (with gene *bbdA*), converting BAM to 2,6 dichlorobenzoic acid (DCBA);⁵⁵ the hydrolysis follows Michaelis–Menten kinetics, with a Michaelis–Menten coefficient of the amidase BbdA of 0.71 μmol/L.⁵⁵ Further degradation steps beyond the hydrolysis have recently been explored by Raes et al.⁵⁶

Aminobacter sp. MSH exhibits a promising BAM mineralization/degradation capacity, not only in well-defined laboratory experiments but also in BAM-contaminated soil/aquifer and pilot sand filters in drinking water treatment plants.^{21, 24, 57-59} Table 1.2 summarizes the studies on BAM degradation and mineralization with *Aminobacter* sp. MSH1 under various experimental conditions, such as different experimental scales (e.g., batch, sand filters), BAM concentrations, and cell densities.

Table 1.2 Overview of BAM degradation and mineralization with the specific degrader strain *Aminobacter* sp. MSH1 in laboratory experiments(Modified from Ellegaard-Jensen et al., 2017²¹)

Experimental type	Experimental setup	Inoculated cell density	Medium/matrix	BAM concentration	Maximum mineralization/BAM removal	Specific degradation rate	Reference
Degradation	Batch-flask	$2-4 \times 10^6$ cells mL ⁻¹	MS *	$1.5 - 50000$ µg L ⁻¹	95.6–99.9%	nd	Sorensen et al. 2007 ²²
Degradation	Batch-flask	OD _{600nm} = 0.9	MS	12000 µg L ⁻¹	~>95%	nd	Reinicke et al. 2012 ⁶⁰
Degradation	Batch-flask	10^7 cells mL ⁻¹	MSNC #	120 µg L ⁻¹	98% (240 min)	$4.4-7.3 \times 10^{-9}$ nmol C cell ⁻¹ min ⁻¹	Simonsen et al. 2012 ⁶¹
Degradation	Flow channel	10^7-10^8 cells mL ⁻¹	MS	$1-1000$ µg L ⁻¹	70–90%	3×10^{-14} to 1×10^{-11} µg BAM cell ⁻¹ min ⁻¹ (at 30 days of growth in starvation conditions)	Sekhar et al. 2016 ⁵¹
		10^8-10^9 cells mL ⁻¹	MS	$1-1000$ µg L ⁻¹	70–90%	4×10^{-12} to 5×10^{-10} µg BAM cell ⁻¹ min ⁻¹ (within minutes of inoculation)	
Degradation	Flow channel	2.5×10^8 cells mL ⁻¹	MS	1 µg L ⁻¹	~50–70%	$\sim 10^{-13-14}$ µg BAM cell ⁻¹ min ⁻¹	Horemans et al. 2017a ⁶²
		2.5×10^8 cells mL ⁻¹	MS	1000 µg L ⁻¹	~70–90%	$\sim 10^{-10-11}$ µg BAM cell ⁻¹ min ⁻¹	
Degradation	Column	$\sim 10^9$ cells mL ⁻¹	Groundwater	2.7 µg L ⁻¹	94–97%	$\sim 10^{-12}$ µg BAM cell ⁻¹ min ⁻¹	Albers et al. 2014 ⁶³
Degradation	Column	10^9 cells mL ⁻¹	Treated wastewater in DWTP &	$0.3-3$ µg L ⁻¹	~100% (until 40 days) ~60% (150 days)	nd	Ellegaard_Jensen et al. 2020 ⁶⁴
Degradation	Pilot-scale sand filter	10^9 cells mL ⁻¹	Groundwater	$0.13-0.22$ µg L ⁻¹	50% (2 days) 5–11% (23 days)	4×10^{-13} µg BAM cell ⁻¹ min ⁻¹	Albers et al. 2015 ⁵⁷

(Table continues)

Degradation	Pilot-scale sand filter	$\sim 10^{10}$ cells mL ⁻¹	Groundwater	0.19 $\mu\text{g L}^{-1}$	80% (~8days) 22% (44 days) 5% (88 days)	nd	Horemans et al.	2017b ⁵⁹
	Pilot-scale sand filter with alginate matrix	$\sim 10^{10}$ cells mL ⁻¹	Groundwater	0.19 $\mu\text{g L}^{-1}$	80% (~8days) 20% (44 days) 15% (88days)	nd		
Mineralization	Batch-flask	$2-4 \times 10^6$ cells mL ⁻¹	MS	1.5–50000 $\mu\text{g L}^{-1}$	Mineralization 15–64 % (within 2–10 days) BAM depletion 95.6–99.9%	nd	Sorensen et al.	2007 ²²
Mineralization	Batch-flask	10^9 cells mL ⁻¹	MSNC	120 $\mu\text{g L}^{-1}$	3.6–7.0% (180 min)	$4.4-7.3 \times 10^{-9}$ nmol C cell ⁻¹ min ⁻¹	Simonsen et al.	2012 ⁶¹
Mineralization	Batch-flask	$\sim 10^6$ cells mL ⁻¹	MS	19000 $\mu\text{g L}^{-1}$	$\sim 70-80\%$ (within 20–105 days)	10^{-16} mol C cell ⁻¹ day ⁻¹	Sjøholm et al.	2010 ⁶⁵
		$\sim 10^6$ cells mL ⁻¹	Groundwater	19000 $\mu\text{g L}^{-1}$	$\sim 5\%$ (115 days)	$10^{-17}-10^{-16}$ mol C cell ⁻¹ day ⁻¹		
		$\sim 7 \times 10^6$ cells mL ⁻¹	Groundwater	19000 $\mu\text{g L}^{-1}$	$\sim 50\%$ (185 days)	10^{-16} mol C cell ⁻¹ day ⁻¹		
Mineralization	Batch-flask		MSNC	1000 $\mu\text{g L}^{-1}$	>50 (24 h)	5×10^{-11} $\mu\text{g BAM cell}^{-1} \text{ min}^{-1}$	Schultz-Jensen et al.	2014 ²⁴
Mineralization	Sand filter	10^5 cells mL ⁻¹ 10^7 cells mL ⁻¹	Soil/sand slurry	100 $\mu\text{g L}^{-1}$ respiked after 28 days	10–100% (7–56 days)		Ekelund et al.	2015 ⁶⁶

* MS is medium salt solution. # MSNC is mineral salt solution with KNO₃ and (NH₄)SO₄ and N sources and glycerol as source. & DWTP is drinking water treatment plant.

Because of the high BAM-degradation potential of *Aminobacter* sp. MSH1, many studies focus on its application in the bioaugmentation of sand filters in drinking water treatment plants.^{21, 23, 57-59, 62, 63} The sand filters were initially inoculated with *Aminobacter* sp. MSH1 and installed after the aerated inlet water with a fast flow.²¹ Bacteria are supposed to adhere to the sediments. Compared to the batch experiments with fresh suspended cultures, reported cell-specific BAM degradation rates in such a sand filter were 10–100 times lower, which was explained by the short hydraulic retention times because of the fast flow rate.⁵¹ In addition, one big challenge of BAM degradation is that the degradation rate decreased with time in the long-time purification process in sand filters.^{21, 57, 65} Two possible explanations were brought forward by researchers. One explanation was the observed loss of inoculated bacteria from sediments, irrespective of whether the sand filters were running with or without backwashing.^{21, 57} Due to the loss of inoculated bacteria, BAM degradation efficiency could decrease to less than 20%, and it was reported to be difficult to maintain efficient degradation for more than two to three weeks.^{57, 65} Compared to the sand filters inoculated with suspended bacteria, the sand filter inoculated with immobilized bacteria in an alginate matrix showed less loss of bacteria after inoculation. However, the final removal rates did not differ between reactors inoculated with suspended and immobilized cells.⁵⁹ The second possible explanation for the poor long-term performance of biofilters is starvation. In the study of Horemans et al.,⁵⁹ even though the degrading biomass in the sand filters should not limit BAM degradation based on theoretical considerations, the specific BAM degradation rates were 100-fold below expectations, which is consistent with the observations of Sekhar et al.^{21, 51} There, cells residing in carbon- and nitrogen-starved biofilms for 30–60 days grew slower compared to the growth rate of fresh cells, likely because of reduced bacterial fitness (physiological limitation).⁵¹ In general, observed degradation efficiency at low BAM concentrations was consistently smaller compared to biodegradation at high BAM concentrations.²² When it comes to the limiting factors determining bacterial fitness for biodegradation of BAM at low concentrations, one limiting factor is mass-transfer limitation (detailed in section 1.2.3), which constrains the transport process of the contaminant from the bulk solution into the bacterial cell (in this thesis denoted as “bioavailable solution”).^{41, 44} Another limiting factor is physiological limitations (detailed in section 1.2.4), such as detachment or death of cells, downregulation of functional genes or reduced activity of catabolic enzymes due to a physiological response to oligotrophic conditions.^{50, 51}

This thesis hypothesizes that mass-transfer limitation and physiological limitation are potentially responsible for the difficulty of eliminating BAM below the threshold limit of 0.1 µg/L. Therefore, it is important to identify/distinguish the respective limiting factors in order to optimize bioremediation approaches. In this thesis, I applied multiple analytical techniques to investigate the limitations during the degradation of BAM. Specifically, the application of compound-specific isotope analysis (CSIA) creates a new opportunity to probe mass-transfer limitation and physiological limitation during biodegradation.

1.3 Compound-specific stable isotope analysis for evaluating biodegradation of organic contaminants in groundwater

1.3.1 Theoretical and analytical basics of CSIA

Compound-specific stable isotope analysis (CSIA) is an advanced method to evaluate the degradation processes and pathways for environmental applications. The isotope value of a substrate is usually expressed as δ [‰],

$$\delta_{\text{sample}} = \frac{R_{\text{sample}} - R_{\text{standard}}}{R_{\text{standard}}} \times 1000 \quad (1.2)$$

in which the heavy to light isotope ratio (e.g., $^{13}\text{C}/^{12}\text{C}$, $^{15}\text{N}/^{14}\text{N}$) of the samples R_{sample} [-] is calibrated by the isotope ratio of the international standard R_{standard} [-]. For example, Vienna PeeDee Belemnite (V-PDB) and Air-N₂ are the international reference standards for carbon and nitrogen isotope values, respectively. In the lab, the carbon and nitrogen isotope values $\delta^{13}\text{C}$ and $\delta^{15}\text{N}$ are usually calculated in relation to a lab reference gas (e.g., the CO₂ gases RM 8562, and NSVEC (N₂)) in the beginning and at the end of each run.

During (bio)transformation, kinetic isotope effects typically favor the transformation of substrates with light isotopes, as expressed by the corresponding isotopic enrichment factor ε [‰],⁴⁴

$$\varepsilon = \left(\frac{h_r/h_c}{l_r/l_c} - 1 \right) \times 1000 \quad (1.3)$$

in which h_r [µmol L⁻¹ s⁻¹] and l_r [µmol L⁻¹ s⁻¹] are the transformation rate of heavy and light isotopologues, respectively; h_c [µmol L⁻¹] and l_c [µmol L⁻¹] are the concentrations of heavy and light isotopologues, respectively.

During (bio)transformation, molecules with heavy isotopes are transformed more slowly, thus, they stay behind and become enriched in the remaining substrate in the bulk solution. The relation between isotope fractionation and (bio)transformation is usually expressed as the so-called Rayleigh equation,

$$\frac{R_t}{R_0} = \frac{\delta_t + 1}{\delta_0 + 1} = f^\varepsilon \quad (1.4)$$

in which isotope values at time zero, δ_0 [‰] and time t , δ_t [‰] are linked to the remaining substrate concentration fraction f [-] by ε .

Hence, when isotope ratios increase within a concentration gradient in groundwater or sediments, this can generally provide direct evidence of natural transformation of a compound, such as of turnover of sulfate,^{67, 68} nitrate,⁶⁹ or methane⁷⁰ in redox gradients, or degradation of organic pollutants (e.g., BTEX, chlorinated ethenes, pesticides, and herbicides)⁷¹⁻⁷⁵ at contaminated sites.

1.3.2 Does diffusion and hydraulic dispersion induce isotope fractionation of organic compounds at natural isotopic abundance in aqueous systems?

Even though diffusion- and/or dispersion-induced isotope fractionation was previously considered to be negligible,^{73, 76-78} this has been challenged by many studies which reported valid diffusion induced isotope fractionation with isotopically labeled compounds,⁷⁹ such as deuterated toluene with enrichment factor $\varepsilon = -37$ ‰, and deuterated ethylbenzene with $\varepsilon = -43$ ‰.⁷⁹

However, rare studies focused on the diffusion-induced isotope fractionation with organic compounds at natural isotopic abundance in the aqueous phase. Small isotope fractionations induced by diffusion in the aqueous phase have been observed in CO₂,⁸⁰ methane,^{81, 82} and chlorinated ethenes⁸³ (with ε between -0.22‰ and -2.23‰). In addition, Wannner and Hunkeler⁸³ reported diffusion induced isotope fractionation of TCE and 1,2 DCA at natural isotope abundance, with $\varepsilon_{carbon} = -0.22$ ‰, $\varepsilon_{chlorine} = -0.37$ ‰ for TCE, and $\varepsilon_{carbon} = -0.23$ ‰, $\varepsilon_{chlorine} = -0.61$ ‰ for 1,2DCA. Jin and Rolle also observed distinct isotope fractionation of TCE ($\varepsilon_{chlorine} = -1.79$ ‰) and cis-DCE ($\varepsilon_{chlorine} = -0.65$ ‰).^{79, 83-85} However,

the organic compounds at natural isotopic abundance in these studies have relatively higher mass ratio between heavy isotopologues and light isotopologues. A study of organic compounds at natural isotopic abundance with relative smaller mass ratio of heavy and light isotopologues has not yet been completed. Therefore, it is necessary to re-examine the isotope fractionation by diffusion and dispersion for organic compounds at natural isotopic abundance.

In order to better understand the underlying theories of the potential isotope fractionation during molecular diffusion in the aqueous phase, various theoretical models that describe the mechanisms of aqueous-phase diffusion and the correlated mass dependence during diffusion are introduced below.

Stokes-Einstein relation

The Stokes-Einstein relation is the most common basis for estimating diffusion coefficients. In the Stokes-Einstein relation, Einstein assumed that the diffusive particles were small rigid spheres that diffuse in a continuum of solvent, and that there is a force acting on the particle.⁸⁶⁻⁸⁸ The diffusion coefficient D [$\text{m}^2 \text{s}^{-1}$] was derived as,

$$D = \frac{k_B T}{f_r} = \frac{k_B T}{6\pi\eta R_i} \quad (1.5)$$

in which f_r [kg s^{-1}] is the friction coefficient of the solute, k_B [J K^{-1}] is the Boltzmann's constant, T [K] is the temperature, η [$\text{kg m}^{-1}\text{s}^{-1}$] is the dynamic viscosity of the solvent, R_i [m] is the radius of the species.

In the Stokes-Einstein relation, the diffusion coefficient is inversely proportional to the viscosity and solute size. However, this relation only holds for a liquid with a small Reynold number. When the solute radius is much smaller (e.g., 5 times smaller) than the solvent radius or if the viscosity is very high, the relation will not be adequate.⁸⁸

Chapman-Enskog relation

The Chapman-Enskog relation was originally derived to estimate the diffusion coefficient of molecular hydrodynamic motion in dilute gases. This relation assumes simple molecular interactions involving collisions between only two molecules at a time.^{89, 90} It was further extended to describe the binary collision dynamics during the diffusion of a solute particle in a dense hard-sphere fluid where the solute particle is also treated as a single hard-sphere.^{88, 91} The diffusion coefficient depends on the solute-solvent size ratio and mass ratio:

$$D = \frac{3}{8\rho R_0^2} \cdot \frac{1}{g_{i0}(R_i + R_0)} \cdot \left(\frac{k_B T}{2\pi\mu}\right)^{0.5} \quad (1.6)$$

in which ρ [kg m⁻³] is the solvent density, R_0 [m] is the radius of the solvent particle, R_i [m] is the radius of the solute particle, g_{i0} is the radial distribution function, k_B [J K⁻¹] is the Boltzmann constant, μ is the reduced mass $\mu = \frac{M_A M_B}{M_A + M_B}$ [kg], where M_A [kg] and M_B [kg] are the molecular masses of the solute and the solvent, respectively.

Furthermore, a similar empirical equation was given by Woch et al.,⁹² where the diffusion coefficient was assumed to be inversely proportional to the molecular mass of the solute with a power law exponent of 0.53.

Wilke-Chang relation

To further evaluate the effect of solvents properties on the diffusion coefficient, Wilke and Chang⁹³ derived an equation based on the Stokes-Einstein relation that depends on the solute molar volume correlated with solvent properties:

$$D = \frac{7.4 \cdot 10^{-12} (xM)^{0.5} T}{\eta V_i^{0.6}} \quad (1.7)$$

In addition to solvent viscosity η [kg m⁻¹s⁻¹], molar volume [m³ mol⁻¹] of the diffusion species i , and the effective molar weight of the solvent xM [kg mol⁻¹] are considered, where x [-] is an empirical solvent parameter ($x = 1$ for water).^{88, 93}

Maxwell-Stefan relation

The Maxwell-Stefan relation was originally derived as a dynamical theory for the diffusion of gases.⁹⁴ However, it was also applied to study the diffusion process in the aqueous phase.^{87, 95} The Maxwell-Stefan relation describes the velocity distribution among molecules under a chemical potential gradient.^{94, 95} The force on the molecules is expressed in terms of the chemical potential gradient, which is balanced by the coefficient of viscosity or frictions between diffusing species.^{94, 95} Instead of assuming molecules as hard elastic bodies acting on each other,⁹⁴ it assumed that the molecules are the bodies repelling each other at a distance, and each molecule is undergoing motions like translation, rotation, and vibration. The diffusion coefficient showed mass dependence of the molecular masses of both the solute and the solvent molecules.⁸⁷

Einstein relation

In contrast to other deterministic relations, the Einstein relation is derived from a statistic/probabilistic perspective. In the Einstein relation, the diffusion coefficient depends on the probability of the Brownian particle experiencing a certain displacement in a given time t , based on the assumptions that this time interval is small but not too small so that (i) the movements of one particle at two intervals can be independent and (ii) the movement of every single particle is independent of other particles:

$$D = \frac{\Delta x^2}{2t} \quad (1.8)$$

in which Δx [m] is the mean displacement which a particle moves on an average and t [s] is a given time. However, the Einstein's theory cannot accurately describe a solute molecule's trajectory on "time-scale", because the motion of a solute molecule is on a small spatial-temporal scale.⁹⁶

Langevin relation

The Langevin relation is a stochastic differential equation to describe the random trajectory of a single solute molecule within the solvent. It departs from Newton's Second Law for the solute molecule. The key assumption is that the force acting on a single solute molecule arises from collisions between the solute molecule and the much smaller solvent molecules. The force is the sum of the drag force—which is proportional to the molecule's velocity but has an opposite direction—and a randomly fluctuating force which is proportional to Gaussian white noise.⁹⁶ When the time interval is large, the Langevin relation converges with the Einstein relation and there is no mass dependence of diffusion coefficient in Langevin's equation. When it is on a short time scale, the diffusion rate shows mass dependence.⁸⁷

Mode-coupling theory analysis

In the Mode-coupling theory analysis, the diffusive motion of a solute molecule is coupled with long-term hydrodynamic motions and short-term binary collision motions.^{87, 97} The diffusion coefficient was derived from the total friction that is contributed from binary collision and density dynamics. The pair potential of solvent-solvent molecules and solute-solvent molecules was described by the Lennard-Jones potential.

Molecular dynamic simulation

In contrast to the models above, which mainly consider the intermolecular forces/interactions during the diffusion processes of solute molecules in the aqueous phase, molecular dynamic simulation has the advantage of also simulating the behavior of every single atom inside the molecule and including intramolecular forces.^{87,98} The long-range interactions between atoms are usually considered as coulombic interactions by assigning partial charges to each atom, and the short-range interactions between the pair atoms are described as Lennard-Jones potential which depends on particle mass.^{87,98} This model was also able to consider the potential energy of each bond, angle, and dihedral in each solute molecule, which represented stretching, bending, and torsional energy between two bonded atoms.

Even though these models proposed various theoretical explanations for molecular diffusion in the aqueous phase, the mass dependence of aqueous-phase diffusion in these models is not constant. In addition, for organic compounds, the rarely observed large diffusion-induced isotope fractionation with strong mass dependence challenges the diffusion theories based on strong mass dependence. Therefore, in section 2.1, I evaluated the mass dependence of organic compounds at natural isotopic abundance during aqueous-phase diffusion and dispersion by calculating the correlation between mass ratio of heavy to light isotopologues and the observed isotope fractionation; and proposed potential theoretical explanations for aqueous phase diffusion of organic compounds at natural isotopic abundance.

1.3.3 Can we use CSIA to identify mass-transfer limitation as the bottleneck of biodegradation of organic micropollutants and follow the changing degradation activity in a groundwater system?

When we assume that physical factors (e.g., diffusion, dispersion, or sorption) do not significantly interfere with or induce isotope fractionation, the increased isotope fractionation within a concentration gradient in groundwater or sediments usually indicates the natural transformation of a compound;⁹⁹ conversely, the absence of isotope fractionation in a concentration gradient is commonly taken as evidence of the absence of turnover.

However, isotope fractionation only follows the Rayleigh equation when the enzyme reaction is the rate-limiting step (enzyme reaction rate \ll mass-transfer rate of the substrate through the cell membrane). In this case the heavy isotopes that are discriminated against by

the enzyme reaction will diffuse out of the cell and make this isotope effect visible in the bulk solution. (Figure 1.2a) In contrast, if the mass transfer is limiting (mass-transfer rate \ll intracellular enzymatic reaction rate), both heavy and light isotopologues, once transferred into the cell, will be completely degraded such that the isotope fractionation of the enzymatic transformation will be masked in the bulk solution (Figure 1.2b).⁴⁴ This masked isotope principle has been recognized in photosynthesis,¹⁰⁰ denitrification,^{101, 102} and sulfate respiration,^{103, 104} through the observed muted isotope fractionation at low concentrations. In addition, evidence is accumulating that a dramatic decrease of isotope fractionation may occur specifically at low concentrations during biodegradation of organic micropollutants, when extracellular substrate concentrations decrease below a threshold close to the Monod or Michaelis–Menten constants of growth or enzymatic turnover, respectively.^{45, 50, 105, 106} Table 1.3 summarizes the observed masked isotope fractionation due to mass-transfer limitation during biodegradation of organic contaminants.

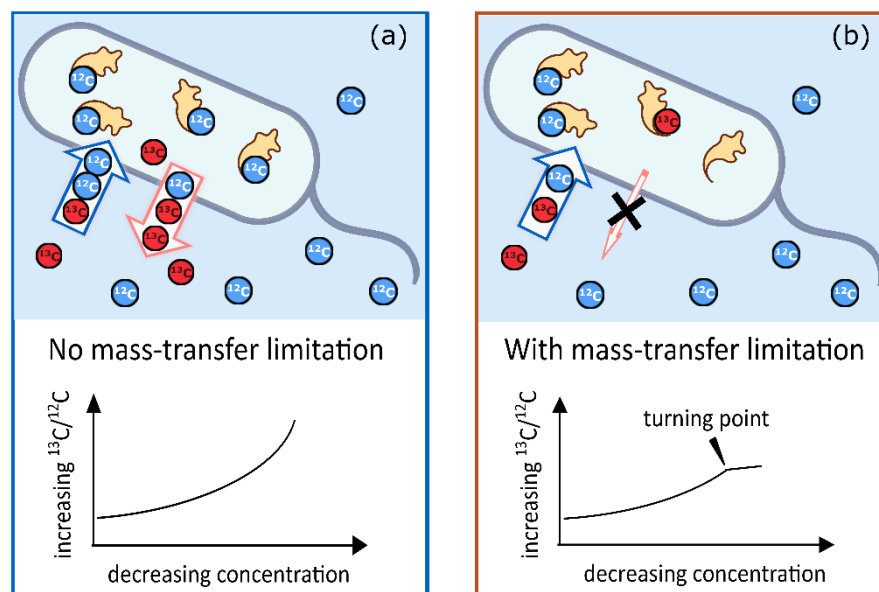


Figure 1.2. Isotope fractionation with decreasing concentration during biodegradation under the hypothesis of (a) no mass-transfer limitation and (b) with mass-transfer limitation.

The masking effect of mass-transfer limitation through the cell membrane on isotope fractionation has been intensively discussed in the process of microbial sulfate reduction. Various factors such as temperature,^{107, 108} carbon source,¹⁰⁷ sulfate supply, and reoxidation of intermediates¹⁰⁹ have been shown to be relevant to the broad variation of sulfur isotope fractionation during microbial sulfur reduction in laboratory and field studies. The mechanisms

by which these factors influence isotope fractionation generally converge to the evaluation of the balance between mass transfer of sulfate through the cell membrane and net sulfate respiration rates. Indeed, isotope fractionation in sulfate reduction was found to show a concentration dependence and to decrease concomitantly with decreasing extracellular sulfate levels.⁶⁸ At low concentrations, when uptake of sulfate is only limited by extracellular sulfate concentrations, forward reactions proceed as fast as sulfur is supplied, and no backward flows are established.¹⁰³ In addition, Habicht et al.¹¹⁰ inferred that the cell demands more energy for sulfate transport into the cell at sulfate concentrations below 300–400 $\mu\text{mol L}^{-1}$ than it does at higher concentrations. In the study of Crowe et al.,¹¹¹ they inferred that the shift of sulfate reduction from organic matter limitation to sulfate limitation is the reason for the muted fractionation at low concentrations.

Table 1.3 Overview of the studies on mass-transfer limitation through the cell membrane with masked isotope fractionation during biotransformation

Compounds	Experiment Setup	Bacteria	Transport type	Isotopes	Concentration [$\mu\text{g/L}$]	* ϵ [‰]	Reference
atrazine	Batch	Polaromonas sp.	passive	C	30–1.4	-3.5	Ehrl, et al., 2018 ¹⁰⁶
		Nea-C-cell ^(N)		N	30–1.4	-1.9	
atrazine	Chemostat	Arthrobacter aurescens	passive	C	82	-5.36	Ehrl et al., 2019 ⁴⁵
				C	62	-4.32	
				C	45	-2.12	
		TC1 ^(P)		N	32	-2.32	
				N	62	1.94	
				N	45	1.04	
atrazine	Chemostat Retentostat	Arthrobacter aurescens	passive	C	30	-4.34	Kundu et al., 2019 ⁵⁰
		TC1 ^(P)		C	12	-0.45	
atrazine	Batch	Rhizobium sp.CX-Z ^(N)	active	C	30–1.2	-1.8	Chen, et al., 2019 ¹¹²
		Rhizobium sp.CX-Z ^(N)		N	30–1.2	0.8	
atrazine	Batch	Rhizobium sp.CX-Z ^(N)	active	C	9.5	-3.5	Chen, et al., 2020 ¹¹³
2-(2,4-dichloro-phenoxy)-propionic acid	Batch	Sphingobium herbicidovorans MH ^(N)	active	C	47000	-0.3	Qiu, et al., 2014 ¹¹⁴
Tetrachloroethylene (PCE)	Batch	Sulfurospirillum multivorans ^(N)	--	C	83000	0.42	Nijenhuis, et al., 2005
Nitrate	Batch	Multiple strains*	passive	N	120–2200	10–15	Kritee, et al., 2005

^(P) Gram positive bacteria. ^(N) Gram negative bacteria.

Furthermore, recent chemostat and retentostat experiments revealed a dramatic decrease in isotope fractionation during biodegradation of atrazine by strain *Arthrobacter auresens* TC1 when atrazine concentration of 30 $\mu\text{g/L}$ and low growth rate were approached.^{45, 50} However, chemostat and retentostat are both controlled liquid culture systems where bacteria were suspended at relatively high cell density in pure liquid culture⁴⁵ rather than colonized on sediments where they more realistically mimic true adaptation to environmental conditions. Hence, the question remains whether an onset of mass-transfer limitation can indeed be observed in a realistic concentration gradient in porous media; if yes, in which substrate concentration range. Therefore, my thesis has the objective to explore the mass-transfer limitation during biodegradation of an organic micropollutant by using CSIA as a performance indicator in a bench-scale aquifer mimicking realistic porous media and, further, to follow the response of the degradation activity in a flow-through sediment system and to pinpoint underlying limitations at different concentrations.

Several models have been developed to explain the concentration dependence of isotope fractionation due to mass-transfer limitation, especially in the field of sulfate reduction. The standard model from Rees¹⁰³ related isotope fractionation to sulfur exchange rate between the extracellular sulfate pool and the intracellular sulfate pool, and to the exchange rate between the intracellular intermediate pools. For an open system, Crowe et al.¹¹¹ developed a reaction-diffusion model, in which a linear decrease of sulfur isotope fractionation factor from 1.070 to 1.000 was applied to the sulfate concentrations below 6 $\mu\text{mol L}^{-1}$. Wing et al.⁶⁸ further developed a quantitative model to explain the near-thermodynamic behavior of sulfur isotope fractionation by associating kinetic sulfur isotope fractionation with selective sulfate uptake into the cytoplasm and equilibrium between extracellular and intracellular sulfur pools. Compared to the models above, the model from Thullner et al.⁴⁴ emphasizes the role of mass-transfer limitation at low concentrations where isotope fractionation may not linearly decrease with concentrations—as suggested by Wing et al.⁶⁸ and implemented by Crowe et al.¹¹¹—but may follow a steeper decline within a narrower range as defined by Michaelis–Menten enzyme kinetics. This corresponds to the intuitive approach by Habicht et al.,¹¹⁰ who used a modified Michaelis–Menten equation to describe isotope fractionation by relating the isotope enrichment factor to sulfate concentration. In section 2.2 of my thesis, the mass-transfer model adapted from Thullner et al.⁴⁴ was coupled into the reactive transport model to simulate the effect of mass-transfer limitation on biodegradation efficiency and isotope fractionation at low concentrations in a quasi-two-dimensional flow-through sediment tank system.

1.4 Transport and degradation mechanisms of contaminants in groundwater

To investigate the bottleneck of biodegradation of organic micropollutants in groundwater, I set up a quasi-two-dimensional flow-through sediment tank mimicking the natural groundwater system. The contaminant (BAM) solution was injected through the single central inlet port of the tank, and the medium solution was injected through all the other inlet ports above and below the central inlet port in parallel. Therefore, the injected BAM solution was considered as a point source contaminant transported through the tank in the form of a quasi-two-dimensional plume. The reactive transport of the contaminant plume and biomass growth were simulated with a two-dimensional reactive transport model that quantitatively elucidates the potential degradation bottlenecks. In this section, the general solute transport equations, Michaelis–Menten kinetics for enzymatic reactions, and Monod microbial growth kinetics are introduced for a better understanding of the models developed in this thesis.

1.4.1 General solute transport equations

Contaminant transport in groundwater usually takes up the form of a plume, driven by advection and hydrodynamic dispersion, migrating with slow groundwater flow. Advection is the main transport process in the direction of the flow, while hydrodynamic dispersion (i.e., mechanical dispersion and molecular diffusion) causes spreading of compounds.

The solute transport process is generally described by the following advection-dispersion partial differential equation:¹⁷

$$\frac{\partial c_i}{\partial t} = -\mathbf{v} \cdot \nabla c_i + \nabla \cdot (\mathbf{D}_{t/\ell} \cdot \nabla c_i) + r \quad (1.9)$$

in which c_i [$\mu\text{mol L}^{-1}$] is the concentration of the contaminant; $\mathbf{D}_{t/\ell}$ [$\text{m}^2 \text{s}^{-1}$] is the dispersion tensor; \mathbf{v} [m s^{-1}] is the velocity vector; t [s^{-1}] is time; r [$\mu\text{mol L}^{-1}\text{s}^{-1}$] is the rate that represents sinks or sources of the contaminant. The velocity \mathbf{v} of the advective transport follows Darcy's law:^{17, 115}

$$\mathbf{v} = \frac{\mathbf{K}}{n_e} \nabla h \quad (1.10)$$

in which \mathbf{K} is the hydraulic conductivity tensor [m s^{-1}] of the system, n_e is the effective porosity [-], and h is the hydraulic head [m].

Hydrodynamic dispersion includes both molecular diffusion and mechanical dispersion caused by pore-scale velocity variations.¹⁷ The standard parameterization assumes that the pore diffusion coefficient D_p [$\text{m}^2 \text{s}^{-1}$] and the mechanical dispersion $D_{\text{mech},t/\ell}$ [$\text{m}^2 \text{s}^{-1}$] are additive:¹⁷

$$D_{t/\ell} = D_p + D_{\text{mech},t/\ell} \quad (1.11)$$

$$D_p = \frac{1}{\tau} D_{\text{aq}} \quad (1.12)$$

in which the index t and ℓ refer to the transverse and longitudinal directions, respectively, and τ [-] is the tortuosity of the porous medium.

The classical parameterization of $D_{\text{mech},t/\ell}$ ¹¹⁶ is compound-independent and linearly proportional to the mean velocity v [m s^{-1}]:

$$D_{\text{mech},t/\ell} = \alpha_{t/\ell} v \quad (1.13)$$

in which $\alpha_{t/\ell}$ is the transverse or longitudinal dispersivity [m].

Another parameterization of transverse dispersion coefficient $D_{\text{mech},t}$ was introduced by Chiogna et al.¹¹⁷, which is a non-linear equation:

$$D_{\text{mech},t} = v \cdot \frac{d_{\text{eff}}}{\sqrt{Pe + 123}} \quad (1.14)$$

in which the mechanical dispersion depends on the grain-Péclet number $Pe = v \cdot d_{\text{eff}}/D_{\text{aq}}$. d_{eff} [m] is the effective grain diameter.

1.4.2 Michaelis–Menten kinetics

Michaelis–Menten kinetics is the typical model that describes saturation-type enzyme kinetics. It was derived based on enzyme–compound interactions which limit the overall removal of the substrate. Under the assumption that back reactions do not occur, the general enzyme-mediated reaction is shown as below,



in which E , S , ES , and P represent enzyme, substrate, enzyme-substrate complex, and product, respectively. The reaction rate of the substrate can be written as,

$$\frac{dc_i}{dt} = r = r_{\text{max}} \frac{c_i}{c_i + K_M} \quad (1.15)$$

in which c_i [$\mu\text{mol L}^{-1}$] is the concentration of substrate i , K_M [$\mu\text{mol L}^{-1}$] is the substrate half-saturation constant, and r_{\max} [$\mu\text{mol L}^{-1} \text{s}^{-1}$] is the maximum reaction rate. When $c_i \ll K_M$, r is linearly proportional to c_i ; when $c_i \gg K_M$, r reaches its maximum r_{\max} . Figure 1.3 depicts the hyperbolic relation between r and c_i .

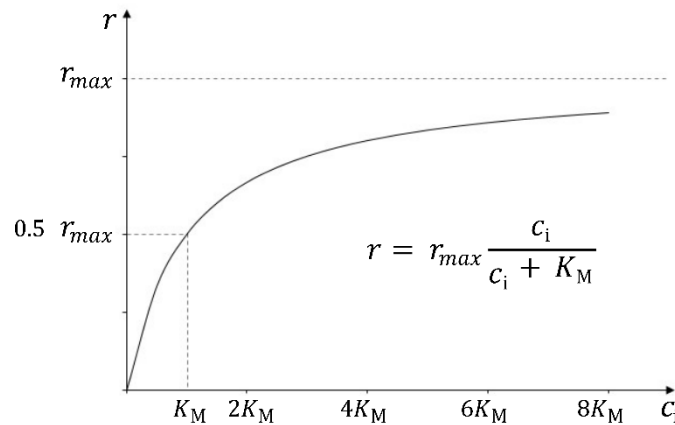


Figure 1.3. Michaelis–Menten Kinetics

When the bioavailable concentration that enzyme experiences is equal to its bulk concentration and saturation-type enzymatic dynamics is considered, degradation of a substrate sometimes can be assumed to follow Michaelis–Menten Kinetics.

1.4.3 Monod microbial growth kinetics

The common mathematical model for bacterial growth is the Monod equation which was empirically proposed by Jacques Monod.¹¹⁸ The Monod equation has the same mathematical form as the Michaelis–Menten kinetics. We can get the Monod equation by replacing the symbols used in the Michaelis–Menten equation—replacing μ for r yields the growth rate, replacing μ_{\max} for r_{\max} yields the maximum growth rate, and replacing K_S for K_M yields the Monod constant. In the Monod equation, the microbial growth rate was related to the concentration of the substrate c_i that is critical for its growth. Like Michaelis–Menten kinetics, growth rate μ and substrate concentration c_i follow a hyperbolic relation.

In the case of dual substrate limiting growth, a modified equation (dual-Monod equation¹¹⁹) that reflects the impacts of both substrates, i and j is written as below,

$$\mu = \mu_{\max} \cdot \frac{c_i}{K_{iM} + c_i} \cdot \frac{c_j}{K_{jM} + c_j} \quad (1.16)$$

in which μ is the specific growth rate [s^{-1}], μ_{\max} is the maximum specific growth rate [s^{-1}], K_{iM} [$\mu\text{mol L}^{-1} s^{-1}$] and K_{jM} [$\mu\text{mol L}^{-1} s^{-1}$] represent the Monod coefficient of species i and j , respectively. For example, i may be electron donor (e.g., BAM), and j may be electron acceptor (e.g., O_2).

Monod microbial growth can also be related to concentration changes of the limiting substrate. To evaluate the degradation rate of the substrate i , yield coefficient Y (cells grown per mole of substrate i used, [$\mu\text{mol-biomass } \mu\text{mol}_i^{-1}$]) was introduced in the equation below,¹¹⁹

$$\frac{dc_i}{dt} = -\frac{\mu \cdot X}{Y} \quad (1.17)$$

in which X [$\mu\text{mol-biomass L}^{-1}$] represents cell abundance.

In this thesis, I used Michaelis–Menten kinetics and Monod equation interchangeably because they are mathematically identical, and both describe saturation-type kinetics.

1.5 Outline and objectives

The objective of this thesis is to investigate the limitations of biodegradation of organic micropollutants in a bench-scale aquifer by applying CSIA. Specifically, I aimed to:

- (1) quantify the diffusion- and dispersion-induced isotope effects of organic compounds at natural isotopic abundance in the aqueous phase and porous media for a more accurate interpretation of observed isotope values in the reactive transport system.
- (2) investigate the potential mass-transfer limitation during biodegradation of the organic micropollutant–BAM by evaluating the relation between isotope fractionation and concentration/biomass profiles in a two-dimensional flow-through sediment tank system that mimics natural groundwater flow in the field.
- (3) explore more effective bioremediation strategies (e.g., priming strategy, intermediate flow fluctuation) for organic contaminants at low concentrations, and to identify potential degradation limitations in various steady states by applying CSIA as a biodegradation indicator.

To achieve these goals, I designed and performed stepwise laboratory experiments with CSIA as a crucial approach. Figure 1.4 illustrates the outline of the Research sections.

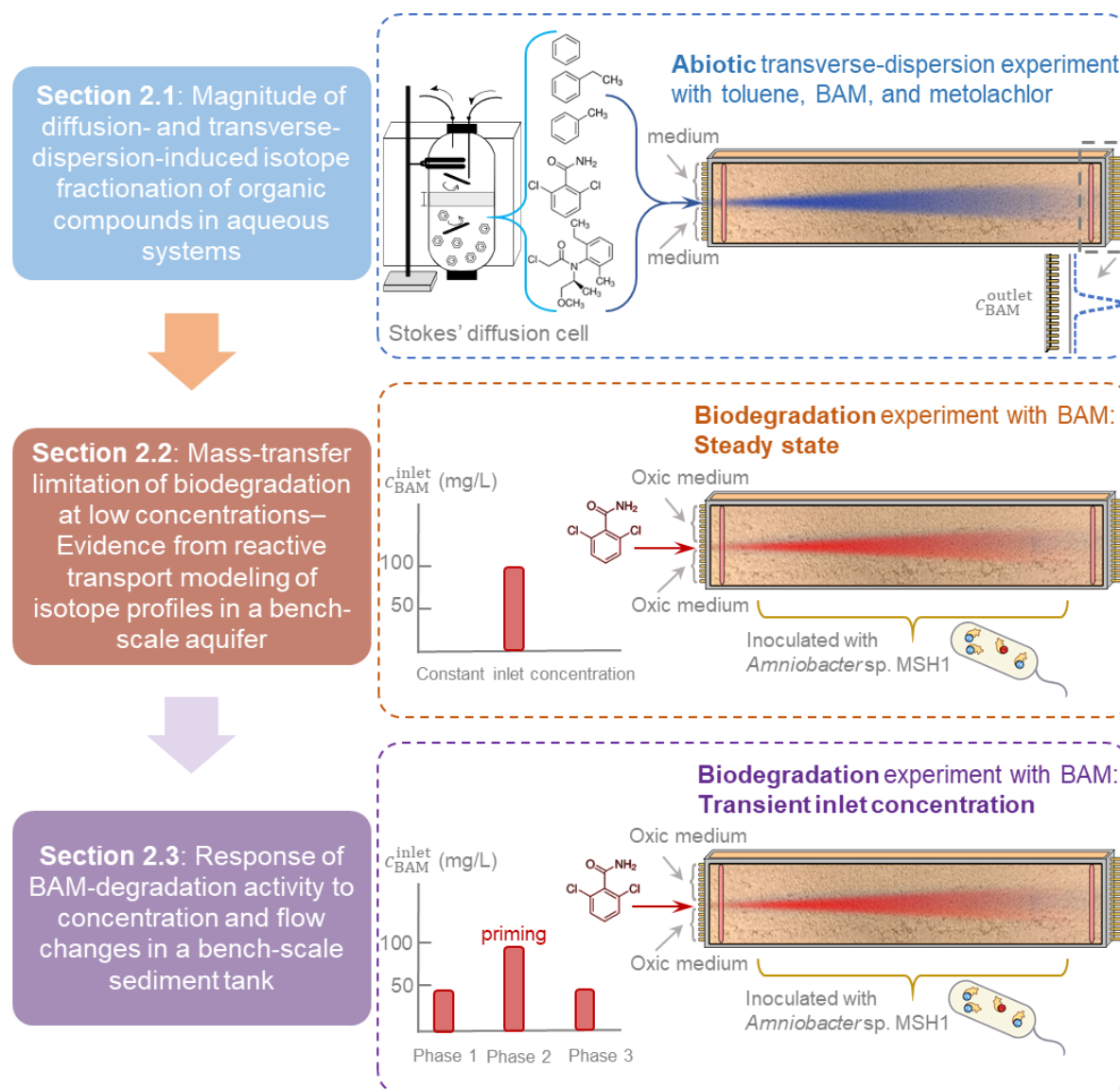


Figure 1.4. Outline of the Research chapter

In order to apply the correlation between isotope values and concentrations as an indicator for biodegradation and potential mass-transfer limitation, as a precondition, it is necessary to exclude diffusion- or dispersion-induced isotope fractionation as artifacts that would potentially bias data interpretation. Therefore, in section 2.1, I performed diffusion and dispersion experiments to evaluate the potential isotopic interference from diffusion and dispersion during contaminant transport. Although many theoretical models (as the diffusion

theories introduced in section 1.3.2, e.g., Enskog relation) proposed that aqueous-phase diffusion was strongly mass-dependent, weak mass dependence of isotope fractionation has been observed in many studies;^{87, 120, 121} in addition, studies on organic compounds at natural isotopic abundance are rare. In order to quantify the diffusion-induced isotope fractionation of organic compounds at natural isotopic abundance in the aqueous phase and the corresponding mass dependence, I conducted modified Stokes' diffusion cell experiments with organic compounds with various molecular masses at natural isotopic abundance. For the study on the isotope effect of transverse dispersion in porous media, abiotic quasi-two-dimensional flow-through sediment tank experiments were conducted with toluene, BAM, and metolachlor at natural isotopic abundance. To further investigate the potential significance of transverse-dispersion-induced isotope fractionation, I compared modeling scenarios with different transverse dispersion equations.

In section 2.2, CSIA was applied to evaluate biodegradation efficiency and potential mass-transfer limitation after evaluating the diffusion- and dispersion-induced isotope effects of organic compounds at natural isotopic abundance in section 2.1. Even though the onset of mass-transfer limitation through the bacterial cell membrane at low substrate concentrations has been observed in the artificially controlled liquid culture systems (e.g., bench, chemostat), whether mass transfer inhibits micropollutant biodegradation in realistic groundwater sediments has not been verified by direct observation. To mimic natural groundwater flow, I set up a quasi-two-dimensional flow-through sediment tank system. By injecting the BAM solution at the central inlet port, transverse concentration cross-gradients of BAM can generate from the center of the plume towards the top and bottom regions of the tank where low steady-state concentrations can be yielded, mimicking the oligotrophic conditions in groundwater. To pinpoint the threshold concentration range below which the onset of mass-transfer limitation can be observed, CSIA in conjunction with concentration measurements was performed. Furthermore, a reactive transport model that accounted for mass-transfer limitation through the cell membrane was developed to verify and elucidate the observations (e.g., isotope values and concentrations). By calculating the apparent isotope enrichment factors along the concentration gradient, a threshold concentration range below which the isotope fractionation was strongly constrained can be estimated.

In the presence of the potential limiting factors detailed in section 1.2.3 and 1.2.4, it has been observed that the degradation rate of organic contaminant decreased with time and

remained low at low substrate concentrations in laboratory experiments and pilot water-treatment facilities (e.g., sand filters). In section 2.3, to stimulate the biodegradation of organic pollutants, especially under low concentration conditions, intermediate system disturbances (i.e., priming strategy and flow fluctuation) were implemented in the two-dimensional flow-through sediment tank system. Based on the study described in section 2.2, the following questions arise: (a) Can we use isotope fractionation in conjunction with other variables (concentrations, cell numbers, metabolite/parent ratios) to follow the response of BAM-degradation activity to perturbations? (b) Can we use isotope fractionation as an indicator of underlying limitations when the system is operating at different quasi-steady states? Therefore, isotope values and other variables (concentrations, cell numbers, metabolite/parent ratios) was monitored under different steady-state conditions. The isotope analysis in different concentration zones under different concentration conditions can be potentially used as an indicator for mass-transfer limitation and physiological limitation.

References

1. Döll, P.; Hoffmann-Dobrev, H.; Portmann, F. T.; Siebert, S.; Eicker, A.; Rodell, M.; Strassberg, G.; Scanlon, B. Impact of water withdrawals from groundwater and surface water on continental water storage variations. *J. Geodyn.* **2012**, *59*, 143-156.
2. Green, T. R.; Taniguchi, M.; Kooi, H.; Gurdak, J. J.; Allen, D. M.; Hiscock, K. M.; Treidel, H.; Aureli, A. Beneath the surface of global change: Impacts of climate change on groundwater. *J. Hydrol.* **2011**, *405* (3-4), 532-560.
3. Wu, W.-Y.; Lo, M.-H.; Wada, Y.; Famiglietti, J. S.; Reager, J. T.; Yeh, P. J.-F.; Ducharne, A.; Yang, Z.-L. Divergent effects of climate change on future groundwater availability in key mid-latitude aquifers. *Nat. Commun.* **2020**, *11* (1), 1-9.
4. Tang, F. H.; Lenzen, M.; McBratney, A.; Maggi, F. Risk of pesticide pollution at the global scale. *Nat. Geosci.* **2021**, *14* (4), 206-210.
5. Schwarzenbach, R. P.; Escher, B. I.; Fenner, K.; Hofstetter, T. B.; Johnson, C. A.; Von Gunten, U.; Wehrli, B. The challenge of micropollutants in aquatic systems. *Science* **2006**, *313* (5790), 1072-1077.
6. Bedient, P. B.; Rifai, H. S.; Newell, C. J. *Groundwater Contamination: Transport and Remediation*. Prentice-Hall International, Inc.: 1994.
7. Smith, R.; Knight, R.; Fendorf, S. Overpumping leads to California groundwater arsenic threat. *Nat. Commun.* **2018**, *9* (1), 2089.
8. Feng, W.; Zhong, M.; Lemoine, J. M.; Biancale, R.; Hsu, H. T.; Xia, J. Evaluation of groundwater depletion in North China using the Gravity Recovery and Climate Experiment (GRACE) data and ground-based measurements. *Water Resour. Res.* **2013**, *49* (4), 2110-2118.
9. Sarkar, T.; Kannaujiya, S.; Taloor, A. K.; Ray, P. K. C.; Chauhan, P. Integrated study of GRACE data derived interannual groundwater storage variability over water stressed Indian regions. *Groundw. Sustain. Dev.* **2020**, *10*, 100376.
10. Voss, K. A.; Famiglietti, J. S.; Lo, M.; De Linage, C.; Rodell, M.; Swenson, S. C. Groundwater depletion in the Middle East from GRACE with implications for transboundary water management in the Tigris-Euphrates-Western Iran region. *Water Resour. Res.* **2013**, *49* (2), 904-914.
11. Kirby, R. M.; Bartram, J.; Carr, R. Water in food production and processing: quantity and quality concerns. *Food Control* **2003**, *14* (5), 283-299.
12. Emmanuel, E.; Pierre, M. G.; Perrodin, Y. Groundwater contamination by microbiological and chemical substances released from hospital wastewater: Health risk assessment for drinking water consumers. *Environ. Int.* **2009**, *35* (4), 718-726.
13. Andrade, L.; O'Dwyer, J.; O'Neill, E.; Hynds, P. Surface water flooding, groundwater contamination, and enteric disease in developed countries: A scoping review of connections and consequences. *Environ. Pollut.* **2018**, *236*, 540-549.
14. Griebler, C.; Avramov, M.; Hose, G. Groundwater ecosystems and their services: current status and potential risks. In *Atlas of Ecosystem Services*, Springer: 2019; pp 197-203.
15. Gleick, P. H. The human right to water. *Water Policy* **1998**, *1* (5), 487-503.
16. Powers, S. E.; Hunt, C. S.; Heermann, S. E.; Corseuil, H. X.; Rice, D.; Alvarez, P. J. J. The transport and fate of ethanol and BTEX in groundwater contaminated by gasohol. *Crit. Rev. Environ. Sci. Technol.* **2001**, *31* (1), 79-123.
17. Bear, J.; Cheng, A. H.-D. *Modeling Groundwater Flow and Contaminant Transport*. Springer Science & Business Media: 2010; Vol. 23.
18. Munoz, A.; Koskinen, W. C.; Cox, L.; Sadowsky, M. J. Biodegradation and mineralization of metolachlor and alachlor by *Candida xestobii*. *J. Agric. Food Chem.* **2011**, *59* (2), 619-27.

19. U.S. Environmental Protection Agency's Integrated Risk Information System (IRIS). "Summary on Metolachlor (51218-45-2)", <https://www.epa.gov/iris/>. Available from March 15, 2000.
20. Si, Y.; Takagi, K.; Iwasaki, A.; Zhou, D. Adsorption, desorption and dissipation of metolachlor in surface and subsurface soils. *Pest Manage. Sci.* **2009**, *65* (9), 956-62.
21. Ellegaard-Jensen, L.; Horemans, B.; Raes, B.; Aamand, J.; Hansen, L. H. Groundwater contamination with 2,6-dichlorobenzamide (BAM) and perspectives for its microbial removal. *Appl. Microbiol. Biotechnol.* **2017**, *101* (13), 5235-5245.
22. Sorensen, S. R.; Holtze, M. S.; Simonsen, A.; Aamand, J. Degradation and mineralization of nanomolar concentrations of the herbicide dichlobenil and its persistent metabolite 2,6-dichlorobenzamide by *Aminobacter* spp. isolated from dichlobenil-treated soils. *Appl. Environ. Microbiol.* **2007**, *73* (2), 399-406.
23. Vandermaesen, J.; Horemans, B.; Degryse, J.; Boonen, J.; Walravens, E.; Springael, D. Mineralization of the common groundwater pollutant 2,6-dichlorobenzamide (BAM) and its metabolite 2,6-dichlorobenzoic acid (2,6-DCBA) in sand filter units of drinking water treatment plants. *Environ. Sci. Technol.* **2016**, *50* (18), 10114-22.
24. Schultz-Jensen, N.; Knudsen, B. E.; Frkova, Z.; Aamand, J.; Johansen, T.; Thykaer, J.; Sorensen, S. R. Large-scale bioreactor production of the herbicide-degrading *Aminobacter* sp. strain MSH1. *Appl. Microbiol. Biotechnol.* **2014**, *98* (5), 2335-44.
25. Clausen, L.; Larsen, F.; Albrechtsen, H.-J. Sorption of the herbicide dichlobenil and the metabolite 2, 6-dichlorobenzamide on soils and aquifer sediments. *Environ. Sci. Technol.* **2004**, *38* (17), 4510-4518.
26. Drinking Water Directive 98/83/EC. European Commission. 1998.
27. Gupta, P. K.; Bharagava, R. N. *Fate and Transport of Subsurface Pollutants*. Springer: 2020.
28. Yang, Y. J.; Spencer, R. D.; Mersmann, M. A.; Gates, T. M. Groundwater contaminant plume differentiation and source determination using BTEX concentration ratios. *Groundwater* **1995**, *33* (6), 927-935.
29. Hansch, C.; Leo, A.; Hoekman, D.; Livingstone, D. *Exploring QSAR: Hydrophobic, Electronic, and Steric Constants*. American Chemical Society Washington, DC: 1995; Vol. 48.
30. NCI Thesaurus, https://ncit.nci.nih.gov/ncitbrowser/ConceptReport.jsp?dictionary=NCI_Thesaurus&ns=NCI_Thesaurus&code=C302. Accessed 18 June, 2021.
31. National Center for Biotechnology Information. "PubChem Annotation Record for TOLUENE, Source: Hazardous Substances Data Bank (HSDB)" PubChem, <https://pubchem.ncbi.nlm.nih.gov/source/hsdb/131>. Accessed 18 June, 2021.
32. National Center for Biotechnology Information. "PubChem Compound Summary for CID 7500, Ethylbenzene" PubChem, <https://pubchem.ncbi.nlm.nih.gov/compound/Ethylbenzene>. Accessed 18 June, 2021.
33. National Center for Biotechnology Information. "PubChem Compound Summary for CID 4169, Metolachlor" PubChem, <https://pubchem.ncbi.nlm.nih.gov/compound/Metolachlor>. Accessed 18 June, 2021.
34. National Center for Biotechnology Information. "PubChem Annotation Record for 2,6-Dichlorobenzamide, Source: Hazardous Substances Data Bank (HSDB)" PubChem, <https://pubchem.ncbi.nlm.nih.gov/source/hsdb/2728>. Accessed 18 June, 2021.
35. Zhang, S.; Mao, G.; Crittenden, J.; Liu, X.; Du, H. Groundwater remediation from the past to the future: A bibliometric analysis. *Water Res.* **2017**, *119*, 114-125.
36. Sethi, R.; Di Molfetta, A. *Groundwater Engineering*. 2019; p 331-409.
37. Aziz, C. E.; Wymore, R. A.; Steffan, R. J. Bioaugmentation considerations. In *Bioaugmentation for Groundwater Remediation*, Springer: 2013; pp 141-169.

38. Cycoń, M.; Mrozik, A.; Piotrowska-Seget, Z. Bioaugmentation as a strategy for the remediation of pesticide-polluted soil: A review. *Chemosphere* **2017**, *172*, 52-71.
39. Pieper, D. H.; Reineke, W. Engineering bacteria for bioremediation. *Curr. Opin. Biotechnol.* **2000**, *11* (3), 262-270.
40. Baveye, P.; Valocchi, A. An evaluation of mathematical models of the transport of biologically reacting solutes in saturated soils and aquifers. *Water Resour. Res.* **1989**, *25* (6), 1413-1421.
41. Bosma, T. N. P.; Middeldorp, P. J. M.; Schraa, G.; Zehnder, A. J. B. Mass transfer limitation of biotransformation: quantifying bioavailability. *Environ. Sci. Technol.* **1997**, *31* (1), 248-252.
42. Hesse, F.; Harms, H.; Attinger, S.; Thullner, M. Linear exchange model for the description of mass transfer limited bioavailability at the pore scale. *Environ. Sci. Technol.* **2010**, *44* (6), 2064-2071.
43. Thullner, M.; Fischer, A.; Richnow, H.-H.; Wick, L. Y. Influence of mass transfer on stable isotope fractionation. *Appl. Microbiol. Biotechnol.* **2013**, *97* (2), 441-452.
44. Thullner, M.; Kampara, M.; Richnow, H. H.; Harms, H.; Wick, L. Y. Impact of bioavailability restrictions on microbially induced stable isotope fractionation. 1. Theoretical calculation. *Environ. Sci. Technol.* **2008**, *42* (17), 6544-6551.
45. Ehrl, B. N.; Kundu, K.; Gharasoo, M.; Marozava, S.; Elsner, M. Rate-limiting mass transfer in micropollutant degradation revealed by isotope fractionation in chemostat. *Environ. Sci. Technol.* **2019**, *53* (3), 1197-1205.
46. Button, D. K. Nutrient uptake by microorganisms according to kinetic parameters from theory as related to cytoarchitecture. *Microbiol. Mol. Biol. Rev.* **1998**, *62* (3), 636-45.
47. Martinez, M. B.; Schendel, F. J.; Flickinger, M. C.; Nelsestuen, G. L. Kinetic properties of enzyme populations in vivo: alkaline phosphatase of the Escherichia coli periplasm. *Biochemistry* **1992**, *31* (46), 11500-9.
48. Shinoda, W. Permeability across lipid membranes. *Biochim. Biophys. Acta, Biomembr.* **2016**, *1858* (10), 2254-2265.
49. Males, R.; Herring, F. A ¹H-NMR study of the permeation of glycolic acid through phospholipid membranes. *Biochim. Biophys. Acta, Biomembr.* **1999**, *1416* (1-2), 333-338.
50. Kundu, K.; Marozava, S.; Ehrl, B.; Merl-Pham, J.; Griebl, C.; Elsner, M. Defining lower limits of biodegradation: atrazine degradation regulated by mass transfer and maintenance demand in *Arthrobacter aurescens* TC1. *ISME J.* **2019**, *13* (9), 2236-2251.
51. Sekhar, A.; Horemans, B.; Aamand, J.; Sorensen, S. R.; Vanhaecke, L.; Bussche, J. V.; Hofkens, J.; Springael, D. Surface colonization and activity of the 2,6-dichlorobenzamide (BAM) degrading *Aminobacter* sp. strain MSH1 at macro- and micropollutant BAM concentrations. *Environ. Sci. Technol.* **2016**, *50* (18), 10123-33.
52. Kjaergaard Nielsen, T.; Horemans, B.; Lood, C.; T'Syen, J.; van Noort, V.; Lavigne, R.; Ellegaard-Jensen, L.; Hylling, O.; Aamand, J.; Springael, D. Analyses of the complete genome sequence of 2, 6-dichlorobenzamide (BAM) degrader *Aminobacter* sp. MSH1 suggests a polyploid chromosome, phylogenetic reassignment, and functions of (un) stable plasmids. *bioRxiv* **2021**.
53. Simonsen, A.; Holtze, M. S.; Sorensen, S. R.; Sorensen, S. J.; Aamand, J. Mineralisation of 2,6-dichlorobenzamide (BAM) in dichlobenil-exposed soils and isolation of a BAM-mineralising *Aminobacter* sp. *Environ. Pollut.* **2006**, *144* (1), 289-95.
54. Holtze, M. S.; Hansen, H. C.; Juhler, R. K.; Sorensen, J.; Aamand, J. Microbial degradation pathways of the herbicide dichlobenil in soils with different history of dichlobenil-exposure. *Environ. Pollut.* **2007**, *148* (1), 343-51.
55. T'Syen, J.; Tassoni, R.; Hansen, L.; Sorensen, S. J.; Leroy, B.; Sekhar, A.; Wattiez, R.; De Mot, R.; Springael, D. Identification of the amidase BbdA that initiates biodegradation of the groundwater micropollutant 2,6-dichlorobenzamide (BAM) in *Aminobacter* sp. MSH1. *Environ. Sci. Technol.* **2015**, *49* (19), 11703-13.

56. Raes, B.; Horemans, B.; Rentsch, D.; T'Syen, J.; Ghequire, M. G. K.; De Mot, R.; Wattiez, R.; Kohler, H.-P. E.; Springael, D. Aminobacter sp. MSH1 mineralizes the groundwater micropollutant 2,6-dichlorobenzamide through a unique chlorobenzoate catabolic pathway. *Environ. Sci. Technol.* **2019**, *53* (17), 10146-10156.
57. Albers, C. N.; Feld, L.; Ellegaard-Jensen, L.; Aamand, J. Degradation of trace concentrations of the persistent groundwater pollutant 2,6-dichlorobenzamide (BAM) in bioaugmented rapid sand filters. *Water Res.* **2015**, *83*, 61-70.
58. Ellegaard-Jensen, L.; Albers, C. N.; Aamand, J. Protozoa graze on the 2, 6-dichlorobenzamide (BAM)-degrading bacterium Aminobacter sp. MSH1 introduced into waterworks sand filters. *Appl. Microbiol. Biotechnol.* **2016**, *100* (20), 8965-8973.
59. Horemans, B.; Raes, B.; Vandermaesen, J.; Simanjuntak, Y.; Brocatus, H.; T'Syen, J.; Degryse, J.; Boonen, J.; Wittebol, J.; Lapanje, A.; Sorensen, S. R.; Springael, D. Biocarriers improve bioaugmentation efficiency of a rapid sand filter for the treatment of 2,6-dichlorobenzamide-contaminated drinking water. *Environ. Sci. Technol.* **2017**, *51* (3), 1616-1625.
60. Reinnicke, S.; Simonsen, A.; Sorensen, S. R.; Aamand, J.; Elsner, M. C and N isotope fractionation during biodegradation of the pesticide metabolite 2,6-dichlorobenzamide (BAM): potential for environmental assessments. *Environ. Sci. Technol.* **2012**, *46* (3), 1447-54.
61. Simonsen, A.; Badawi, N.; Anskjaer, G. G.; Albers, C. N.; Sorensen, S. R.; Sorensen, J.; Aamand, J. Intermediate accumulation of metabolites results in a bottleneck for mineralisation of the herbicide metabolite 2,6-dichlorobenzamide (BAM) by Aminobacter spp. *Appl. Microbiol. Biotechnol.* **2012**, *94* (1), 237-45.
62. Horemans, B.; Vandermaesen, J.; Sekhar, A.; Rombouts, C.; Hofkens, J.; Vanhaecke, L.; Springael, D. Aminobacter sp. MSH1 invades sand filter community biofilms while retaining 2,6-dichlorobenzamide degradation functionality under C- and N-limiting conditions. *FEMS Microbiol. Ecol.* **2017**, *93* (6).
63. Albers, C. N.; Jacobsen, O. S.; Aamand, J. Using 2,6-dichlorobenzamide (BAM) degrading Aminobacter sp. MSH1 in flow through biofilters--initial adhesion and BAM degradation potentials. *Appl. Microbiol. Biotechnol.* **2014**, *98* (2), 957-67.
64. Ellegaard-Jensen, L.; Schostag, M. D.; Nikbakht Fini, M.; Badawi, N.; Gobbi, A.; Aamand, J.; Hansen, L. H. Bioaugmented sand filter columns provide stable removal of pesticide residue from membrane retentate. *Front. water.* **2020**, *2* (55), 603567.
65. Sjöholm, O. R.; Nybroe, O.; Aamand, J.; Sorensen, J. 2,6-Dichlorobenzamide (BAM) herbicide mineralisation by Aminobacter sp. MSH1 during starvation depends on a subpopulation of intact cells maintaining vital membrane functions. *Environ. Pollut.* **2010**, *158* (12), 3618-25.
66. Ekelund, F.; Harder, C. B.; Knudsen, B. E.; Aamand, J. Aminobacter MSH1-mineralisation of BAM in sand-filters depends on biological diversity. *PLoS One* **2015**, *10* (6), e0128838.
67. Brunner, B.; Bernasconi, S. M.; Kleikemper, J.; Schroth, M. H. A model for oxygen and sulfur isotope fractionation in sulfate during bacterial sulfate reduction processes. *Geochim. Cosmochim. Acta* **2005**, *69* (20), 4773-4785.
68. Wing, B. A.; Halevy, I. Intracellular metabolite levels shape sulfur isotope fractionation during microbial sulfate respiration. *Proc. Natl. Acad. Sci. U. S. A.* **2014**, *111* (51), 18116-18125.
69. Kritee, K.; Sigman, D. M.; Granger, J.; Ward, B. B.; Jayakumar, A.; Deutsch, C. Reduced isotope fractionation by denitrification under conditions relevant to the ocean. *Geochim. Cosmochim. Acta* **2012**, *92*, 243-259.
70. Humez, P.; Mayer, B.; Nightingale, M.; Becker, V.; Kingston, A.; Taylor, S.; Bayegnak, G.; Millot, R.; Kloppmann, W. Redox controls on methane formation, migration and fate in shallow aquifers. *Hydrol. Earth Syst. Sci.* **2016**, *20* (7), 2759-2777.

71. Kolhatkar, R.; Kuder, T.; Philip, P.; Allen, J.; Wilson, J. T. Use of compound-specific stable carbon isotope analyses to demonstrate anaerobic biodegradation of MTBE in groundwater at a gasoline release site. *Environ. Sci. Technol.* **2002**, *36*, 5139.
72. Koster van Groos, P. G.; Hatzinger, P. B.; Streger, S. H.; Vainberg, S.; Philp, R. P.; Kuder, T. Carbon isotope fractionation of 1,2-dibromoethane by biological and abiotic processes. *Environ. Sci. Technol.* **2018**, *52* (6), 3440-3448.
73. Kuder, T.; Wilson, J. T.; Kaiser, P.; Kolhatkar, R.; Philp, P.; Allen, J. Enrichment of stable carbon and hydrogen isotopes during anaerobic biodegradation of MTBE: Microcosm and field evidence. *Environ. Sci. Technol.* **2005**, *39*, 213.
74. Wu, L.; Verma, D.; Bondgaard, M.; Melvej, A.; Vogt, C.; Subudhi, S.; Richnow, H. H. Carbon and hydrogen isotope analysis of parathion for characterizing its natural attenuation by hydrolysis at a contaminated site. *Water Res.* **2018**, *143*, 146-154.
75. Fischer, A.; Theuerkorn, K.; Stelzer, N.; Gehre, M.; Thullner, M.; Richnow, H. H. Applicability of stable isotope fractionation analysis for the characterization of benzene biodegradation in a BTEX-contaminated aquifer. *Environ. Sci. Technol.* **2007**, *41* (10), 3689-96.
76. Elsner, M.; McKelvie, J.; Lacrampe Couloume, G.; Sherwood Lollar, B. Insight into methyl tert-butyl ether (MTBE) stable isotope fractionation from abiotic reference experiments. *Environ. Sci. Technol.* **2007**, *41* (16), 5693-5700.
77. Hofstetter, T. B.; Schwarzenbach, R. P.; Bernasconi, S. M. Assessing transformation processes of organic compounds using stable isotope fractionation. *Environ. Sci. Technol.* **2008**, *42* (21), 7737-7743.
78. Schmidt, T. C.; Schirmer, M.; Weiss, H.; Haderlein, S. B. Microbial degradation of methyl tert-butyl ether and tert-butyl alcohol in the subsurface. *J. Contam. Hydrol.* **2004**, *70*, 173.
79. Rolle, M.; Jin, B. Normal and inverse diffusive isotope fractionation of deuterated toluene and benzene in aqueous systems. *Environ. Sci. Technol. Lett.* **2017**, *4* (7), 298-304.
80. O'Leary, M. H. Measurement of the isotope fractionation associated with diffusion of carbon dioxide in aqueous solution. *J. Phys. Chem.* **1984**, *88* (4), 823-825.
81. Zhang, T.; Krooss, B. M. Experimental investigation on the carbon isotope fractionation of methane during gas migration by diffusion through sedimentary rocks at elevated temperature and pressure. *Geochim. Cosmochim. Acta* **2001**, *65* (16), 2723-2742.
82. Schloemer, S.; Krooss, B. M. Molecular transport of methane, ethane and nitrogen and the influence of diffusion on the chemical and isotopic composition of natural gas accumulations. *Geofluids* **2004**, *4* (1), 81-108.
83. Wanner, P.; Hunkeler, D. Carbon and chlorine isotopologue fractionation of chlorinated hydrocarbons during diffusion in water and low permeability sediments. *Geochim. Cosmochim. Acta* **2015**, *157*, 198-212.
84. Jin, B.; Rolle, M.; Li, T.; Haderlein, S. B. Diffusive fractionation of BTEX and chlorinated ethenes in aqueous solution: Quantification of spatial isotope gradients. *Environ. Sci. Technol.* **2014**, *48* (11), 6141-50.
85. LaBolle, E. M.; Fogg, G. E.; Eweis, J. B.; Gravner, J.; Leaist, D. G. Isotopic fractionation by diffusion in groundwater. *Water Resour. Res.* **2008**, *44* (7), W07405.
86. Einstein, A. *Investigations on the Theory of the Brownian Movement*. Courier Corporation: 1956.
87. Wanner, P.; Hunkeler, D. Isotope fractionation due to aqueous phase diffusion - What do diffusion models and experiments tell? - A review. *Chemosphere* **2019**, *219*, 1032-1043.
88. Tyrrell, H. J. V.; Harris, K. *Diffusion in Liquids: A theoretical and Experimental Study*. Butterworth-Heinemann: 2013.

89. Cussler, E. L.; Cussler, E. L. *Diffusion: Mass Transfer in Fluid Systems*. Cambridge University Press: 1997.
90. Chapman, S. The kinetic theory of simple and composite monatomic gases: viscosity, thermal conduction, and diffusion. *Proc. R. Soc. London, Ser. A* **1916**, 93 (646), 1-20.
91. Alder, B. J.; Alley, W. E.; Dymond, J. H. Studies in molecular dynamics. XIV. Mass and size dependence of the binary diffusion coefficient. *J. Chem. Phys.* **1974**, 61 (4), 1415-1420.
92. Worch, E. Eine neue gleichung zur berechnung von diffusionskoeffizienten gelöster stoffe. *Vom Wasser* **1993**, 81, 289-297.
93. Wilke, C.; Chang, P. Correlation of diffusion coefficients in dilute solutions. *AIChE J.* **1955**, 1 (2), 264-270.
94. Maxwell, J. C. On the Dynamical Theory of Gases. [Abstract]. *Proceedings of the Royal Society of London* **1866**, 15, 167-171.
95. Krishna, R.; Wesselingh, J. A. The Maxwell-Stefan approach to mass transfer. *Chemical Engineering Science* **1997**, 52 (6), 861-911.
96. Gillespie, D. T.; Seitaridou, E. *Simple Brownian Diffusion: An Introduction to the Standard Theoretical Models*. Oxford University Press: 2013.
97. Bhattacharyya, S.; Bagchi, B. Power law mass dependence of diffusion: A mode coupling theory analysis. *Phys. Rev. E* **2000**, 61 (4), 3850.
98. Wanner, P.; Hunkeler, D. Molecular dynamic simulations of carbon and chlorine isotopologue fractionation of chlorohydrocarbons during diffusion in liquid water. *Environ. Sci. Technol. Lett.* **2019**, 6 (11), 681-685.
99. Meckenstock, R. U.; Morasch, B.; Griebler, C.; Richnow, H. H. Stable isotope fractionation analysis as a tool to monitor biodegradation in contaminated aquifers. *J. Contam. Hydrol.* **2004**, 75 (3-4), 215-55.
100. O'Leary, M. H. Carbon isotopes in photosynthesis. *Bioscience* **1988**, 38 (5), 328-336.
101. Wunderlich, A.; Heipieper, H. J.; Elsner, M.; Einsiedl, F. Solvent stress-induced changes in membrane fatty acid composition of denitrifying bacteria reduce the extent of nitrogen stable isotope fractionation during denitrification. *Geochim. Cosmochim. Acta* **2018**, 239, 275-283.
102. Sigman, D. M.; Casciotti, K. L.; Andreani, M.; Barford, C.; Galanter, M.; Böhlke, J. K. A bacterial method for the nitrogen isotopic analysis of nitrate in seawater and freshwater. *Anal. Chem.* **2001**, 73 (17), 4145-4153.
103. Rees, C. A steady-state model for sulphur isotope fractionation in bacterial reduction processes. *Geochim. Cosmochim. Acta* **1973**, 37 (5), 1141-1162.
104. Mangalo, M.; Einsiedl, F.; Meckenstock, R. U.; Stichler, W. Influence of the enzyme dissimilatory sulfite reductase on stable isotope fractionation during sulfate reduction. *Geochim. Cosmochim. Acta* **2008**, 72 (6), 1513-1520.
105. Kampara, M.; Thullner, M.; Richnow, H. H.; Harms, H.; Wick, L. Y. Impact of bioavailability restrictions on microbially induced stable isotope fractionation. 2. Experimental evidence. *Environ. Sci. Technol.* **2008**, 42 (17), 6552-6558.
106. Ehrl, B. N.; Gharasoo, M.; Elsner, M. Isotope fractionation pinpoints membrane permeability as a barrier to atrazine biodegradation in gram-negative *Polaromonas* sp. Nea-C. *Environ. Sci. Technol.* **2018**, 52 (7), 4137-4144.
107. Canfield, D. E. Isotope fractionation by natural populations of sulfate-reducing bacteria. *Geochim. Cosmochim. Acta* **2001**, 65 (7), 1117-1124.
108. Canfield, D. E.; Olesen, C. A.; Cox, R. P. Temperature and its control of isotope fractionation by a sulfate-reducing bacterium. *Geochim. Cosmochim. Acta* **2006**, 70 (3), 548-561.

109. Mangalo, M.; Meckenstock, R. U.; Stichler, W.; Einsiedl, F. Stable isotope fractionation during bacterial sulfate reduction is controlled by reoxidation of intermediates. *Geochim. Cosmochim. Acta* **2007**, *71* (17), 4161-4171.
110. Habicht, K. S.; Salling, L.; Thamdrup, B.; Canfield, D. E. Effect of low sulfate concentrations on lactate oxidation and isotope fractionation during sulfate reduction by *Archaeoglobus fulgidus* Strain Z. *Appl. Environ. Microbiol.* **2005**, *71* (7), 3770-3777.
111. Crowe, S. A.; Paris, G.; Katsev, S.; Jones, C.; Kim, S.-T.; Zerkle, A. L.; Nomosatryo, S.; Fowle, D. A.; Adkins, J. F.; Sessions, A. L.; Farquhar, J.; Canfield, D. E. Sulfate was a trace constituent of Archean seawater. *Science* **2014**, *346* (6210), 735-739.
112. Chen, S.; Zhang, K.; Jha, R. K.; Chen, C.; Yu, H.; Liu, Y.; Ma, L. Isotope fractionation in atrazine degradation reveals rate-limiting, energy-dependent transport across the cell membrane of gram-negative rhizobium sp. CX-Z. *Environ. Pollut.* **2019**, *248*, 857-864.
113. Chen, S.; Zhang, K.; Jha, R. K.; Ma, L. Impact of atrazine concentration on bioavailability and apparent isotope fractionation in Gram-negative Rhizobium sp. CX-Z. *Environ. Pollut.* **2020**, *257*, 113614.
114. Qiu, S.; Gözdereliler, E.; Weyrauch, P.; Lopez, E. C. M.; Kohler, H.-P. E.; Sørensen, S. R.; Meckenstock, R. U.; Elsner, M. Small $^{13}\text{C}/^{12}\text{C}$ fractionation contrasts with large enantiomer fractionation in aerobic biodegradation of phenoxy acids. *Environ. Sci. Technol.* **2014**, *48* (10), 5501-5511.
115. Whitaker, S. Flow in porous media I: A theoretical derivation of Darcy's law. *Transp. Porous Media* **1986**, *1* (1), 3-25.
116. Scheidegger, A. E. General theory of dispersion in porous media. *J. Geophys. Res.* **1961**, *66* (10), 3273-3278.
117. Chiogna, G.; Eberhardt, C.; Grathwohl, P.; Cirpka, O. A.; Rolle, M. Evidence of compound-dependent hydrodynamic and mechanical transverse dispersion by multitracer laboratory experiments. *Environmental science & technology* **2010**, *44* (2), 688-693.
118. Monod, J.; Wyman, J.; Changeux, J.-P. On the nature of allosteric transitions: a plausible model. *J. Mol. Biol.* **1965**, *12* (1), 88-118.
119. Schwarzenbach, R. P.; Gschwend, P. M.; Imboden, D. M. *Environmental Organic Chemistry*. John Wiley & Sons: 2016.
120. Wanner, P.; Parker, B. L.; Chapman, S. W.; Aravena, R.; Hunkeler, D. Quantification of degradation of chlorinated hydrocarbons in saturated low permeability sediments using compound-specific isotope analysis. *Environ. Sci. Technol.* **2016**, *50* (11), 5622-30.
121. Kopinke, F.-D.; Georgi, A. H/D-isotope fractionation due to aqueous phase diffusion – Deuterated hydrocarbons revisited. *Chemosphere* **2020**, *258*, 127357.

2. Research

2.1 Magnitude of diffusion- and transverse-dispersion-induced isotope fractionation of organic compounds in the aqueous systems

Published in *Environmental Science & Technology* **2021**, 55,8,4772-4782,

<https://pubs.acs.org/doi/10.1021/acs.est.0c06741>

by Fengchao Sun, Jan Peters, Martin Thullner, Olaf A. Cirpka, and Martin Elsner

Reprinted with permission. Further permissions related to the material excerpted should be directed to the ACS.

Synopsis

The objective of this section is to determine whether diffusion and dispersion in the aqueous phase induce isotope fractionation of the organic compounds at natural isotopic abundance.

Firstly, diffusion experiments with benzene, toluene, ethylbenzene, BAM and metolachlor at natural isotopic abundances were conducted in modified Stokes' diaphragm diffusion cells. The residual concentrations and the isotope values of the organic compounds in the lower compartment of the cells were measured in different experimental periods. Concentrations of benzene, toluene and ethylbenzene were measured on GC-MS, and concentrations of BAM and metolachlor were measured on HPLC. Carbon and nitrogen isotope values were measured on GC-IRMS. The diffusion-induced isotope fractionation of the compounds at natural isotopic abundance in the aqueous phase was found to be negligible and the corresponding diffusion coefficients exhibited a weak power-law or insignificant mass dependence; including reported literature data, values of β were typically in the range of 0.008–0.082. In addition, a further analysis of the relations between isotope fractionation and masses of ions, noble gases, and labeled organic compounds from literature indicate that organic compounds should be treated differently from ions and noble gases due to their stronger intramolecular motions (e.g., vibrations, rotations). Specifically, the diffusion of labeled organic compounds vs. organic compounds at natural isotopic abundance should be treated differently.

Subsequently, transverse-dispersion experiments with toluene, BAM, and metolachlor at natural isotopic abundance were conducted in a quasi-two-dimensional flow-through sediment tank system. By injecting the contaminant solution into the central port of the tank, due to transverse dispersion, a concentration gradient from high concentration to low concentration developed from the center towards the upper and lower boundaries of the tank. Samples for concentration and isotope measurements were collected at steady state when concentrations were stable. This system allowed a long-term large-volume sample collection at steady state for isotope measurement. The transverse dispersion processes of organic contaminants at natural isotopic abundance did not lead to noticeable isotope fractionation. This challenges the common approach of modeling isotope data by coupling the Enskog or Worch equation to an equation brought forward by Chiogna et al. in numerical simulations. These expressions would greatly overestimate isotope fractionation induced by transverse dispersion, which leads to larger predicted isotope fractionation than observed in this study.

Author contributions

Fengchao Sun designed the experiments with the supervision of Prof. Martin Elsner, conducted analytical measurements, and compiled and analyzed the data and results. Under the supervision of Prof. Olaf A. Cirpka, Fengchao Sun developed the numerical model. Jan Peters conducted the abiotic quasi-two-dimensional flow-through sediment tank experiment with toluene. All authors discussed the results. Fengchao Sun wrote the manuscript with input from all authors.

Magnitude of Diffusion- and Transverse Dispersion-Induced Isotope Fractionation of Organic Compounds in Aqueous Systems

Fengchao Sun, Jan Peters, Martin Thullner, Olaf A. Cirpka, and Martin Elsner*



Cite This: *Environ. Sci. Technol.* 2021, 55, 4772–4782



Read Online

ACCESS |



Metrics & More



Article Recommendations

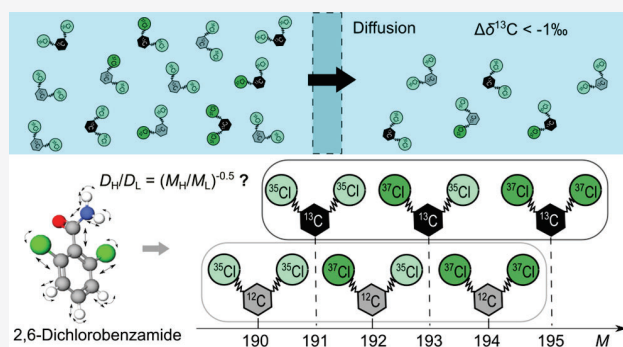


Supporting Information

ABSTRACT: Determining whether aqueous diffusion and dispersion lead to significant isotope fractionation is important for interpreting the isotope ratios of organic contaminants in groundwater. We performed diffusion experiments with modified Stokes diaphragm cells and transverse-dispersion experiments in quasi-two-dimensional flow-through sediment tank systems to explore isotope fractionation for benzene, toluene, ethylbenzene, 2,6-dichlorobenzamide, and metolachlor at natural isotopic abundance. We observed very small to negligible diffusion- and transverse-dispersion-induced isotope enrichment factors ($\epsilon < -0.4\text{‰}$), with changes in carbon and nitrogen isotope values within $\pm 0.5\text{‰}$ and $\pm 1\text{‰}$, respectively. Isotope effects of diffusion did not show a clear correlation with isotopologue mass with calculated power-law exponents β close to zero ($0.007 < \beta < 0.1$).

In comparison to ions, noble gases, and labeled compounds, three aspects stand out. (i) If a mass dependence is derived from collision theory, then isotopologue masses of polyatomic molecules would be affected by isotopes of multiple elements resulting in very small expected effects. (ii) However, collisions do not necessarily lead to translational movement but can excite molecular vibrations or rotations minimizing the mass dependence. (iii) Solute–solvent interactions like H-bonds can further minimize the effect of collisions. Modeling scenarios showed that an inadequate model choice, or erroneous choice of β , can greatly overestimate the isotope fractionation by diffusion and, consequently, transverse dispersion. In contrast, available data for chlorinated solvent and gasoline contaminants at natural isotopic abundance suggest that in field scenarios, a potential additional uncertainty from aqueous diffusion or dispersion would add to current instrumental uncertainties on carbon or nitrogen isotope values ($\pm 1\text{‰}$) with an additional $\pm 1\text{‰}$ at most.

KEYWORDS: BTEX, Compound-specific isotope analysis, Stokes diaphragm cell, Flow-through tank system, Mass dependence, Metolachlor, Organic contaminants, 2,6-dichlorobenzamide



INTRODUCTION

Changes in compound-specific stable isotope values of organic compounds can be used to infer the extent of degradation.^{1–4} In groundwater systems, solute concentrations are influenced by both (bio)chemical degradation and physical transport, namely advection, dispersion, diffusion, and interphase mass transfer.^{5–8} While advection is the main mass transport process in the direction of the flow, dispersion, and diffusion cause spreading of the compounds due to the physical or chemical variability of the system. In contrast to concentrations, isotope ratios are thought to be little affected by hydrodynamic dispersion (including mechanical dispersion and diffusion) or diffusion because all isotopologues essentially undergo the same dilution.^{9–12} If true, then changes in isotope values can serve as a particularly robust indicator of degradation that is little affected by these physical processes. However, it can be challenging to adequately identify and quantify the influence of dispersion and diffusion on isotope fractionation of organic compounds when evaluating the changes in isotope ratios as

evidence of (bio)chemical reactions in the field. One challenge is that dispersion and diffusion may affect the concentration profiles and level out the degradation-induced gradients of the isotope ratios⁵ while another complicating factor may be that the diffusion coefficients of different isotopologues differ, thus potentially causing reaction-independent isotope fractionation by the process of diffusion itself.¹³

Although such diffusion-induced isotope fractionation in the aqueous phase was repeatedly considered to be negligible,^{9–12} significant diffusion-induced isotope fractionation has been reported in some studies with isotopically labeled organic compounds,^{6,7,14–19} such as deuterated alcohols (with isotope

Received: October 6, 2020

Revised: February 8, 2021

Accepted: February 22, 2021

Published: March 17, 2021



enrichment factors ε between -2.6‰ and -7.0‰),¹⁴ benzene, toluene, and ethylbenzene (ε between -40‰ and 19‰).^{7,15,19} By contrast, recent studies reported negligible isotope fractionation for labeled benzene, toluene, and cyclohexane.^{20,21} For compounds at natural isotopic abundance, finally, much smaller isotope fractionation has been observed, such as with CO₂,^{16,22} methane,^{17,18} ethane,¹⁸ and chlorinated ethenes⁶ (ε between -0.22‰ and -2.23‰).

Various theoretical models have conceptualized diffusion in the aqueous phase to be driven by intermolecular or intramolecular interactions between the solute and solvent molecules.^{13,23–26} A prime focus has been on the collision of solute and solvent molecules, conceptualized as hard-sphere particles, which is usually described by the Enskog relation (eq 1),²⁷

$$D_{\text{aq}} \propto \left(\frac{M_1 M_2}{M_1 + M_2} \right)^{-\beta}, \quad \beta = 0.5 \quad (1)$$

in which D_{aq} [m²/s] is the diffusion coefficient of the solute particle in the aqueous phase, M_1 [Da] is the molecular mass of the solute, and M_2 [Da] is the molecular mass of the solvent. If in the dilute water phase the hydrogen-bonded water network is assumed to act as “effective particle”,⁶ then M_2 is infinitively large so that $D_{\text{aq}} \propto M_1^{-0.5}$. The resulting eq 2 is usually applied to predict the ratio of diffusion coefficients of heavy and light isotopes or isotopologues D_{aq}^{H} and D_{aq}^{L}

$$\frac{D_{\text{aq}}^{\text{H}}}{D_{\text{aq}}^{\text{L}}} = \left(\frac{M_{\text{H}}}{M_{\text{L}}} \right)^{-\beta}, \quad \beta = 0.5 \quad (2)$$

in which M_{H} [Da] and M_{L} [Da] are the molecular masses of the heavy and light isotopes or isotopologues, respectively.

However, a power-law mass dependence of isotope fractionation with $\beta = 0.5$ has been rarely observed for aqueous-phase diffusion.²⁸ For noble gases, weak or negligible power-law mass-dependent isotope fractionation has been observed for Ne, Kr, and Xe with $\beta < 0.2$.^{29,30} An even weaker dependence has been observed for ions (e.g., Li⁺, Na⁺, Cl⁻, and Br⁻) with $\beta < 0.07$.^{13,31,32} Also for organic compounds at natural isotopic abundance, observed mass-dependent isotope fractionation was weak with $\beta < 0.1$ for trichloroethene (TCE), 1,2-dichloroethane (1,2-DCA), and *cis*-dichloroethene (*cis*-DCE).^{6,7} In contrast, a much stronger mass dependence has been observed for the diffusion-induced isotope fractionation of labeled organic compounds (e.g., deuterated benzene and toluene).^{7,20,21}

Mode-Coupling Theory Analysis and Molecular Dynamic Simulations were brought forward to explain the weak mass dependence of diffusion-induced isotope effects observed for noble gases and ions.^{13,31,33} These theories still conceptualize the molecules of the solutes and the surrounding water as rigid masses and neglect the influence of intramolecular vibrations and rotations. The Mode-Coupling Theory assumes that diffusion can be explained by frictions in series,¹³ i.e., $\frac{1}{\text{Friction}_{\text{total}}} = \frac{1}{\text{Friction}_{\text{collisions}}} + \frac{1}{\text{Friction}_{\text{hydrodynamic}}}$, in which the collision term $1/\text{Friction}_{\text{collisions}}$ would show a squared power-law mass dependence and the hydrodynamic-motion term $1/\text{Friction}_{\text{hydrodynamic}}$ shows no mass dependence at all, explaining a weaker dependence on the molecular mass, which is actually not even a power law. Considering this shaky theoretical basis, it is remarkable that all interpretations of experimental data

have so far relied on the power-law mass dependence of diffusion coefficients (eq 2), merely adapting the positive exponent β . On the basis of this relationship, diffusion-induced isotope effects are hypothesized to increase in a systematic way with increasing relative mass difference between the isotopologues, where the β -value is left open for adjusting the relation between the magnitude of diffusion-induced isotope fractionation and mass difference between the isotopologues.

If there are isotope effects on molecular diffusion, then it is further still unclear how they scale up to dispersion, which describes the effective mixing and dilution in flowing groundwater. Hydrodynamic dispersion includes both mechanical dispersion caused by pore-scale velocity variations and molecular diffusion. The standard parametrization assumes that the pore diffusion coefficient D_{p} [m²/s] and the mechanical dispersion $D_{\text{mech},t/l}$ [m²/s] are additive,

$$D_{t/l} = D_{\text{p}} + D_{\text{mech},t/l} \quad (3)$$

$$D_{\text{p}} = \frac{1}{\tau} D_{\text{aq}} \quad (4)$$

in which the index t and l refer to the transverse and longitudinal directions, respectively, and τ [–] is the tortuosity of the porous medium. In the classical parametrization,³⁴ the mass dependence of molecular diffusion is relevant only at very low groundwater velocities because $D_{\text{mech},t/l}$ is believed to be compound-independent and to scale linearly with the mean velocity v [m/s]:

$$D_{\text{mech},t/l} = \alpha_{t/l} v \quad (5)$$

in which $\alpha_{t/l}$ is the transverse or longitudinal dispersivity [m], which is supposed to depend linearly on the effective grain diameter d_{eff} [m] in homogeneous sand packs (e.g., $\alpha_t = 3 \times d_{\text{eff}}/16$).³⁵

On the basis of high-resolution transverse concentration profiles using different tracers at different velocities, however, Chiogna et al.³⁶ introduced a nonlinear parametrization of the transverse dispersion coefficient:

$$D_t = D_{\text{p}} + v \cdot \frac{d_{\text{eff}}}{\sqrt{Pe + 123}} \quad (6)$$

in which the mechanical dispersion depends on the grain-Péclet number $Pe = v \times d_{\text{eff}}/D_{\text{aq}}$, implying that the transverse dispersion scales with the square roots of the velocity and the molecular diffusion coefficient at high velocities.

The latter work inspired many modeling studies to reconsider the isotope fractionation due to transverse dispersion in saturated porous media.^{19,37–39} In such simulations, diffusion coefficients of heavy and light isotopologues were usually estimated by the Enskog²⁷ or the Worch relation,⁴⁰ implying an exponent $\beta = 0.5$ or 0.53 in eq 2, which resulted in large dispersion-induced isotope fractionation in these models.^{15,19,37,38,41}

This study aims at experimentally re-examining isotope fractionation by diffusion and transverse dispersion for organic compounds at natural isotopic abundance. We applied compound-specific isotope analysis to investigate the diffusion-induced isotope fractionation with increasing molecular mass and decreasing mass ratio of heavy to light isotopologues for benzene, toluene, ethylbenzene, 2,6-dichlorobenzamide (BAM), and metolachlor in the aqueous phase. We determined the diffusion coefficients of the heavy and light isotopologues of each compound by conducting modified Stokes diffusion-

cell experiments.⁶ We then reconsidered the mass dependence of diffusion-induced isotope fractionation by comparing the theoretical models (e.g., Enskog relation) with our measured isotope ratios and published experimental data from previous diffusion studies on labeled organic compounds, noble gases, and ions. To investigate the potential significance of isotopic effects on transverse dispersion, we conducted steady-state transport experiments in flow-through sediment tanks and compared transverse profiles with numerical-modeling results using the classical transverse dispersion parametrization and the expression of Chiogna et al., coupled to the Enskog relation.

MATERIALS AND METHODS

Diffusion Cell Experiment. The Stokes diffusion cell is a classical and commonly used approach to determine liquid-phase diffusion coefficients of dissolved species.^{6,13,21,42,43} We adopted the setup of diffusion cell experiments from the design of Wanner and Hunkeler.⁶ The diffusion cell was separated into upper and lower compartments (with a volume of each compartment of 38 mL) by a silica frit in between. The lower compartment was filled with a solution of the dissolved organic compound, while the upper compartment was filled with deionized water, which was continuously replaced at a pumping rate of 10 mL/min to keep the concentration in the upper compartment close to zero (Figure 1). Therefore,

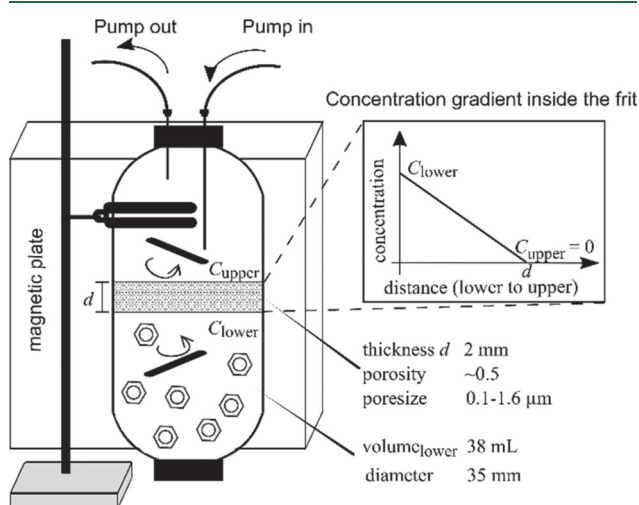


Figure 1. Setup of Stokes' diffusion cell experiment.

the isotope fractionation in the lower compartment follows a Rayleigh type behavior. The solution of each compartment was well mixed by a Teflon-coated stirring bar to ensure a homogeneous concentration distribution. Because of the concentration gradient through the frit, the small pore size, and the uniform composition in each compartment maintained by vigorous stirring, diffusion is the exclusive transport process of the dissolved organic compounds through the frit.^{13,42} The design parameters and the estimation of the characteristic factor of each diffusion cell can be found in Figure 1 and Table S2 of the Supporting Information (SI). We conducted two sets of experiments: one set with benzene, toluene, and ethylbenzene; and the other with BAM and metolachlor. Experiments were performed in parallel for different durations; in each experiment the concentrations and isotope values of the

solution in the lower compartment were measured at the beginning and the end of each time period.

Upon diffusion from the lower to the upper compartment through the silica frit, the concentrations in the lower compartment meet the following expression:⁶

$$C(t) = C(0) \cdot e^{-D_{aq} \cdot \sigma \cdot t} \quad (7)$$

in which $C(0)$ [mg/L] is the initial concentration in the lower compartment of the diffusion cell, and $C(t)$ [mg/L] is the concentration at time t [s]. $\sigma = \frac{\phi \cdot \tau \cdot A}{d \cdot V_{low}}$ [m⁻²] is the cell calibration factor, with ϕ [-], τ [-], A [m²], d [m], and V_{low} [m³] being the porosity, tortuosity, cross-sectional area, thickness of the frit, and the volume of the lower compartment, respectively. From this we can derive a Rayleigh-fractionation equation:⁶

$$\ln\left(\frac{R_t}{R_0}\right) = \ln\left(\frac{\delta_t + 1}{\delta_0 + 1}\right) = \underbrace{\left(\frac{D_{aq}^H}{D_{aq}^L} - 1\right)}_{=\varepsilon_D} \times \ln\left(\frac{C(t)}{C(0)}\right) \quad (8)$$

in which R_0 [-] and R_t [-] represent the isotope ratios at times zero and t , respectively, δ_0 [-] and δ_t [-] are the corresponding δ isotope values [-], and $\varepsilon_D = \frac{D_{aq}^H}{D_{aq}^L} - 1$ [-] is the isotope-enrichment factor due to diffusion.

Flow-Through Sediment-Tank Experiment. To investigate the effect of transverse dispersion on the isotope fractionation of organic compounds in saturated porous media, we conducted two-dimensional flow-through sediment-tank experiments. The setup of the tank (Figure S1) was adapted from Bauer et al.⁴⁴ and is detailed in the SI. At the inlet and outlet boundaries of the tank, 16 equally spaced ports (distance 1.0 cm) were pumped with a constant rate of $45 \pm 2 \mu\text{L}/\text{min}$ per port. A solution with the target compounds (inlet solution with BAM 400 mg/L and metolachlor 100 mg/L in the first setup, and inlet solution with toluene 34.2 mg/L in the second setup) at natural isotopic abundance was injected into the central inlet port ($z = 8$ cm) of the tank, whereas a compound-free solution was injected into the remaining inlet ports. We sampled the 16 outlet ports to obtain concentration and isotope profiles at the outflow boundary of the domain. Sampling for isotope measurements of BAM and metolachlor was conducted from day 5 to day 20; sampling for isotope measurements of toluene was conducted from day 5 to day 8.

Chemicals. A list of chemicals is provided in the SI.

Carbon and Nitrogen Isotope Analysis of BAM, Metolachlor, Benzene, Toluene, and Ethylbenzene. Samples from the tank experiments were frozen at -20 °C immediately after sampling until enough samples were collected for isotope analysis. For carbon and nitrogen isotope measurements of BAM and metolachlor, the samples from the diffusion cell experiments (40 mL) and tank experiments (1 L) were first filtered through a $0.2 \mu\text{m}$ Nalgene Rapid-Flow filter (Thermo Fisher Scientific, Germany) and concentrated in ethyl acetate after solid-phase extraction as detailed in the SI. All isotope measurements were conducted on a GC-IRMS system in which a TRACE GC Ultra gas chromatograph (Thermo Fisher Scientific, Italy) with a DB-5 analytical column (60 m, 0.25 mm i.d., 1 μm film, Agilent Technologies, Germany) was coupled to a Finnigan MAT 253 isotope-ratio mass spectrometer through a Finnigan GC Combustion III interface (Thermo Fisher Scientific, Germany). For carbon-

Table 1. Experimental Results for Measured Diffusion Coefficients D_{aq} , Diffusion Coefficient Ratios D_{aq}^H/D_{aq}^L of Heavy to Light Isotopologues, Isotope Enrichment Factors ϵ and Calculated β -Values of Organic Compounds at Natural Isotope Abundance from This Study and Literature^a

compound	isotopologues	D_{aq}^H/D_{aq}^L	ϵ (%)	β	D_{aq} -measured (m ² /s)	references
CO ₂	¹³ CO ₂ /CO ₂ ^b	0.99927 ± 0.00019	-0.73 ± 0.19	0.032 ± 0.009		O'Leary, 1984 ¹⁶
	¹³ CO ₂ /CO ₂ ^c	0.99913 ± 0.00005	-0.87 ± 0.05	0.039 ± 0.002		Jahne et al., 1987 ²²
CH ₄	¹³ CH ₄ /CH ₄ ^b	0.99978 ± 0.00008	-2.23 ± 0.82	0.037 ± 0.014		Zhang and Krooss, 2001 ¹⁷
	¹³ CH ₄ /CH ₄ ^b	0.99978 ± 0.00012	-2.17 ± 1.12	0.036 ± 0.023		Schloemer and Krooss, 2004 ¹⁸
C ₂ H ₆	¹³ CCH ₆ /C ₂ H ₆ ^b	0.99888 ± 0.00008	-1.23 ± 0.76	0.038 ± 0.023		Schloemer and Krooss, 2004 ¹⁸
DCM	¹³ CH ₂ Cl ₂ /CH ₂ Cl ₂ ^b	0.99972 ± 0.00009	-0.28 ± 0.09	-0.025 ± 0.008		Wanner et al., 2017 ¹⁵
cis-DCE	C ₂ H ₃ ³⁷ ClCl/C ₂ H ₃ Cl ₂ ^{b,d}	0.99882 ± 0.00003	-1.80 ± 0.3	0.088 ± 0.017		Jin et al., 2014 ⁷
1,2-DCA	¹³ CCH ₄ Cl ₂ /C ₂ H ₄ Cl ₂	0.99977 ± 0.00004	-0.23 ± 0.04	0.023 ± 0.004		Wanner and Hunkeler, 2015 ⁶
TCE	C ₂ H ₄ ³⁷ ClCl/C ₂ H ₄ Cl ₂	0.99939 ± 0.00003	-0.61 ± 0.03	0.031 ± 0.002		Wanner and Hunkeler, 2015 ⁶
	¹³ CCHClCl ₃ /C ₂ HCl ₃	0.99978 ± 0.00006	-0.22 ± 0.06	0.029 ± 0.008		Wanner and Hunkeler, 2015 ⁶
	C ₂ H ³⁷ ClCl ₂ /C ₂ HCl ₃	0.99963 ± 0.00003	-0.37 ± 0.03	0.024 ± 0.002		Wanner and Hunkeler, 2015 ⁶
	C ₂ H ³⁷ ClCl ₂ /C ₂ HCl ₃ ^{b,d}	0.99993 ± 0.00002	-0.67 ± 0.2	0.043 ± 0.009		Jin et al., 2014 ⁷
Benzene	¹³ CC ₆ H ₆ /C ₆ H ₆	0.99991 ± 0.00001	-0.09 ± 0.01	0.007 ± 0.001	(11.2 ± 3.2) × 10 ⁻¹⁰	this study
Toluene	¹³ CC ₆ H ₈ /C ₇ H ₈	0.99991 ± 0.00006	-0.09 ± 0.06	0.008 ± 0.006	(10.6 ± 4.2) × 10 ⁻¹⁰	this study
Ethylbenzene	¹³ CC ₇ H ₁₀ /C ₈ H ₁₀	0.99991 ± 0.00005	-0.09 ± 0.05	0.010 ± 0.005	(10.4 ± 4.8) × 10 ⁻¹⁰	this study
BAM	¹³ CC ₈ H ₅ Cl ₂ NO/C ₇ H ₅ Cl ₂ NO	0.99992 ± 0.00016	-0.08 ± 0.16	0.015 ± 0.030	(6.08 ± 0.51) × 10 ⁻¹⁰	this study
Metolachlor	C ₇ H ₅ Cl ₂ ¹⁵ NO/C ₇ H ₅ Cl ₂ NO	0.99980 ± 0.00022	-0.20 ± 0.22	0.038 ± 0.042		
	¹³ CC ₁₄ H ₂₂ ClNO ₂ /C ₁₃ H ₂₂ ClNO ₂	0.99964 ± 0.00036	-0.36 ± 0.36	0.102 ± 0.102	(5.02 ± 0.56) × 10 ⁻¹⁰	this study
	C ₁₅ H ₂₂ Cl ¹⁵ NO ₂ /C ₁₅ H ₂₂ ClNO ₂	0.99994 ± 0.00035	-0.06 ± 0.35	0.017 ± 0.099		

^aUncertainties of D_{aq} -values were the standard deviation, uncertainties of D_{aq}^H/D_{aq}^L and ϵ -values were calculated based on the 95% confidence intervals of regressions according to eq 8. Also, literature data were evaluated with respect to 95% confidence intervals to enable comparisons on an equal basis. Uncertainties of β -values were calculated based on Gauss' error propagation law by using the uncertainty of D_{aq}^H/D_{aq}^L .^bUncertainties of D_{aq}^H/D_{aq}^L and ϵ -values represent the recalculated 95% confidence interval based on the published standard deviation or data set; uncertainties of β -values were calculated based on Gauss' error propagation by using the uncertainty of D_{aq}^H/D_{aq}^L .^cUncertainties of D_{aq}^H/D_{aq}^L and ϵ -values were published system deviations; uncertainties of β -values were calculated based on Gauss' error propagation by using the uncertainty of D_{aq}^H/D_{aq}^L .^d D_{aq}^H/D_{aq}^L , ϵ , and β -values were calculated based on $D_{aq}^{6,8,10,12,13,14}$ values in Table S2 from Jin et al.

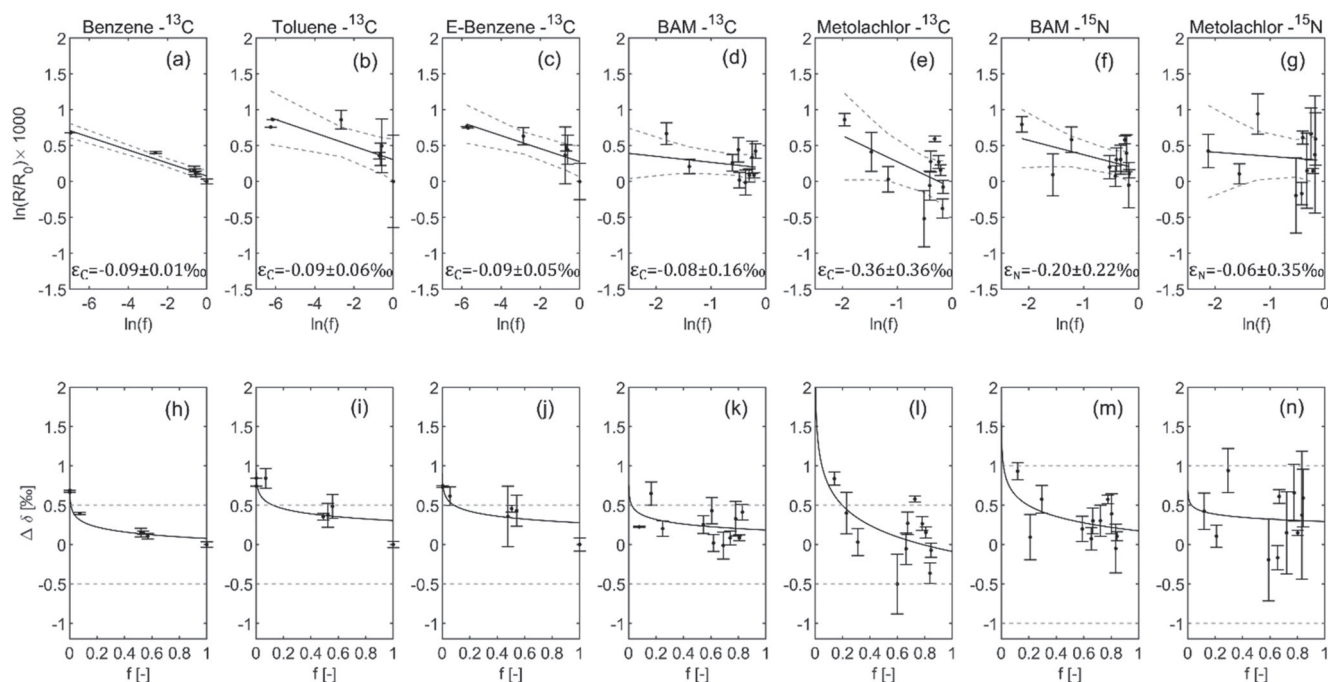


Figure 2. Diffusion-induced isotope fractionations observed for benzene, toluene, ethylbenzene, BAM, and metolachlor. Panels (a–g) represent evaluations of the isotope fractionation factor ϵ of each compound according to the Rayleigh equation (eq 8) with 95% confidence intervals. Dashed lines indicate 95% confidence intervals of the regression line. Panels (h–n) represent the correlation between the remaining concentration fractionation $f(C(t)/C(0))$ and $\Delta\delta^{13}\text{C}$ for each compound and $\Delta\delta^{15}\text{N}$ for BAM and metolachlor. Dashed lines indicate the instrument uncertainties of $\pm 0.5\text{‰}$ for carbon-isotope measurements and of $\pm 1\text{‰}$ for nitrogen-isotope measurements. Error bars represent standard deviations of the measurements.

isotope measurements of benzene, toluene, and ethylbenzene, a Velocity XPT purge-and-trap sample concentrator with an AQUATEk 70 liquid autosampler (Teledyne Tekmar, Mason, OH) was connected to the gas chromatograph. Detailed information about the method can be found in the SI.

Concentration Measurements. BAM and metolachlor concentrations were measured using a Prominence HPLC system (Schimadzu Corp., Japan) with a $75 \times 4.6 \text{ mm}^2$ Kinetex $2.6 \mu\text{m}$ C18 100 Å column (Phenomenex Inc., Golden, CO). Benzene, toluene, and ethylbenzene concentrations were measured on a Trace DSQ GC-MS system (Thermo Electron, Germany) equipped with a Combi PAL autosampler (CTC Analytics, Switzerland) with a DB-5 analytical column (30 m, 0.25 mm i.d., 0.5 μm film, Agilent Technologies, Germany). Chloride (Cl^-) concentrations in the diffusion-cell experiments were analyzed by ion chromatography (Dionex 500, Dionex, Sunnyvale, CA). Concentrations of the conservative tracer uranine in the tank experiment were measured on VICTOR Multilabel Plate Reader (PerkinElmer, U.S.A.). A detailed description of the methods is provided in the SI.

Governing Equations and Numerical Method. The solute transport in the 2D flow-through sediment-tank was described by the following advection-dispersion partial differential equation in two dimensions:

$$\frac{\partial C_i}{\partial t} = -\mathbf{v} \cdot \nabla C_i + \nabla \cdot (\mathbf{D} \cdot \nabla C_i) \quad (9)$$

in which C_i [$\mu\text{mol L}^{-1}$] are the concentrations of BAM with heavy (e.g., ^{13}C or ^{15}N) or light isotopes (e.g., ^{12}C or ^{14}N), respectively; \mathbf{D} [$\text{m}^2 \text{s}^{-1}$] is the dispersion tensor; \mathbf{v} [m s^{-1}] is the velocity vector; and t [s^{-1}] is time.

We compared the transverse dispersion behavior of heavy and light isotopologues in the modeling scenarios with the classical transverse dispersion equation (eq 5) and the Chiogna et al. transverse dispersion equation (eq 6) in MATLAB. The solute transport process was solved in the homogeneous domain with a spatial discretization of 1 mm in vertical direction and 10 mm in horizontal direction by the Finite Volume Method. Global implicit method was adopted for the transport.

RESULTS AND DISCUSSION

Diffusion Cell Experiments Showed Weak to Negligible Diffusion-Induced Isotope Fractionation of Organic Compounds at Natural Isotopic Abundance. The initial and final concentrations of benzene, toluene, ethylbenzene, BAM, and metolachlor in the lower compartment of the diffusion cell in each of the experiments conducted over different time periods can be found in Table S1. Concentrations of all organic compounds in the lower compartments of the diffusion cells decreased with extending experimental duration and followed eq 7 (Figure S2). Table 1 shows the diffusion coefficients of the compounds calculated according to eq 7, which are in the upper range of the literature values (Table S3) within uncertainties.

Even after an extended duration of diffusion, and with target compounds at low remaining concentrations (down to 0.1% of initial values) carbon- and nitrogen-isotope values $\Delta\delta$ of all investigated organic compounds fell within a range of -1‰ , which essentially coincides with the uncertainty of $\pm 0.5\text{‰}$ for carbon-isotope measurements and of $\pm 1\text{‰}$ for nitrogen-isotope measurements, respectively (Figure 2). When isotope enrichment factors ϵ_C for carbon and ϵ_N for nitrogen were

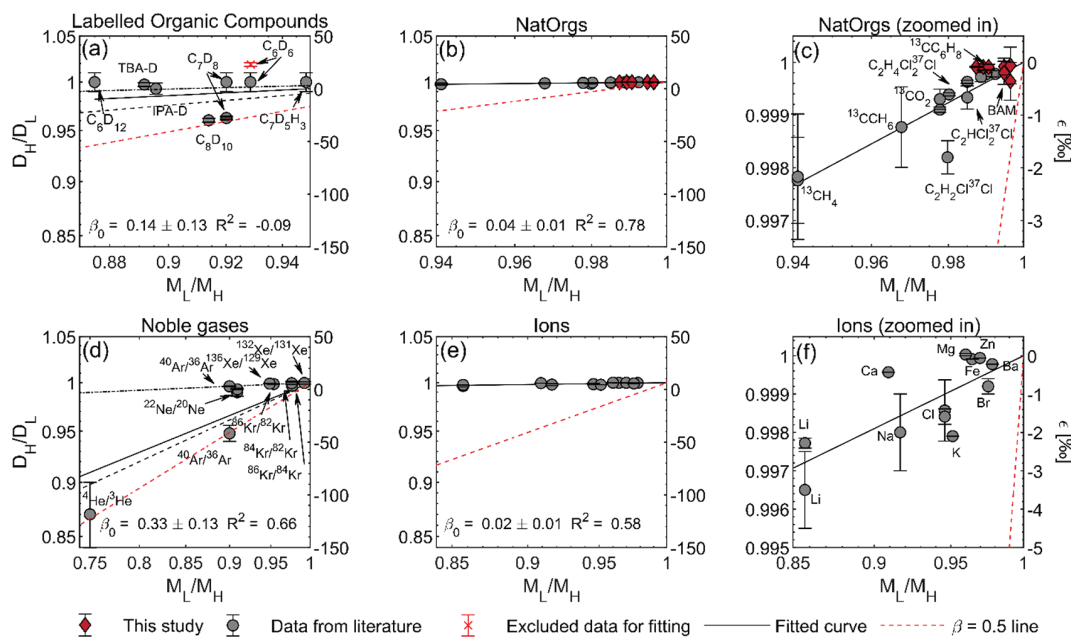


Figure 3. D_H/D_L (left y axis) as a function of M_L/M_H in logarithmic scale, corresponding to the enrichment factor ϵ [‰] on the right y axis. For organic compounds at natural isotopic abundance (NatOrgs), M_L/M_H was calculated based on the most abundant isotopologues with one or zero heavy isotopes in one molecule. Solid lines show the determination of β_0 by a regression curve based on eq 2, where red crosses represent data excluded from the fit. Red dashed lines represent calculated trends in isotope values with $\beta = 0.5$. In panel (a), the black dashed line represents the regression ($\beta_0 = 0.24$) without the data of labeled benzene, toluene and cyclohexane with $D_H/D_L = 1$,^{20,21} and the black dashed-dotted line represents the regression ($\beta_0 = 0.07$) without the data of labeled toluene and ethylbenzene with comparatively small D_H/D_L -values.¹⁵ In panel (d), the black dashed line represents the regression ($\beta_0 = 0.37$) without the anomalously high D_H/D_L value of Ar isotopes,⁴⁶ and the black dash-dotted line represents the regression ($\beta_0 = 0.04$) without low D_H/D_L -values of Ar and He isotopes data.^{22,30} Most of the compounds data points are labeled with compound names except for some of the NatOrgs due to the limit of space. Error bars represent the uncertainties listed in Tables 1 and S5. Detailed data are available in Tables 1 and S5.

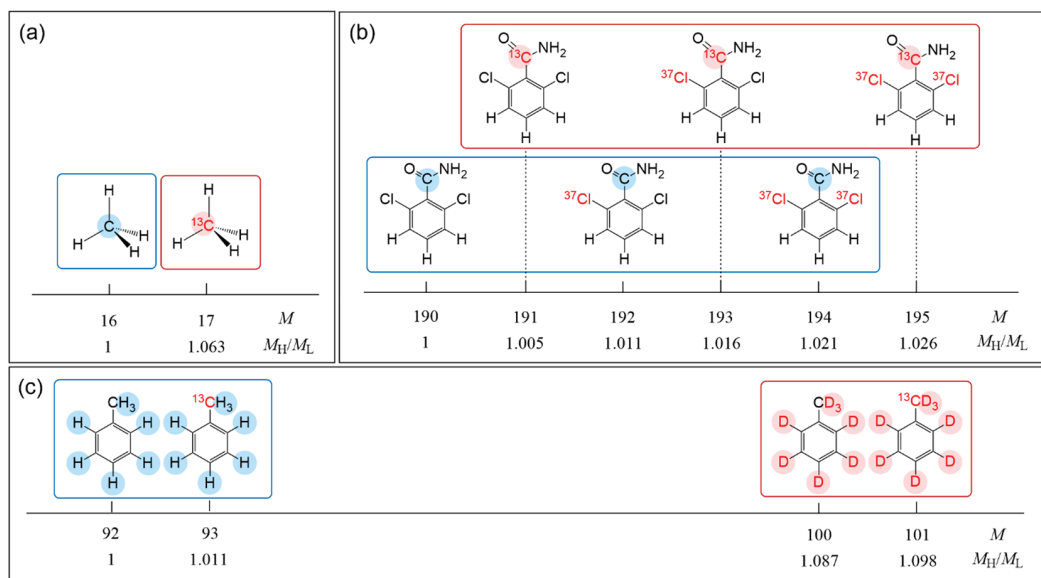


Figure 4. Mass and mass ratio of heavy to light isotopologues of (a) methane and (b) BAM at natural isotopic abundance, and (c) deuterated and nondeuterated toluene.

calculated based on the Rayleigh equation (eq 8), values were smaller than -0.36‰ corresponding to a diffusion coefficient ratio for each organic compound isotopologue pair of close to 1.0 (Table 1). Therefore, the observed isotope fractionation induced by diffusion of benzene, toluene, ethylbenzene, BAM,

and metolachlor at natural isotopic abundance in aqueous phase was weak to negligible.

The calculated β -values of the isotopologue pairs for our target compounds are without exception smaller than 0.1 showing a similarly weak mass dependence as observed in other studies^{6,7,16–18} for CO_2 , CH_4 , C_2H_6 , TCE, 1,2-DCA, and

cis-DCE at natural isotopic abundance (Table 1). This dependence is particularly weak when compared to much larger β -values ($\beta = 0.4$ to 0.5) reported for labeled toluene and ethylbenzene^{7,15,19} (Figure 3; note that we have omitted stark outliers from labeled studies in this comparison, which will be discussed later on). This raises the question of the underlying reasons for the different behavior of labeled and nonlabeled organic compounds.

If a mass dependence is hypothesized based on collision theory, then diffusion-induced isotope fractionation depends on differences in molecular mass, irrespective of the element of the isotopic substitution by which these mass differences are caused (eq 2). In order to illustrate two important influences, Figure 4 shows molecular masses of isotopologues and the mass ratios of heavy to light isotopologues of labeled and nonlabeled organic compounds. The first, widely recognized, influence is that compounds at natural isotopic abundance show a much smaller relative mass difference than labeled substances so that also the expected fractionation is much smaller. This consequence is exemplified in the mass ratios of $M_{\text{H}}/M_{\text{L}} = 93/92 = 1.01$ for ¹³C-substituted toluene vs $M_{\text{H}}/M_{\text{L}} = 100/92 = 1.09$ for perdeuterated toluene in Figure 4c, and it is the underlying reason for the hypothesized power law dependence of eq 2. The second, possibly less obvious influence is illustrated by comparing the mass and mass ratio of heavy to light isotopologues of methane, BAM, and perdeuterated toluene in Figure 4. Perdeuterated isotopologues are clearly separated in mass from nonlabeled toluene isotopologues, and this separation is not significantly affected by the additional isotopic substitution of ¹³C at natural abundance (Figure 4c). In the case of methane (Figure 4a) isotopologues of mass 17 at natural isotopic abundance can be derived from substitution by either ¹³C or ²H. Due to the low natural abundance of ²H, however, isotopologues of mass 17 are almost exclusively composed of ¹³CH₄ so that also here, mass separation can be attributed to only one specific element (¹³C vs ¹²C, Figure 4a). Figure 4b illustrates that this is different with isotopes of different elements in a multielement organic compound at natural isotopic abundance such as BAM. Here, substitution by isotopes of other elements (e.g., ³⁷Cl, ¹⁵N) lends isotopologues a higher molecular mass, even though they may contain only ¹²C. Hence, isotope separation of ¹³C vs ¹²C within the isotopologues can never be as sharp as that for methane or labeled organic compounds. While this effect may be taken into account by explicitly modeling all isotopologues including all elements,⁷ it is neglected by a power-law mass dependence that concentrates on only one element. However, Figure 3c suggests that such an approach may not even be adequate. The diffusion isotope effects of BAM, toluene, and methane do not follow the same trend, where toluene shows much smaller isotope effects than expected from the regression line between methane and BAM. This warrants a closer critical evaluation of this widely postulated mass dependence.

Critical Evaluation of the Mass Dependence of Diffusion-Induced Isotope Fractionation. To further investigate the relation between diffusion-induced isotope fractionation and the mass ratio of heavy-to-light isotopes or isotopologues, we compared the mass dependence of organic compounds at natural isotopic abundance, labeled organic compounds, ions, and noble gases (Figure 3) by estimating β_0 based on eq 2. To qualitatively understand the factors affecting diffusion-induced isotope fractionation of organic compounds, we first considered noble gases and ions as monatomic species

with either very strong (ions), or very weak (noble gases) solute–solvent interactions.

Diffusion of ions in water shows small isotope fractionation ($M_{\text{L}}/M_{\text{H}} > 0.95$, $|\epsilon| < 2\%$), with a very weak to negligible mass dependence of diffusion coefficients of $\beta_0 = 0.02 \pm 0.01$. Strong ionic interactions between water molecules and charged ions lead to an intimately bound solvation shell around the ions.³¹ Hence, collisions between ions and surrounding water molecules are not expected to directly lead to translational movement of the ion, but rather to vibrations and rotations within the network of hydrogen bonds inside the solvation shell.³¹ In contrast, for noble gases the mass dependence of diffusion-induced isotope fractionation in the aqueous phase is inconsistent, with $\beta_0 = 0.33 \pm 0.13$ when all data are included. For individual isotope pairs of Ne, Kr, and Xe, the determined β -values vary between -0.09 and 0.192 ,^{29,30,46,47} whereas Ar showed an inconsistent mass dependence with $\beta = 0.508$ in the study of Tyroller et al.³⁰ and $\beta = 0.035$ and 0.037 in the study of Tempest and Emerson⁴⁶ and Seltzer et al.⁴⁷ Similar to the strong mass dependence of Ar observed by Tyroller et al.,³⁰ the β -value of He reported by Jähne et al.²² is also high ($\beta = 0.486$). Since noble gases are monatomic gases without the formation of ionic or hydrogen bounds with water, the picture of collisions between simplified hard spheres (i.e., solute and solvent molecules) in the Enskog relation seems to be appropriate at first sight. However, the weak mass dependence of Ne, Kr, and Xe isotope fractionation and the contradictory mass dependence of Ar put this picture into question. Molecular-dynamic simulations have suggested that the coupling of short-range and long-range interactions may lead to the weak mass dependence of Ne, Kr, and Xe; while quantum tunneling might be the reason for the strong mass dependence of He^{13,31,33} and the mass dependence of Ar diffusion-induced isotope fractionation is still under debate.

Among the labeled organic compounds (Figure 3a), deuterated isopropyl alcohol (IPA) and *tert*-butyl alcohol (TBA) showed comparatively low diffusion-induced isotope effects. In contrast to benzene, toluene, or ethylbenzene (Figure 3a), these alcohols can form hydrogen bonds resulting in strong interactions with water molecules. In a similar way as with ionic interactions of dissolved ions (Figure 3f), such strongly directed interactions in the solvent shell may compete with the short-range interaction following the Enskog relation so that they weaken the mass dependence of diffusion. In this light the data in Figure 3a suggest that a power-law dependence on molecular mass may not necessarily be observable across all organic molecules. Instead, the compound-specific ability to undergo specific interactions with solvent molecules (dependent on functional groups) may be an important factor unaccounted for in the Enskog relation. Another compound-specific factor that is not considered are molecular vibrations and rotations. In collision theory, organic molecules are treated as single solid balls, even though they consist of multiple atoms and bonds. Each molecule has its degree of freedom which is the sum of translation, rotation, and vibration modes. Treating a polyatomic molecule such as toluene like a noble gas is therefore a gross simplification, even though it may have a similar molecular mass (e.g., Kr: 84, toluene: 92). While for Kr every collision leads to a (short-range) translational movement, collisions of toluene may excite rotations and vibrations instead, which do not result in molecular diffusion. Hence, omitting vibrations and rotations is

likely a further confounding factor to the simplified description by eq 2.

Finally, stark outliers have been reported for labeled molecules, where the inconsistent diffusion-induced isotope fractionation of labeled benzene and toluene in different experimental setups stand out. Rolle et al.¹⁵ observed significant normal diffusion-induced isotope fractionation for labeled toluene and ethylbenzene, and reverse isotope fractionation for labeled benzene, whereas Kopinke et al.²⁰ reported negligible isotope fractionation of labeled benzene, toluene, and cyclohexane and hypothesized that the different solvent matrix (aqueous diffusion in agar gel vs water) may induce the contradictory mass dependence. Presently, it is difficult to explain this inconsistency—future studies may explore whether it can be traced back to specific features of the experimental setups, or even to measurement protocols, the linearity and accuracy of which are not as stringently established for GC–MS as for GC–IRMS. Currently it can therefore be concluded that perdeuterated compounds appear to be poor models for studies of aqueous diffusion of organic compounds at natural isotopic abundance.

For organic compounds at natural isotopic abundance (Figure 3b, c), in contrast, a comparatively consistent picture emerges: β -values are generally smaller than 0.1 and the fitted β_0 of 0.04 indicates a weak to negligible mass dependence. Specifically, the enrichment factor of the diffusion-induced isotope fractionation $|\epsilon|$ is smaller than 1‰ when $M_L/M_H > 0.98$. Only CO₂, methane, and ethane are reported to exhibit higher enrichment factors due to the large mass difference between heavy and light isotopologues, and the negligible interference by isotopes of other elements (discussed in Figure 4). In summary, our critical discussion of the mass-dependence of isotope fractionation provides multiple arguments as to why a power law with $\beta = 0.5$ as expressed in the Enskog relation is not adequate for organic compounds at natural isotopic abundance. First, as discussed in the Introduction, this relationship is inconsistent with the Mode-Coupling Theory. Second, solute–solvent interactions and, third, intramolecular movements are neglected. Fourth, the equation applies to multiatomic isotopologues rather than isotopes. Therefore, data from compound-specific isotope analysis by GC–IRMS cannot be directly evaluated. Finally, our considerations show that data on labeled compounds cannot be extrapolated to model substances at natural isotopic abundance. In particular, an exponent of $\beta = 0.5$ is not adequate and would lead to a gross overestimation of diffusion-induced isotope effects. In contrast, our data obtained with BTEX contaminants and pesticides, which all contained at least 6 carbon atoms per molecule, gave very small ¹³C/¹²C and ¹⁵N/¹⁴N isotope effects of aqueous diffusion: between -0.1‰ and -0.4‰ . This magnitude is in agreement with ¹³C/¹²C effects between -0.2‰ and -0.3‰ determined by Wanner and Hunkeler⁶ in the same Stokes' cell setup for diffusion of representative chlorinated groundwater pollutants (trichloroethylene, dichloroethane, and dichloromethane).^{6,45} In combination, these data put an upper limit of about -0.2‰ to -0.4‰ to the magnitude of aqueous diffusion isotope effects to be expected for typical pollutants at contaminated sites including petroleum and chlorinated hydrocarbons (but not natural gas constituents such as methane, ethane, etc.). Under these boundary conditions, simulations of Wanner and Hunkeler for low permeability sediments (aquifers) suggest

that the resulting diffusion-induced changes in $\delta^{13}\text{C}$ -values would be below $\Delta\delta^{13}\text{C} = 1.5\text{‰}$.⁶

Two-Dimensional Flow-through Sediment Tank Experiments Showed Negligible Isotope Fractionation by Transverse Dispersion. Figure 5 shows the steady-state,

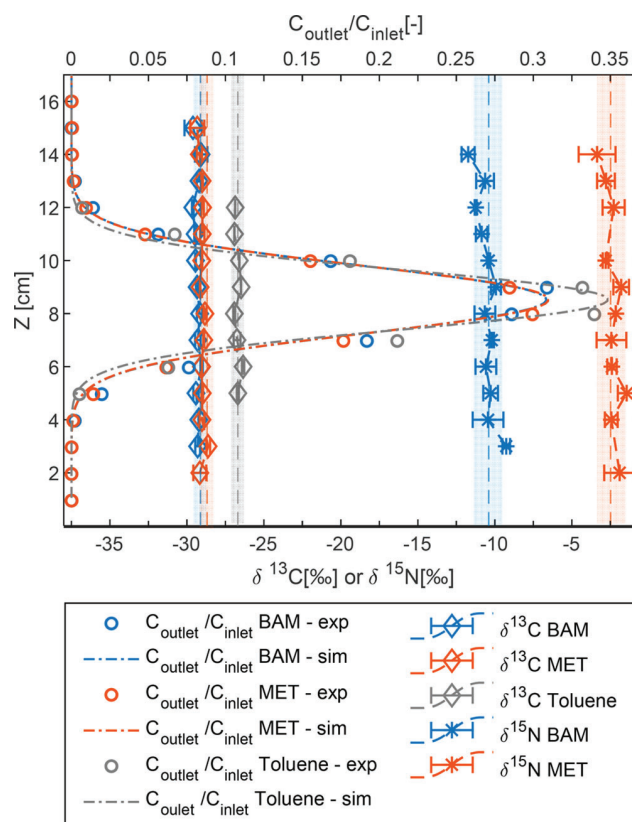


Figure 5. Measured concentrations, $\delta^{13}\text{C}$ - and $\delta^{15}\text{N}$ -values of BAM and MET, and $\delta^{13}\text{C}$ -values of toluene at the outlets of the tank. Dash-dotted lines indicate fitted numerical simulations for conservative transport. Error bars represent standard deviations of the measurements. Color zones with dashed lines represent $\pm 0.5\text{‰}$ uncertainty for the standard C isotope values and $\pm 1\text{‰}$ uncertainty for the standard N isotope values.

conservative, transverse profiles of concentrations and isotope values of BAM, metolachlor, and toluene in the outflow of the flow-through tank. The transverse concentration profiles meet the expected Gaussian distributions. The fitted transverse dispersion coefficients of BAM, metolachlor, and toluene were $2.99 \times 10^{-9} \text{ m}^2/\text{s}$, $2.94 \times 10^{-9} \text{ m}^2/\text{s}$, and $1.72 \times 10^{-9} \text{ m}^2/\text{s}$, respectively. Additional modeling parameters can be found in Table S4.

As shown in Figure 5, the $\delta^{13}\text{C}$ - and $\delta^{15}\text{N}$ -values of BAM were in the range of -29.6‰ to -29.0‰ and -11.7‰ to -9.3‰ , respectively, the $\delta^{13}\text{C}$ and $\delta^{15}\text{N}$ values of metolachlor were in the range of -29.3‰ to -28.6‰ and -3.4‰ to -1.4‰ , respectively, whereas the $\delta^{13}\text{C}$ -values of toluene were in the range of -26.9‰ to -26.3‰ . In general, the absolute difference between the observed isotope values and the standard isotope values of the target compounds was smaller than 0.5‰ for carbon, and smaller than 1‰ for nitrogen. Thus, we did not observe significant isotope fractionation induced by transverse dispersion that was above the uncertainty of the analytical methods (± 0.5 for carbon or

$\pm 1\%$ for nitrogen, respectively), even at very small concentrations ($C_{\text{outlet}}/C_{\text{inlet}} < 0.1\%$) at the top and bottom of the tank. This observation is consistent with previous observations of negligible BAM isotope fractionation by transverse dispersion in a mesoscale aquifer model.⁴⁸

ENVIRONMENTAL SIGNIFICANCE

The parametrization of Chiogna et al. leads to a square-root dependence of the transverse dispersion coefficient on the diffusion coefficient at high velocities, which predicts significant isotope fractionation by transverse dispersion if the diffusion coefficient is assumed to be strongly mass dependent. Numerous published solute-transport models^{15,19,37,38,41} coupled the parametrization of Chiogna et al. to the Enskog or Worch equations to compute the isotopologue-specific transverse dispersion coefficients of organic contaminants. In combination with the use of labeled substrates, β -values as high as 0.5 (e.g., $\beta = 0.53$ for PCE,⁴¹ ethylbenzene,³⁸ and deuterated ethylbenzene¹⁹) were assumed. For a critical re-evaluation in the light of this study's evidence, we simulated the expected isotope fractionation in advective-dispersive transport of heavy and light isotopologues of BAM. They were treated as distinct species with different diffusion coefficients following eq 2 in the 2D flow-through system in two scenarios using (a) the classical linear equation (eq 5), and (b) the Chiogna et al. equation (eq 6) to parametrize the transverse dispersion. We used β -values of 0.01, 0.1, and 0.5 and showed the computed dispersion-induced isotope fractionation in Figure 6. Both scenarios showed negligible isotope fractionation ($|\Delta\delta| < 1\%$) when the mass dependence of the diffusion was weak ($\beta = 0.01$). As expected, the computed isotope fractionation induced by transverse dispersion was larger and more sensitive to β -values in scenario (b) with the Chiogna et al. parametrization than in scenario (a).

In addition, we simulated isotope fractionations $\Delta\delta_{\text{max}}$ at the outmost vertical outlet port of the tank system induced by transverse dispersion as a function of β and the mass ratio of heavy-to-light isotopologues $M_{\text{H}}/M_{\text{L}}$ (Figure S3). Consistent with the simulations in Figure 6, the $\Delta\delta$ -values predicted by the parametrization of Chiogna et al. (Figure S3a,c) are about twice as large as those predicted by the classical equation (Figure S3b,d). The results also indicate that both scenarios predict very large isotope fractionations when a β -value of 0.5 is assumed; for $M_{\text{H}}/M_{\text{L}} = 1.05$, $\Delta\delta = -25.4\%$ using the classical parametrization, and with $\Delta\delta = -66.7\%$ using the Chiogna et al. parametrization. As such strong isotope fractionation has not been observed, these results strengthen the point that the Enskog and Worch relations with $\beta = 0.5$ or 0.53 greatly overestimate the isotope fractionation induced by diffusion and transverse dispersion.

In contrast, our diffusion experiments, the other studies presented in Figure 3, and the results from our tank experiments suggest that the mass dependence of diffusion coefficients is weak or negligible, especially for organic compounds at natural isotopic abundance. Available data (Table 1) suggest that organic compounds at natural isotopic abundance show small to negligible diffusion- and dispersion-induced isotope effects with isotope enrichment factors $\epsilon < -0.4\%$. With $\epsilon < -0.4\%$, the simulated $\Delta\delta$ in our tank system (with $D_t = 2.99 \times 10^{-9} \text{ m}^2/\text{s}$) is smaller than -1.2% even using eq 6 from Chiogna et al. (Figure 6, red zone). For the simulation at even lower remaining concentrations ($C_{\text{outlet}}/$

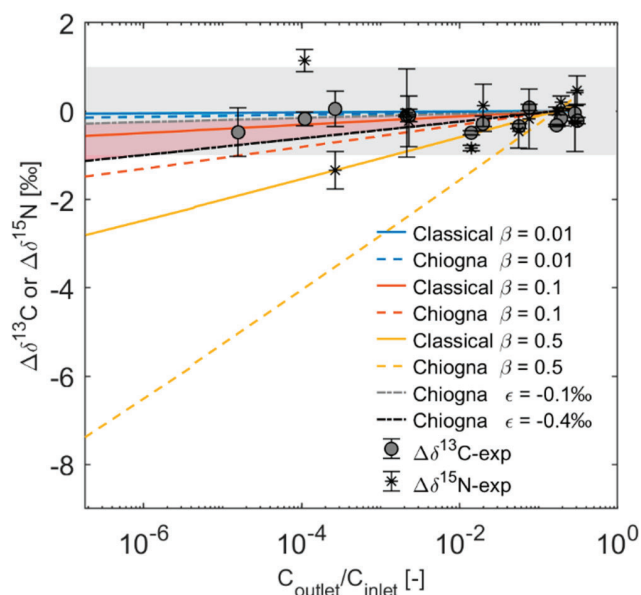


Figure 6. Simulated isotope fractionations $\Delta\delta^{13}\text{C}$ or $\Delta\delta^{15}\text{N}$ induced by transverse dispersion at different outlet-to-inlet concentration ratios $C_{\text{outlet}}/C_{\text{inlet}}$ using different β -values and ϵ -values. Solid lines: with classical linear parametrization of transverse dispersion; dashed lines: with nonlinear parametrization by Chiogna et al.; we used light and heavy isotopologues of BAM ($M_{\text{L}} = 190.02 \text{ Da}$, $M_{\text{H}} = 191.02 \text{ Da}$) as the target compounds, with $D_{\text{L}} = 6.08 \times 10^{-10} \text{ m}^2/\text{s}$. Both dispersion scenarios with the transverse dispersion coefficient $D_t = 2.99 \times 10^{-9} \text{ m}^2/\text{s}$ fitted to the experimental concentration data, with the effective grain size $d_{\text{eff}} = 1.0 \text{ mm}$ in the classical equation, and $d_{\text{eff}} = 2.5 \text{ mm}$ in eq 6 from Chiogna et al. Gray zone represents the $\pm 1\%$ tolerated standard deviation of the original standard isotope value. Red zone represents the isotope fractionation range predicted using eq 6 from Chiogna et al. with $\epsilon = -0.1$ (gray dotted-dashed line) and -0.4% (black dotted-dashed line).

$C_{\text{inlet}} = 10^{-11}$; Figure S4, simulation with $D_t = 1.5 \times 10^{-9} \text{ m}^2/\text{s}$) the estimated $\Delta\delta$ (with $\epsilon = -0.4\%$) was smaller than -1.8% using eq 6 which was consistent with the carbon isotope change below 1.5‰ of TCE aqueous diffusion in low permeability sediments estimated by Wanner and Hunkeler.⁶ We note, however, that such residual concentrations would come to lie below the sensitivity of current compound-specific isotope analysis. On the basis of the results from this and other studies,^{6,13,45} we therefore recommend that conservative interpretations of CSIA field data may be accomplished if an additional uncertainty in carbon isotope values of $\pm 1\%$ is considered in addition to the present analytical uncertainty of $\pm 2\%$ suggested by EPA.⁴⁹ This would apply to contaminations by chlorinated solvents and gasoline contaminants (but not natural gases such as methane or ethane) and would be adequate to consider the effect of aqueous diffusion and dispersion (but not the influence from sorption, volatilization or gas phase diffusion). Compared to recent predictions from simulations^{15,19,37,38,41} this significantly reduces uncertainties and enables more reliable interpretation of CSIA data in the field (e.g., source identification or discrimination, assessment of degradation).

ASSOCIATED CONTENT

Supporting Information

The Supporting Information is available free of charge at <https://pubs.acs.org/doi/10.1021/acs.est.0c06741>.

More detailed experimental section and description of the numerical simulations (PDF)

AUTHOR INFORMATION

Corresponding Author

Martin Elsner – Institute of Groundwater Ecology, Helmholtz Zentrum München, 85764 Neuherberg, Germany; Chair of Analytical Chemistry and Water Chemistry, Technical University of Munich, 81377 Munich, Germany; orcid.org/0000-0003-4746-9052; Phone: +49 89 2180-78232; Email: m.elsner@tum.de

Authors

Fengchao Sun – Institute of Groundwater Ecology, Helmholtz Zentrum München, 85764 Neuherberg, Germany; Chair of Analytical Chemistry and Water Chemistry, Technical University of Munich, 81377 Munich, Germany

Jan Peters – Institute of Groundwater Ecology, Helmholtz Zentrum München, 85764 Neuherberg, Germany; Center for Applied Geoscience, University of Tübingen, 72074 Tübingen, Germany

Martin Thullner – Department of Environmental Microbiology, UFZ—Helmholtz Centre for Environmental Research, 04318 Leipzig, Germany; orcid.org/0000-0001-9723-4601

Olaf A. Cirpka – Center for Applied Geoscience, University of Tübingen, 72074 Tübingen, Germany

Complete contact information is available at: <https://pubs.acs.org/10.1021/acs.est.0c06741>

Author Contributions

The manuscript was written through the contributions of all authors. All authors have given approval to the final version of the manuscript.

Funding

This work was funded by an ERC consolidator grant (“MicroDegrad”, grant no. 616861) awarded by the European Research Council.

Notes

The authors declare no competing financial interest.

ACKNOWLEDGMENTS

We acknowledge Armin H. Meyer from Helmholtz Zentrum München for his contribution on the isotope measurements of the toluene samples from the tank experiment.

REFERENCES

- (1) Elsner, M. Stable isotope fractionation to investigate natural transformation mechanisms of organic contaminants: Principles, prospects and limitations. *J. Environ. Monit.* **2010**, *12* (11), 2005–31.
- (2) Kuntze, K.; Eisenmann, H.; Richnow, H.-H.; Fischer, A. Compound-specific stable isotope analysis (CSIA) for evaluating degradation of organic pollutants: An overview of field case studies. In *Anaerobic Utilization of Hydrocarbons, Oils, and Lipids*; Boll, M., Ed. Springer: Cham: 2019; pp 323–360.
- (3) Elsner, M.; Imfeld, G. Compound-specific isotope analysis (CSIA) of micropollutants in the environment - Current developments and future challenges. *Curr. Opin. Biotechnol.* **2016**, *41*, 60–72.
- (4) Elsner, M.; Jochmann, M. A.; Hofstetter, T. B.; Hunkeler, D.; Bernstein, A.; Schmidt, T. C.; Schimmelmann, A. Current challenges in compound-specific stable isotope analysis of environmental organic contaminants. *Anal. Bioanal. Chem.* **2012**, *403* (9), 2471–91.
- (5) Thullner, M.; Centler, F.; Richnow, H.-H.; Fischer, A. Quantification of organic pollutant degradation in contaminated aquifers using compound specific stable isotope analysis – Review of recent developments. *Org. Geochem.* **2012**, *42* (12), 1440–1460.
- (6) Wanner, P.; Hunkeler, D. Carbon and chlorine isotopologue fractionation of chlorinated hydrocarbons during diffusion in water and low permeability sediments. *Geochim. Cosmochim. Acta* **2015**, *157*, 198–212.
- (7) Jin, B.; Rolle, M.; Li, T.; Haderlein, S. B. Diffusive fractionation of BTEX and chlorinated ethenes in aqueous solution: Quantification of spatial isotope gradients. *Environ. Sci. Technol.* **2014**, *48* (11), 6141–50.
- (8) Kopinke, F. D.; Georgi, A.; Voskamp, M.; Richnow, H. H. Carbon isotope fractionation of organic contaminants due to retardation on humic substances: Implications for natural attenuation studies in aquifers. *Environ. Sci. Technol.* **2005**, *39*, 6052.
- (9) Elsner, M.; McKelvie, J.; Lacrampe Couloume, G.; Sherwood Lollar, B. Insight into methyl tert-butyl ether (MTBE) stable isotope fractionation from abiotic reference experiments. *Environ. Sci. Technol.* **2007**, *41* (16), 5693–5700.
- (10) Hofstetter, T. B.; Schwarzenbach, R. P.; Bernasconi, S. M. Assessing transformation processes of organic compounds using stable isotope fractionation. *Environ. Sci. Technol.* **2008**, *42* (21), 7737–7743.
- (11) Schmidt, T. C.; Schirmer, M.; Weiss, H.; Haderlein, S. B. Microbial degradation of methyl tert-butyl ether and tert-butyl alcohol in the subsurface. *J. Contam. Hydrol.* **2004**, *70*, 173.
- (12) Kuder, T.; Wilson, J. T.; Kaiser, P.; Kolhatkar, R.; Philp, P.; Allen, J. Enrichment of stable carbon and hydrogen isotopes during anaerobic biodegradation of MTBE: Microcosm and field evidence. *Environ. Sci. Technol.* **2005**, *39*, 213.
- (13) Wanner, P.; Hunkeler, D. Isotope fractionation due to aqueous phase diffusion - What do diffusion models and experiments tell? - A review. *Chemosphere* **2019**, *219*, 1032–1043.
- (14) LaBolle, E. M.; Fogg, G. E.; Eweis, J. B.; Gravner, J.; Leaist, D. G. Isotopic fractionation by diffusion in groundwater. *Water Resour. Res.* **2008**, *44* (7), W07405.
- (15) Rolle, M.; Jin, B. Normal and inverse diffusive isotope fractionation of deuterated toluene and benzene in aqueous systems. *Environ. Sci. Technol. Lett.* **2017**, *4* (7), 298–304.
- (16) O’Leary, M. H. Measurement of the isotope fractionation associated with diffusion of carbon dioxide in aqueous solution. *J. Phys. Chem.* **1984**, *88* (4), 823–825.
- (17) Zhang, T.; Krooss, B. M. Experimental investigation on the carbon isotope fractionation of methane during gas migration by diffusion through sedimentary rocks at elevated temperature and pressure. *Geochim. Cosmochim. Acta* **2001**, *65* (16), 2723–2742.
- (18) Schloemer, S.; Krooss, B. M. Molecular transport of methane, ethane and nitrogen and the influence of diffusion on the chemical and isotopic composition of natural gas accumulations. *Geofluids* **2004**, *4* (1), 81–108.
- (19) Rolle, M.; Chiogna, G.; Bauer, R.; Griebler, C.; Grathwohl, P. Isotopic fractionation by transverse dispersion: Flow-through microcosms and reactive transport modeling study. *Environ. Sci. Technol.* **2010**, *44* (16), 6167–6173.
- (20) Kopinke, F. D.; Georgi, A.; Roland, U. Isotope fractionation in phase-transfer processes under thermodynamic and kinetic control - Implications for diffusive fractionation in aqueous solution. *Sci. Total Environ.* **2018**, *610–611*, 495–502.
- (21) Kopinke, F.-D.; Georgi, A. H/D-isotope fractionation due to aqueous phase diffusion – Deuterated hydrocarbons revisited. *Chemosphere* **2020**, *258*, 127357.
- (22) Jähne, B.; Heinz, G.; Dietrich, W. Measurement of the diffusion coefficients of sparingly soluble gases in water. *J. Geophys. Res.* **1987**, *92* (C10), 10767–10776.
- (23) Einstein, A. *Investigations on the Theory of the Brownian Movement*; Courier Corporation: North Chelmsford, MA, 1956.
- (24) Maxwell, J. C. On the dynamical theory of gases. *Proc. R. Soc. London* **1866**, *15*, 167–171.

- (25) Lemons, D. S.; Gythiel, A. Paul Langevin's 1908 paper "On the theory of Brownian motion" ["Sur la théorie du mouvement brownien," C. R. Acad. Sci. (Paris) 146, 530–533 (1908)]. *Am. J. Phys.* **1997**, *65* (11), 1079–1081.
- (26) Ali, S. M.; Samanta, A.; Ghosh, S. K. Mode coupling theory of self and cross diffusivity in a binary fluid mixture: Application to Lennard-Jones systems. *J. Chem. Phys.* **2001**, *114* (23), 10419–10429.
- (27) Tyrrell, H. J. V.; Harris, K. *Diffusion in Liquids: A Theoretical and Experimental Study*; Butterworth-Heinemann: Waltham, MA, 2013.
- (28) Wanner, P.; Hunkeler, D. Molecular dynamic simulations of carbon and chlorine isotopologue fractionation of chlorohydrocarbons during diffusion in liquid water. *Environ. Sci. Technol. Lett.* **2019**, *6* (11), 681–685.
- (29) Tyroller, L.; Brennwald, M. S.; Busemann, H.; Maden, C.; Baur, H.; Kipfer, R. Negligible fractionation of Kr and Xe isotopes by molecular diffusion in water. *Earth Planet. Sci. Lett.* **2018**, *492*, 73–78.
- (30) Tyroller, L.; Brennwald, M. S.; Mächler, L.; Livingstone, D. M.; Kipfer, R. Fractionation of Ne and Ar isotopes by molecular diffusion in water. *Geochim. Cosmochim. Acta* **2014**, *136*, 60–66.
- (31) Bourg, I. C.; Richter, F. M.; Christensen, J. N.; Sposito, G. Isotopic mass dependence of metal cation diffusion coefficients in liquid water. *Geochim. Cosmochim. Acta* **2010**, *74* (8), 2249–2256.
- (32) Rodushkin, I.; Stenberg, A.; Andren, H.; Malinovsky, D.; Baxter, D. C. Isotopic fractionation during diffusion of transition metal ions in solution. *Anal. Chem.* **2004**, *76* (7), 2148–2151.
- (33) Bhattacharyya, S.; Bagchi, B. Power law mass dependence of diffusion: A mode coupling theory analysis. *Phys. Rev. E: Stat. Phys., Plasmas, Fluids, Relat. Interdiscip. Top.* **2000**, *61* (4), 3850.
- (34) Scheidegger, A. E. General theory of dispersion in porous media. *J. Geophys. Res.* **1961**, *66* (10), 3273–3278.
- (35) De Josselin de Jong, G. Longitudinal and transverse diffusion in granular deposits. *Trans., Am. Geophys. Union* **1958**, *39* (1), 67–74.
- (36) Chiogna, G.; Eberhardt, C.; Grathwohl, P.; Cirpka, O. A.; Rolle, M. Evidence of compound-dependent hydrodynamic and mechanical transverse dispersion by multitracer laboratory experiments. *Environ. Sci. Technol.* **2010**, *44* (2), 688–693.
- (37) Xu, S.; Sherwood Lollar, B.; Sleep, B. E. Rethinking aqueous phase diffusion related isotope fractionation: Contrasting theoretical effects with observations at the field scale. *Sci. Total Environ.* **2017**, *607–608*, 1085–1095.
- (38) Eckert, D.; Rolle, M.; Cirpka, O. A. Numerical simulation of isotope fractionation in steady-state bioreactive transport controlled by transverse mixing. *J. Contam. Hydrol.* **2012**, *140–141*, 95–106.
- (39) Eckert, D.; Qiu, S.; Elsner, M.; Cirpka, O. A. Model complexity needed for quantitative analysis of high resolution isotope and concentration data from a toluene-pulse experiment. *Environ. Sci. Technol.* **2013**, *47* (13), 6900–7.
- (40) Worch, E. Eine neue gleichung zur berechnung von diffusionskoeffizienten gelöster stoffe. *Vom Wasser* **1993**, *81*, 289–297.
- (41) Van Breukelen, B. M.; Rolle, M. Transverse hydrodynamic dispersion effects on isotope signals in groundwater chlorinated solvents' plumes. *Environ. Sci. Technol.* **2012**, *46* (14), 7700–8.
- (42) Stokes, R. H. An improved diaphragm-cell for diffusion studies, and some tests of the method. *J. Am. Chem. Soc.* **1950**, *72* (2), 763–767.
- (43) Asfour, A. F. A. Improved and simplified diaphragm cell design and analysis technique for calibration. *Rev. Sci. Instrum.* **1983**, *54* (10), 1394–1396.
- (44) Bauer, R. D.; Maloszewski, P.; Zhang, Y.; Meckenstock, R. U.; Griebler, C. Mixing-controlled biodegradation in a toluene plume—Results from two-dimensional laboratory experiments. *J. Contam. Hydrol.* **2008**, *96* (1–4), 150–68.
- (45) Wanner, P.; Parker, B. L.; Chapman, S. W.; Aravena, R.; Hunkeler, D. Does sorption influence isotope ratios of chlorinated hydrocarbons under field conditions? *Appl. Geochem.* **2017**, *84*, 348–359.
- (46) Tempest, K. E.; Emerson, S. Kinetic isotopic fractionation of argon and neon during air–water gas transfer. *Mar. Chem.* **2013**, *153*, 39–47.
- (47) Seltzer, A. M.; Ng, J.; Severinghaus, J. P. Precise determination of Ar, Kr and Xe isotopic fractionation due to diffusion and dissolution in fresh water. *Earth Planet. Sci. Lett.* **2019**, *514*, 156–165.
- (48) Schurner, H. K.; Maier, M. P.; Eckert, D.; Brejcha, R.; Neumann, C. C.; Stumpp, C.; Cirpka, O. A.; Elsner, M. Compound-specific stable isotope fractionation of pesticides and pharmaceuticals in a mesoscale aquifer model. *Environ. Sci. Technol.* **2016**, *50* (11), 5729–39.
- (49) Hunkeler, D.; Meckenstock, R. U.; Sherwood Lollar, B.; Schmidt, T. C.; Wilson, J.; Schmidt, T.; Wilson, J. *A Guide for Assessing Biodegradation and Source Identification of Organic Ground Water Contaminants Using Compound Specific Isotope Analysis (CSIA)*; US EPA: Oklahoma, 2008; <https://pubs.fdlp.gov/GPO/LPS115694>.

Supporting Information for

Magnitude of diffusion- and transverse dispersion-induced isotope fractionation of organic compounds in aqueous systems

Fengchao Sun, Jan Peters, Martin Thullner, Olaf A. Cirpka, and Martin Elsner

Supplementary Table of Contents

Supporting Environmental Section	48
Chemicals	48
Setup of the two-dimensional flow-through sediment tank experiment	48
Sample preparation and solid-phase extraction (SPE)	49
Concentration measurements on HPLC-UV-DAD	49
Concentration measurements on GC-MS	50
Carbon and nitrogen isotope measurements on GC-IRMS	50
Tracer test with uranine	52
Supporting Figures	53
Figure S1 Setup of the two-dimensional flow-through sediment tank experiment	53
Figure S2 Concentration change with increasing duration in the diffusion cell experiments of (a) BAM and metolachlor (MET) and (b) benzene, toluene and ethylbenzene	53
Figure S3. Dependence of $\Delta\delta_{\max}$ induced by transverse dispersion on the β -value and the ratio between molecular mass of heavy and light isotopologues M_H/M_L	54
Figure S4. Simulated isotope fractionation $\Delta\delta^{13}\text{C}$ or $\Delta\delta^{15}\text{N}$ induced by transverse dispersion at different outlet-to-inlet concentration ratios $C_{\text{outlet}}/C_{\text{inlet}}$	54
Supporting Tables	55
Table S1 Initial and final concentrations and calculated remaining fraction and diffusion coefficient of each compound in each diffusion cell experiment	55
Table S2 Estimation of the characteristic factor σ of each diffusion cell	56
Table S3 Measured D_{aq} of benzene, toluene, ethylbenzene, BAM and metolachlor	56
Table S4 Parameters for transport modeling	57
Table S5 Summary of diffusion-induced isotope fractionation $\varepsilon_{\text{diff}}$ and exponents of an assumed power law mass dependency of labelled organic compounds, noble gases and ions from literature.	58
References	60

Supporting Environmental Section

Chemicals

The following chemicals were used: benzene, toluene and ethylbenzene from Riedel-de Haën, supplied by Sigma Aldrich, Germany, 2,6-dichlorobenzamide (Sigma Aldrich, Germany), s-metolachlor (Chemos GmbH & Co. KG, Germany), potassium chloride (Sigma Aldrich, Germany), uranine (Sigma Aldrich, Germany), and sodium hydroxide (Sigma Aldrich, Germany).

Setup of the two-dimensional flow-through sediment tank experiment

The setup of the two-dimensional (2D) flow-through sediment tank experiment (Figure S1) was adapted from Bauer et al¹. The tank was built with two glass sheets fitted into the frame made of teflon and aluminum and had the dimensions of 0.955 m × 0.185 m × 0.012 m (L × H × W); the small width of the tank simplified the flow-through system to be two-dimensional. Sixteen inlet and outlet ports were vertically distributed along the left-hand and the right-hand boundaries of the tank with a 1 cm vertical distance between each port. Two peristaltic pumps (Ismatec, Germany) with the same pumping rate ($45 \pm 2 \mu\text{L}/\text{min}$ per port) at the inlet and outlet boundaries established constant and homogeneous flow conditions within the flow-through tank system. Pumping rates of the pumps with a maximum standard deviation of 8% were calibrated before the experiments. The inlet and outlet ports consisted of stainless steel capillaries (1/16 inch, Alltech, USA) that penetrated the Teflon at the sides of the 2D tank which were connected at the outer side with Viton pump-tubes (ID: 1.02 mm; Ismatec, Glattbrugg, CH) of the peristaltic pumps. At the outlet each steel capillary was in addition covered by steel wire gauze inside the tank to prevent blockage by sands. The tank was sterilized with 12 g/L NaOH solution and rinsed with autoclaved ultra-pure MQ water before each experiment. Autoclaved sands (diameter 0.8-1.2 mm in the BAM and metolachlor experiment, diameter 0.4-0.8mm in the toluene experiment, MKK Märkische Kies- und Kalksandsteinwerke GmbH, Germany) were homogeneously wet packed into the tank. A solution containing the target compounds (BAM 400 mg/L, metolachlor 100 mg/L and toluene 34.2 mg/l) at natural isotopic abundance was introduced through the central inlet port ($z = 8$ cm) of the tank, and the medium solution was pumped in through the rest of the inlet ports. Sampling of BAM and metolachlor were assessed by collecting samples from the 16 outlet ports; sampling of toluene was carried out with a syringe pump (Ismatec, Germany). Sampling

for the isotope measurements started when steady-state conditions had been established. For BAM and metolachlor sampling was conducted from day 5 to day 20; for toluene sampling was conducted from day 5 to day 8.

Sample preparation and solid-phase extraction (SPE)

Samples from tank experiments were frozen at $-20\text{ }^{\circ}\text{C}$ immediately after each sampling until enough sample volume was collected for isotope analysis. For carbon and nitrogen isotope measurements of BAM and metolachlor samples from diffusion cell experiments (40 mL) and tank experiments (1 L) were first filtered through $0.2\text{ }\mu\text{M}$ PES filter (Nalgene Thermo Scientific, Germany) and then were concentrated by SPE.

The SPE method was adapted from Torrentó et al². 0.2 g hydrophobic polymer-based sorbent Bakerbond SDB-1 (J.T. Baker, USA) was self-packed in the 6 mL empty PP SPE cartridge with PE frit ($20\text{ }\mu\text{m}$ pore size; Sigma Aldrich, Germany). The SPE steps are illustrated in the figure below.

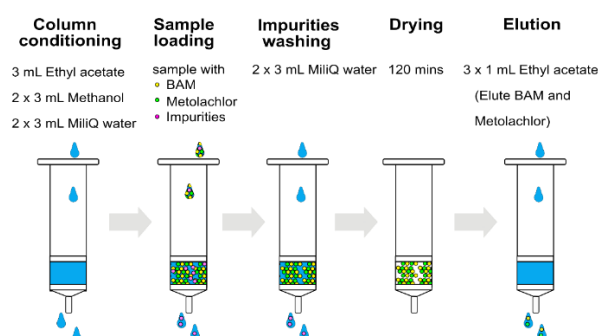


Figure 1 SPE steps

Concentration measurements on HPLC-UV-DAD

BAM and metolachlor concentrations were measured on Prominence HPLC (Shimadzu Corp., Japan) with a $75 \times 4.6\text{ mm}$ Kinetex $2.6\mu\text{m}$ C18 100 \AA column and a SecurityGuard ULTRA cartridge for C18 UHPLC (both from Phenomenex Inc., Golden, CO). The volume of injected sample was $50\text{ }\mu\text{L}$. Separation was performed with a binary gradient flow rate of 1 mL/min at $40\text{ }^{\circ}\text{C}$. The mobile phase A was a 5 mM KH_2PO_4 (pH 7) buffer solution, and the mobile phase B was pure acetonitrile. The initial mobile phase composition was 90% A and 10% B with a 4 min gradient ending with a composition of 70% A and 30% B, followed by a 4 min gradient ending with a composition of 22% A and 78% B. This composition was held

for 2 min thereafter returning to the initial conditions in 0.5 min. BAM was detected with UV absorbance at 201 nm, and metolachlor was detected with UV absorbance at 215 nm. All peaks were quantified by LabSolutions V 5.71 SP2 (Shimadzu Corp., Japan).

Concentration measurements on GC-MS

The method of concentration measurements of volatile organic compounds on GC-MS was adapted from Anneser et al.³ Concentrations of benzene, toluene and ethylbenzene were measured on a Trace DSQ GC-MS system (Thermo Electron, Germany) equipped with a Combi PAL autosampler (CTC Analytics, Switzerland). A DB-5 analytical column (30 m, 0.25 mm i.d., 0.5 μ m film, Agilent Technologies, Germany) with carrier gas He at a flow rate of 1 mL/min was used for separation. 250 μ L gas sample were injected at a split ratio of 1:10 in the headspace measurement. The oven temperature started at 80 °C, where it was held for 1 min, then increased to 140 °C at a rate of 15 °C/min, then increased to a final temperature of 220 °C at a rate of 25 °C/min and held for 1.8 min. The MS was operated in the selected ion monitoring mode (SIM). Internal standards of fluorobenzene and 1,4-dichlorobenzene (EPA 524 internal Standard Mix, Supelco, Bellefonte, PA) were added to the samples and standards.

Carbon and nitrogen isotope measurements on GC-IRMS

For the carbon and nitrogen isotope measurements, the samples concentrated in ethyl acetate after SPE were measured on a GC-IRMS system in which a TRACE GC Ultra gas chromatograph (Thermo Fisher Scientific, Italy) was coupled to a Finnigan MAT 253 isotope ratio mass spectrometer (IRMS) through a Finnigan GC Combustion III interface (Thermo Fisher Scientific, Germany). In addition, for carbon isotope measurements of benzene, toluene and ethylbenzene, a Velocity XPT purge and trap sample concentrator with an AQUATEk 70 liquid autosampler (Teledyne Tekmar) was connected before the gas chromatograph. The IRMS was operated with a vacuum in the ion source of 2.1×10^6 mbar, an accelerating potential of 9 kV and an emission energy of 1.5 mA for carbon isotope analysis and 2 mA for nitrogen analysis. A DB-5 analytical column (30 m, 0.25 mm i.d., 0.5 μ m film, Agilent Technologies, Germany) was used in the gas chromatograph for separation. Helium (grade 5.0) was used as the carrier gas. Samples were injected using a GC Pal autosampler (CTC, Switzerland). For the measurements of high concentrations of BAM and metolachlor the Thermo injector in the split/split-less injection mode was used; for the measurements of BAM and metolachlor at low concentrations and the measurements of benzene, toluene and ethylbenzene, a programmable

injector controlled by an Optic 3 system with liquid N₂-cryofocusing (ATAS GL, distributed by Axel Semrau, Germany) was used. BAM and metolachlor at low concentrations were measured in the on-column injection mode in which a Rxi retention gap (fused silica, 3 m × 0.53 mm inner diameter) (RESTEK, Germany) was connected to a custom made on-column liner, whereas benzene, toluene and ethylbenzene were measured after purge and trap by cryofocusing in a split injection liner.

Vienna PeeDee Belemnite (V-PDB) and Air-N₂ were applied to determine the carbon isotope values $\delta^{13}\text{C}$ [‰] and nitrogen isotope values $\delta^{15}\text{N}$ [‰] of the samples. The carbon and nitrogen isotope values $\delta^{13}\text{C}$ and $\delta^{15}\text{N}$ of the samples were calculated in relation to a lab reference gas (CO₂ and N₂, respectively) which was measured against V-PDB and air in the beginning and the end of each run by using international reference materials (provided by IAEA), e.g. the CO₂ gases RM 8562, RM8563 for CO₂, and RM 8564 and NSVEC (N₂) for N₂.

For the measurements of BAM and metolachlor in the split/split-less injection mode, the GC method for BAM and metolachlor started at 80 °C, and then increased to a final temperature of 280 °C at a ramp rate of 15 °C/min, after which the temperature was held for 7 min. A constant flow rate of 1.4 mL/min was maintained during the measurement. The method of on-column injection was adapted from Ehrl et al.⁴ The GC oven started at 35 °C, was held for 30 s, and then increased to 80 °C at a ramp rate of 5 °C/min to allow a complete solvent evaporation and compound transfer from the retention gap to the analytical column. Then the temperature increased from 80 °C to 280 °C at a ramp rate of 15 °C/min. The method in the Optic 3 started at an initial temperature of 40 °C, which was held for 300 s and then increased to 250 °C at a ramp rate of 2 °C/s. The column flow rate started from 0.3 mL/min, which was held for 120 s and then increased to 1.4 mL/min within 2 min. Thus, a stable flow rate of 1.4 mL/min was established before the GC temperature program started.

The method for carbon isotope analysis of benzene, toluene and ethylbenzene on the GC-IRMS was adapted from Qiu et al.⁵ The GC oven temperature started at 50 °C, was held for 120 s, and was then increased to 150 °C at a ramp rate of 10 °C/min, where it was held for 1 min. Then the temperature increased with a second ramp rate of 100 °C/min to 250 °C, where it was held for 13 min. The method in the Optic 3 started at an initial temperature -80 °C, where it was held for 10 s, then it was increased to 250 °C at a ramp rate of 10 °C/s. The flow rate was kept constant at 1.4 mL/min.

Tracer test with uranine

To determine the properties of the flow system and to validate the numerical simulation of solute transport, we conducted tracer tests with uranine before the transport experiments. For the tracer test before the experiment with BAM and metolachlor, a 30 $\mu\text{g/L}$ uranine solution was continuously injected into the middle inlet port ($z = 8 \text{ cm}$) of the tank, at a constant pumping rate of $45 \pm 2 \mu\text{L}/\text{min}/\text{port}$. For the tracer test before the experiment with toluene, the pumping rate was $44 \pm 2 \mu\text{L}/\text{min}/\text{port}$. The concentration of uranine was measured at the outlets. Figure 2 shows the vertical distribution curve and the breakthrough curve of the measured outlet-to-inlet concentration ratio of uranine $C_{\text{out}}/C_{\text{in}}$. The measured results were fitted by the numerical simulation. The determined seepage velocity, and longitudinal and transverse dispersivity can be found in Table S3.

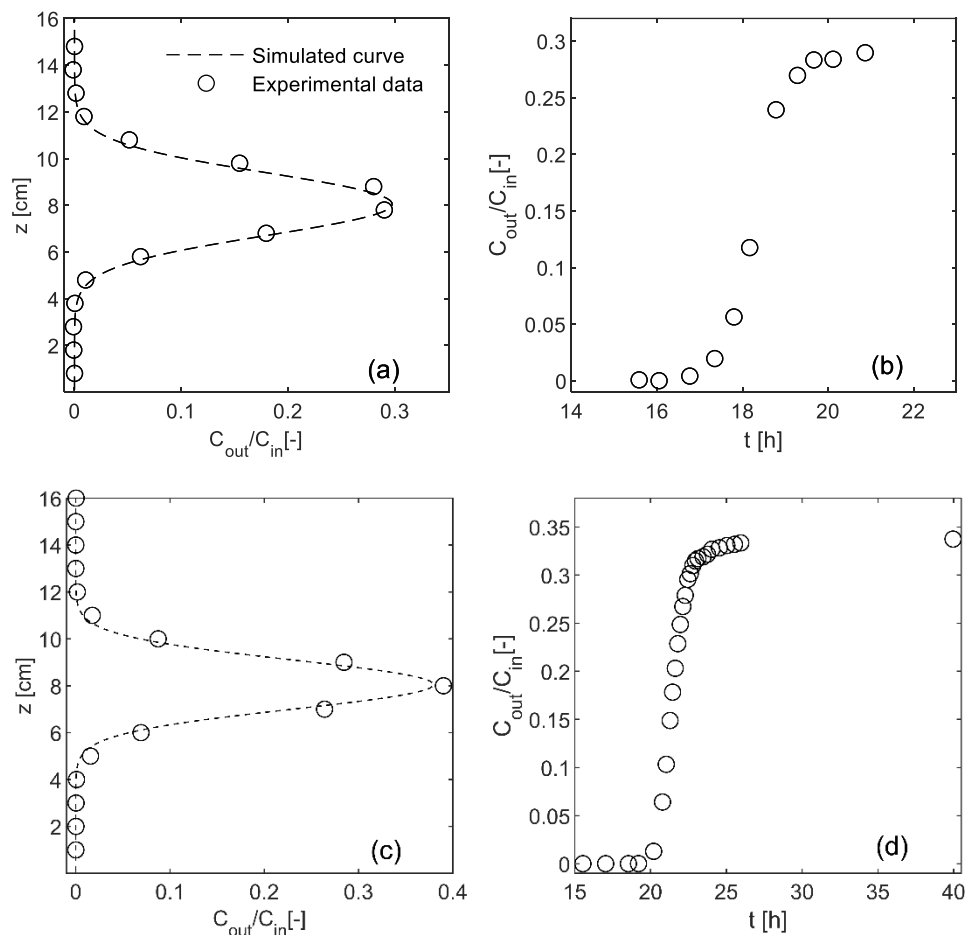


Figure 2 Tracer test results for the continuous injection of uranine before the flow-through tank experiments with (a)-(b) BAM and *s*-metolachlor, and (c)-(d) with toluene: (a), (c) vertical concentration distribution along the outlet profile; (b), (d) breakthrough of uranine at the central outlet port located at $z = 8 \text{ cm}$.

Supporting Figures

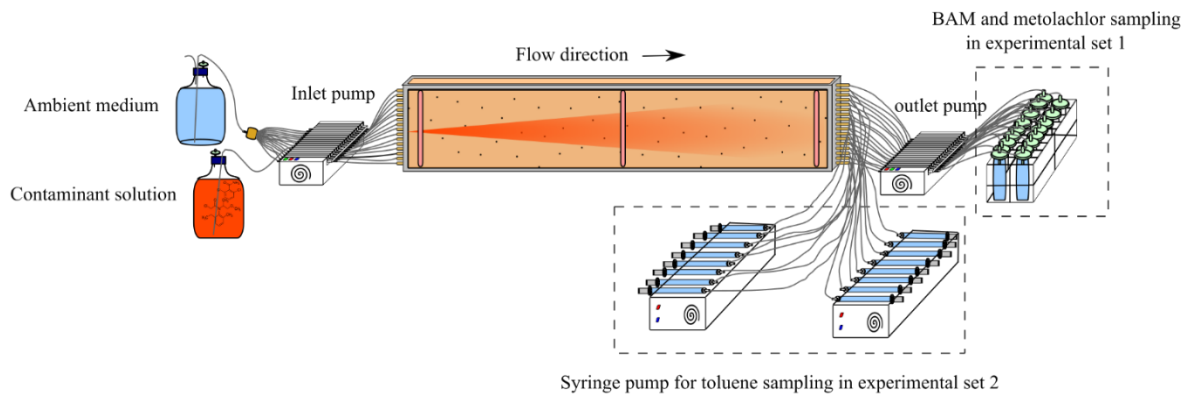


Figure S1 Setup of the two-dimensional flow-through sediment tank experiment

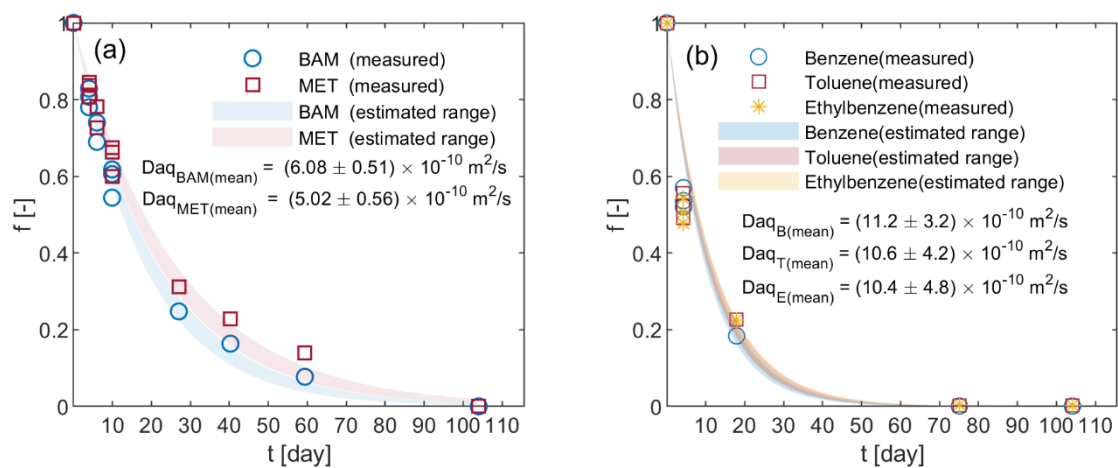


Figure S2 Concentration change with increasing duration in the diffusion cell experiments of (a) BAM and metolachlor (MET) and (b) benzene, toluene, and ethylbenzene.

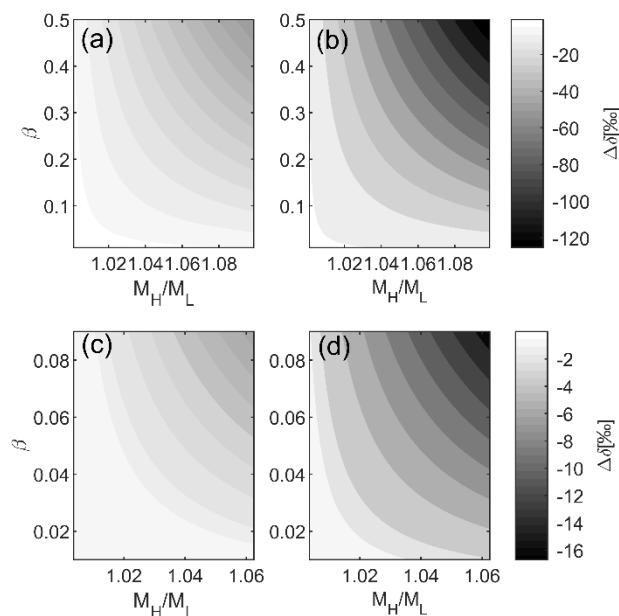


Figure S3 Dependence of $\Delta\delta$ induced by transverse dispersion on the β -value and the ratio between molecular mass of heavy to light isotopologues M_H/M_L . $\Delta\delta$ was the maximum isotope fractionation at the lowest concentration site along the vertical outlet profile of the tank system. Panel (a, b): simulations for a test range of $\beta = (0.01–0.5)$ and $M_H/M_L = (1.001–1.099)$ by using classical equation and Chiogna et al. equation, respectively; panel (c, d): simulations for organic compounds at natural isotopic abundance for a test range of $\beta = (0.01–0.09)$ and $M_H/M_L = (1.004–1.063)$ by using classical equation and Chiogna et al. equation, respectively. The lightest regions in the contour plots represent absolute $\Delta\delta$ -values smaller than 1‰. The initial isotope ratio $^{13}\text{C}/^{12}\text{C}$ was arbitrarily set to be 0.0108.

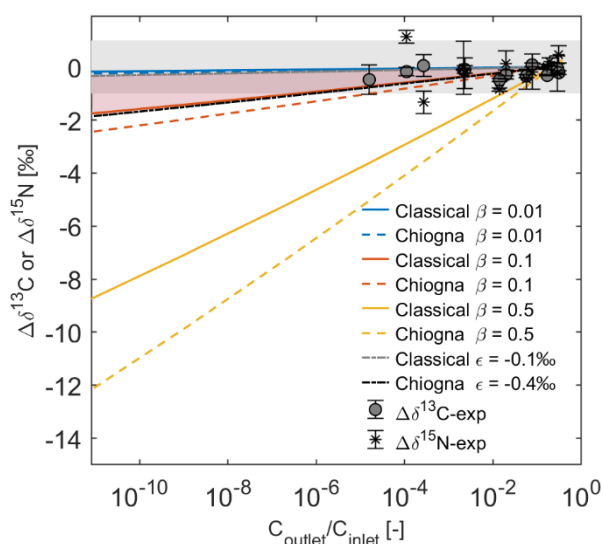


Figure S4. Simulated isotope fractionations $\Delta\delta^{13}\text{C}$ or $\Delta\delta^{15}\text{N}$ induced by transverse dispersion at different outlet-to-inlet concentration ratios $C_{\text{outlet}}/C_{\text{inlet}}$ using different β -values and ϵ -values. Solid lines: with classical linear parameterization of transverse dispersion; dashed lines: with nonlinear

parameterization by Chiogna et al.; dotted-dashed lines: nonlinear parameterization by Chiogna et al. with $\varepsilon = -0.1$ and -0.4% . We used light and heavy isotopologues of BAM ($M_H = 190.02$ Da, $M_L = 191.02$ Da) as the target compounds, with $D_L = 6.08 \times 10^{-10}$ m²/s. Both dispersion scenarios with the transverse dispersion coefficient $D_t = 1.5 \times 10^{-9}$ m²/s. Gray zone represents the $\pm 1\%$ tolerated standard deviation of the original standard isotope value. Red zone represents the isotope fractionation range predicted by using Chiogna et al. equation with $\varepsilon = -0.1$ and -0.4% .

Supporting Tables

Table S1 Initial and final concentrations and calculated remaining fraction and diffusion coefficient of each compound in each diffusion cell experiment running for a different time period

Compound	$C(0)$ [mg/L]	$C(t)$ [mg/L]	f [-]	t [day]	σ [m ²]	Da_q [m ² /s]	Da_q' [m ² /s]	$Da_{q_{mean}}$ [m ² /s]	STDEV [m ² /s]	$Da_{q_{ref}}$ [m ² /s]
Benzene	48.47	26.01	0.5366	4.27	1053	1.60×10^{-9}				
Benzene	48.47	25.22	0.5204	4.27	1053	1.68×10^{-9}	1.58×10^{-9}			
Benzene	48.47	27.64	0.5703	4.27	1053	1.45×10^{-9}		1.12×10^{-9}	3.16×10^{-10}	$(9.40-11.60) \times 10^{-10}$
Benzene	195.22	35.91	0.1839	17.92	1053	1.04×10^{-9}	1.04×10^{-9}			
Benzene	488.97	0.47	0.0010	75.08	1053	1.02×10^{-9}	1.02×10^{-9}			
Benzene	488.97	0.41	0.0008	104.13	927	8.48×10^{-10}	8.48×10^{-10}			
Toluene	18.87	9.88	0.5237	4.27	1053	1.66×10^{-9}				
Toluene	18.87	9.25	0.4903	4.27	1053	1.83×10^{-9}	1.67×10^{-9}			
Toluene	18.87	10.50	0.5566	4.27	1053	1.51×10^{-9}		1.06×10^{-9}	4.15×10^{-10}	$(8.34-9.70) \times 10^{-10}$
Toluene	41.99	9.54	0.2272	17.92	1053	9.09×10^{-10}	9.09×10^{-10}			
Toluene	135.81	0.29	0.0021	75.08	1053	9.00×10^{-10}	9.00×10^{-10}			
Toluene	135.81	0.26	0.0019	104.13	927	7.49×10^{-10}	7.49×10^{-9}			
Ethylbenzene	5.76	2.91	0.5056	4.27	1053	1.76×10^{-10}				
Ethylbenzene	5.76	2.75	0.4778	4.27	1053	1.90×10^{-10}	1.74×10^{-9}			
Ethylbenzene	5.76	3.12	0.5421	4.27	1053	1.58×10^{-10}		1.04×10^{-9}	4.75×10^{-10}	$(7.85-9.20) \times 10^{-10}$
Ethylbenzene	12.79	2.89	0.2256	17.92	1053	9.13×10^{-10}	9.13×10^{-10}			
Ethylbenzene	50.85	0.17	0.0034	75.08	1053	8.33×10^{-10}	8.33×10^{-10}			
Ethylbenzene	50.85	0.16	0.0032	104.13	927	6.90×10^{-10}	6.90×10^{10}			
BAM	360.65	291.17	0.8074	3.97	886	7.05×10^{-10}				
BAM	360.65	298.92	0.8288	3.97	927	5.91×10^{-10}	6.62×10^{-10}			
BAM	360.65	281.33	0.7801	3.97	1053	6.88×10^{-10}				
BAM	360.65	266.87	0.7400	6.00	886	6.56×10^{-10}	6.68×10^{-10}			
BAM	360.65	248.71	0.6896	6.00	1053	6.81×10^{-10}		6.08×10^{-10}	5.08×10^{-11}	4.32×10^{-10}
BAM	360.65	218.45	0.6057	9.90	886	6.62×10^{-10}				
BAM	360.65	222.87	0.6180	9.90	927	6.08×10^{-10}	6.48×10^{-10}			
BAM	360.65	196.29	0.5443	9.90	1053	6.76×10^{-10}				
BAM	360.65	89.36	0.2478	27.02	1053	5.68×10^{-10}	5.68×10^{-10}			
BAM	360.65	58.98	0.1636	40.26	886	5.88×10^{-10}	5.88×10^{-10}			

BAM	360.65	27.87	0.0773	59.38	927	5.39×10^{-10}	5.39×10^{-10}			
BAM	360.65	0.03	0.0001	104.00	1773	5.86×10^{-10}	5.86×10^{-10}			
Metolachlor	93.37	78.14	0.8369	3.97	886	5.87×10^{-10}				
Metolachlor	93.37	78.91	0.8451	3.97	927	5.30×10^{-10}	5.70×10^{-10}			
Metolachlor	93.37	75.35	0.8070	3.97	1053	5.94×10^{-10}				
Metolachlor	93.37	72.92	0.7809	6.00	886	5.39×10^{-10}	5.61×10^{-10}			
Metolachlor	93.37	67.91	0.7273	6.00	1053	5.83×10^{-10}				
Metolachlor	93.37	61.93	0.6633	9.90	886	5.42×10^{-10}				
Metolachlor	93.37	62.99	0.6746	9.90	927	4.97×10^{-10}	5.36×10^{-10}	5.02×10^{-10}	5.64×10^{-11}	$(4.82-5.16) \times 10^{-10}$
Metolachlor	93.37	55.93	0.5990	9.90	1053	5.69×10^{-10}				
Metolachlor	93.37	29.06	0.3113	27.02	1053	4.75×10^{-10}	4.75×10^{-10}			
Metolachlor	93.37	21.36	0.2288	40.26	886	4.79×10^{-10}	4.79×10^{-10}			
Metolachlor	93.37	13.11	0.1404	59.38	927	4.13×10^{-10}	4.13×10^{-10}			
Metolachlor	93.37	0.05	0.0005	104.00	1773	4.77×10^{-10}	4.77×10^{-10}			

Table S2 Estimation of the characteristic factor σ of each diffusion cell, with Cl^- as test solute*

No.cell	$C(0)$ [g/L]	$C(t)$ [g/L]	f [-]	time [h]	σ [cm^{-2}]	σ_{mean} [m^{-2}]	STDEV [m^{-2}]
new 1	3.52	3.07	0.87	22	0.08812	886	6.5
new 1	4.42	3.29	0.74	47	0.08903		
new 2	4.42	3.12	0.71	47	0.10503	1053	4.3
new 2	3.84	1.92	0.50	93	0.10563		
new 3	3.52	3.04	0.86	22	0.09444	927	25.3
new 3	4.42	3.27	0.74	47	0.09087		
new' 4	3.48	1.25	0.36	75.2	0.19305	1773	222.5
new' 4	3.35	1.59	0.48	65.3	0.16158		

* Test experiments were conducted with 0.1 mol/L KCl solution. $D_{\text{aq-Cl}^-} = 1.96 \times 10^{-9} \text{m}^2/\text{s}$

Table S3 Measured D_{aq} of benzene, toluene, ethylbenzene, BAM and metolachlor

Compound	D_{aq} -measured [m^2/s]	D_{aq} -from literature [m^2/s]
Benzene	$11.2 \pm 3.2 \times 10^{-10}$ *	$(9.40-11.60) \times 10^{-10}$ (6-8)
Toluene	$10.6 \pm 4.2 \times 10^{-10}$	$(8.34-9.70) \times 10^{-10}$ (6-8)
Ethylbenzene	$10.4 \pm 4.8 \times 10^{-10}$	$(7.85-9.20) \times 10^{-10}$ (7-9)
BAM	$6.08 \pm 0.51 \times 10^{-10}$	4.32×10^{-10} (10)
Metolachlor	$5.02 \pm 0.56 \times 10^{-10}$	$(4.82-5.16) \times 10^{-10}$ (7, 11)

*Uncertainties express standard deviations.

Table S4 Parameters for transport modeling

Symbol	Parameter	Values	Unit	References
Transport parameters				
$v_{(BAM, MET)}$	seepage velocity	1.25	[m day ⁻¹]	experimental
$v_{(toluene)}$	seepage velocity	1.16	[m day ⁻¹]	experimental
$d_{eff(BAM, MET)}$	effective grain size for classical equation	0.001	[m]	fitted
$d_{eff(BAM)-Chiogna}$	effective grain size for Chiogna et al. equation	0.0025	[m]	fitted
$d_{eff(toluene)}$	effective grain size for classical equation	0.0005	[m]	fitted
$\Phi_{(BAM, MET)}$	porosity	0.450	[-]	experimental
$\Phi_{(toluene)}$	porosity	0.434	[-]	experimental
$\alpha_l(BAM, MET)$	longitudinal dispersivity	6×10^{-4}	[m]	fitted
$\alpha_l(toluene)$	longitudinal dispersivity	2×10^{-4}	[m]	fitted
$\alpha_t(BAM, MET)$	transverse dispersivity	1.9×10^{-4}	[m]	$\alpha_t = d_{eff} \times 3/16$
$\alpha_t(toluene)$	transverse dispersivity	9.4×10^{-5}	[m]	$\alpha_t = d_{eff} \times 3/16$
D_{aq}^{BAM}	diffusion coefficient of BAM	6.08×10^{-10}	[m ² s ⁻¹]	diffusion experiment
D_{aq}^{MET}	diffusion coefficient of metolachlor	5.02×10^{-10}	[m ² s ⁻¹]	diffusion experiment
$D_{aq}^{toluene}$	diffusion coefficient of toluene	1.06×10^{-9}	[m ² s ⁻¹]	diffusion experiment
D_t^{BAM}	Transverse dispersion coefficient of BAM	2.99×10^{-9}	[m ² s ⁻¹]	$D_t = \alpha_t v + D_{aq} \Phi$
D_t^{MET}	Transverse dispersion coefficient of metolachlor	2.94×10^{-9}	[m ² s ⁻¹]	$D_t = \alpha_t v + D_{aq} \Phi$
$D_t^{Toluene}$	Transverse dispersion coefficient of toluene	1.72×10^{-9}	[m ² s ⁻¹]	$D_t = \alpha_t v + D_{aq} \Phi$
Inflow concentrations				
C_{in}^{BAM}	Inlet concentration of BAM	400	[mg L ⁻¹]	experimental
C_{in}^{MET}	Inlet concentration of metolachlor	100	[mg L ⁻¹]	experimental
$C_{in}^{Toluene}$	Inlet concentration of toluene	34.2	[mg L ⁻¹]	experimental

Table S5 Summary of diffusion-induced isotope fractionation ϵ_{diff} and exponents of an assumed power law mass dependency of labelled organic compounds, noble gases and ions from literature.

Species	Heavy to light isotopes isotopologues	D_H/D_L	ϵ_{diff} [‰]	β [-]**	References
Labeled organic compounds					
Isopropyl alcohol	C_3D_7HO/C_3H_8O	0.993 ± 0.006^a	-7 ± 6^a	0.06 ± 0.05^b	LaBolle et al., 2008 ¹²
tert-Butyl alcohol	$C_4D_9HO/C_4H_{10}O$	0.997 ± 0.002^a	-3 ± 2^a	0.023 ± 0.023^b	LaBolle et al., 2008 ¹²
benzene	C_6D_6/C_6H_6	1.019 ± 0.002^a	19 ± 2^a	-0.247 ± 0.026^a	Rolle and Jin, 2017 ⁶
		1.000 ± 0.005^c	0 ± 5^c	0.0 ± 0.1^b	Kopinke et al., 2020 ¹³
		1.00 ± 0.01^c	0 ± 10^c	0.0 ± 0.1^b	Kopinke et al., 2018 ^{14*}
cyclohexane	C_6D_{12}/C_6H_{12}	1.00 ± 0.01^c	0 ± 10^c	0.0 ± 0.1^b	Kopinke et al., 2018 ^{14*}
toluene	C_7D_8/C_7H_8	0.962 ± 0.002^a	-38 ± 2^a	0.46 ± 0.02^a	Rolle and Jin, 2017 ⁶
		0.963 ± 0.002^a	-37 ± 2^a	0.455 ± 0.023^a	Jin et al., 2014 ⁹
		1.00 ± 0.01^c	0 ± 10^c	0.0 ± 0.1^b	Kopinke et al., 2018 ^{14*}
		1.00 ± 0.01^c	0 ± 10^c	0.0 ± 0.1^b	Kopinke et al., 2020 ¹³
ethylbenzene	$C_7D_5H_3/C_7H_8$	1.00 ± 0.01^c	0 ± 10^c	0.0 ± 0.1^b	Kopinke et al., 2018 ^{14*}
		C_8D_{10}/C_8H_{10}	0.960 ± 0.02^a	-40 ± 2^a	0.455 ± 0.027^a
Noble gases					
He	$^4He/^3He$	0.87 ± 0.03^d	-130 ± 30^d	0.486 ± 0.012^b	Jahne et al., 1987 ¹⁵
Ne	$^{22}Ne/^{20}Ne$	0.990 ± 0.003^a	-10 ± 3^a	0.104 ± 0.032^b	Tyroller et al., 2018 ¹⁶
		0.9931 ± 0.0008^c	-6.9 ± 0.8^c	0.073 ± 0.008^b	Tempest and Emerson, 2013 ^{17*}
Ar	$^{40}Ar/^{36}Ar$	0.948 ± 0.004^a	-52 ± 4^a	0.508 ± 0.040^b	Tyroller et al., 2014 ¹⁸
		0.9961 ± 0.0003^c	-3.90 ± 0.3^c	0.037 ± 0.003^b	Tempest and Emerson, 2013 ^{17*}
		0.9963 ± 0.0003^a	-3.69 ± 0.25^a	0.035 ± 0.002^b	Seltzer et al., 2019 ^{19*}
Kr	$^{84}Kr/^{82}Kr$	0.9995 ± 0.0023^c	-0.50 ± 0.23^c	0.021 ± 0.050^b	Tyroller et al., 2018 ¹⁶
		0.9995^g	-0.50^g	0.021^g	Seltzer et al., 2019 ^{19*}
		0.9986^g	-1.40^g	0.029^g	Seltzer et al., 2019 ^{19*}

	$^{84}\text{Kr}/^{83}\text{Kr}$	0.998 ± 0.010^c	-2 ± 10^c	0.200 ± 0.423^b	Tyroller et al., 2018 ¹⁶
	$^{86}\text{Kr}/^{84}\text{Kr}$	0.9965 ± 0.0052^c	-3.50 ± 0.52^c	0.149 ± 0.111^b	Tyroller et al., 2018 ¹⁶
Xe	$^{132}\text{Xe}/^{129}\text{Xe}$	1.0015 ± 0.0025^c	1.5 ± 2.5^c	-0.065 ± 0.056^b	Tyroller et al., 2018 ¹⁶
	$^{136}\text{Xe}/^{129}\text{Xe}$	0.9990^g	-1.00^g	0.019^g	Seltzer et al., 2019 ^{19*}
	$^{132}\text{Xe}/^{131}\text{Xe}$	0.9997 ± 0.0012^c	-0.3 ± 1.2^c	0.039 ± 0.079^b	Tyroller et al., 2018 ¹⁶
	$^{136}\text{Xe}/^{132}\text{Xe}$	0.9993 ± 0.0020^c	-0.7 ± 2.0^c	0.023 ± 0.035^b	Tyroller et al., 2018 ¹⁶
	$^{134}\text{Xe}/^{132}\text{Xe}$	1.0014 ± 0.0018^c	1.40 ± 1.8^c	-0.093 ± 0.060^b	Tyroller et al., 2018 ¹⁶
Ions					
Li	$^7\text{Li}/^6\text{Li}$	0.9965^g	-3.5^g	0.023^g	Kunze and Fuoss, 1962 ²⁰
	$^7\text{Li}/^6\text{Li}$	0.99772 ± 0.00013^f	-2.28 ± 0.13^f	0.015 ± 0.001^b	Richter et al., 2006 ²¹
	$^7\text{Li}/^6\text{Li}$	0.989 ± 0.002^f	-11 ± 2^f	0.071 ± 0.010^b	Fritz, 1992 ²²
Na	$^{24}\text{Na}/^{22}\text{Na}$	0.998 ± 0.002^a	-2 ± 2^a	0.023 ± 0.020^b	Pikal, 1972 ²³
Mg	$^{25}\text{Mg}/^{24}\text{Mg}$	1.00003 ± 0.00003^f	0.03 ± 0.03^f	0.0007 ± 0.0007^b	Richter et al., 2006 ²¹
K	$^{41}\text{K}/^{39}\text{K}$	0.9979^g	-2.10^g	0.042 ± 0.002^j	Bourg et al., 2010 ²⁴
Ca	$^{44}\text{Ca}/^{40}\text{Ca}$	0.9997^g	-0.43^g	0.0045 ± 0.0005^j	Bourg et al., 2010 ²⁴
Fe	$^{56}\text{Fe}/^{54}\text{Fe}$	0.99991 ± 0.00002^i	-0.09 ± 0.02^i	0.0024 ± 0.0001^b	Rodushkin et al., 2004 ²⁵
Zn	$^{66}\text{Zn}/^{64}\text{Zn}$	0.9999 ± 0.00001^i	-0.06 ± 0.01^i	0.0019 ± 0.0000^b	Rodushkin et al., 2004 ²⁵
Ba	$^{137}\text{Ba}/^{134}\text{Ba}$	0.99978^g	-0.22^g	0.010 ± 0.002^h	Van Zuilen et al., 2016 ²⁶
Cl	$^{37}\text{Cl}/^{35}\text{Cl}$	0.99857 ± 0.0004^f	-1.43 ± 0.04^f	0.025 ± 0.007^b	Richter et al., 2006 ²¹
	$^{37}\text{Cl}/^{35}\text{Cl}$	0.99836 ± 0.00020^a	-1.64 ± 0.20^a	0.030 ± 0.004^b	Eggenkamp and Coleman, 2009 ²⁷
Br	$^{81}\text{Br}/^{79}\text{Br}$	0.99920 ± 0.00017^a	-0.80 ± 0.17^a	0.032 ± 0.007^b	Eggenkamp and Coleman, 2009 ²⁷

^a Published or calculated standard deviation based on the data in literature, ^b β uncertainty calculated according to Gauss' error propagation law by including the uncertainty of D_H/D_L , ^c published system uncertainty, ^d unclear uncertainty, ^e standard deviation recalculated based on published standard error, ^f standard deviation recalculated from reported 2 times standard deviation, ^g uncertainty not available, ^h estimated uncertainty range, ⁱ standard deviation of isotope ratio measurements, ^j uncertainty from linear regression. *Studies on mass transfer of species between two phases (water/gas phase^{17, 19} or water/n-octane phase¹⁴). ** β values were either the published values or recalculated based on eq 2.

References

1. Bauer, R. D.; Maloszewski, P.; Zhang, Y.; Meckenstock, R. U.; Griebler, C., Mixing-controlled biodegradation in a toluene plume--results from two-dimensional laboratory experiments. *J. Contam. Hydrol.* **2008**, *96* (1-4), 150-68.
2. Torrentó, C.; Bakkour, R.; Ryabenko, E.; Ponsin, V.; Prasuhn, V.; Hofstetter, T. B.; Elsner, M.; Hunkeler, D., Fate of four herbicides in an irrigated field cropped with corn: lysimeter experiments. *Procedia Earth Planet. Sci.* **2015**, *13*, 158-161.
3. Anneser, B.; Einsiedl, F.; Meckenstock, R. U.; Richters, L.; Wisotzky, F.; Griebler, C., High-resolution monitoring of biogeochemical gradients in a tar oil-contaminated aquifer. *Appl. Geochem.* **2008**, *23* (6), 1715-1730.
4. Ehrl, B. N.; Kundu, K.; Gharasoo, M.; Marozava, S.; Elsner, M., Rate-limiting mass transfer in micropollutant degradation revealed by isotope fractionation in chemostat. *Environ. Sci. Technol.* **2019**, *53* (3), 1197-1205.
5. Qiu, S.; Eckert, D.; Cirpka, O. A.; Huenniger, M.; Knappett, P.; Maloszewski, P.; Meckenstock, R. U.; Griebler, C.; Elsner, M., Direct experimental evidence of non-first order degradation kinetics and sorption-induced isotopic fractionation in a mesoscale aquifer: ¹³C/¹²C analysis of a transient toluene pulse. *Environ. Sci. Technol.* **2013**, *47* (13), 6892-9.
6. Rolle, M.; Jin, B., Normal and inverse diffusive isotope fractionation of deuterated toluene and benzene in aqueous systems. *Environ. Sci. Technol. Lett.* **2017**, *4* (7), 298-304.
7. EPA On-line Tools for Site Assessment Calculation. <https://www3.epa.gov/ceampubl/learn2model/part-two/onsite/estdiffusion.html>.
8. Rowe, R. K.; Mukunoki, T.; Sangam, H. P., BTEX diffusion and sorption for a geosynthetic clay liner at two temperatures. *J. Geotech. Geoenviron. Eng.* **2005**, *131* (10), 1211-1221.
9. Jin, B.; Rolle, M.; Li, T.; Haderlein, S. B., Diffusive fractionation of BTEX and chlorinated ethenes in aqueous solution: quantification of spatial isotope gradients. *Environ. Sci. Technol.* **2014**, *48* (11), 6141-50.
10. Jorgensen, P. R.; Klint, K. E.; Kistrup, J. P., Monitoring well interception with fractures in clayey till. *Ground Water* **2003**, *41* (6), 772-9.
11. Martínez, L.; Lechón, Y.; Sánchez-Brunete, C.; Tadeo, J. L., Persistence of metolachlor, atrazine and deethylatrazine in soil and its simulation by deterministic models. *Toxicol. Environ. Chem.* **1996**, *54* (1-4), 219-232.
12. LaBolle, E. M.; Fogg, G. E.; Eweis, J. B.; Gravner, J.; Leaist, D. G., Isotopic fractionation by diffusion in groundwater. *Water Resour. Res.* **2008**, *44* (7), W07405.
13. Kopinke, F.-D.; Georgi, A., H/D-isotope fractionation due to aqueous phase diffusion – Deuterated hydrocarbons revisited. *Chemosphere* **2020**, *258*, 127357.
14. Kopinke, F. D.; Georgi, A.; Roland, U., Isotope fractionation in phase-transfer processes under thermodynamic and kinetic control - Implications for diffusive fractionation in aqueous solution. *Sci. Total Environ.* **2018**, *610-611*, 495-502.
15. Jähne, B.; Heinz, G.; Dietrich, W., Measurement of the diffusion coefficients of sparingly soluble gases in water. *J. Geophys. Res.: Oceans* **1987**, *92* (C10), 10767-10776.
16. Tyroller, L.; Brennwald, M. S.; Busemann, H.; Maden, C.; Baur, H.; Kipfer, R., Negligible fractionation of Kr and Xe isotopes by molecular diffusion in water. *Earth Planet. Sci. Lett.* **2018**, *492*, 73-78.
17. Tempest, K. E.; Emerson, S., Kinetic isotopic fractionation of argon and neon during air–water gas transfer. *Mar. Chem.* **2013**, *153*, 39-47.
18. Tyroller, L.; Brennwald, M. S.; Mächler, L.; Livingstone, D. M.; Kipfer, R., Fractionation of Ne and Ar isotopes by molecular diffusion in water. *Geochim. Cosmochim. Acta* **2014**, *136*, 60-66.

19. Seltzer, A. M.; Ng, J.; Severinghaus, J. P., Precise determination of Ar, Kr and Xe isotopic fractionation due to diffusion and dissolution in fresh water. *Earth Planet. Sci. Lett.* **2019**, *514*, 156-165.
20. Kunze, R. W.; Fuoss, R. M., Conductance of the alkali Halides. III. The isotopic lithium chlorides. *J. Phys. Chem.* **1962**, *66* (5), 930-931.
21. Richter, F. M.; Mendybaev, R. A.; Christensen, J. N.; Hutcheon, I. D.; Williams, R. W.; Sturchio, N. C.; Beloso Jr, A. D., Kinetic isotopic fractionation during diffusion of ionic species in water. *Geochim. Cosmochim. Acta* **2006**, *70* (2), 277-289.
22. Fritz, S. J., Measuring the ratio of aqueous diffusion coefficients between 6Li^+ Cl^- and 7Li^+ Cr^- by osmometry. *Geochim. Cosmochim. Acta* **1992**, *56* (10), 3781-3789.
23. Pikal, M. J., Isotope effect in tracer diffusion. Comparison of the diffusion coefficients of $^{24}\text{Na}^+$ and $^{22}\text{Na}^+$ in aqueous electrolytes. *J. Phys. Chem.* **1972**, *76* (21), 3038-3040.
24. Bourg, I. C.; Richter, F. M.; Christensen, J. N.; Sposito, G., Isotopic mass dependence of metal cation diffusion coefficients in liquid water. *Geochim. Cosmochim. Acta* **2010**, *74* (8), 2249-2256.
25. Rodushkin, I.; Stenberg, A.; Andrén, H.; Malinovsky, D.; Baxter, D. C., Isotopic fractionation during diffusion of transition metal ions in solution. *Anal. Chem.* **2004**, *76* (7), 2148-2151.
26. van Zuilen, K.; Müller, T.; Nägler, T. F.; Dietzel, M.; Küsters, T., Experimental determination of barium isotope fractionation during diffusion and adsorption processes at low temperatures. *Geochim. Cosmochim. Acta* **2016**, *186*, 226-241.
27. Eggenkamp, H. G. M.; Coleman, M. L., The effect of aqueous diffusion on the fractionation of chlorine and bromine stable isotopes. *Geochim. Cosmochim. Acta* **2009**, *73* (12), 3539-3548.

2.2 Mass-transfer limitation of biodegradation at low concentrations- Evidence from reactive transport modeling of isotope profiles in a bench-scale aquifer

Published in Environmental Science & Technology 2021, 55, 11, 7386–7397,

<https://pubs.acs.org/doi/10.1021/acs.est.0c08566>

by Fengchao Sun, Adrian Mellage, Mehdi Gharasoo, Aileen Melsbach, Xin Cao, Ralf Zimmermann, Christian Griebler, Martin Thullner, Olaf A. Cirpka, and Martin Elsner

Reprinted with permission. Further permissions related to the material excerpted should be directed to the ACS.

Synopsis

The objective of this chapter is to investigate mass-transfer limitation of biodegradation of organic contaminants at low concentrations in a flow-through sediment tank system by applying CSIA in conjunction with concentration measurements. A reactive transport model considering mass-transfer through the bacterial cell membrane was developed to elucidate the observed carbon and nitrogen isotope values along the concentration cross gradient. In addition, the model further pinpointed the threshold concentration range below which isotope fractionation would be strongly masked.

To mimic oligotrophic conditions in groundwater, I set up a quasi-two-dimensional flow-through sediment tank and homogeneously inoculated it with the BAM degrader *Aminobacter* sp. MSH1. BAM solution was injected at the central inlet port of the tank, developing a concentration gradient from high to low concentration from the center of the tank towards the bottom and top boundaries because of transverse dispersion. Thus, the low BAM concentrations at the lower and upper region of the tank mimicked oligotrophic conditions in the field. To evaluate the bottleneck of biodegradation and the effect of mass-transfer limitation, concentrations of BAM, 2,6-DCBA, DO (dissolved oxygen), total washed-out cell number, ATP of the cells, and the carbon and nitrogen isotope values during the quasi-steady state were analyzed. Decreased isotope fractionation along the concentration downgradient indicated that mass-transfer limitation became the limiting step for biodegradation of organic compounds at low concentrations. In addition, representations of isotope fractionation against residual BAM

concentrations revealed three zones of different limitations: (i) at high substrate concentration, isotope fractionation follows Rayleigh relation suggesting that the substrate BAM was present in excess and that oxygen availability was the limiting factor; (ii) when substrate concentration decreased to a threshold region of about 600 $\mu\text{g/L}$, a drastic decrease in isotope fractionation gave direct evidence of substrate mass-transfer limitation; (iii) when substrate concentrations were even lower, isotope fractionation indicated that mass transfer was still limiting, but at the same time the extent of degradation became smaller. Hence, at this point intrinsic biodegradation activity must have been limited also by physiological adaptation.

To capture this process in quantitative terms, I developed a reactive transport model, combining effects of transverse dispersion and mass transfer through the bacterial cell membrane. The simulated apparent isotope enrichment factor ϵ decreased strongly below a simulated threshold BAM concentration of 600 $\mu\text{g/L}$. In addition, simulations without the consideration of mass-transfer limitation would show strong isotope fractionation, which strongly suggests that mass-transfer limitations on the cellular level must be accounted for in reactive transport models.

Author contributions

Fengchao Sun conceptualized and designed the experiment with the supervision of Prof. Martin Elsner, Prof. Olaf A. Cirpka, and Dr. Martin Thullner; set up the tank system with the help of Prof. Christian Griebler; and developed the numerical model with the help of Prof. Olaf A. Cirpka, Dr. Adrian Mellage, and Dr. Mehdi Gharasoo. Dr. Adrian Mellage performed sensitivity analysis of the model. Dr. Aileen Melsbach helped to perform part of the nitrogen isotope measurements. Fengchao Sun conducted the measurements on LC-MS/MS with assistance of Xin Cao and Prof. Ralf Zimmermann. Fengchao Sun conducted analytical measurements and interpreted data and results; and wrote the manuscript with input from Dr. Adrian Mellage, Dr. Mehdi Gharasoo, Xin Cao, Prof. Christian Griebler, Dr. Martin Thullner, Prof. Olaf A. Cripka, and Prof. Martin Elsner. All authors commented on the manuscript.

Mass-Transfer-Limited Biodegradation at Low Concentrations—Evidence from Reactive Transport Modeling of Isotope Profiles in a Bench-Scale Aquifer

Fengchao Sun, Adrian Mellage, Mehdi Gharasoo, Aileen Melsbach, Xin Cao, Ralf Zimmermann, Christian Griebler, Martin Thullner, Olaf A. Cirpka, and Martin Elsner*



Cite This: *Environ. Sci. Technol.* 2021, 55, 7386–7397



Read Online

ACCESS |

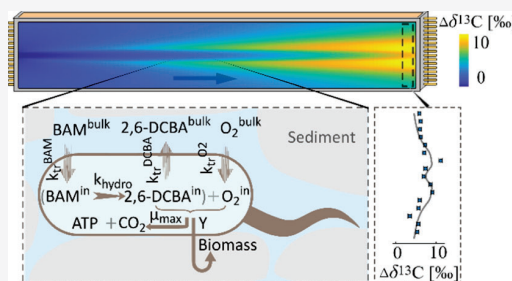
Metrics & More

Article Recommendations

Supporting Information

ABSTRACT: Organic contaminant degradation by suspended bacteria in chemostats has shown that isotope fractionation decreases dramatically when pollutant concentrations fall below the (half-saturation) Monod constant. This masked isotope fractionation implies that membrane transfer is slow relative to the enzyme turnover at $\mu\text{g L}^{-1}$ substrate levels. Analogous evidence of mass transfer as a bottleneck for biodegradation in aquifer settings, where microbes are attached to the sediment, is lacking. A quasi-two-dimensional flow-through sediment microcosm/tank system enabled us to study the aerobic degradation of 2,6-dichlorobenzamide (BAM), while collecting sufficient samples at the outlet for compound-specific isotope analysis. By feeding an anoxic BAM solution through the center inlet port and dissolved oxygen (DO) above and below, strong transverse concentration cross-gradients of BAM and DO yielded zones of low ($\mu\text{g L}^{-1}$) steady-state concentrations. We were able to simulate the profiles of concentrations and isotope ratios of the contaminant plume using a reactive transport model that accounted for a mass-transfer limitation into bacterial cells, where apparent isotope enrichment factors ϵ decreased strongly below concentrations around $600 \mu\text{g/L}$ BAM. For the biodegradation of organic micropollutants, mass transfer into the cell emerges as a bottleneck, specifically at low ($\mu\text{g L}^{-1}$) concentrations. Neglecting this effect when interpreting isotope ratios at field sites may lead to a significant underestimation of biodegradation.

KEYWORDS: bioavailability, 2,6-dichlorobenzamide, reactive-transport model, flow-through system, GC-IRMS, CSIA



INTRODUCTION

The combined interpretation of solute concentrations and isotope ratios in sediment profiles and groundwater samples is a common approach to unravel natural transformations of nutrients and organic compounds, most prominently organic pollutants.^{1–4} The interpretation relies on the phenomenon that kinetic isotope effects typically favor the transformation of molecules with light isotopes so that molecules with heavy isotopes become enriched in the remaining substrate.^{5,6} Hence, an increase of isotope ratios, such as of $^{13}\text{C}/^{12}\text{C}$ or $^{15}\text{N}/^{14}\text{N}$, along a transport path in groundwater or sediments can provide direct evidence of the natural transformation of a compound. This has been applied in the analysis of sulfate,^{7,8} nitrate,⁹ and methane,¹⁰ among others, along with redox gradients and organic pollutants (e.g., BTEX, chlorinated ethenes, pesticides, and herbicides)^{11–17} at contaminated sites. Conversely, the absence of isotope fractionation, despite a concentration decrease, is commonly interpreted as evidence of the absence of reactive turnover.

However, recent studies with suspended cells in chemostats have shown that isotope fractionation may no longer be observable at low concentrations, even though transformation

still occurs.^{18–27} When the mass transfer of a substrate at the cellular level (i.e., through the cell membrane into and out of the cell) is limited, both heavy and light isotopologues are degraded completely inside the cell before they may diffuse out. Consequently, the isotope fractionation of the enzymatic transformation inside the cell can no longer be observed outside of the cell where samples are taken for analysis.²⁸ Such masking of isotope fractionation has been widely recognized in photosynthesis,²⁰ denitrification,^{21,29} and sulfate respiration.^{8,22,23,30,31} Because the phenomenon occurs if membrane transfer is slower than the enzymatic turnover, theoretical considerations predict that mass-transfer limitations may become particularly relevant at extracellular substrate concentrations below the Monod or Michaelis–Menten constants of growth and enzymatic turnover when enzyme kinetics shift

Received: December 18, 2020

Revised: April 9, 2021

Accepted: April 9, 2021

Published: May 10, 2021



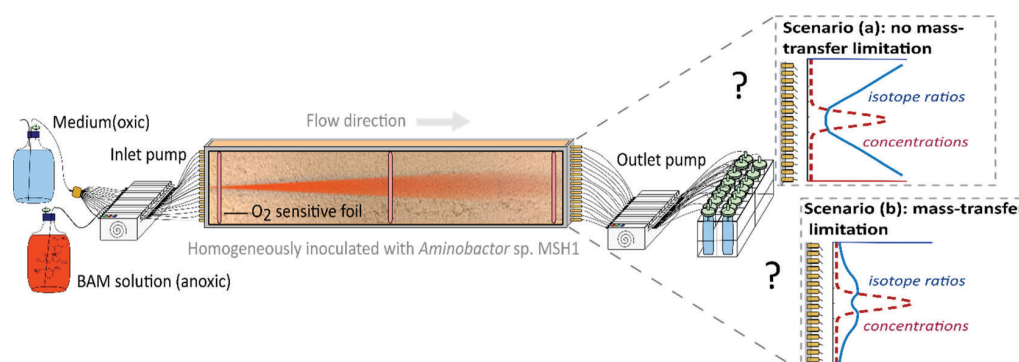


Figure 1. Schematic illustration of the 2-D flow-through sediment tank and expected profiles of isotope ratios at the outlet. Scenario (a): in the absence of mass-transfer limitation, isotope values (blue solid line) are expected to increase strongly with degradation at low concentrations. Scenario (b): with mass-transfer limitation, isotope fractionation would be masked at low concentrations.

from zero- to first-order.^{28,32} Indeed, recent biodegradation experiments of atrazine in chemostats and retentostats showed dramatically decreased isotope fractionation when atrazine concentrations dropped below 30 $\mu\text{g/L}$.^{18,19,33,34}

Thus far, however, this phenomenon has been demonstrated only in well-mixed liquid culture systems (e.g., chemostats,^{19,33,34} retentostats,³³ or batch reactors^{18,25,27,35,36}) where bacteria were suspended at relatively high cell densities in a liquid culture rather than being attached to sediments. In these cultivations, bacteria were either not adapted to low concentrations (e.g., in batch reactors^{18,25,27,35,36}), or they were adapted to low concentrations, but still they experienced a relatively high substrate flux (e.g., in chemostats^{19,33,34}). Hence, insights from these systems are not directly transferable to the physiology of microorganisms in field sediments. There, bacteria are mainly attached to sediments in subsurface environments with contaminant concentrations in groundwater governed by advection and dispersion coupled to the reactive turnover. Under such circumstances, a low extent of isotope fractionation is normally interpreted as evidence of the decreasing degradation rate with depth³⁷ or isotopologue-specific transverse dispersion,^{38,39} where concentration trends are explained by dilution¹³ or heterogeneity of groundwater systems.^{40,41} While mass-transfer limitation due to aquifer heterogeneities is well recognized,^{40–42} the possible relevance of slow transfer through the bacterial cell wall and its influence on observable isotope fractionation is currently overlooked in the evaluation of degradation at field sites. Neglecting mass transfer through the cell wall may overestimate the effect of dilution, dispersion, or heterogeneity on the observed isotope values. More importantly, such slow membrane permeation may constitute an overlooked bottleneck for degradation that could explain the widely observed persistence of organic micropollutants specifically at low concentrations in the environment.

Hence, the question arises whether and at which concentration an onset of mass-transfer limitation into bacterial cells can be observed during biodegradation in porous media under realistic *in situ* conditions. To investigate this phenomenon, sediment-attached degrading bacteria would have to be exposed to different steady-state contaminant concentrations over a longer time so that they can adapt their physiology to prevailing substrate fluxes. Sampling would need to allow for a closed mass balance to determine the true turnover. While pronounced degradation-induced isotope

fractionation would be observable at high concentrations, isotope fractionation may or may not be masked at low concentrations depending on the absence or presence of mass transfer limitations, respectively.

Unfortunately, large-scale studies in natural aquifers lack the high sampling resolution needed for such an in-depth characterization. We therefore set up a two-dimensional (2-D) flow-through sediment microcosm/tank system⁴³ which allowed (i) establishing a closed mass balance with (ii) sufficient sample resolution at the outlet (every 1 cm) to capture the defined steady-state concentrations within gradients, while (iii) allowing us to collect sufficiently large samples over time for compound-specific isotope analysis (CSIA) at low concentrations. By feeding an anoxic pollutant solution into the center port of the tank, and a medium containing dissolved oxygen (DO) above and below, strong transverse concentration cross-gradients of the organic substrate and DO were established. The organic substrate concentration ranged from high values, at the plume center, to low steady-state levels toward the upper and lower boundaries. Under otherwise identical conditions, bacteria could therefore adapt to different steady-state concentrations, with oligotrophic conditions in the upper and lower regions of the tank (Figure 1).

Figure 1 illustrates our targeted hypotheses. Greater changes in isotope values are expected when the fraction of remaining contaminant decreases by degradation. In the plume center, contaminant concentrations are so high that much turnover is needed to significantly decrease the fraction relative to its initial value. Because such a large extent of degradation is limited by the availability of oxygen, only moderate changes in isotope values are expected. In contrast, larger changes in the isotope values could arise at low concentrations toward the upper and lower boundaries of the tank where degradation is not limited by oxygen availability. Here, isotope values are expected to increase strongly with degradation in the absence of mass transfer (Figure 1, scenario a). In contrast, despite ongoing degradation such a trend would not become apparent if mass transfer into the bacterial cell is limiting (Figure 1, scenario b). Hence, the predicted trends can be tested by the observations, where interpretations are supported by mass balance calculations and via a reactive transport model that accounts for mass transfer into bacterial cells, among other factors controlling solute transport and turnover.

To target a particularly relevant scenario, 2,6-dichlorobenzamide (BAM), a metabolite of the herbicides dichlobenil and chlorthiamide, was chosen as a model compound.⁴⁴ BAM has been frequently detected at low concentrations in groundwater, exceeding drinking water guidelines (0.1 $\mu\text{g/L}$) and causing problems for drinking water production in many European countries.^{44–47} The bacterial degrader inoculated here was *Aminobacter* sp. MSH1, an aerobic, Gram-negative, motile bacterium,⁴⁸ exhibiting a documented potential for the purification of BAM-contaminated water in bioaugmented sand filters.^{44,46,49} Furthermore, BAM is highly water soluble ($K_{\text{ow}} = 0.77^{50}$), ruling out sorption to the sediment as a confounding factor.

The primary objective of this study was to investigate whether mass transfer into bacterial cells limits the *in situ* biodegradation of BAM at low substrate concentrations in groundwater. Following the hypotheses of Figure 1, CSIA together with concentration and biomass data were applied to calibrate and validate a reactive transport model. The model, in turn, allowed a quantitative elucidation of the interactions between mass transfer, degradation kinetics, solute transport, and isotope fractionation. In addition, by simultaneously evaluating changes in concentrations and isotope values, the model allowed estimating a threshold concentration range below which biodegradation became strongly limited by mass transfer into the cells.

EXPERIMENTAL SECTION

2-D Flow-Through Sediment-Tank Experiment. We adapted the experimental setup of Bauer et al.⁴³ At the inlet and outlet of the tank, 16 ports (distance: 1 cm) were equally spaced to accurately inject different constituents at specified depths at the inlet and to sample with a high-depth resolution at the outlet. Via depth-resolved sampling at steady state, enough sample volume could be collected at the outlet ports of the tank to enable isotope analysis in a low ($\mu\text{g/L}$) concentration range. The inner dimensions of the domain were 95 cm \times 18 cm \times 1 cm (L \times H \times W), such that the tank represents a quasi-2-D system. A detailed description of the setup is provided in the Supporting Information, as are additional details regarding chemicals, media preparation, and bacterial cultivation.

The water-saturated, sand-packed tank was inoculated with the bacterial strain *Aminobacter* sp. MSH1 by injecting an inoculum containing 1×10^7 cells/mL across all inlet ports, except the central one, at a pumping rate of $45 \pm 2 \mu\text{L}/\text{min}/\text{port}$ for 24 h. During the inoculation, a 50 mg/L anoxic BAM solution was continuously injected at the central inlet port. After inoculation, the flow was stopped for 3 h to give bacteria time to adhere to the sediment. Subsequently, an anoxic 50 mg/L BAM solution was continuously introduced through the central inlet port and an oxic medium solution without an additional carbon or nitrogen source was continuously pumped in through all other inlet ports at a pumping rate of $45 \pm 2 \mu\text{L}/\text{min}/\text{port}$. This initial injection of BAM resulted in transient breakthrough profiles. The system did not reach steady state during the initial period of 4 weeks. Specifically, the biomass exhibited a transient planktonic behavior, which was likely an artifact from previous growth under well-mixed conditions. Consequently, the time period of the 50 mg/L injection was considered as a preliminary injection phase, where bacteria were still undergoing physiological adaptations after their

inoculation, and this initial phase was not considered in the present study.

After 4 weeks, the inlet concentration of BAM was increased to 100 mg/L. The system reached a steady state in the 7th week, that is, 3 weeks after increasing the concentration, as indicated by stable BAM concentrations at the outflow. In this study, *Aminobacter* sp. MSH1 used BAM as the sole source of carbon, nitrogen, and energy. It is well established that in the catalytic breakdown of BAM, hydrolysis of BAM to 2,6-dichlorobenzoic acid (2,6-DCBA) by *Aminobacter* sp. MSH1 is the initial, irreversible step,^{44,51,52} which is associated with a large normal isotope fractionation for both carbon ($\epsilon_{\text{C}} = -7.8 \pm 0.2\text{‰}$) and nitrogen ($\epsilon_{\text{N}} = -13.5 \pm 0.2\text{‰}$).⁵³

For sample collection, the outflow solution was filtered through 0.22 μm syringe filters (Merck KGaA, Germany; filter exchange every 12 h) and pumped into separate sampling vials for each outlet port. The sterilizing filtration can remove the bacteria from the outflow and stop the biodegradation in the solution right after filtration. Samples were collected and stored at $-20 \text{ }^\circ\text{C}$ from week 8 to week 12 and from week 12 to week 16 (where sampling time is in relation to the start time of inoculation). Each sampling period lasted for 30 days until a sufficient sample volume (2 L) was collected at each outlet port to enable CSIA of low substrate concentrations. The Results and Discussion section presents data from this second sampling period.

Carbon and Nitrogen Isotope Analysis of BAM.

Carbon and nitrogen isotope values of BAM were measured on a GC-IRMS system. A DB-5 analytical column (60 m, 0.25 mm i.d., 0.5 μm film, Agilent Technologies, Germany) was used in a TRACE GC Ultra gas chromatograph (Thermo Fisher Scientific, Italy) which was coupled to a Finnigan MAT 253 isotope-ratio mass spectrometer through a Finnigan GC Combustion III interface (Thermo Fisher Scientific, Germany). The typical total uncertainty of carbon isotope measurements is $\pm 0.5\text{‰}$, and the uncertainty of nitrogen isotope measurements is $\pm 1\text{‰}$. The method, including solid-phase extraction before CSIA, is described by Sun et al.⁵⁴ and provided in the Supporting Information.

Concentration Measurements of BAM, DO, ATP, and Total Cell Counts. The concentrations of BAM and 2,6-DCBA were measured every 3–5 days. After solid-phase extraction, measurements were conducted via liquid chromatography tandem mass spectrometry (LC–MS/MS) by adapting the method of Jensen et al.⁵⁵ LC was conducted on an Agilent 1100 HPLC system (Agilent Technologies Inc, USA); MS was performed on a QTrap 4000 system using electrospray ionization (ESI) (Sciex, USA); and separation was carried out on a Kinetex C18 column (2.6 μm , 10 nm, 100 \times 2.1 mm i.d., Phenomenex, USA) at $40 \text{ }^\circ\text{C}$, with 5 mM of ammonium acetate at pH 2.4 as the mobile phase A and acetonitrile as mobile phase B. A detailed method description is provided in the Supporting Information.

DO concentrations were measured daily via oxygen-sensitive polymer optode foils (18 cm \times 0.5 cm; PreSens GmbH, Regensburg, Germany) glued onto the inner side of the tank and read out by a FIBOX2 Fiber-optic oxygen meter (PreSens, Regensburg, Germany). The intracellular ATP concentrations were measured on a Glomax luminometer (Turner Biosystems, Sunnyvale, CA), according to a method adapted from Hammes et al.⁵⁶ For total cell counts, samples were collected every 3–5 days from the outlet ports of the tank, fixed with 2.5% glutaraldehyde, and stored at $4 \text{ }^\circ\text{C}$ in the fridge until

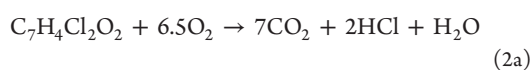
measurement. The samples were stained with SYBR Green I and measured on a Cytomics FC 500 flow cytometer (Beckmann Coulter, Hebron, KY) according to the method of Bayer et al.⁵⁷

Conceptual Model. The model accounts for the possibility of substrate mass transfer through the cell membrane due to passive diffusion driven by concentration differences. The intracellular irreversible hydrolysis of BAM to 2,6-DCBA via an amidase enzyme (Reaction 1) was simulated to follow Michaelis–Menten kinetics (eq 10) and to be the sole step that led to carbon and nitrogen isotope fractionation, resulting in an enrichment of heavy isotopologues of BAM within the cells.⁵³ Subsequently, this enrichment may or may not equilibrate with BAM in the bulk solution depending on the rate of back diffusion through the cell membrane relative to the rate of the enzyme turnover. For the calculation of mass balances, it is assumed that no other reactive intermediates accumulated and that 2,6-DCBA was either degraded to CO₂ via aerobic respiration (Reaction 2a) or utilized for biomass synthesis (C₅H₇O₂N), that is, cell growth (Reaction 2b). All microbially mediated reactions were assumed to take place inside the bacterial cells and, thus, to depend on the kinetics of the mass transfer into the bacterial cells.²⁸

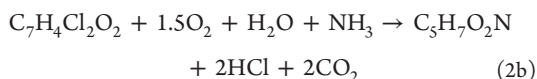
BAM to 2, 6-DCBA:



2, 6-DCBA to CO₂:



2, 6-DCBA to biomass:



Both mobile (planktonic cells) and immobile biomass (cells attached onto the sediment matrix) were considered in the model. Partitioning between mobile and immobile biomass was described by the growth-mediated release of daughter cells and by the first-order attachment of mobile cells onto the sand.⁵⁸ Because the planktonic cells made up only a very small fraction^{58–60} (<5%) of the total biomass in the tank, only the immobile biomass was assumed to be responsible for biodegradation.^{61–65} Biomass was generated by growth from the aerobic degradation of 2,6-DCBA, as parameterized by a dual-Monod kinetic rate expression (eq 12). (Note: Carbon isotope fractionation arising from 2,6-DCBA degradation was not considered in our model formulation because this transformation occurred after the first irreversible step, i.e., the hydrolysis of BAM). Herein, we refer to both Michaelis–Menten kinetics and Monod kinetics interchangeably when referring to saturation-type kinetics, as they are mathematically identical. For rate expressions containing both an electron acceptor and donor dependence, we explicitly state that these are dual-Monod expressions.

Upon the calibration of the model with the experimentally determined high-resolution vertical profiles of concentrations and isotope ratios, we could convert concentration measurements into rates, determine all rate coefficients, and quantify the influence of mass transfer on the reactive turnover at a high

spatial resolution under conditions that mimic field applications.

Governing Equations. The 2-D reactive transport of substrates in the bulk solution, and the mass transfer and reactions inside the cell, coupled to the microbial dynamics in the model are described by the following set of partial differential equations.

In the bulk solution

$$\frac{\partial c_{\text{bulk}}^i}{\partial t} = -\mathbf{v} \cdot \nabla c_{\text{bulk}}^i + \nabla \cdot (\mathbf{D} \cdot \nabla c_{\text{bulk}}^i) - r_{\text{mt}}^i \frac{X^{\text{im}}}{\rho_{\text{bio}}} \quad (3)$$

$$\frac{\partial X^{\text{mob}}}{\partial t} = -\mathbf{v} \cdot \nabla X^{\text{mob}} + \nabla \cdot (\mathbf{D} \cdot \nabla X^{\text{mob}}) + r_{\text{daughter}} - r_{\text{attach}} \quad (4)$$

$$\frac{\partial X^{\text{im}}}{\partial t} = r_{\text{growth}}^{\text{im}} - r_{\text{daughter}} + r_{\text{attach}} \quad (5)$$

Inside the bacterial cell

$$\frac{\partial c_{\text{int}}^{\text{BAM}}}{\partial t} = l_{\text{mt}}^{\text{BAM}} - l_{\text{deg}}^{\text{BAM}} \quad (6)$$

$$\frac{\partial c_{\text{int}}^{\text{DCBA}}}{\partial t} = r_{\text{mt}}^{\text{DCBA}} + l_{\text{deg}}^{\text{BAM}} + h_{\text{deg}}^{\text{BAM}} - r_{\text{deg}}^{\text{DCBA}} \quad (7)$$

$$\frac{\partial c_{\text{int}}^{\text{O}_2}}{\partial t} = r_{\text{mt}}^{\text{O}_2} - r_{\text{deg}}^{\text{O}_2} \quad (8)$$

in which c_{bulk}^i [$\mu\text{mol L}^{-1}$] is the concentrations of substrate i (heavy or light isotopologues of BAM, 2,6-DCBA, or oxygen) in the bulk solution; X^{mob} [$\mu\text{mol}_{\text{bio}} \text{L}^{-1}$] is the mobile biomass concentration; X^{im} [$\mu\text{mol}_{\text{bio}} \text{L}^{-1}$] is the immobile biomass concentration; $l_{\text{mt}}^{\text{BAM}}$ [$\mu\text{mol}_{\text{bio}} \text{L}^{-1} \text{s}^{-1}$] is the intracellular concentration of light and heavy BAM isotopologues, respectively; $c_{\text{int}}^{\text{DCBA}}$ [$\mu\text{mol L}^{-1}$] and $c_{\text{int}}^{\text{O}_2}$ [$\mu\text{mol L}^{-1}$] are the intracellular concentrations of 2,6-DCBA and oxygen, respectively; \mathbf{D} [$\text{m}^2 \text{s}^{-1}$] is the dispersion tensor of different substrates and mobile biomass, respectively; \mathbf{v} [m s^{-1}] is the velocity vector; r_{mt}^i [$\mu\text{mol L}_{\text{cell}}^{-1} \text{s}^{-1}$] is the mass-transfer rate of each substrate through the cell membrane; r_{daughter} [$\mu\text{mol}_{\text{bio}} \text{L}^{-1} \text{s}^{-1}$] is the growth-dependent detachment rate; r_{attach} [$\mu\text{mol}_{\text{bio}} \text{L}^{-1} \text{s}^{-1}$] is the bacterial attachment rate; $l_{\text{deg}}^{\text{BAM}}$ [$\mu\text{mol}_{\text{bio}} \text{L}_{\text{int}}^{-1} \text{s}^{-1}$] is the intracellular hydrolysis rate of either the heavy ($l_{\text{deg}}^{\text{BAM}}$) or the light ($l_{\text{deg}}^{\text{BAM}}$) isotopologue of BAM to 2,6-DCBA; $r_{\text{deg}}^{\text{DCBA}}$ [$\mu\text{mol L}_{\text{int}}^{-1} \text{s}^{-1}$] is the intracellular degradation rate of 2,6-DCBA; $r_{\text{deg}}^{\text{O}_2}$ [$\mu\text{mol L}_{\text{int}}^{-1} \text{s}^{-1}$] is the consumption rate of oxygen during the degradation of 2,6-DCBA; and ρ_{bio} [$\mu\text{mol}_{\text{bio}} \text{L}_{\text{int}}^{-1}$] is the molar density of the bacteria, which is defined as biomass (M_{cell} [$\mu\text{mol}_{\text{bio}}$]) per bacterial cell volume (V_{cell} [L_{int}]).

The mass-transfer rate r_{mt}^i of each substrate through the bacterial cell membrane from the bulk solution to the location of the enzymes is approximated via a linear-driving force model⁶⁶

$$r_{\text{mt}}^i = k_{\text{tr}}^i (c_{\text{bulk}}^i - c_{\text{int}}^i) \quad (9)$$

in which k_{tr}^i [s^{-1}] is the first-order mass-transfer coefficient of compound i for diffusion into and out of the cell. We assumed that the mass-transfer coefficients of heavy and light isotopologues of BAM are identical due to the negligible difference of their diffusion coefficients.⁵⁴ In the presence of BAM, the intermediate product 2,6-DCBA is transformed

inside the bacterial cell, such that the direction of the mass transfer of 2,6-DCBA is in the opposite direction.

The hydrolysis of both the heavy and light isotopologues of BAM to 2,6-DCBA inside the cell follows Michaelis–Menten kinetics⁵²

$$l_{r_{\text{deg}}}^{\text{BAM}} = r_{\text{max}}^{\text{hydro}} \cdot \frac{l_{c_{\text{int}}}^{\text{BAM}}}{c_{\text{int}}^{\text{BAM}_{\text{total}}} + K_{\text{m}}^{\text{BAM}}} \quad (10)$$

$$h_{r_{\text{deg}}}^{\text{BAM}} = \alpha \cdot r_{\text{max}}^{\text{hydro}} \cdot \frac{h_{c_{\text{int}}}^{\text{BAM}}}{c_{\text{int}}^{\text{BAM}_{\text{total}}} + K_{\text{m}}^{\text{BAM}}} \quad (11)$$

in which $r_{\text{max}}^{\text{hydro}}$ [$\mu\text{mol L}_{\text{int}}^{-1} \text{s}^{-1}$] is the maximum hydrolysis reaction rate and $K_{\text{m}}^{\text{BAM}}$ [$\mu\text{mol L}_{\text{int}}^{-1}$] is the half-saturation constant. During the hydrolysis reaction of BAM, 2,6-DCBA is produced inside the cell. The fractionation coefficient α [-] describes the ratio of the pseudo first-order rate coefficient

$i_{\text{deg}}^{\text{BAM}}/i_{\text{int}}^{\text{BAM}}$ between the heavy and the light isotopologues. The fractionation may either be caused by differences between the isotopologues in the maximum hydrolysis rate, or by differences in the half-saturation concentration.

The rate of 2,6-DCBA degradation, $r_{\text{deg}}^{\text{DCBA}}$ [$\mu\text{mol L}_{\text{int}}^{-1} \text{s}^{-1}$], was parameterized as a dual-Monod kinetic rate expression

$$r_{\text{deg}}^{\text{DCBA}} = \mu_{\text{max}} \cdot \frac{\rho_{\text{bio}}}{Y} \cdot \frac{c_{\text{int}}^{\text{DCBA}}}{K_{\text{m}}^{\text{DCBA}} + c_{\text{int}}^{\text{DCBA}}} \cdot \frac{c_{\text{int}}^{\text{O}_2}}{K_{\text{m}}^{\text{O}_2} + c_{\text{int}}^{\text{O}_2}} \quad (12)$$

in which the maximum degradation rate of 2,6-DCBA inside the cell is expressed as $\mu_{\text{max}} \rho_{\text{bio}}/Y$, μ_{max} [s^{-1}] is the specific growth rate of the bacteria, Y [$\mu\text{mol}_{\text{bio}} \mu\text{mol}^{-1}$] is the growth yield coefficient, and $K_{\text{m}}^{\text{DCBA}}$ and $K_{\text{m}}^{\text{O}_2}$ [$\mu\text{mol L}_{\text{int}}^{-1}$] are the half-saturation constants of 2,6-DCBA and O_2 , respectively.

The total transformation of 1 mol of BAM to CO_2 needs 6.5 mol O_2 (Reaction 2a) and the total transformation from 1 mol BAM to biomass ($\text{C}_5\text{H}_7\text{O}_2\text{N}$) requires 1.5 mol O_2 (Reaction 2b). Thus, the specific stoichiometric ratio for O_2 to degrade 2,6-DCBA to CO_2 was computed from a linear combination of both reactions

$$p = 6.5 - 5Y \quad (13)$$

in which p is the effective stoichiometric coefficient for O_2 . Thus, the oxygen consumption rate $r_{\text{deg}}^{\text{O}_2}$ [$\mu\text{mol L}_{\text{int}}^{-1} \text{s}^{-1}$] is

$$r_{\text{deg}}^{\text{O}_2} = p \cdot r_{\text{deg}}^{\text{DCBA}} \quad (14)$$

The growth rate of immobile biomass $r_{\text{growth}}^{\text{im}}$ [$\mu\text{mol}_{\text{bio}} \text{L}^{-1} \text{s}^{-1}$] depends on the biodegradation rate of 2,6-DCBA $r_{\text{deg}}^{\text{DCBA}}$, immobile biomass in the bulk solution X^{im} [$\mu\text{mol}_{\text{bio}} \text{L}^{-1}$], cell density ρ_{bio} , and yield coefficient Y ,

$$r_{\text{growth}}^{\text{im}} = r_{\text{deg}}^{\text{DCBA}} \cdot \frac{X^{\text{im}}}{\rho_{\text{bio}}} \cdot Y \quad (15)$$

r_{daughter} [$\mu\text{mol}_{\text{bio}} \text{L}^{-1} \text{s}^{-1}$] is the growth-dependent detachment rate. The release of daughter cells r_{daughter} depends on the proximity of the attached cell concentration X^{im} to the maximum carrying capacity X_{max} [$\mu\text{mol}_{\text{bio}} \text{L}^{-1}$]. Thus, as the attached population approaches its maximum capacity, all newly produced cells (via growth) are effectively expelled into the mobile phase

$$r_{\text{daughter}} = r_{\text{growth}}^{\text{im}} \cdot \left(\frac{X^{\text{im}}}{X_{\text{max}}} \right) \quad (16)$$

In addition, we assumed that only new grown cells can detach and there was no detachment due to mortality. The adhesion of the planktonic bacteria onto the sediment is represented as the attachment rate r_{attach}

$$r_{\text{attach}} = k_{\text{att}} \cdot X^{\text{mob}} \cdot \left(1 - \frac{X^{\text{im}}}{X_{\text{max}}} \right) \quad (17)$$

in which k_{att} [s^{-1}] is the first-order rate coefficient for attachment. With increasing attachment, the corresponding reduction in carrying capacity (or maximum allowable attached biomass concentration) was assumed to inhibit the attachment rate via: $(1 - X^{\text{im}}/X_{\text{max}})$.

The isotope ratio of the heavy and light isotopologues of BAM was evaluated by

$$\delta_{\text{sample}} = \frac{R_{\text{sample}} - R_{\text{standard}}}{R_{\text{standard}}} = \frac{R_{\text{sample}}}{R_{\text{standard}}} - 1 \quad (18)$$

in which R_{sample} is the ratio of heavy to light isotopologues of the substrate ($^h\text{c}/^l\text{c}$) and R_{standard} is the reference isotope ratio.

The standard model to predict changes in isotope ratios is the Rayleigh equation^{67,68}

$$\frac{(^h\text{c}/^l\text{c})_t}{(^h\text{c}/^l\text{c})_0} = \frac{R_t}{R_0} = \frac{\delta^{13}\text{C}_t + 1}{\delta^{13}\text{C}_0 + 1} = f^{\alpha-1} = f^\varepsilon \quad (19)$$

in which isotope values at time zero, $\delta^{13}\text{C}_0$, and time t , $\delta^{13}\text{C}_t$, are linked to the remaining substrate concentration fraction f by $\varepsilon = \alpha - 1$.⁵ The Rayleigh model, however, requires that the isotope fractionating step of a reaction is also the rate-limiting one. Hence, we do not expect that the Rayleigh model holds in the given setup over the whole concentration range if mass transfer becomes limiting at low concentrations, as shown in Figure 1, scenario b.

Numerical Method. The coupled system of equations for the multidimensional reactive transport was solved in MATLAB following the approach of Eckert et al.⁶² and Mellage et al.⁵⁸ in which the spatial discretization was done by the cell-centered Finite Volume Method ($\Delta z = 0.001$ m and $\Delta x = 0.01$ m) with the upwind differentiation of the advective term, and physical transport was coupled to the reactions via a global implicit approach. The Newton–Raphson method was applied to linearize the system of equations. The experiment was simulated with an adaptive time stepping.

RESULTS AND DISCUSSION

Stoichiometry of Bacterial Growth and Model Fit.

Figure 2 shows the quasi-steady-state profiles with a 100 mg/L BAM inlet concentration at the center port (from week 12 to week 16). The concentration of each species (Figures 2 and 3) was adequately simulated using the calibrated parameters (Table S2) of the reactive transport model, which reached steady state after a simulated time of 17 days (Figure S2). Steep oxygen concentration gradients showed that oxygen was limiting in the plume center, where BAM and 2,6-DCBA concentrations were highest. In contrast, high oxygen concentrations evidenced sufficient O_2 supply for aerobic BAM degradation at the plume fringes. A mass balance of the measured concentrations gave a reduction of the total mass flux of BAM from $34.1 \pm 1.5 \mu\text{mol}/\text{d}$ in the inlet to $6.2 \pm 1.6 \mu\text{mol}/\text{d}$ in the outlet (total reduction by 82%). Concurrently, fluxes of total DO decreased from $237 \pm 12 \mu\text{mol}/\text{d}$ at the inlet to $151 \pm 5 \mu\text{mol}/\text{d}$ at the outlet and $14.9 \pm 2.3 \mu\text{mol}/\text{d}$

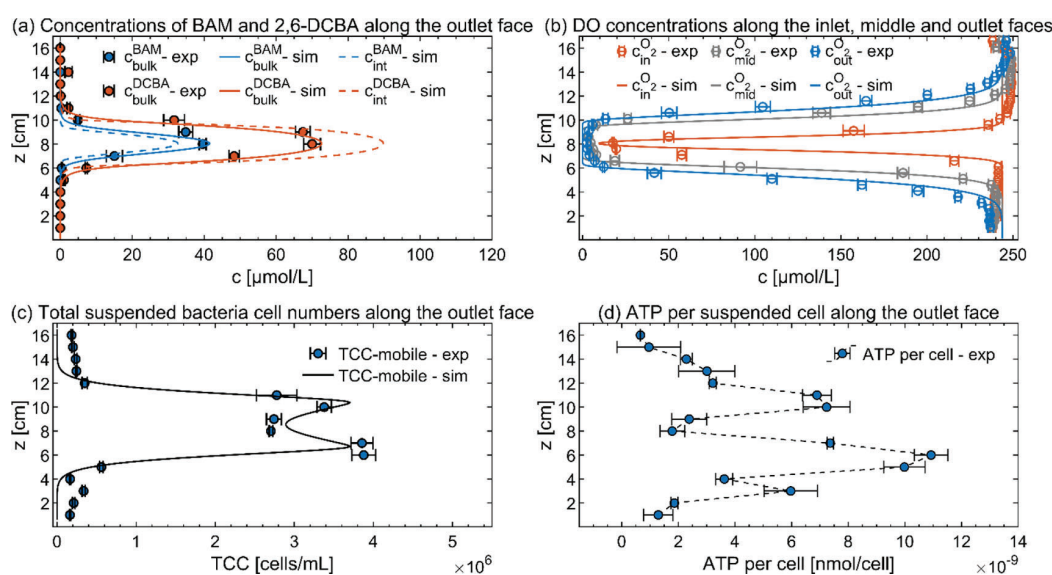


Figure 2. Experimental and simulated concentrations of (a) BAM and 2,6-DCBA in the bulk solution (circles with error bars, solid lines) and inside the cell (dashed lines) along the outlet vertical face, (b) oxygen in the bulk solution along the vertical inlet, middle, and outlet faces, (c) total suspended bacterial (mobile) cell numbers at the outlet ports, and (d) ATP per cell calculated by dividing the measured total ATP by the total suspended bacterial cell number at the outlet ports. Error bars represent the standard errors of measurements during the sampling period in a quasi-steady state.

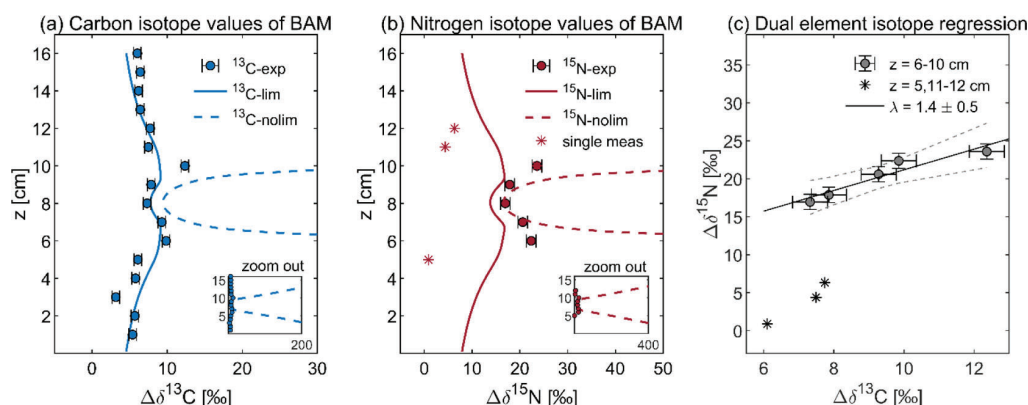


Figure 3. Carbon and nitrogen isotope values of BAM at the outlet of the tank for a BAM inlet concentration of 100 mg/L. $\Delta\delta^{13}\text{C}$ and $\Delta\delta^{15}\text{N}$ represent the carbon- and nitrogen isotope value difference between the outlet samples and the BAM inlet solution. Panels (a) and (b): $\Delta\delta^{13}\text{C}$ and $\Delta\delta^{15}\text{N}$ profiles along the outlet face. Solid lines and dashed lines represent the simulated isotope values with and without the assumption of mass-transfer limitations, respectively. Asterisk symbols represent the data of one-time measurements due to the limited analyte mass at low concentrations, which were not considered for modeling (panel b) and regression (panel c). A dual element isotope plot ($\Delta\delta^{13}\text{C}$ vs $\Delta\delta^{15}\text{N}$), with 95% confidence intervals, is shown in panel (c). Error bars represent the instrument uncertainties of $\pm 0.5\%$ for carbon isotope measurements and of $\pm 1\%$ for nitrogen isotope measurements.

out of the produced 2,6-DCBA were not further degraded but reached the outlet, likely because of depleted DO at the plume center. Estimated conversion rates from BAM to 2,6-DCBA were $27.9 \pm 1.2 \mu\text{mol/d}$ and from 2,6-DCBA to biomass and CO_2 were $13.0 \pm 0.6 \mu\text{mol/d}$, resulting in a molar ratio of oxygen to converted 2,6-DCBA of 6.6. This is close to the stoichiometric factor of 6.5 for oxygen in Reaction 2a suggesting that the consumed 2,6-DCBA was primarily used for respiration rather than for growth. Independently, a fitted yield coefficient Y of 0.24 could be derived from the reactive transport model (Table S2), which implies that 24% of the transformed 2,6-DCBA was used in biomass growth whereas 76% was respired, resulting in a stoichiometry of oxygen to 2,6-DCBA of 5.3 (eq 13). While both results confirm that

respiratory- and maintenance-driven carbon consumptions were greater than carbon assimilation via growth, the reactive transport model considers additional biomass data so that the value of 5.3 is more reliable to represent the effective stoichiometry of the catabolic reaction.

Even though biomass was depleted at the upper and lower boundaries of the tank, where BAM and 2,6-DCBA concentrations were the lowest ($< 0.1 \mu\text{mol/L}$), suspended cell concentrations from 1×10^5 to 5×10^5 cells/mL cells were continuously detected in outflow samples. This continuous outwash may be explained by: (i) trace dissolved organic carbon or nitrogen contained in the medium solution that may have provided an additional low-level source of carbon and

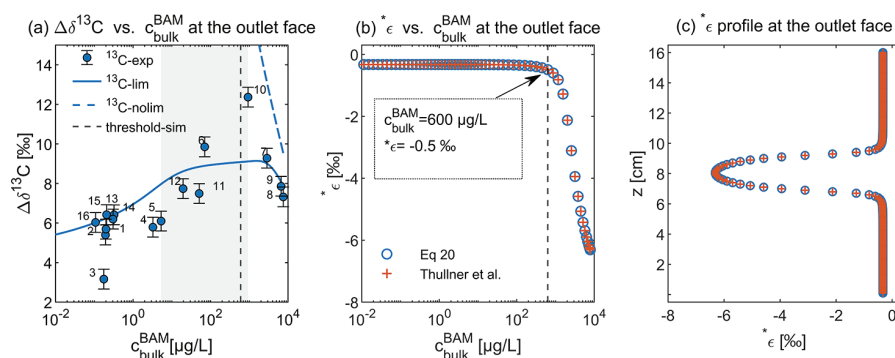


Figure 4. Threshold concentration for mass-transfer limitation determined by the distribution curve of the observed carbon isotope values $\Delta\delta^{13}\text{C}$, and the simulated apparent enrichment factor $^*\epsilon$. (a) Carbon isotope fractionation plotted against the BAM bulk concentration in the outlet. Blue solid lines and dashed lines represent the simulated isotope values with and without the assumption of mass-transfer limitations, respectively. Measured data were labeled with the position of each outlet port ($z = 1\text{--}16$ cm). The gray zone represents the estimated threshold concentration range where the observed isotope values indicate the influence of mass-transfer limitations. (b) Simulated apparent enrichment factor $^*\epsilon$ based on eq 20 (circles) and Thullner et al. (plus signs, eq S29) vs the corresponding bulk concentration and (c) along the outlet vertical profile. The vertical black dashed lines in panels (a) and (b) represent a simulated BAM threshold concentration of $600 \mu\text{g/L}$ ($^*\epsilon = -0.5\text{‰}$).

nitrogen for bacterial growth^{61,69} and/or (ii) some washed-out cells were remnants of the initial inoculation.

Evidence of High Cell Activity at the Plume Fringes.

The distribution pattern of the suspended bacterial cell numbers informs about the adaptation of the degrader strain *Aminobacter* sp. MSH1 to different concentrations along the concentration profile (Figure 2). At the plume fringes, the breakthrough of the suspended cells [$(3.38 \pm 0.36) \times 10^6$ cells/mL to $(3.88 \pm 0.60) \times 10^6$ cells/mL] and the ATP concentrations [$(7.2 \pm 1.4) \times 10^{-9}$ nmol/cell to $(10.9 \pm 1.0) \times 10^{-9}$ nmol/cell] were the highest, indicating that biodegradation was most active where BAM and oxygen were well mixed via transverse dispersion (Figure 2c,d). In contrast, at the center of the plume, the comparatively lower bacterial cell numbers indicated that degradation was limited by the depletion of the electron acceptor (i.e., oxygen). This is supported by the observation that although a large number of cells [$(2.70 \pm 0.09) \times 10^6$ cells/mL] were washed out from the center of the plume, the measured ATP of those cells [$(1.78 \pm 0.75) \times 10^{-9}$ nmol/cell] was lower than the ATP at the fringes [$(1.09 \pm 0.10) \times 10^{-8}$ nmol/cell] (Figure 2d).

Mass-Transfer Limitation Revealed by Decreased Isotope Fractionation. Figure 3 shows the experimental and simulated profiles of carbon and nitrogen isotope values of BAM in the form of the differences in $\delta^{13}\text{C}$ and $\delta^{15}\text{N}$ values between the outlet and the inlet of the tank. The dual-element isotope plot of $\Delta\delta^{13}\text{C}$ vs $\Delta\delta^{15}\text{N}$ (Figure 3c) shows a slope λ of 1.4 ± 0.5 , which is consistent with a value of 1.75 ± 0.03 expected for bacterial BAM hydrolysis reported by Reinicke et al.⁵³ We experimentally observed the strongest changes in isotope values ($\Delta\delta^{13}\text{C}$ values between 9.3 ± 0.5 and $12.4 \pm 0.5\text{‰}$, $\Delta\delta^{15}\text{N}$ values between 21 ± 1 and $24 \pm 1\text{‰}$) at the fringes where the electron donor and acceptor were mixed, bacterial activity was high (see Figure 2), and BAM concentrations ranged from $0.4 \pm 0.6 \mu\text{mol/L}$ to $15 \pm 9 \mu\text{mol/L}$ ($z = 6, 7$ and 10 cm). In contrast, and as expected, the center of the plume ($z = 8$ cm and $z = 9$ cm) showed comparatively small changes in isotope values ($\Delta\delta^{13}\text{C} = 7.3 \pm 0.5$ and $7.9 \pm 0.5\text{‰}$, $\Delta\delta^{15}\text{N} = 17 \pm 1$ and $18 \pm 1\text{‰}$). Here, biodegradation was limited by the lack of the electron acceptor (i.e., oxygen).

At the upper and lower boundaries of the plume, where the electron acceptor was in excess, the residual BAM concentrations were $0.1\text{--}50 \mu\text{g/L}$ ($z = 1\text{--}5, 11\text{--}16$ cm), corresponding to the concentrations at which BAM is often detected in groundwater across Europe.^{44–47} In these zones, where BAM concentrations decreased most strongly, isotope values did not strongly increase but rather decreased significantly. This was contrary to the expected behavior depicted in Figure 1, scenario (a), and to the simulation results in the absence of mass transfer (dashed lines in Figure 3a,b). The drop in δ -values at low concentrations was accurately reproduced by our model that considered the mass transfer of the substrate into and out of the bacteria (solid lines in Figure 3a,b corresponding to the predictions in Figure 1, scenario (b)). Thus, both experimental and simulated results indicate that mass transfer through the cell membrane masked the isotope fractionation at low concentrations in the flow-through porous-media system. This is consistent with the hypothesis of concentration-dependent mass transfer limitation predicted by Thullner et al.,^{27,28} and the observation that atrazine isotope fractionation was masked at low concentrations in batch and chemostat experiments.^{18,19}

Mass Transfer of BAM Through the Cell Membrane. If the substrate supply into the cell is rate limiting, the intracellular substrate will be used up, resulting in smaller concentrations compared to the concentrations outside at steady state. At high surrounding concentrations in the plume center, when the enzyme reaction was still the rate-determining step, model predictions imply that this intracellular substrate depletion was not yet strongly pronounced. The simulated intracellular BAM concentration still reached 80% of the bulk-phase concentration (Figure S3c), and the isotope fractionation of BAM observed in the bulk phase largely reflected the fractionation by the enzyme. In contrast, at low bulk concentrations, where mass transfer through the cell membrane was the limiting factor (Figure 3a), model simulations predicted a much steeper concentration gradient across the cell membrane so that the simulated intracellular BAM concentration made up only 4% of the surrounding bulk-phase concentration (Figure S3c).

The model simulations resulted in a well-constrained mass transfer coefficient of BAM of $7.6 \pm 0.5 \text{ s}^{-1}$, which can be

converted (eq S1) to an estimated apparent permeation coefficient P_{app}^{BAM} of $(1.1 \pm 0.1) \times 10^{-6} \text{ m s}^{-1}$ that describes how fast BAM permeates through the two lipid bilayers of the cell wall. P_{app} is proportional to the effective membrane diffusion coefficient D_{mem} and the lipid–water distribution coefficient K_{lipw} .⁷⁰ Compared to the permeation coefficient derived for mass transfer of atrazine through the cell membrane of *Arthrobacter aureus* TC1, $P_{app}^{atrazine} = 3.5 \times 10^{-5} \text{ m s}^{-1}$, the smaller permeation coefficient of BAM is likely attributable to a smaller lipid–water distribution coefficient ($K_{lipw}^{BAM} = 11$ vs $K_{lipw}^{atrazine} = 741$).¹⁹ Hence, BAM does not penetrate as easily through the lipid membrane because it is more hydrophilic than atrazine. In contrast, the modeled effective membrane diffusion coefficients agree within one order of magnitude ($D_{mem}^{BAM} = (1.0 \pm 0.1) \times 10^{-15} \text{ m}^2 \text{ s}^{-1}$ vs $D_{mem}^{atrazine} = 1.9 \times 10^{-16} \text{ m}^2 \text{ s}^{-1}$),¹⁹ which is in very good agreement considering that different organisms with different cell walls were involved.

In Which Concentration Range Does a Mass-Transfer Limitation Appear? To estimate the concentration range in which mass transfer became limiting, we plotted the changes in carbon isotope values against the concentrations of BAM and visually assessed the concentration at which the carbon isotope fractionation became strongly masked (Figure 4a). The experimental data suggested a BAM threshold range between 5.3 ± 7.6 and $70 \pm 112 \mu\text{g/L}$ ($z = 5\text{--}6 \text{ cm}$) in the lower region of the plume and a threshold range between 51 ± 78 and $900 \pm 400 \mu\text{g/L}$ ($z = 10\text{--}11 \text{ cm}$) in the upper region of the plume (grey zone in Figure 4a). To quantitatively analyze the masked isotope fractionation due to mass transfer limitation, we calculated the apparent carbon isotope fractionation enrichment factor ϵ^* based on eq 20 (derivation is provided in the Supporting Information) which is analogous to the expression brought forward by Thullner et al.²⁸

$$\begin{aligned} \epsilon^* = \alpha^* - 1 = & \alpha_0 \left[c_{bulk}^{BAM} + K_m^{BAM} + \frac{r_{max}^{hydro}}{k_{tr}^{BAM}} \right. \\ & + \sqrt{\left(c_{bulk}^{BAM} - K_m^{BAM} - \frac{r_{max}^{hydro}}{k_{tr}^{BAM}} \right)^2 + 4c_{bulk}^{BAM} \cdot K_m^{BAM}} \\ & \left. \left/ \left[c_{bulk}^{BAM} + K_m^{BAM} + (2\alpha_0 - 1) \frac{r_{max}^{hydro}}{k_{tr}^{BAM}} \right] \right. \\ & \left. + \sqrt{\left(c_{bulk}^{BAM} - K_m^{BAM} - \frac{r_{max}^{hydro}}{k_{tr}^{BAM}} \right)^2 + 4c_{bulk}^{BAM} \cdot K_m^{BAM}} \right] - 1 \end{aligned} \quad (20)$$

With fitted values of r_{max}^{hydro} ($67.3 \pm 1.3 \mu\text{mol L}_{cell}^{-1} \text{ s}^{-1}$), K_m^{BAM} ($0.38 \pm 0.03 \mu\text{mol L}_{int}^{-1}$), and k_{tr}^{BAM} ($7.6 \pm 0.5 \text{ s}^{-1}$) and a fixed enzymatic fractionation factor α_0 of 0.992 ($\epsilon_0 = -8\text{‰}$),⁵³ the calculated value of ϵ^* in the outflow was in the range between -6.3 and -0.33‰ (Figure 4b,c). The turning point at which $|\epsilon^*| \leq 0.5\text{‰}$ was at a bulk concentration value of $600 \mu\text{g/L}$ (Figure 4b), which was in agreement with the observed threshold range between 51 ± 78 and $900 \pm 400 \mu\text{g/L}$ ($z = 10\text{--}11 \text{ cm}$). In this threshold range, mass transfer would start to become strongly limiting, as evidenced by masked isotope fractionation. This estimated threshold concentration value of

$600 \mu\text{g/L}$ was somewhat higher than the fitted K_m^{BAM} ($72 \pm 6 \mu\text{g L}_{int}^{-1}$) and a reported K_m of BAM in the literature ($K_m = 135 \pm 17 \mu\text{g/L}$),⁵² which is consistent with the prediction that the threshold domain may extend over a certain range because masking is predicted to depend on the magnitude of several rate parameters relative to each other (i.e., K_m^{BAM} , r_{max}^{hydro} , and k_{tr}^{BAM}).²⁸ Even at a relatively high substrate concentration of $8000 \mu\text{g/L}$, the enzymatic fractionation factor was already masked with $\epsilon^* = -6.3\text{‰}$, which was comparable to the observed reduced atrazine isotope fractionation factor of atrazine hydrolysis with $\epsilon^* = -3.5\text{‰}$ at an atrazine concentration of $4000 \mu\text{g/L}$.¹⁸

Implications for Interpretation of Isotope Fractionation to Assess Biodegradation in Field Studies. The recognition of cellular mass transfer as a limiting factor in field settings has implications for both interpretations of isotope fractionation and the understanding of bottlenecks in micropollutant degradation. For the interpretation of isotope fractionation at contaminated sites, mass transfer on the cellular level has received little attention thus far. Instead, the Rayleigh equation has been extended to explain cases of small isotope fractionation by introducing different additional factors: (a) variable degradation rates,⁷¹ (b) diffusion- or dispersion-induced isotope fractionation,^{38,39} (c) an isotopic interference from mixing by dispersion or from secondary sources,^{72,73} and (d) the diminishing effect of a mixing-controlled transport process,^{13,42,74} or other physical and chemical heterogeneity.^{40,41}

- Regarding variable degradation rates, Wanner and Hunkeler observed decreased changes in carbon isotope ratios with depth in contaminated clay, which were explained by a nonuniform, depth-dependent degradation rate due to nutrient availability in the aquitard.³⁷ Our results suggest that mass-transfer limitation by cell–wall permeation could provide an alternative explanation.
- As per dispersion, several studies have assumed that isotopologue-specific transverse dispersion may explain isotope patterns observed in transverse profiles of steady-state plumes.^{38,39} In contrast, recent work from our lab demonstrates that diffusion- and transverse dispersion-induced isotope fractionation of BAM at natural isotopic abundance in a 2-D flow-through sediment system is negligible.⁵⁴ Diffusion- and transverse dispersion-induced isotope enrichment factors ϵ were smaller than -0.4‰ , and changes in carbon and nitrogen isotope values were within ± 0.5 and $\pm 1\text{‰}$, respectively. Thus, isotope effects of the dispersion can be excluded as an explanation of the observed isotope patterns in the present study.
- With regard to mixing with a secondary source, Prommer et al.⁷² observed muted carbon isotope fractionation of toluene with decreasing toluene concentration at a tar oil-contaminated field site. The failure to detect strong changes in the isotope gradient at low concentrations was explained as the combined result of the additional dissolution of fresh toluene that would dwarf any degradation-induced changes, and a lack of degradation. Muted isotope fractionation was also reported for N_2O when tracing microbial N_2O production and consumption, where Wenk et al.⁷³ observed significantly weaker N and O isotope effects

than expected in lake basins at $N_2O < 80 \mu\text{mol/L}$. Therein, the interference from sedimentary N_2O consumption or production was considered as the potential reason. Alternatively, our study brings forward mass-transfer limitation at the cellular level as a possible explanation.

- (d) When mass transfer is considered, aquifer heterogeneity is commonly assumed to be the main factor during the reactive transport of contaminants. Druhan and Maher⁴² simulated diminished isotope fractionation by describing the reactive transport with a travel time distribution as a modifying factor in the Rayleigh equation. Our results show that observable isotope fractionation can be strongly masked by membrane mass transfer even in a homogeneous system.

Our findings are, however, in line with the work on microbial sulfate reduction, where studies^{22,75–77} converge to a balance between the mass transfer of sulfate through the cell membrane and net sulfate respiration rates, with decreasing isotope fractionation at decreasing extracellular sulfate levels.^{7,8,22,30,31} Wing and Halevy⁸ combined kinetic sulfur isotope fractionation, selective sulfate uptake, and equilibrium between extracellular and intracellular sulfur pools. Our model, in contrast, suggests that isotope fractionation may not decrease linearly with concentrations—as conceptualized by Wing and Halevy⁸ and implemented by Crowe et al.³¹—but would follow a steeper decline within a narrower range as defined by Michaelis–Menten enzyme kinetics, as hypothesized by Habicht et al.³⁰

To further highlight the impact of mass transfer through the cell membrane, Figure 5b compares simulations using the Rayleigh equation (red solid line) and simulations from a reactive transport model with (blue solid line) and without (blue dashed line) cellular mass transfer. According to Figure 5b, a direct application of the Rayleigh equation at low remaining concentrations would significantly underestimate the extent of degradation. Even reactive transport modeling without the mass-transfer limitation on the cellular level would fail to explain the extent by which observable isotope fractionation was diminished at low concentrations. This illustrates that it is important to consider mass transfer at the cellular level in reactive transport models.

Implications for Bacterial Adaptation to Biodegradation at Low Concentrations. Figure 5a reveals three different concentration regimes that give rise to different limitations and adaptations of bacterial activity. In regime (i), where BAM concentrations were higher than the threshold of around $600 \mu\text{g/L}$ ($z = 7–10 \text{ cm}$, blue data points in Figure 5a) isotope fractionation followed a trend close to Rayleigh-type isotope fractionation, indicating an unlimited substrate supply into the cells. In regime (ii), at the plume fringes ($z = 6$ and 11 cm , green data points in Figure 5a), the combination of lower concentrations and higher biomass created a constellation in which mass transfer became limiting and isotope fractionation started to become masked. When moving further toward the low-concentration regime ($z = 5, 11–13 \text{ cm}$) isotope values continued to decline due to the mass-transfer limitation. In regime (iii), when substrate concentrations became even lower ($z = 1–4, 14–16 \text{ cm}$, purple data points in Figure 5a), changes in isotope values remained equally small. At the same time, however, the remaining concentration fraction f was higher corresponding to a smaller extent of degradation. Therefore,

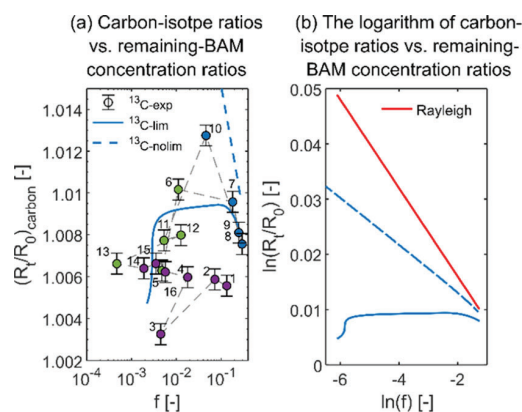


Figure 5. (a) $\Delta\delta^{13}\text{C}$ plotted against the remaining fraction of BAM in the bulk solution after normalization to conservative transport concentrations $f(z) = c_{\text{react}}(z)/c_{\text{conservative}}(z)$. Measured data were labeled with the position of each outlet port ($z = 1–16 \text{ cm}$, from the lower to upper boundary). Regime (i) (blue data points) represents $\Delta\delta^{13}\text{C}$ with none-to-little mass-transfer limitation; Regime (ii) (green data points) represents $\Delta\delta^{13}\text{C}$ with strong mass-transfer limitation; Regime (iii) (purple data points) represents $\Delta\delta^{13}\text{C}$ with the combined effect of strong mass-transfer limitation and physiological limitation. Panel (b) represents the relation between $\ln(f)$ and $\ln(R_t/R_0)$. The blue solid line represents the simulated trend in isotope ratios when considering both dispersion and mass-transfer limitations on the cellular level. The blue dashed line neglects the cellular mass transfer but accounts for the effect of the dispersion on degradation-induced isotope ratio gradients. The red solid line represents the classical Rayleigh relation that would be observed in a well-mixed experimental batch with $\epsilon^{\text{carbon}} = -8\text{‰}$.

these greater values of f indicated a slowdown of biodegradation, which may point to physiological adaptation or decreased biomass at such lower concentrations. Given that in this very low-concentration region bacteria were less metabolically active,⁶¹ degradation was likely not only mass-transfer limited but in addition limited by subsequent bacterial adaptation. The reactive transport model (solid blue line in Figure 5a) accurately simulated the trend in f values and the decrease of isotope values in regime (i) and (ii). However, because the model did not include bacterial adaptation, it did not capture the countertrend toward larger f values at even lower concentrations in regime (iii).

The results of this study revealed a concentration-dependent microbial degradation in a bench-scale physical aquifer model that was limited by mass transfer at the cellular level, at low concentrations, and, possibly, subsequent bacterial adaptation. The results further demonstrate that the assumption of a constant isotopic enrichment factor over the entire substrate concentration range would not be appropriate when evaluating such biodegradation and bacterial activity at low concentrations. To account for this, reactive transport models need to be complemented by a term accounting for mass transfer through the bacterial cell membrane. Finally, the relationship between degradation, $\ln(f)$, and isotope fractionation, $\ln(R_t/R_0)$ (Figure 5a), holds potential to recognize underlying limitations (mass transfer vs physiological adaptation) during ongoing biodegradation. The approach may, therefore, help to identify optimum substrate concentrations for maximum degradation (points farthest to the left in Figure 5a) in bioremediation schemes.

■ ASSOCIATED CONTENT

SI Supporting Information

The Supporting Information is available free of charge at <https://pubs.acs.org/doi/10.1021/acs.est.0c08566>.

More detailed experimental section, description of numerical simulations, parameters of target analytes on MS, flow, and transport parameters and reaction rate coefficients, parameter sensitivities plotted at each measurement location, simulated transient development, and concentration difference (PDF)

■ AUTHOR INFORMATION

Corresponding Author

Martin Elsner – Institute of Groundwater Ecology, Helmholtz Zentrum München, Neuherberg 85764, Germany; Chair of Analytical Chemistry and Water Chemistry, Technical University of Munich, Munich 81377, Germany; orcid.org/0000-0003-4746-9052; Phone: +49 89 2180-78232; Email: m.elsner@tum.de

Authors

Fengchao Sun – Institute of Groundwater Ecology, Helmholtz Zentrum München, Neuherberg 85764, Germany; Chair of Analytical Chemistry and Water Chemistry, Technical University of Munich, Munich 81377, Germany

Adrian Mellage – Center for Applied Geoscience, University of Tübingen, Tübingen 72076, Germany; orcid.org/0000-0003-2708-4518

Mehdi Gharasoo – Institute of Groundwater Ecology, Helmholtz Zentrum München, Neuherberg 85764, Germany; Department of Earth and Environmental Sciences, Ecohydrology, University of Waterloo, Waterloo N2L 3G1, Canada

Aileen Melsbach – Institute of Groundwater Ecology, Helmholtz Zentrum München, Neuherberg 85764, Germany; Chair of Analytical Chemistry and Water Chemistry, Technical University of Munich, Munich 81377, Germany

Xin Cao – Joint Mass Spectrometry Centre, Comprehensive Molecular Analytics (CMA) Cooperation Group Helmholtz Zentrum, Munich 81379, Germany

Ralf Zimmermann – Joint Mass Spectrometry Centre, Comprehensive Molecular Analytics (CMA) Cooperation Group Helmholtz Zentrum, Munich 81379, Germany

Christian Griebler – Department of Functional and Evolutionary Ecology, University of Vienna, Vienna 1090, Austria

Martin Thullner – Department of Environmental Microbiology, UFZ—Helmholtz Centre for Environmental Research, Leipzig 30418, Germany; orcid.org/0000-0001-9723-4601

Olaf A. Cirpka – Center for Applied Geoscience, University of Tübingen, Tübingen 72076, Germany; orcid.org/0000-0003-3509-4118

Complete contact information is available at: <https://pubs.acs.org/doi/10.1021/acs.est.0c08566>

Author Contributions

The manuscript was written through contributions of all the authors. All the authors have given approval to the final version of the manuscript.

Notes

The authors declare no competing financial interest.

■ ACKNOWLEDGMENTS

This work was funded by an ERC consolidator grant (“MicroDegrade”, grant no. 616861) awarded by the European Research Council. We acknowledge Prof. Dr. Jens Aamand from the Department of Geochemistry, GEUS Geological Survey of Denmark and Greenland for his contribution in providing the strain *Aminobacter* sp. MSH1. We thank Prof. Christine Stumpff (University of Natural Resources and Life Sciences Vienna), Dr. Sviatlana Marozava, Dr. Benno N. Ehrl, and Dr. Kankana Kundu (Helmholtz Zentrum München) for valuable discussions.

■ REFERENCES

- (1) Meckenstock, R. U.; Morasch, B.; Griebler, C.; Richnow, H. H. Stable isotope fractionation analysis as a tool to monitor biodegradation in contaminated aquifers. *J. Contam. Hydrol.* **2004**, *75*, 215–255.
- (2) Kuntze, K.; Eisenmann, H.; Richnow, H.-H.; Fischer, A. Compound-specific stable isotope analysis (CSIA) for evaluating degradation of organic pollutants: An overview of field case studies. In *Anaerobic Utilization of Hydrocarbons, Oils, and Lipids*; Boll, M., Ed.; Springer: Cham, 2019; pp 323–360.
- (3) Fischer, A.; Manefield, M.; Bombach, P. Application of stable isotope tools for evaluating natural and stimulated biodegradation of organic pollutants in field studies. *Curr. Opin. Biotechnol.* **2016**, *41*, 99–107.
- (4) Braeckvelt, M.; Fischer, A.; Kästner, M. Field applicability of compound-specific isotope analysis (CSIA) for characterization and quantification of in situ contaminant degradation in aquifers. *Appl. Microbiol. Biotechnol.* **2012**, *94*, 1401–1421.
- (5) Elsner, M. Stable isotope fractionation to investigate natural transformation mechanisms of organic contaminants: Principles, prospects and limitations. *J. Environ. Monit.* **2010**, *12*, 2005–2031.
- (6) Elsner, M.; Zwank, L.; Hunkeler, D.; Schwarzenbach, R. P. A new concept linking observable stable isotope fractionation to transformation pathways of organic pollutants. *Environ. Sci. Technol.* **2005**, *39*, 6896–6916.
- (7) Brunner, B.; Bernasconi, S. M.; Kleikemper, J.; Schroth, M. H. A model for oxygen and sulfur isotope fractionation in sulfate during bacterial sulfate reduction processes. *Geochim. Cosmochim. Acta* **2005**, *69*, 4773–4785.
- (8) Wing, B. A.; Halevy, I. Intracellular metabolite levels shape sulfur isotope fractionation during microbial sulfate respiration. *Proc. Natl. Acad. Sci. U.S.A.* **2014**, *111*, 18116–18125.
- (9) Kritee, K.; Sigman, D. M.; Granger, J.; Ward, B. B.; Jayakumar, A.; Deutsch, C. Reduced isotope fractionation by denitrification under conditions relevant to the ocean. *Geochim. Cosmochim. Acta* **2012**, *92*, 243–259.
- (10) Humez, P.; Mayer, B.; Nightingale, M.; Becker, V.; Kingston, A.; Taylor, S.; Bayegnak, G.; Millot, R.; Kloppmann, W. Redox controls on methane formation, migration and fate in shallow aquifers. *Hydrol. Earth Syst. Sci.* **2016**, *20*, 2759–2777.
- (11) Kolhatkar, R.; Kuder, T.; Philp, P.; Allen, J.; Wilson, J. T. Use of compound-specific stable carbon isotope analyses to demonstrate anaerobic biodegradation of MTBE in groundwater at a gasoline release site. *Environ. Sci. Technol.* **2002**, *36*, 5139.
- (12) Koster van Groos, P. G.; Hatzinger, P. B.; Streger, S. H.; Vainberg, S.; Philp, R. P.; Kuder, T. Carbon isotope fractionation of 1,2-dibromoethane by biological and abiotic processes. *Environ. Sci. Technol.* **2018**, *52*, 3440–3448.
- (13) Kuder, T.; Wilson, J. T.; Kaiser, P.; Kolhatkar, R.; Philp, P.; Allen, J. Enrichment of stable carbon and hydrogen isotopes during anaerobic biodegradation of MTBE: Microcosm and field evidence. *Environ. Sci. Technol.* **2005**, *39*, 213.
- (14) Wu, L.; Verma, D.; Bondgaard, M.; Melvej, A.; Vogt, C.; Subudhi, S.; Richnow, H. H. Carbon and hydrogen isotope analysis of

parathion for characterizing its natural attenuation by hydrolysis at a contaminated site. *Water Res.* **2018**, *143*, 146–154.

(15) Fischer, A.; Theuerkorn, K.; Stelzer, N.; Gehre, M.; Thullner, M.; Richnow, H. H. Applicability of stable isotope fractionation analysis for the characterization of benzene biodegradation in a BTEX-contaminated aquifer. *Environ. Sci. Technol.* **2007**, *41*, 3689–3696.

(16) Höhener, P.; Elsner, M.; Eisenmann, H.; Atteia, O. Improved constraints on in situ rates and on quantification of complete chloroethene degradation from stable carbon isotope mass balances in groundwater plumes. *J. Contam. Hydrol.* **2015**, *182*, 173–182.

(17) Höhener, P.; Li, Z. M.; Julien, M.; Nun, P.; Robins, R. J.; Remaud, G. S. Simulating stable isotope ratios in plumes of groundwater pollutants with BIOSCREEN-AT-ISO. *Groundwater* **2017**, *55*, 261–267.

(18) Ehrl, B. N.; Gharasoo, M.; Elsner, M. Isotope Fractionation Pinpoints Membrane Permeability as a Barrier to Atrazine Biodegradation in Gram-negative *Polaromonas* sp. Nea-C. *Environ. Sci. Technol.* **2018**, *52*, 4137–4144.

(19) Ehrl, B. N.; Kundu, K.; Gharasoo, M.; Marozava, S.; Elsner, M. Rate-limiting mass transfer in micropollutant degradation revealed by isotope fractionation in chemostat. *Environ. Sci. Technol.* **2019**, *53*, 1197–1205.

(20) O'Leary, M. H. Carbon isotopes in photosynthesis. *Bioscience* **1988**, *38*, 328–336.

(21) Wunderlich, A.; Heipieper, H. J.; Elsner, M.; Einsiedl, F. Solvent stress-induced changes in membrane fatty acid composition of denitrifying bacteria reduce the extent of nitrogen stable isotope fractionation during denitrification. *Geochim. Cosmochim. Acta* **2018**, *239*, 275–283.

(22) Rees, C. E. A steady-state model for sulphur isotope fractionation in bacterial reduction processes. *Geochim. Cosmochim. Acta* **1973**, *37*, 1141–1162.

(23) Mangalo, M.; Einsiedl, F.; Meckenstock, R. U.; Stichler, W. Influence of the enzyme dissimilatory sulfite reductase on stable isotope fractionation during sulfate reduction. *Geochim. Cosmochim. Acta* **2008**, *72*, 1513–1520.

(24) Qiu, S.; Gözdereliler, E.; Weyrauch, P.; Lopez, E. C. M.; Kohler, H.-P. E.; Sorensen, S. R.; Meckenstock, R. U.; Elsner, M. Small $^{13}\text{C}/^{12}\text{C}$ Fractionation Contrasts with Large Enantiomer Fractionation in Aerobic Biodegradation of Phenoxy Acids. *Environ. Sci. Technol.* **2014**, *48*, 5501–5511.

(25) Chen, S.; Zhang, K.; Jha, R. K.; Chen, C.; Yu, H.; Liu, Y.; Ma, L. Isotope fractionation in atrazine degradation reveals rate-limiting, energy-dependent transport across the cell membrane of gram-negative rhizobium sp. CX-Z. *Environ. Pollut.* **2019**, *248*, 857–864.

(26) Nijenhuis, I.; Andert, J.; Beck, K.; Kästner, M.; Diekert, G.; Richnow, H.-H. Stable isotope fractionation of tetrachloroethene during reductive dechlorination by *Sulfurospirillum* multivorans and *Desulfitobacterium* sp. strain PCE-S and abiotic reactions with cyanocobalamin. *Appl. Environ. Microbiol.* **2005**, *71*, 3413–3419.

(27) Kampara, M.; Thullner, M.; Richnow, H. H.; Harms, H.; Wick, L. Y. Impact of bioavailability restrictions on microbially induced stable isotope fractionation. 2. Experimental evidence. *Environ. Sci. Technol.* **2008**, *42*, 6552–6558.

(28) Thullner, M.; Kampara, M.; Richnow, H. H.; Harms, H.; Wick, L. Y. Impact of bioavailability restrictions on microbially induced stable isotope fractionation. 1. Theoretical calculation. *Environ. Sci. Technol.* **2008**, *42*, 6544–6551.

(29) Sigman, D. M.; Casciotti, K. L.; Andreani, M.; Barford, C.; Galanter, M.; Böhlke, J. K. A bacterial method for the nitrogen isotopic analysis of nitrate in seawater and freshwater. *Anal. Chem.* **2001**, *73*, 4145–4153.

(30) Habicht, K. S.; Salling, L.; Thamdrup, B.; Canfield, D. E. Effect of Low Sulfate Concentrations on Lactate Oxidation and Isotope Fractionation during Sulfate Reduction by *Archaeoglobus fulgidus* Strain Z[†]. *Appl. Environ. Microbiol.* **2005**, *71*, 3770–3777.

(31) Crowe, S. A.; Paris, G.; Katsev, S.; Jones, C.; Kim, S.-T.; Zerkle, A. L.; Nomosatryo, S.; Fowle, D. A.; Adkins, J. F.; Sessions, A. L.;

Farquhar, J.; Canfield, D. E. Sulfate was a trace constituent of Archean seawater. *Science* **2014**, *346*, 735–739.

(32) Thullner, M.; Fischer, A.; Richnow, H.-H.; Wick, L. Y. Influence of mass transfer on stable isotope fractionation. *Appl. Microbiol. Biotechnol.* **2013**, *97*, 441–452.

(33) Kundu, K.; Marozava, S.; Ehrl, B.; Merl-Pham, J.; Griebler, C.; Elsner, M. Defining lower limits of biodegradation: atrazine degradation regulated by mass transfer and maintenance demand in *Arthrobacter aureus* TC1. *ISME J.* **2019**, *13*, 2236–2251.

(34) Gharasoo, M.; Ehrl, B. N.; Cirpka, O. A.; Elsner, M. Modeling of contaminant biodegradation and compound-specific isotope fractionation in chemostats at low dilution rates. *Environ. Sci. Technol.* **2019**, *53*, 1186–1196.

(35) Marozava, S.; Meyer, A. H.; Pérez-de-Mora, A.; Gharasoo, M.; Zhuo, L.; Wang, H.; Cirpka, O. A.; Meckenstock, R. U.; Elsner, M. Mass transfer limitation during slow anaerobic biodegradation of 2-methylnaphthalene. *Environ. Sci. Technol.* **2019**, *53*, 9481–9490.

(36) Cichocka, D.; Imfeld, G.; Richnow, H.-H.; Nijenhuis, I. Variability in microbial carbon isotope fractionation of tetra- and trichloroethene upon reductive dechlorination. *Chemosphere* **2008**, *71*, 639–648.

(37) Wanner, P.; Parker, B. L.; Chapman, S. W.; Aravena, R.; Hunkeler, D. Quantification of degradation of chlorinated hydrocarbons in saturated low permeability sediments using compound-specific isotope analysis. *Environ. Sci. Technol.* **2016**, *50*, 5622–5630.

(38) Rolle, M.; Chiogna, G.; Bauer, R.; Griebler, C.; Grathwohl, P. Isotopic fractionation by transverse dispersion: Flow-through microcosms and reactive transport modeling study. *Environ. Sci. Technol.* **2010**, *44*, 6167–6173.

(39) Van Breukelen, B. M.; Rolle, M. Transverse hydrodynamic dispersion effects on isotope signals in groundwater chlorinated solvents' plumes. *Environ. Sci. Technol.* **2012**, *46*, 7700–7708.

(40) Abe, Y.; Hunkeler, D. Does the Rayleigh equation apply to evaluate field isotope data in contaminant hydrogeology? *Environ. Sci. Technol.* **2006**, *40*, 1588–1596.

(41) Thullner, M.; Centler, F.; Richnow, H.-H.; Fischer, A. Quantification of organic pollutant degradation in contaminated aquifers using compound specific stable isotope analysis - Review of recent developments. *Org. Geochem.* **2012**, *42*, 1440–1460.

(42) Druhan, J. L.; Maher, K. The influence of mixing on stable isotope ratios in porous media: A revised Rayleigh model. *Water Resour. Res.* **2017**, *53*, 1101–1124.

(43) Bauer, R. D.; Maloszewski, P.; Zhang, Y.; Meckenstock, R. U.; Griebler, C. Mixing-controlled biodegradation in a toluene plume - Results from two-dimensional laboratory experiments. *J. Contam. Hydrol.* **2008**, *96*, 150–168.

(44) Ellegaard-Jensen, L.; Horemans, B.; Raes, B.; Aamand, J.; Hansen, L. H. Groundwater contamination with 2,6-dichlorobenzamide (BAM) and perspectives for its microbial removal. *Appl. Microbiol. Biotechnol.* **2017**, *101*, 5235–5245.

(45) Vandermaesen, J.; Horemans, B.; Degryse, J.; Boonen, J.; Walravens, E.; Springael, D. Mineralization of the common groundwater pollutant 2,6-dichlorobenzamide (BAM) and its metabolite 2,6-dichlorobenzoic acid (2,6-DCBA) in sand filter units of drinking water treatment plants. *Environ. Sci. Technol.* **2016**, *50*, 10114–10122.

(46) Albers, C. N.; Feld, L.; Ellegaard-Jensen, L.; Aamand, J. Degradation of trace concentrations of the persistent groundwater pollutant 2,6-dichlorobenzamide (BAM) in bioaugmented rapid sand filters. *Water Res.* **2015**, *83*, 61–70.

(47) Pukkila, V.; Kontro, M. H. Dichlobenil and 2,6-dichlorobenzamide (BAM) dissipation in topsoil and deposits from groundwater environment within the boreal region in southern Finland. *Environ. Sci. Pollut. Res.* **2014**, *21*, 2289–2297.

(48) Sorensen, S. R.; Holtze, M. S.; Simonsen, A.; Aamand, J. Degradation and mineralization of nanomolar concentrations of the herbicide dichlobenil and its persistent metabolite 2,6-dichlorobenzamide by *Aminobacter* spp. isolated from dichlobenil-treated soils. *Appl. Environ. Microbiol.* **2007**, *73*, 399–406.

- (49) Albers, C. N.; Jacobsen, O. S.; Aamand, J. Using 2,6-dichlorobenzamide (BAM) degrading *Aminobacter* sp. MSH1 in flow through biofilters-initial adhesion and BAM degradation potentials. *Appl. Microbiol. Biotechnol.* **2014**, *98*, 957–967.
- (50) Clausen, L.; Larsen, F.; Albrechtsen, H.-J. Sorption of the Herbicide Dichlobenil and the Metabolite 2,6-Dichlorobenzamide on Soils and Aquifer Sediments. *Environ. Sci. Technol.* **2004**, *38*, 4510–4518.
- (51) T'Syen, J.; Raes, B.; Horemans, B.; Tassoni, R.; Leroy, B.; Lood, C.; van Noort, V.; Lavigne, R.; Wattiez, R.; Kohler, H. E.; Springael, D. Catabolism of the groundwater micropollutant 2,6-dichlorobenzamide beyond 2,6-dichlorobenzoate is plasmid encoded in *Aminobacter* sp. MSH1. *Appl. Microbiol. Biotechnol.* **2018**, *102*, 7963–7979.
- (52) T'Syen, J.; Tassoni, R.; Hansen, L.; Sorensen, S. J.; Leroy, B.; Sekhar, A.; Wattiez, R.; De Mot, R.; Springael, D. Identification of the amidase BbdA that initiates biodegradation of the groundwater micropollutant 2,6-dichlorobenzamide (BAM) in *Aminobacter* sp. MSH1. *Environ. Sci. Technol.* **2015**, *49*, 11703–11713.
- (53) Reinnicke, S.; Simonsen, A.; Sorensen, S. R.; Aamand, J.; Elsner, M. C and N isotope fractionation during biodegradation of the pesticide metabolite 2,6-dichlorobenzamide (BAM): potential for environmental assessments. *Environ. Sci. Technol.* **2012**, *46*, 1447–1454.
- (54) Sun, F.; Peters, J.; Thullner, M.; Cirpka, O. A.; Elsner, M. Magnitude of diffusion- and transverse dispersion-induced isotope fractionation of organic compounds in aqueous systems. *Environ. Sci. Technol.* **2021**, *55*, 4772–4782.
- (55) Jensen, G. G.; Björklund, E.; Simonsen, A.; Halling-Sorensen, B. Determination of 2,6-dichlorobenzamide and its degradation products in water samples using solid-phase extraction followed by liquid chromatography-tandem mass spectrometry. *J. Chromatogr. A* **2009**, *1216*, 5199–5206.
- (56) Hammes, F.; Goldschmidt, F.; Vital, M.; Wang, Y.; Egli, T. Measurement and interpretation of microbial adenosine tri-phosphate (ATP) in aquatic environments. *Water Res.* **2010**, *44*, 3915–3923.
- (57) Bayer, A.; Drexler, R.; Weber, N.; Griebler, C. Quantification of aquatic sediment prokaryotes-A multiple-steps optimization testing sands from pristine and contaminated aquifers. *Limnologia* **2016**, *56*, 6–13.
- (58) Mellage, A.; Eckert, D.; Grösbacher, M.; Inan, A. Z.; Cirpka, O. A.; Griebler, C. Dynamics of suspended and attached aerobic toluene degraders in small-scale flow-through sediment systems under growth and starvation conditions. *Environ. Sci. Technol.* **2015**, *49*, 7161–7169.
- (59) Grösbacher, M.; Eckert, D.; Cirpka, O. A.; Griebler, C. Contaminant concentration versus flow velocity: Drivers of biodegradation and microbial growth in groundwater model systems. *Biodegradation* **2018**, *29*, 211–232.
- (60) Lehman, R. M.; Colwell, F. S.; Bala, G. A. Attached and unattached microbial communities in a simulated basalt aquifer under fracture- and porous-flow conditions. *Appl. Environ. Microbiol.* **2001**, *67*, 2799–2809.
- (61) Sekhar, A.; Horemans, B.; Aamand, J.; Sorensen, S. R.; Vanhaecke, L.; Bussche, J. V.; Hofkens, J.; Springael, D. Surface Colonization and Activity of the 2,6-Dichlorobenzamide (BAM) Degrading *Aminobacter* sp. Strain MSH1 at Macro- and Micro-pollutant BAM Concentrations. *Environ. Sci. Technol.* **2016**, *50*, 10123–10133.
- (62) Eckert, D.; Kürzinger, P.; Bauer, R.; Griebler, C.; Cirpka, O. A. Fringe-controlled biodegradation under dynamic conditions: Quasi 2-D flow-through experiments and reactive-transport modeling. *J. Contam. Hydrol.* **2015**, *172*, 100–111.
- (63) Eckert, D.; Rolle, M.; Cirpka, O. A. Numerical simulation of isotope fractionation in steady-state bioreactive transport controlled by transverse mixing. *J. Contam. Hydrol.* **2012**, *140–141*, 95–106.
- (64) Cirpka, O. A.; Valocchi, A. J. Two-dimensional concentration distribution for mixing-controlled bioreactive transport in steady state. *Adv. Water Resour.* **2007**, *30*, 1668–1679.
- (65) Ballarini, E.; Beyer, C.; Bauer, R. D.; Griebler, C.; Bauer, S. Model based evaluation of a contaminant plume development under aerobic and anaerobic conditions in 2D bench-scale tank experiments. *Biodegradation* **2014**, *25*, 351–371.
- (66) Hesse, F.; Harms, H.; Attinger, S.; Thullner, M. Linear exchange model for the description of mass transfer limited bioavailability at the pore scale. *Environ. Sci. Technol.* **2010**, *44*, 2064–2071.
- (67) Rayleigh, L. L. Theoretical considerations respecting the separation of gases by diffusion and similar processes. *Mag. J. Sci.* **1896**, *42*, 493–498.
- (68) Hoefs, J. *Stable Isotope Geochemistry*; Springer Verlag: Chicago, 1987.
- (69) Helbling, D. E.; Hammes, F.; Egli, T.; Kohler, H.-P. E. Kinetics and yields of pesticide biodegradation at low substrate concentrations and under conditions restricting assimilable organic carbon. *Appl. Environ. Microbiol.* **2014**, *80*, 1306–1313.
- (70) Ehrl, B. N.; Mogusu, E. O.; Kim, K.; Hofstetter, H.; Pedersen, J. A.; Elsner, M. High permeation rates in liposome systems explain rapid glyphosate biodegradation associated with strong isotope fractionation. *Environ. Sci. Technol.* **2018**, *52*, 7259–7268.
- (71) Wanner, P.; Hunkeler, D. Carbon and chlorine isotopologue fractionation of chlorinated hydrocarbons during diffusion in water and low permeability sediments. *Geochim. Cosmochim. Acta* **2015**, *157*, 198–212.
- (72) Prommer, H.; Anneser, B.; Rolle, M.; Einsiedl, F.; Griebler, C. Biogeochemical and isotopic gradients in a BTEX/PAH contaminant plume: Model-based interpretation of a high-resolution field data set. *Environ. Sci. Technol.* **2009**, *43*, 8206–8212.
- (73) Wenk, C. B.; Frame, C. H.; Koba, K.; Casciotti, K. L.; Veronesi, M.; Niemann, H.; Schubert, C. J.; Yoshida, N.; Toyoda, S.; Makabe, A.; Zopf, J.; Lehmann, M. F. Differential N2 O dynamics in two oxygen-deficient lake basins revealed by stable isotope and isotopomer distributions. *Limnol. Oceanogr.* **2016**, *61*, 1735–1749.
- (74) Xu, S.; Sherwood Lollar, B.; Sleep, B. E. Rethinking aqueous phase diffusion related isotope fractionation: Contrasting theoretical effects with observations at the field scale. *Sci. Total Environ.* **2017**, *607–608*, 1085–1095.
- (75) Canfield, D. E. Isotope fractionation by natural populations of sulfate-reducing bacteria. *Geochim. Cosmochim. Acta* **2001**, *65*, 1117–1124.
- (76) Canfield, D. E.; Olesen, C. A.; Cox, R. P. Temperature and its control of isotope fractionation by a sulfate-reducing bacterium. *Geochim. Cosmochim. Acta* **2006**, *70*, 548–561.
- (77) Mangalo, M.; Meckenstock, R. U.; Stichler, W.; Einsiedl, F. Stable isotope fractionation during bacterial sulfate reduction is controlled by reoxidation of intermediates. *Geochim. Cosmochim. Acta* **2007**, *71*, 4161–4171.

Supporting Information for

Mass Transfer-Limited Biodegradation at Low Concentrations– Evidence from Reactive Transport Modeling of Isotope Profiles in a Bench-Scale Aquifer

Fengchao Sun, Adrian Mellage, Mehdi Gharasoo, Aileen Melsbach, Xin Cao, Ralf Zimmermann,
Christian Griebler, Martin Thullner, Olaf A. Cirpka, and Martin Elsner

Supplementary Table of Contents

Chemicals.....	77
Sample Preparation and Solid-phase Extraction (SPE)	77
BAM and 2,6-DCBA Concentration Measurements on LC-MS/MS	78
Table S1. Parameters of target analytes on MS	78
Carbon and Nitrogen Isotope Measurements on GC-IRMS	79
Medium Preparation and Bacteria Cultivation	79
Set-up of the Two-dimensional Flow-through Sediment-Tank Experiment	80
Additional Equations for the Mass-Transfer Limitation Scenario.....	80
Governing Equations for the Scenario without Mass-Transfer Limitation	81
Parameter Uncertainties and Sensitivities.....	82
Table S2. Flow and transport parameters and reaction rate coefficients, for the reactive transport model	84
Figure S1. Parameter sensitivities plotted at each measurement location.	86
Derivation of the Apparent Enrichment Factor (Equation 18)	87
Additional Supporting Figures.....	90
Figure S2. Simulated transient development of $\Delta\delta^{13}\text{C}$, $c_{\text{bulk}}^{\text{BAM}}$, and TCC.	90
Figure S3. Concentration difference between $c_{\text{bulk}}^{\text{BAM}}$ and $c_{\text{int}}^{\text{BAM}}$	90
References.....	91

Chemicals

The following chemicals were used: 2,6-dichlorobenzamide (Sigma Aldrich, Germany), 2,6-dichlorobenzamide-3,4,5-d₃, 98.4%-d₃ (Alfa Chemistry, Ronkonkoma, NY).

The following chemicals were used for the medium preparation: disodium phosphate (6 g/L), monopotassium phosphate ($\geq 99\%$), ammonium chloride ($\geq 99\%$), magnesium sulfate heptahydrate ($\geq 98\%$), calcium chloride dihydrate ($\geq 99\%$), boric acid ($\geq 99.5\%$), manganese sulfate monohydrate ($\geq 99\%$), copper sulfate pentahydrate ($\geq 98\%$), zinc chloride ($\geq 98\%$), cobalt chloride hexahydrate ($\geq 98\%$), sodium molybdate monohydrate ($\geq 99\%$), glucose, and ferric chloride ($\geq 98\%$). All the chemicals were from Sigma Aldrich, Germany.

Sample Preparation and Solid-phase Extraction (SPE)

Samples for carbon and nitrogen isotope analysis were filtered through 0.2 μM PES filter (Nalgene Thermo Scientific, Germany) and frozen at $-20\text{ }^{\circ}\text{C}$ immediately after each sampling event until enough sample volume (2 L) was collected. Samples for concentration measurements were filtered through 0.22 μM syringe filters (Merck KGaA, Germany), adjusted to pH 1.7 with HCl and spiked with internal standard 2,6-dichlorobenzamide-3,4,5-d₃ before solid phase extraction (SPE). The SPE method was adapted from Torrentó et al.¹ and Jensen et al.². For the SPE of isotope samples, 0.2 g of hydrophobic polymer-based sorbent Bakerbond SDB-1 (J.T. Baker, USA) was self-packed into empty 6 mL PP SPE cartridges with PE frit (20 μm pore size; Sigma Aldrich, Germany). The cartridges were conditioned with 3 mL ethyl acetate, followed by 2×3 mL methanol and 2×3 mL Milli-Q water. 200 – 2000 mL samples were loaded to the SPE columns at a rate of 3 mL/min. After sample loading, the cartridges were washed twice with 3 mL of Milli-Q water and dried for 2 hours. BAM was eluted with 3 mL ethyl acetate, dried under a gentle stream of nitrogen at room temperature, and re-dissolved in 100–1000 μl ethyl acetate for CSIA. For the SPE method of concentration samples, 50 mg sorbent was packed in the 1 mL empty PP SPE cartridge with PE frit (20 μm pore size; Sigma Aldrich, Germany). The cartridges were conditioned with 1 mL ethyl acetate, followed by 2×1 mL methanol and 2×1 mL Milli-Q water. 1 mL samples were slowly loaded to the SPE columns. After sample loading, the cartridges were washed twice with 1 mL Milli-Q water and dried for 1 hour. Compounds were eluted with 1 mL acetonitrile, dried under a gentle stream of nitrogen at room temperature, and re-dissolved in 100–1000 μl 10% acetonitrile water solution for LC-MS/MS measurements.

BAM and 2,6-DCBA Concentration Measurements on LC-MS/MS

The method of the concentration measurement of BAM and 2,6-DCBA on LC-MS/MS was adapted from Jensen et al.² Briefly, liquid chromatography (LC) was performed on an Agilent 1100 HPLC system including a column compartment, an autosampler, a binary pump system, and a degasser (Agilent Technologies Inc, USA). Mass spectrometry (MS) was operated on a QTrap 4000 system using electrospray ionization (ESI) (Sciex, USA). Separation was carried out on a Kinetex® C18 column (2.6 μm , 10 nm, 100 \times 2.1 mm i.d., Phenomenex, USA) at 40 °C. Mobile phase A was 5 mM of ammonium acetate with pH of 2.4 (adjusted by formic acid). Mobile phase B was acetonitrile. A gradient flow of 300 $\mu\text{L}/\text{min}$ was used as follows: 0–5 min, 90% A; 5–9 min, 90%–10% A; 9–10 min, 10%–90% A; 10–15 min, 90% A. The injection volume was 10 μL . Each sample was analyzed twice in multiple reaction monitoring (MRM) mode with a temperature of 450 °C, a nebulizer gas at 50 psi, a heater gas at 40 psi, a curtain gas at 20 psi, and a collision gas at 11 psi. 2,6-Dichlorobenzamide and 2,6-dichlorobenzamide-3,4,5- d_3 (internal standard) were analyzed in positive mode with a capillary voltage at 4.5 kV. 2,6-Dichlorobenzoic acid was analyzed in negative mode with a capillary voltage at -4.5 kV. For each sample, two transitions were selected. The first transition was used for quantification and the second transition was used for qualification (shown in Table S1).

Table S1. Parameters of target analytes on MS

Compound	Precursor ion (m/z)	Product ion (m/z)	Declustering potential (V)	Entrance potential (V)	Collision energy (V)	Cell exit potential (V)
2,6-Dichlorobenzamide	190	173	75	10	29	7
	190	145.3	75	10	40	7
2,6-dichlorobenzamide-3,4,5- d_3	193.1	176.1	70	10	27	7
	193.1	148.0	70	10	42	7
2,6-dichlorobenzoic acid	189	144.9	-26	-3	-13	-8
	189	35.2	-26	-3	-33	-3

Carbon and Nitrogen Isotope Measurements on GC-IRMS

This method was described by Sun et al.³. Briefly, a TRACE GC Ultra gas chromatograph (Thermo Fisher Scientific, Italy) and a Finnigan MAT 253 isotope ratio mass spectrometer (IRMS) were coupled through a Finnigan GC Combustion III interface (Thermo Fisher Scientific, Germany). A DB-5 analytical column (30 m, 0.25 mm i.d., 0.5 μ m film, Agilent Technologies, Germany) was used to separate BAM in the gas chromatograph. Helium (grade 5.0) was the carrier gas. For the isotope measurement of the high BAM concentration samples, we used a Thermo injector in the split/split-less injection mode; for the isotope measurement of the low BAM concentration samples, we applied a programmable injector controlled by an Optic 3 system with liquid N₂-cryofocusing (ATAS GL, distributed by Axel Semrau, Germany) in on-column injection mode, in which a Rxi retention gap (fused silica, 3 m \times 0.53 mm inner diameter) (RESTEK, Germany) was connected to a custom made on-column liner.

In the split/split-less injection mode, the GC method started at 80 °C. At a ramp rate of 15 °C/min, temperature increased to 280 °C and was held for 7 min. The flow rate was kept constant at 1.4 mL/min. In the on-column injection mode, the GC oven started at 35 °C and was held for 30 s. At a ramp rate of 5 °C/min, temperature increased to 80 °C. Then at a ramp rate of 15 °C/min, temperature increased from 80 °C to 280 °C. In the Optic 3, the method started at an initial temperature of 40 °C and was held for 300 s. Then temperature increased to 250 °C at a ramp rate of 2 °C/s. The initial flow rate was 0.3 mL/min and was held for 120 s. Then it was increased to 1.4 mL/min within 2 min. Thus, before the GC temperature program started a stable flow rate of 1.4 mL/min was established.

We used Vienna PeeDee Belemnite (V-PDB) and Air-N₂ to determine the carbon isotope values $\delta^{13}\text{C}$ [‰] and nitrogen isotope values $\delta^{15}\text{N}$ [‰] of the samples. We calculated the carbon and nitrogen isotope values $\delta^{13}\text{C}$ and $\delta^{15}\text{N}$ of the samples in relation to a lab reference gas (CO₂ and N₂, respectively). In the beginning and the end of each run, the reference gas was measured against V-PDB and air by using international reference materials (provided by IAEA), e.g., the CO₂ gases RM 8562, RM8563 for CO₂, and RM 8564 and NSVEC (N₂) for N₂.

Medium Preparation and Bacteria Cultivation

The medium for the growth of *Aminobacter* sp. Strain MSH1 in the biotic tank experiment was adapted from Schultz-Jensen et al.⁴ Briefly, medium solution was prepared with Na₂HPO₄ (6 g/L), KH₂PO₄ (3 g/L), NH₄Cl (1 g/L), MgSO₄ \times 7H₂O (0.2 g/L), CaCl₂ \times 2H₂O (0.01 g/L)

and autoclaved at 120 °C. After autoclaving, 10 mL from the trace element stock solution was filtered through 0.22 μ m syringe filters (Merck KGaA, Germany) and added to 1 L medium solution. The trace elements stock solution was H₃BO₃ (39 mg/L), MnSO₄ × H₂O (84.5 mg/L), CuSO₄ × 5H₂O (125 mg/L), ZnCl₂ (69 mg/L), CoCl₂ × 6H₂O (119.5 mg/L), and Na₂MoO₄ × H₂O (121 mg/L).

Aminobacter sp. Strain MSH1 was from the Department of Geochemistry, the Geological Survey of Denmark and Greenland (GEUS), Denmark. The strain on the sterile plates was transferred to the medium solution with a sterile needle. Precultures were made in 1 L shaker flask containing 200 mL medium solution. 2 mL of autoclaved glucose were added to 200 mL medium solution as carbon source. To ensure that the culture maintain its BAM-degrading ability, BAM was added to the medium (10 mg/L). The preculture was incubated in an orbital shaker at 130 rpm at 20 °C until an optical density (OD) of 1 was reached. The preculture with OD = 1 was centrifuged in four 50 mL centrifuge tubes at 4000 rpm for 5 min. Cell pellets were resuspended and washed in 10 mL medium solution (without glucose or BAM) for three times to remove the remaining glucose or BAM in the preculture. Finally, the suspended bacterial cell pellets were resuspended in 2 L medium solution (without glucose or BAM); the experimental culture with OD value of 0.1 was ready for the inoculation to the tank.

Set-up of the Two-dimensional Flow-through Sediment Tank Experiment

The quasi-two-dimensional tank was made up of two glass plates, separated by a Teflon spacer, and all fitted into two aluminum rims at either side of the chamber which were screwed together. The tank respectively was fitted with sixteen, equally spaced (at 1.0 cm distance each), ports at the inlet and outlet to accurately inject different constituents at specified depths and to sample with a high depth resolution at the outlet. The inner dimensions of the domain were 95 cm × 18 cm × 1 cm (L × H × W), so that the tank represents a quasi-two-dimensional system. The tank was wet packed with sterilized sand (0.8–1.2 mm grain diameter). Stainless steel capillaries and tygon pump-tubes are used to connect to inflow and outflow peristaltic pumps (Ismatec, Germany). The pumping rate was maintained at 45 ± 2 μ L/min per port. The seepage velocity was 1.25 m/d. The tank was sterilized with 12 g/L NaOH solution and rinsed with autoclaved Milli-Q water before the experiment.

Additional Equations for the Mass-Transfer limitation Scenario

We assume that k_{tr} [1/s], the mass transfer rate coefficient, primarily describes the transfer through the cell membrane and neglect the transfer resistance from the bulk solution to the cell. The mass transfer through the cell membrane between the bulk phase and the cytoplasm has different effects on the bulk-phase concentration than on the intracellular concentrations because of the disproportionate bulk solution vs. single cell volumes. Therefore, eq 1, in the main manuscript, and the following equations, which describe the degradation rates in the bulk solution, contain the ratio of the biomass concentration over the mass density of bacterial cells. While the concentration in the cell interior may be expressed in moles of substrate per volume of pore space, this would not be the concentration experienced by the enzymes. Thus, comparisons between studies using pure enzymes and those involving bacterial cells may not be valid.

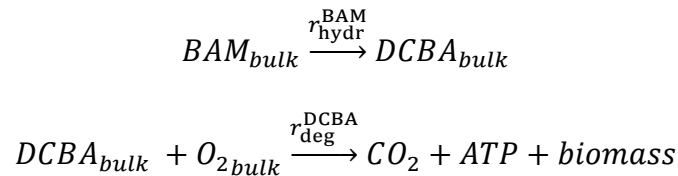
The fitted value of the coefficient, k_{tr} can be used to estimate the effective diffusion coefficient D_{eff} [m² s⁻¹], and the apparent permeability of the cell membrane P_{app} [m s⁻¹],⁵⁻⁷

$$k_{tr} = \frac{P_{app} \times A_{cell}}{V_{cell}} = \frac{D_{eff} \times K_{lipw} \times A_{cell}}{\sigma \times V_{cell}} \quad (S1)$$

where K_{lipw} [L_{water} L_{membrane}⁻¹] (value of 11) is the lipid-water distribution coefficient of BAM,⁸ A_{cell} and V_{cell} are the surface area and volume of a single cell, 6 μm² and 0.9 μm³, respectively,^{9, 10} and we can assume that the diffusive distance, σ [nm], from the substrates in the bulk solution to the location of the enzyme is the thickness of two lipid bilayer of the gram-negative bacterial strain *Aminobacter* sp. MSH1, $\sigma = 10$ nm.^{11, 12}

Governing Equations for the Scenario without Mass-Transfer Limitation

In the simulation scenario without mass transfer limitation, the mass transfer process through the cell membrane was neglected, thus only the substrate concentrations in the bulk solution were simulated. The BAM degradation pathway can be simplified as,



in which BAM was irreversibly hydrolyzed to the main intermediate 2,6-DCBA via an amidase enzyme, then 2,6-DCBA is either degraded to CO₂ and ATP via aerobic respiration or utilized for the synthesis of biomass (C₅H₇O₂N).

The reactive transport of substrates in the bulk solution was coupled to microbial dynamics and was described by the following equations in two dimensions:

$$\frac{\partial c_{\text{bulk}}^{\text{l,h,BAM}}}{\partial t} = -\mathbf{v} \cdot \nabla c_{\text{bulk}}^{\text{l,h,BAM}} + \nabla \cdot (\mathbf{D}_{\text{BAM}} \cdot \nabla c_{\text{bulk}}^{\text{l,h,BAM}}) - {}^{\text{l,h}}r_{\text{hydr}}^{\text{BAM}} \quad (\text{S2})$$

$$\frac{\partial c_{\text{bulk}}^{\text{O}_2}}{\partial t} = -\mathbf{v} \cdot \nabla c_{\text{bulk}}^{\text{O}_2} + \nabla \cdot (\mathbf{D}_{\text{O}_2} \cdot \nabla c_{\text{bulk}}^{\text{O}_2}) - r_{\text{deg}}^{\text{O}_2} \quad (\text{S3})$$

$$\begin{aligned} \frac{\partial c_{\text{bulk}}^{\text{DCBA}}}{\partial t} = & -\mathbf{v} \cdot \nabla c_{\text{bulk}}^{\text{DCBA}} + \nabla \cdot (\mathbf{D}_{\text{DCBA}} \cdot \nabla c_{\text{bulk}}^{\text{DCBA}}) + {}^{\text{l}}r_{\text{hydr}}^{\text{BAM}} + {}^{\text{h}}r_{\text{hydr}}^{\text{BAM}} \\ & - r_{\text{deg}}^{\text{DCBA}} \end{aligned} \quad (\text{S4})$$

$$\frac{\partial X^{\text{im}}}{\partial t} = r_{\text{growth}}^{\text{im}} - r_{\text{daughter}} - r_{\text{decay}}^{\text{im}} \quad (\text{S5})$$

$$\frac{\partial X^{\text{mob}}}{\partial t} = -\mathbf{v} \cdot \nabla X^{\text{mob}} + \nabla \cdot (\mathbf{D} \cdot \nabla X^{\text{mob}}) + r_{\text{daughter}} \quad (\text{S6})$$

$${}^{\text{l}}r_{\text{hydr}}^{\text{BAM}} = r_{\text{max}}^{\text{hydro}} \cdot \frac{{}^{\text{l}}c_{\text{bulk}}^{\text{BAM}}}{c_{\text{bulk}}^{\text{BAM}_{\text{total}}} + K_{\text{m}}^{\text{BAM}}} \quad (\text{S7})$$

$${}^{\text{h}}r_{\text{hydr}}^{\text{BAM}} = \alpha \cdot r_{\text{max}}^{\text{hydro}} \cdot \frac{{}^{\text{h}}c_{\text{int}}^{\text{BAM}}}{c_{\text{bulk}}^{\text{BAM}_{\text{total}}} + K_{\text{m}}^{\text{BAM}}} \quad (\text{S8})$$

$$r_{\text{deg}}^{\text{DCBA}} = \mu_{\text{max}} \cdot \frac{\rho_{\text{bio}}}{Y} \cdot \frac{c_{\text{bulk}}^{\text{DCBA}}}{K_{\text{m}}^{\text{DCBA}} + c_{\text{int}}^{\text{DCBA}}} \cdot \frac{c_{\text{bulk}}^{\text{O}_2}}{K_{\text{m}}^{\text{O}_2} + c_{\text{bulk}}^{\text{O}_2}} \quad (\text{S9})$$

$$r_{\text{deg}}^{\text{O}_2} = p \cdot r_{\text{deg}}^{\text{DCBA}} \quad (\text{S10})$$

Parameter Uncertainties and Sensitivities

We fitted the log-parameter values ($n = 10$) using *lsqnonlin*, a MATLAB built-in nonlinear least squares data-fitting function, via minimization between model computed and measured concentration values. The delogarithmized fitted parameter values are presented alongside additional, fixed, physical parameters in Table S2.

Results of a local sensitivity analysis, performed by perturbing each parameter value by 10% and comparing the model outcome to that of the optimal case, are presented for all relevant

model output in Figure . The sensitivities presented in Figure are calculated by comparing the model outcome to measurements at each depth-location. Thus, Figure shows the spatial dependence of each parameter's sensitivity, that is, where along the depth profile does a parameter most influence the model outcome. A linearized uncertainty quantification was performed on the log-parameter values considering the sum of squared residuals (obtained from *lsqnonlin*) and parameter sensitivities obtained from the local sensitivity analysis. The relative parameter uncertainties are presented, for each parameter, along the legend of Figure . Thus, the relative uncertainty range for each parameter value is given by the multiple and quotient (\times/\div) of the fitted value and its relative uncertainty. That is, the closer the relative uncertainty is equal to 1, the more accurate the estimated parameter.

The results from our uncertainty quantification suggest that most parameters are well constrained, in particular, the parameters, k_{tr}^{BAM} , r_{max}^{hydro} , K_m^{BAM} , Y and X_{max} exhibited a narrow uncertainty range (low relative uncertainty) and these were also the parameters that the model outcome was most sensitive to. The relative uncertainty for k_{att} was not reported, because a 10% perturbation of the fitted parameter value did not yield a quantifiable change in the model output, and thus the absolute value of k_{att} was poorly constrained.

Table S2. Flow and transport parameters and reaction rate coefficients, for the reactive transport model, used as either fixed values obtained from the literature or fitted to measured data.

Symbol	Parameter	Values	Unit	References
Transport parameters				
d_{grain}	grain size	0.001	[m]	experimental
ϕ	porosity	0.45	[-]	experimental
α_l	longitudinal dispersivity	6×10^{-4}	[m]	fitted
α_t	transverse dispersivity	1.9×10^{-4}	[m]	$\alpha_t = d_{grain} \times 3 / 16$
D_m^{bio}	bacteria diffusion coefficient	1.5×10^{-11}	[m ² s ⁻¹]	Kathryn, et al. ¹³
D_m^{BAM}	diffusion coefficient	4.3×10^{-10}	[m ² s ⁻¹]	Jorgensen, et al. ¹⁴
	diffusion coefficient		[m ² s ⁻¹]	Ferrel and Himmelblau ¹⁵
$D_m^{O_2}$		2.2×10^{-9}		
Biokinetic parameters				
k_{tr}^{BAM}	mass transfer coefficient of BAM	7.6	[s ⁻¹]	fitted
k_{tr}^{DCBA}	mass transfer coefficient of DCBA	3.9	[s ⁻¹]	fitted
$k_{tr}^{O_2}$	mass transfer coefficient of O ₂	3×10^6	[s ⁻¹]	fitted
K_m^{BAM}	Michaelis Menten coefficient of BAM for the hydrolysis to form 2,6-DCBA	0.38	[$\mu\text{mol L}_{int}^{-1}$]	fitted
K_m^{DCBA}	Monod coefficient of 2,6-DCBA for further degradation	10.8	[$\mu\text{mol L}_{int}^{-1}$]	fitted
$K_m^{O_2}$	Monod coefficient of O ₂ for further degradation of DCBA	3.9	[$\mu\text{mol L}_{int}^{-1}$]	fitted
r_{max}^{hydro}	maximum hydrolysis rate constant from BAM to 2,6-DCBA	67.3	[$\mu\text{mol L}_{int}^{-1} \text{s}^{-1}$]	fitted
k_{att}	bacterial attachment rate constant	6.2×10^{-6}	[s ⁻¹]	fitted
μ_{max}	maximum specific growth rate constant	1.5×10^{-5}	[s ⁻¹]	fitted
X_{max}	maximum carrying capacity for biomass growth	97	[$\mu\text{mol}_{biomass} \text{L}^{-1}$]	fitted
Y	yield coefficient	0.24	[$\mu\text{mol}_{biomass} \mu\text{mol}^{-1}$]	fitted
V_{cell}	single cell volume	0.9	[μm^3]	Ellegaard, et al. ¹⁰
M_{cell}	dry weight per cell volume	3×10^{-7}	[$\mu\text{g}_{biomass}$]	Schultz-Jensen, et al. ⁴
ρ_{bio}	biomass density	3×10^6	[$\mu\text{mol}_{biomass} \text{L}_{int}^{-1}$]	$\rho_{bio} = M_{cell} / V_{cell}$
Isotope parameters				
ϵ^C	C isotope enrichment factor	-8	[‰]	Reinicke, et al. ¹⁶
ϵ^N	N isotope enrichment factor	-13.7	[‰]	Reinicke, et al. ¹⁶
Inflow concentrations				
c_{in}^{BAM}	BAM inlet concentration	100	[$\mu\text{mol L}^{-1}$]	experimental
$c_{in}^{O_2}$	O ₂ inlet concentration	244	[$\mu\text{mol L}^{-1}$]	experimental
X_{in}^{bio}	Biomass inlet concentration	32.6	[$\mu\text{mol L}^{-1}$]	fitted

The fitted parameters in the model were obtained via the automated model calibration. Other parameters were determined either by laboratory measurements or from literature.

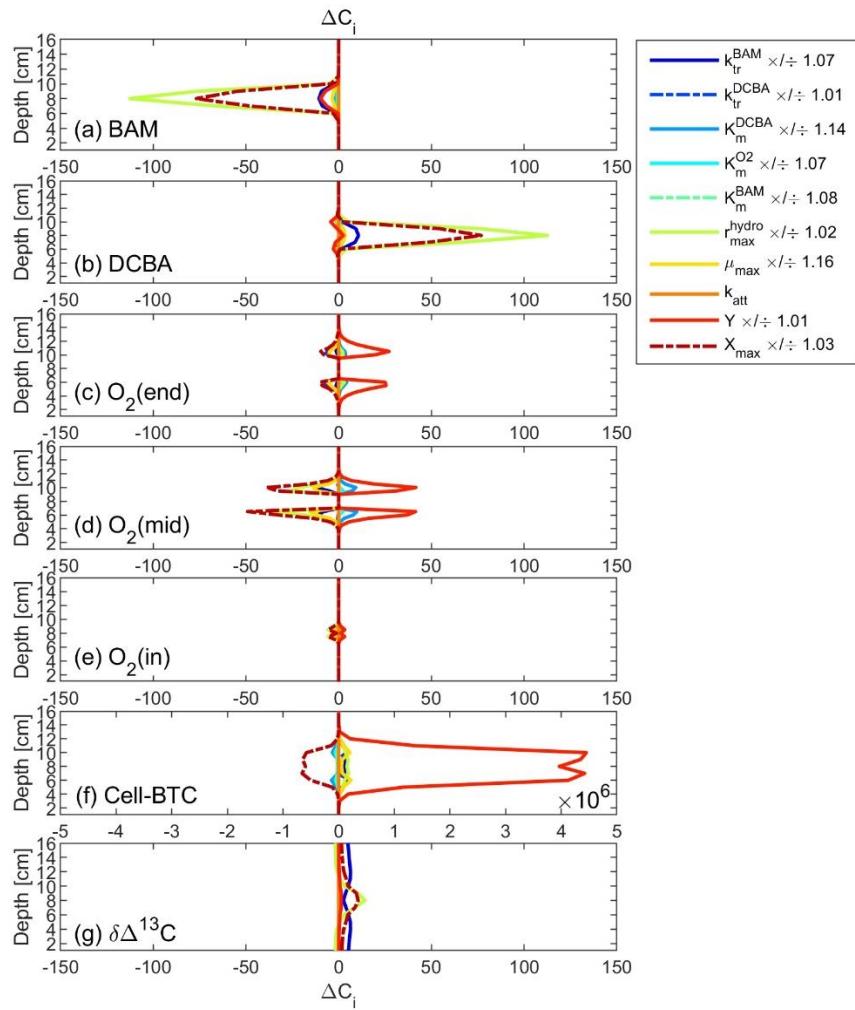


Figure S1. Parameter sensitivities plotted at each measurement location along the column depth-profile, where C_i denotes the i -th model outcome and p_j the j -th parameter ($n = 10$). Relative parameter errors (that is, \times/\div the fitted parameter value) are presented alongside each parameter in the figure legend. Parameters with a relative error close to 1 are well constrained. The uncertainty for k_{att} is not reported, because a 10% perturbation of the parameter did not yield a change in the model output.

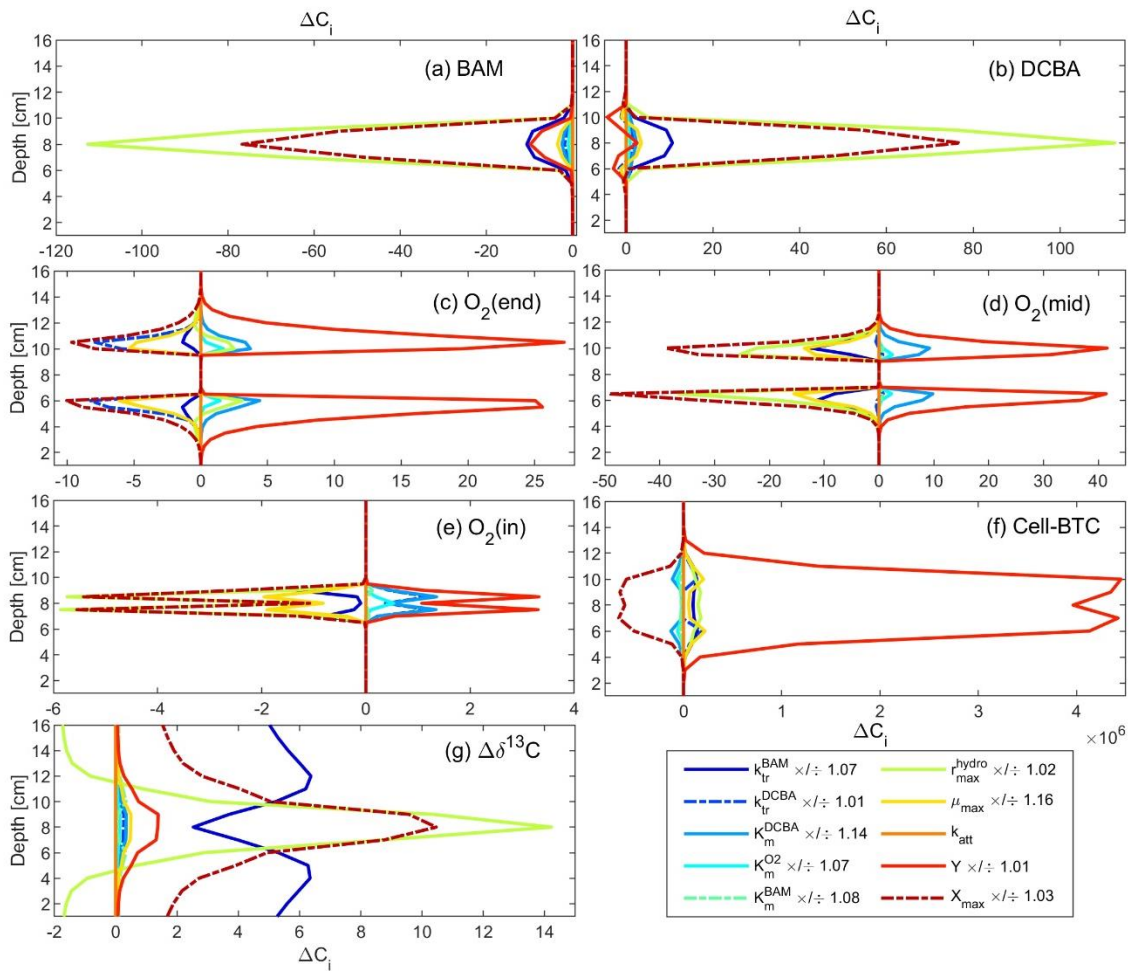


Figure S1 plotted in different x -scales.

Derivation of the Apparent Enrichment Factor (Equation 18)

The theoretical background of the derivation of eq 18 is based Thullner et al.¹⁷ Governing equations without consideration of isotopologues:

$$\frac{\partial c_{\text{bulk}}}{\partial t} = \frac{X^{\text{im}}}{\rho_{\text{bio}}} \cdot k_{\text{tr}} \cdot (c_{\text{int}} - c_{\text{bulk}}) \quad (\text{S11})$$

$$\frac{\partial c_{\text{int}}}{\partial t} = k_{\text{tr}} \cdot (c_{\text{bulk}} - c_{\text{int}}) - r_{\text{max}}^{\text{hydro}} \cdot \frac{c_{\text{int}}}{c_{\text{int}} + K_{\text{m}}} \quad (\text{S12})$$

Assume quasi-steady state in the bacterial cell interior:

$$k_{\text{tr}} \cdot (c_{\text{bulk}} - c_{\text{int}}) - r_{\text{max}}^{\text{hydro}} \cdot \frac{c_{\text{int}}}{c_{\text{int}} + K_{\text{m}}} = 0 \quad (\text{S13})$$

$$\Rightarrow (c_{\text{bulk}} - c_{\text{int}}) \cdot (c_{\text{int}} + K_{\text{m}}) - \frac{r_{\text{max}}^{\text{hydro}}}{k_{\text{tr}}} \cdot c_{\text{int}} = 0 \quad (\text{S14})$$

$$\Rightarrow -c_{\text{int}}^2 + \left(c_{\text{bulk}} - K_{\text{m}} - \frac{r_{\text{max}}^{\text{hydro}}}{k_{\text{tr}}} \right) \cdot c_{\text{int}} + c_{\text{bulk}} \cdot K_{\text{m}} = 0 \quad (\text{S15})$$

yields the quasi steady-state interior concentration:

$$\Rightarrow c_{\text{int}} = \frac{c_{\text{bulk}} - K_{\text{m}} - \frac{r_{\text{max}}^{\text{hydro}}}{k_{\text{tr}}} + \sqrt{\left(c_{\text{bulk}} - K_{\text{m}} - \frac{r_{\text{max}}^{\text{hydro}}}{k_{\text{tr}}} \right)^2 + 4c_{\text{bulk}} \cdot K_{\text{m}}}}{2} \quad (\text{S16})$$

Now we consider the light and heavy isotopologues:

$$\frac{\partial c_{\text{bulk}}^{\text{light}}}{\partial t} = \frac{X^{\text{im}}}{\rho_{\text{bio}}} \cdot k_{\text{tr}} \cdot (c_{\text{int}}^{\text{light}} - c_{\text{bulk}}^{\text{light}}) \quad (\text{S17})$$

$$\frac{\partial c_{\text{int}}^{\text{light}}}{\partial t} = k_{\text{tr}} \cdot (c_{\text{bulk}}^{\text{light}} - c_{\text{int}}^{\text{light}}) - r_{\text{max}}^{\text{hydro}} \cdot \frac{c_{\text{int}}^{\text{light}}}{c_{\text{int}}^{\text{light}} + K_{\text{m}}} \quad (\text{S18})$$

$$\frac{\partial c_{\text{bulk}}^{\text{heavy}}}{\partial t} = \frac{X^{\text{im}}}{\rho_{\text{bio}}} \cdot k_{\text{tr}} \cdot (c_{\text{int}}^{\text{heavy}} - c_{\text{bulk}}^{\text{heavy}}) \quad (\text{S19})$$

$$\frac{\partial c_{\text{int}}^{\text{heavy}}}{\partial t} = k_{\text{tr}} \cdot (c_{\text{bulk}}^{\text{heavy}} - c_{\text{int}}^{\text{heavy}}) - \alpha \cdot r_{\text{max}}^{\text{hydro}} \cdot \frac{c_{\text{int}}^{\text{heavy}}}{c_{\text{int}}^{\text{heavy}} + K_{\text{m}}} \quad (\text{S20})$$

With c_{int} as derived above, quasi-steady state in the interior implies:

$$k_{tr} \cdot (c_{bulk}^{light} - c_{int}^{light}) - r_{max}^{hydro} \cdot \frac{c_{int}^{light}}{c_{int} + K_m} = 0 \quad (S21)$$

$$k_{tr} \cdot (c_{bulk}^{heavy} - c_{int}^{heavy}) - \alpha \cdot r_{max}^{hydro} \cdot \frac{c_{int}^{heavy}}{c_{int} + K_m} = 0 \quad (S22)$$

$$\Rightarrow c_{int}^{light} = \frac{c_{bulk}^{light}}{1 + \frac{r_{max}^{hydro}}{k_{tr} \cdot (c_{int} + K_m)}} \quad (S23)$$

$$\Rightarrow c_{int}^{heavy} = \frac{c_{bulk}^{heavy}}{1 + \frac{\alpha \cdot r_{max}^{hydro}}{k_{tr} \cdot (c_{int} + K_m)}} \quad (S24)$$

Rate of change of concentration in the bulk phase:

$$\begin{aligned} \frac{\partial c_{bulk}^{light}}{\partial t} &= \frac{X^{im}}{\rho_{bio}} \cdot k_{tr} \cdot (c_{int}^{light} - c_{bulk}^{light}) \\ &= \frac{X^{im}}{\rho_{bio}} \cdot k_{tr} \cdot c_{bulk}^{light} \cdot \left(\frac{1}{1 + \frac{r_{max}^{hydro}}{k_{tr}(c_{int} + K_m)}} - 1 \right) \end{aligned} \quad (S25)$$

$$\begin{aligned} \frac{\partial c_{bulk}^{heavy}}{\partial t} &= \frac{X^{im}}{\rho_{bio}} \cdot k_{tr} \cdot (c_{int}^{heavy} - c_{bulk}^{heavy}) \\ &= \frac{X^{im}}{\rho_{bio}} \cdot k_{tr} \cdot c_{bulk}^{heavy} \cdot \left(\frac{1}{1 + \frac{\alpha \cdot r_{max}^{hydro}}{k_{tr} \cdot (c_{int} + K_m)}} - 1 \right) \end{aligned} \quad (S26)$$

Apparent fractionation factor:

$$\begin{aligned} \alpha^* &= \frac{\frac{dc_{bulk}^{heavy}}{dt} \cdot c_{bulk}^{light}}{\frac{dc_{bulk}^{light}}{dt} \cdot c_{bulk}^{heavy}} \\ &= \frac{\frac{1}{1 + \frac{\alpha \cdot r_{max}^{hydro}}{k_{tr} \cdot (c_{int} + K_m)}} - 1}{\frac{1}{1 + \frac{r_{max}^{hydro}}{k_{tr} \cdot (c_{int} + K_m)}} - 1} \end{aligned} \quad (S27)$$

$$\begin{aligned}
& \frac{c_{\text{int}} + K_m}{c_{\text{int}} + K_m + \frac{\alpha \cdot r_{\text{max}}^{\text{hydro}}}{k_{\text{tr}}}} - 1 \\
= & \frac{\frac{c_{\text{int}} + K_m}{c_{\text{int}} + K_m + \frac{r_{\text{max}}^{\text{hydro}}}{k_{\text{tr}}}} - 1}{\frac{\alpha}{c_{\text{int}} + K_m + \frac{\alpha \cdot r_{\text{max}}^{\text{hydro}}}{k_{\text{tr}}}}} \\
= & \frac{1}{\frac{c_{\text{int}} + K_m + \frac{r_{\text{max}}^{\text{hydro}}}{k_{\text{tr}}}}{\alpha}} \\
= & \alpha \frac{c_{\text{int}} + K_m + \frac{r_{\text{max}}^{\text{hydro}}}{k_{\text{tr}}}}{c_{\text{int}} + K_m + \frac{\alpha \cdot r_{\text{max}}^{\text{hydro}}}{k_{\text{tr}}}}
\end{aligned}$$

Substitute eq S16 into eq S27, we will get the final equation:

$$\begin{aligned}
& \alpha^* \tag{S28} \\
= & \alpha \frac{c_{\text{bulk}} + K_m + \frac{r_{\text{max}}^{\text{hydro}}}{k_{\text{tr}}} + \sqrt{\left(c_{\text{bulk}} - K_m - \frac{r_{\text{max}}^{\text{hydro}}}{k_{\text{tr}}}\right)^2 + 4c_{\text{bulk}} \cdot K_m}}{c_{\text{bulk}} + K_m + (2\alpha - 1) \cdot \frac{r_{\text{max}}^{\text{hydro}}}{k_{\text{tr}}} + \sqrt{\left(c_{\text{bulk}} - K_m - \frac{r_{\text{max}}^{\text{hydro}}}{k_{\text{tr}}}\right)^2 + 4c_{\text{bulk}} \cdot K_m}}
\end{aligned}$$

The calculation based on eq 18 and the one based on Thullner et al (eq S29) yielded same estimations (Figure 4).

$$\alpha^* = \alpha \cdot \frac{1 + \frac{1}{2} \left(\frac{a}{k_{\text{tr}}} - \frac{c_{\text{bulk}}}{K_m} - 1 \right) + \sqrt{\frac{a}{k_{\text{tr}}} + \frac{1}{4} \cdot \left(\frac{a}{k_{\text{tr}}} - \frac{c_{\text{bulk}}}{K_m} - 1 \right)^2}}{1 + \alpha_0 \cdot \left[\frac{1}{2} \left(\frac{a}{k_{\text{tr}}} - \frac{c_{\text{bulk}}}{K_m} - 1 \right) + \sqrt{\frac{a}{k_{\text{tr}}} + \frac{1}{4} \cdot \left(\frac{a}{k_{\text{tr}}} - \frac{c_{\text{bulk}}}{K_m} - 1 \right)^2} \right]} \tag{S29}$$

Additional Supporting Figures

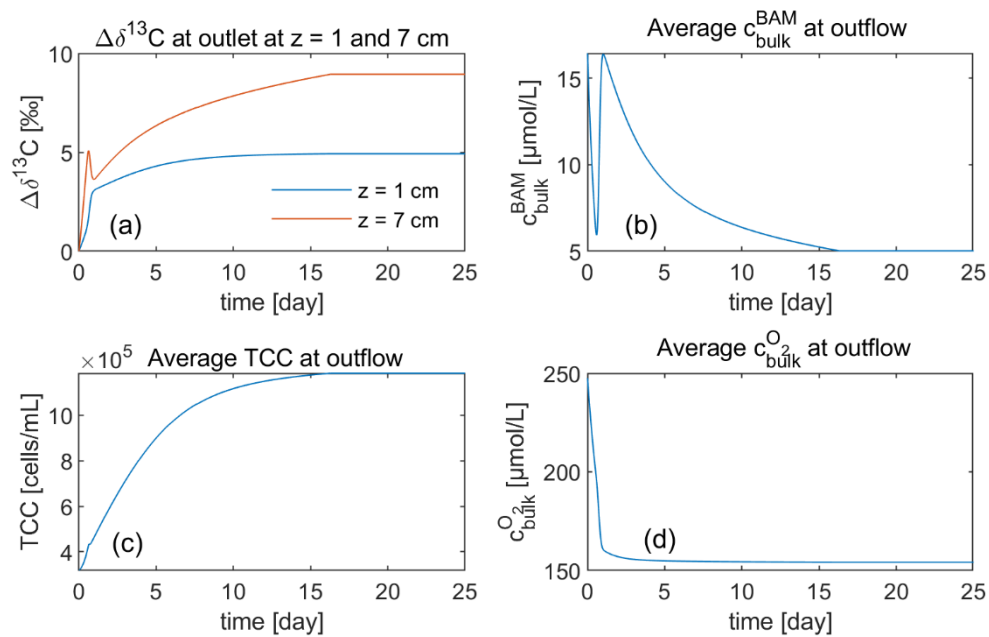


Figure S2. Simulated transient development of isotope values $\Delta\delta^{13}\text{C}$, BAM concentration $c_{\text{bulk}}^{\text{BAM}}$, total washed-out cell number TCC , and oxygen concentration $c_{\text{bulk}}^{\text{O}_2}$ at outflow. System reached to steady state on day 17.

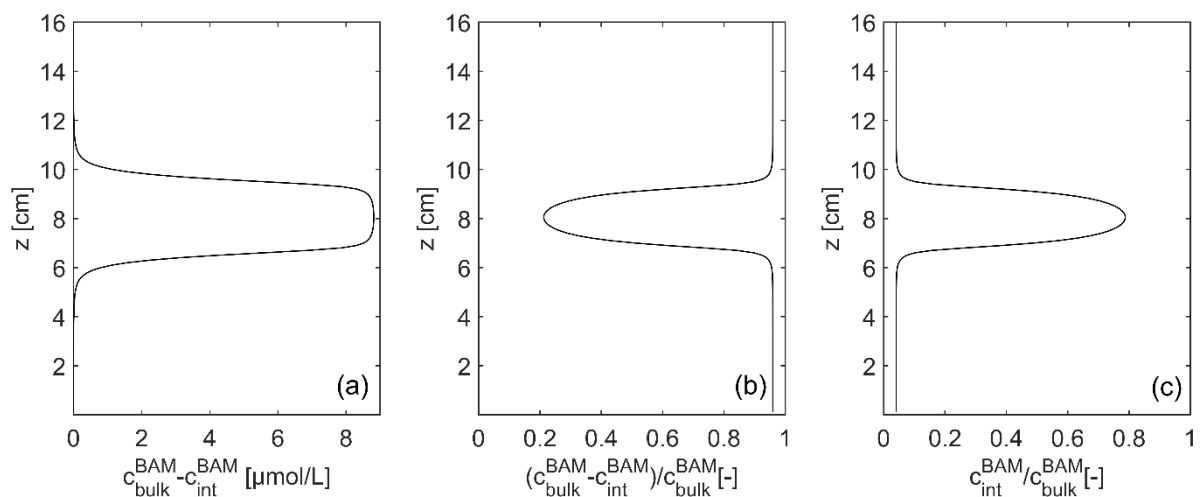


Figure S3. Concentration difference between the bulk solution $c_{\text{bulk}}^{\text{BAM}}$ and the intracellular solution $c_{\text{int}}^{\text{BAM}}$ along the vertical outlet profile.

References

1. Torrentó, C.; Bakkour, R.; Ryabenko, E.; Ponsin, V.; Prasuhn, V.; Hofstetter, T. B.; Elsner, M.; Hunkeler, D. Fate of four herbicides in an irrigated field cropped with corn: lysimeter experiments. *Procedia Earth Planet. Sci.* **2015**, *13*, 158-161.
2. Jensen, G. G.; Bjorklund, E.; Simonsen, A.; Halling-Sorensen, B. Determination of 2,6-dichlorobenzamide and its degradation products in water samples using solid-phase extraction followed by liquid chromatography-tandem mass spectrometry. *J. Chromatogr. A* **2009**, *1216* (27), 5199-206.
3. Sun, F.; Peters, J.; Thullner, M.; Cirpka, O. A.; Elsner, M. Magnitude of diffusion- and transverse dispersion-induced isotope fractionation of organic compounds in aqueous systems. *Environ. Sci. Technol.* **2020**, submitted for publication.
4. Schultz-Jensen, N.; Knudsen, B. E.; Frkova, Z.; Aamand, J.; Johansen, T.; Thykaer, J.; Sorensen, S. R. Large-scale bioreactor production of the herbicide-degrading *Aminobacter* sp. strain MSH1. *Appl. Microbiol. Biotechnol.* **2014**, *98* (5), 2335-44.
5. Shinoda, W. Permeability across lipid membranes. *Biochim. Biophys. Acta, Biomembr.* **2016**, *1858* (10), 2254-2265.
6. Males, R.; Herring, F. A ¹H-NMR study of the permeation of glycolic acid through phospholipid membranes. *Biochim. Biophys. Acta, Biomembr.* **1999**, *1416* (1-2), 333-338.
7. Ehrl, B. N.; Kundu, K.; Gharasoo, M.; Marozava, S.; Elsner, M. Rate-limiting mass transfer in micropollutant degradation revealed by isotope fractionation in chemostat. *Environ. Sci. Technol.* **2019**, *53* (3), 1197-1205.
8. Ulrich, N.; Endo, S.; Brown, T. N.; Watanabe, N.; Bronner, G.; Abraham, M. H.; Goss, K. U. UFZ-LSER database v 3.2 [Internet]. **2017**.
9. Young, K. D. The selective value of bacterial shape. *Microbiol. Mol. Biol. Rev.* **2006**, *70* (3), 660-703.
10. Ellegaard-Jensen, L.; Albers, C. N.; Aamand, J. Protozoa graze on the 2, 6-dichlorobenzamide (BAM)-degrading bacterium *Aminobacter* sp. MSH1 introduced into waterworks sand filters. *Appl. Microbiol. Biotechnol.* **2016**, *100* (20), 8965-8973.
11. Ehrl, B. N.; Gharasoo, M.; Elsner, M. Isotope Fractionation Pinpoints Membrane Permeability as a Barrier to Atrazine Biodegradation in Gram-negative *Polaromonas* sp. Nea-C. *Environ. Sci. Technol.* **2018**, *52* (7), 4137-4144.
12. Ayman, E.-H.; Jayaram, S. H. In *Effect of biological cell size and shape on killing efficiency of pulsed electric field*, 2008 IEEE International Conference on Dielectric Liquids, IEEE: 2008; pp 1-4.
13. Strobel, K. L.; McGowan, S.; Bauer, R. D.; Griebler, C.; Liu, J.; Ford, R. M. Chemotaxis increases vertical migration and apparent transverse dispersion of bacteria in a bench-scale microcosm. *Biotechnol. Bioeng.* **2011**, *108* (9), 2070-2077.
14. Jorgensen, P. R.; Klint, K. E.; Kistrup, J. P. Monitoring well interception with fractures in clayey till. *Ground Water* **2003**, *41* (6), 772-9.
15. Ferrell, R. T.; Himmelblau, D. M. Diffusion coefficients of nitrogen and oxygen in water. *J. Chem. Eng. Data* **1967**, *12* (1), 111-115.
16. Reinnicke, S.; Simonsen, A.; Sorensen, S. R.; Aamand, J.; Elsner, M. C and N isotope fractionation during biodegradation of the pesticide metabolite 2,6-dichlorobenzamide (BAM): potential for environmental assessments. *Environ. Sci. Technol.* **2012**, *46* (3), 1447-54.
17. Thullner, M.; Kampara, M.; Richnow, H. H.; Harms, H.; Wick, L. Y. Impact of bioavailability restrictions on microbially induced stable isotope fractionation. 1. Theoretical calculation. *Environ. Sci. Technol.* **2008**, *42* (17), 6544-6551.

2.3 Response of BAM-degradation activity to concentration and flow changes in a bench-scale sediment tank

2.3.1 Introduction

Anthropogenic groundwater pollution by organic chemicals, which are discharged from industrial production, domestic and agricultural activities, has become a prominent concern for potable water supply, human health, and natural ecosystems.¹⁻³ Although many organic pollutants are biodegradable, they are frequently found in the environment at microgram- to nanogram-per-liter concentrations, exceeding maximum contaminant levels or health advisory levels and raising toxicological concerns.¹ Understanding the reasons for the slow degradation of organic micropollutants - or their persistent metabolites - at such low concentrations, and finding solutions for better management and bioremediation strategies are, therefore, prominent current research challenges.¹

BAM (2,6-dichlorobenzamide) is a metabolite of the widely applied herbicide dichlobenil and of the fungicide fluopicolide. It has a high water solubility of 2.7 g/L with a log K_{ow} of 0.77,⁴ and it is a ubiquitous organic micropollutant frequently detected above drinking water thresholds (0.1 µg/L)⁵ in groundwater in many European countries.⁶⁻⁹ To purify BAM-polluted groundwater, bioremediation is an effective approach both *in-situ* and *ex-situ*.^{6, 10-12} Specifically, by implementing bioaugmented sand filters, BAM can be degraded or mineralized to low concentration levels.^{6, 13-16} The most well-studied strain for the bioaugmentation of sand filters is *Aminobacter* sp. MSH1, an aerobic, Gram-negative, motile but potentially non-chemotactic¹⁷ strain that utilizes BAM as the sole source of carbon, nitrogen, and energy.⁶

However, a specific challenge of bioremediation is that the rate of BAM degradation appears to decrease over time in long-term purification schemes.^{6, 13, 18} BAM degradation efficiency can decrease to less than 20%, and it can be difficult to maintain efficient degradation for more than two to three weeks due to the loss of inoculated bacteria (e.g., predation, wash out).^{13, 14, 16, 18} A manifestation of this phenomenon is the observation that the degree of biodegradation, that is, the extent to which concentrations decrease relative to their initial value for a given residence time drops at low BAM concentrations.^{6, 18, 19} Studies have argued that a potential limiting factor for biodegradation of BAM at low concentrations is rate-limiting mass transfer of the contaminant from the bulk solution into the bacterial cell.^{20, 21} Further,

physiological limitations that decrease the overall enzymatic activities inside bacterial cells may be a factor, such as detachment or death of cells, down-regulation of functional genes, or reduced activity of catabolic enzymes due to a physiological response to oligotrophic conditions.^{19, 22}

Perturbations via transient contaminant supply in flow-through sediment systems have shown promise in enhancing the efficiency of bacterial biodegradation of contaminants.^{12, 23} A potential explanation is that bacteria pre-adapted to a given target contaminant at a certain threshold concentration may stay active even at low contaminant concentrations or regain biodegradation ability faster than bacteria that have not been exposed to the contaminant before.^{12, 23-27} A possible alternative mechanism is that transient flow and/or transient contaminant load may spread microbial biomass over a larger area, potentially yielding an improved degradation capacity.^{23, 28-31} Currently, there remain knowledge gaps regarding (i) how microbial activity responds to different system perturbations, (ii) whether system perturbations can yield promising degradation efficiency over a long time, and (iii) how to recognize the underlying limitations (physiological vs. mass-transfer limitation) in response to system perturbations.

To address these knowledge gaps, we applied compound-specific stable isotope analysis (CSIA) — an advanced approach for the interpretation of biodegradation. Since both chemical and enzymatic reactions typically favor light isotopes, molecules with heavy isotopes are transformed more slowly and thus become enriched in the remaining substrate. Therefore, changes in stable-isotope values of the contaminant over time can provide evidence of biodegradation.^{12, 32-36} In the specific case that the enzymatic reaction is rate limiting and that the pseudo first-order rate coefficient of two isotopologues are in a fixed ratio, the observable isotope fractionation in the bulk phase and the remaining fraction of the substrate follows the Rayleigh relation^{37, 38} (Figure 2.1c, left):

$$\frac{({}^h\text{C}/{}^l\text{C})_t}{({}^h\text{C}/{}^l\text{C})_0} = \frac{\delta_t + 1}{\delta_0 + 1} = f^\varepsilon \quad (2.1)$$

in which ${}^h\text{C}$ and ${}^l\text{C}$ represent the concentration of heavy and light isotopologues, respectively; $f = c_t/c_0$ represents the remaining fraction of the substrate; and δ_0 , and δ_t represent the isotope values at time zero and at time t , respectively.

Recent research has probed the behavior of isotope fractionation, driven by inhibited biodegradation under mass transfer (into the bacterial cells) limiting conditions.^{20, 39-41} As long as enzyme turnover is slow in comparison to mass transfer into and out of the bacterial cell, isotope effects of the underlying intracellular enzyme reactions can be measured in the bulk phase, because molecules that have experienced this isotopic discrimination diffuse out of the cell. This is more likely to occur at high concentrations.⁴²⁻⁴⁵ At low concentrations, by contrast, mass transfer becomes rate-limiting if the catabolic activity remains high whereas the substrate supply is limited, such that the enzymatic turnover is rapid in comparison.²⁰ Consequently, substrate molecules are converted before they can diffuse back to the outside of the cell so that changes in substrate isotope ratios of the cell interior are no longer reflected in the bulk solution (observable isotope fractionation is masked, Figure 2.1c, right).^{20, 40, 41} If isotope fractionation according to the Rayleigh equation can nonetheless be observed at low concentrations (Figure 2.1c, left), the mass transfer is either sufficiently fast also at small concentrations, or the bacteria have downregulated overall enzyme activity in response to the surrounding low concentrations, slowing down enzymatic turnover to match the slow mass transfer (physiological adaptation).²² A decrease in isotope fractionation at low concentrations, beyond the trend expected from Rayleigh fractionation, is indicative of mass-transfer limitations that have been observed in various experimental setups with either suspended cells or attached cells on sediments adapted to oligotrophic concentrations.^{40, 41, 46, 47} These results suggest that isotope fractionation may be used as a performance indicator to characterize changes in biodegradation activity: (i) use isotope fractionation in conjunction with other variables (e.g., concentrations, cell numbers, metabolite/parent ratios) to follow the change of the system in response to perturbations; (ii) use isotope fractionation as an indicator of underlying limitations when the system is operating under different quasi-steady-state conditions.

In this study, we characterized the response of microbial BAM degradation in a flow-through sediment tank inoculated with the BAM-degrading bacterial strain *Aminobacter* sp. MSH1, which was exposed to a transient supply of elevated contaminant concentrations as a priming strategy. In addition, we took advantage of an inadvertent temporal flow fluctuation in the sediment system to investigate how the perturbations changed bacterial activity and the associated biodegradation efficiency in space and over time. By injecting a BAM solution through a single, central inlet port of the tank while injecting a BAM-free oxygen-saturated solution through parallel ports above and below, we created transverse cross-gradients of BAM and dissolved oxygen. Thus, concentrations ($\mu\text{g/L}$) at the fringes of the BAM plume mimicked

typical oligotrophic conditions in groundwater or raw water-treatment facilities (e.g., sand filters). In addition, the upper and lower regions of the tank could be regarded as physical/technical replicates because they were operated under identical external conditions. We expected that they would give identical mirror images of hydrochemical profiles. We increased the inlet substrate concentration as a priming strategy to stimulate biomass growth and the degradation activity of the bacterial strain. Subsequently, we decreased the inlet concentration back to the initial conditions. In a recent study, we have modeled a subset of this experimental data corresponding to a momentary steady-state profile as a proof-of-principle to reveal the relevance of mass transfer through the cell membrane as a limiting factor for biodegradation at low contaminant concentrations.⁴⁰ The present study takes one step further and analyzes the long-term adaptation of the system and its response to concentration and flow changes. Isotope analysis served to explore which factors (namely mass transfer or bacterial physiology) were limiting under different quasi-steady-state conditions, specifically at low concentrations and with improved system adaptation over time.

2.3.2 Methods

Setup of the Quasi-Two-Dimensional Flow-through Sediment-Tank.

The setup of the tank system was adapted from Bauer et al.⁴⁸ and has been detailed in Sun et al.^{40, 49} Briefly, the tank with inner dimensions of 95 cm × 18 cm × 1 cm (Figure 2.1a, quasi-two-dimensional) was wet-packed with uniform quartz sand (diameter of 0.8–1.2 mm). Sixteen equally spaced (1.0 cm) ports were emplaced at the inlet and outlet of the tank. An anoxic BAM solution was injected at the center of the inlet ports (at $z = 8$ cm), whereas oxic medium was introduced through the other inlet ports, and samples were collected at quasi-steady state at the outlet ports. Detailed information about the preparation and setup of the tank experiment, chemicals, liquid media, and bacterial cultures is provided in the supporting information (SI).

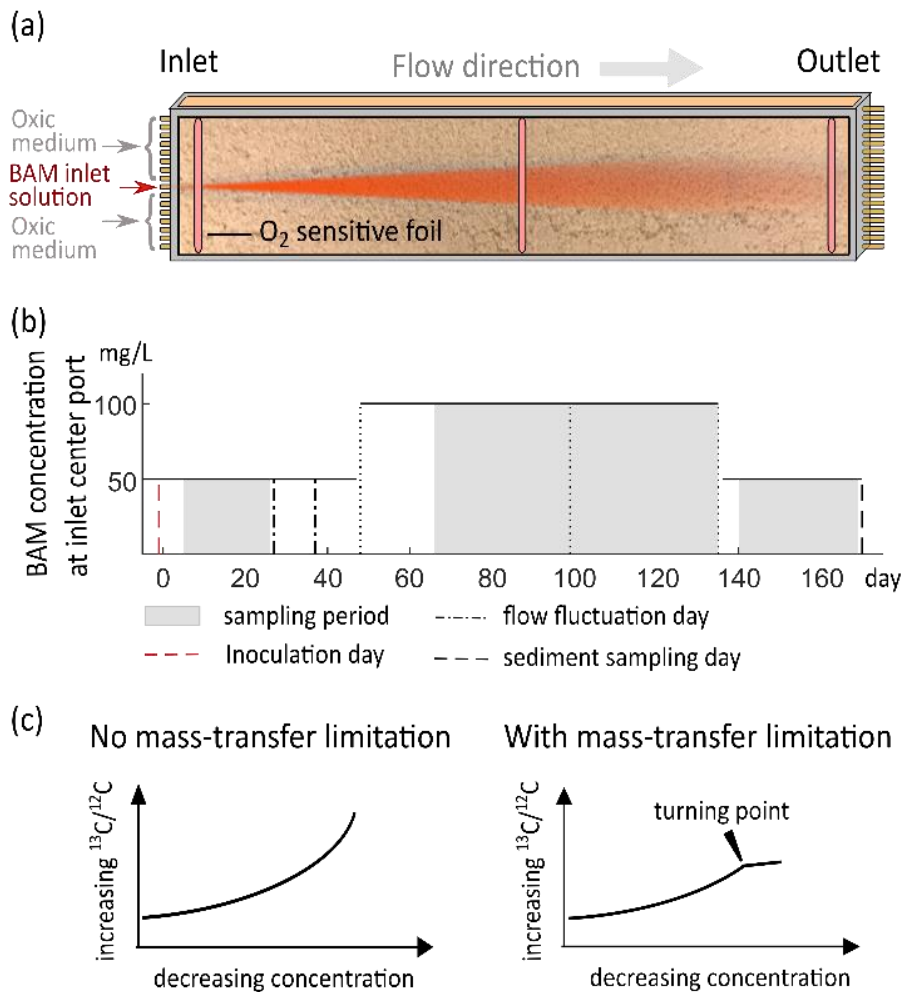


Figure 2.1 (a) Simplified tank setup and the sketch of the plume shape. (b) Sequence of experimental phases with BAM inlet concentration of 50 mg/L (phase 1), 100 mg/L (phase 2), and 50 mg/L (phase 3) at the central inlet port ($z = 8$ cm). Grey shades: periods over which integrated samples were taken for isotope analysis at quasi-steady state; red dashed line: day of inoculation; dash-dotted lines: days of flow fluctuation; dashed line: day of sediment sampling for attached bacterial cell number counting (day 170). (c) Conceptual sketches of expected isotope fractionation with decreasing concentrations without (left) and with (right) mass-transfer limitation.

Before the inoculation, the tank was operated in an abiotic experimental phase to establish a stable, conservative concentration distribution in the tank by continuously injecting a 50 mg/L sterilized, anoxic BAM solution at the central inlet port (at $z = 8$ cm) and a sterilized oxic medium through all other inlet ports. The pumping rate of all ports was maintained at 45 ± 2 $\mu\text{L}/\text{min}/\text{port}$. After running the abiotic experiment for four days, a stable, conservative plume established.⁴⁹ Subsequently, we started the biotic experiment by introducing an inoculum (without carbon or nitrogen source) of the strain *Aminobacter* sp. MSH1 (with a cell density of

1×10^7 cells/mL) at a flow rate of 45 ± 2 $\mu\text{L}/\text{min}/\text{port}$ to all ports except the central one for 24 hours. After inoculation, we stopped the flow for three hours to allow the bacteria to adhere to the sediment. The first day after the inoculation was denoted day 1. The experiment consisted of three phases (Figure 2.1b), with sequential changes of the BAM inlet concentration through the central port from 50 mg/L (phase 1) to 100 mg/L (phase 2), and back to 50 mg/L again (phase 3). Specifically, in phase 1, we injected a 50 mg/L BAM solution through the central port, and all concentrations in the respective outlet ports were at quasi-steady state from day 5 to day 26. On day 27 and day 35, flow inadvertently fluctuated due to partial blockage of individual tubes connected to the outlet ports such that the system was not at steady state anymore during a short intermittence. After normal flow was reestablished, we started phase 2 of the experiment by increasing the BAM inlet concentration through the central port to 100 mg/L on day 50. The concentrations in the outlet reached a quasi-steady state on day 66. The system continued running at 100 mg/L BAM inlet concentration till day 135. On day 136, we decreased the inlet BAM concentration through the central port back to 50 mg/L (phase 3). During the last experimental period from day 140 to day 169, changes of concentrations were minimal, yielding a quasi-steady state. At the end of the experiment (day 170), sediment samples were collected from the tank in different depths along different vertical cross-sections.

Samples for concentration measurements of BAM and its metabolite 2,6-dichlorobenzoic acid (2,6-DCBA), isotope measurements, and bacterial cell counting (TCC_{out}) were collected at each outlet port. In each experimental phase, concentration samples (1 mL) were taken every three to five days, while samples for isotope analysis were continuously collected until one to two liters of sample for isotope analysis had accumulated at each outlet position. In phase 1, with 50 mg/L BAM inlet concentration at the central port, samples for isotope analysis were collected from day 5 to day 26. In phase 2, with a 100 mg/L BAM inlet concentration at the central port, we collected isotope samples over two periods, from day 66 to day 98 and from day 99 to day 135. The quasi-steady-state data from the second sampling period (phase 2) has been presented by Sun et al.⁴⁰ as a subset of the results discussed in full here. In phase 3, with the BAM inlet concentration at the central port back to 50 mg/L, we collected isotope samples from day 140 to day 169 (Note: All sampling times are given in days after inoculation). Samples for concentration and isotope measurements were all filtered through 0.22 μM syringe filters (Merck KGaA, Germany) and stored at -20 $^{\circ}\text{C}$ until analysis.

Carbon Isotope Analysis of BAM.

Biodegradation of BAM by *Aminobacter* sp. MSH1 has previously been shown to induce strong carbon isotope fractionation with isotopic enrichment factors $\varepsilon_C = -7.8 \pm 0.2\%$ at high concentrations in batch experiments.⁴² For the carbon isotope measurements of BAM, samples concentrated in ethyl acetate after solid-phase extraction (SPE) were measured on a GC-IRMS system in which a TRACE GC Ultra gas chromatograph (Thermo Fisher Scientific, Italy) was coupled to a Finnigan MAT 253 isotope-ratio mass spectrometer (IRMS) through a Finnigan GC Combustion III interface (Thermo Fisher Scientific, Germany). The separation was carried out on a DB-5 analytical column (60 m, 0.25 mm i.d., 0.5 μm film, Agilent Technologies, Germany). The typical uncertainty of carbon isotope measurements is $\pm 0.5\%$. A detailed method description, including sample preparation and SPE, is provided in the SI.

Concentration Measurements of BAM, DO, and Total Cell Counts.

By adopting the method of Jensen et al.,⁵⁰ concentrations of BAM and 2,6-DCBA were measured by liquid chromatograph-tandem mass spectrometry (LC-MS/MS) after SPE for sample preparation. Compound separation was performed using a Kinetex® C18 column (2.6 μm , 10 nm, 100 \times 2.1 mm i.d., Phenomenex, USA) at 40 °C. A detailed method description is provided in the SI. We calculated the fraction f of residual BAM concentrations $c_{\text{BAM}}^{\text{biotic}}$ relative to the initial BAM concentrations that would be expected in the absence of biodegradation ($c_{\text{BAM}}^{\text{abiotic}}$) based on the concentration profile on the fourth day of the initial abiotic experiment (see above and Sun et al.⁴⁹) by:

$$f = c_{\text{BAM}}^{\text{biotic}} / c_{\text{BAM}}^{\text{abiotic}} \quad (2.2)$$

DO concentrations along the vertical cross-sections at the inlet, in the middle, and at the outlet of the tank were monitored by reading oxygen-sensitive polymer optode foils (18 cm \times 0.5 cm, PreSens GmbH, Regensburg, Germany) in the inner side of the tank with a FIBOX2 Fiber-optic oxygen meter (PreSens, Regensburg, Germany). For total cell counts of the washed-out bacteria, samples (1.5 mL) were collected every 3–5 days from the outlet ports of the tank, fixed with glutaraldehyde (2.5% final concentration), and stored at 4 °C. For the total cell counts of the attached bacteria on the sediments, sediment samples (2 mL) were collected at the end of the experiment on day 170. All samples were treated according to the method of Bayer et al.⁵¹ before staining with SYBR Green I and quantification on a Cytomics FC 500 flow cytometer (Beckmann Coulter, Hebron, KY). To further confirm the presence of the strain

Aminobacter sp. MSH1 at all depths (z) of the tank, terminal restriction fragment length polymorphism (T-RFLP) analysis was performed to target bacterial 16S rRNA genes. DNA isolation was done for samples collected at each depth at the end of the experiment according to the protocol described in Pilloni et al.⁵² The PCR thermo profile and T-RFLP process are further described in the SI.

2.3.3 Results and discussion

Distribution of Solutes and Biomass.

Figure 2.2 summarizes results of the three experimental phases with BAM inlet concentrations in the central port of 50 mg/L, 100 mg/L, and 50 mg/L, respectively, as well as snapshots during the phase of flow-fluctuation at the end of phase 1. The vertical profiles in the three phases show the typical plume-fringe pattern,^{12, 23, 48, 53-55} that is, the hot spots of biomass growth (reflected in the washed-out cell number) were located at the plume fringes where BAM and DO mixed due to transverse dispersion, with steep DO concentration gradients developed towards the plume center. At the hot spots in the plume fringes, BAM degradation was most efficient, indicated by the lowest fraction f and the highest ratio of 2,6-DCBA to BAM concentrations (Figure 2.2 e, f). In the plume center, the washed-out cell numbers (as a proxy for growth) were lower than at the plume fringes, and the remaining BAM and 2,6-DCBA concentrations were highest, indicating that the lack of electron acceptor (i.e., DO) limited biodegradation of BAM and biomass growth. In the uppermost and lowermost regions of the tank, the washed-out cell numbers and BAM concentrations were the lowest. At these locations, the electron acceptor was in excess, but the degradation efficiency was lower than at the plume fringes, with a higher f -value and a lower molar concentration ratio of 2,6-DCBA to BAM. The observed decrease in BAM degradation capacity with decreasing BAM concentrations (from the plume fringes to the uppermost and lowermost regions of the plume, Figure 2.2f) were consistent with the reduced BAM degradation activity of *Aminobacter* sp. MSH1 at low concentrations observed in batch and flow channel studies.^{9, 19, 56} The lower bacterial degradation activity at low concentrations will be discussed together with the results from isotope analysis below.

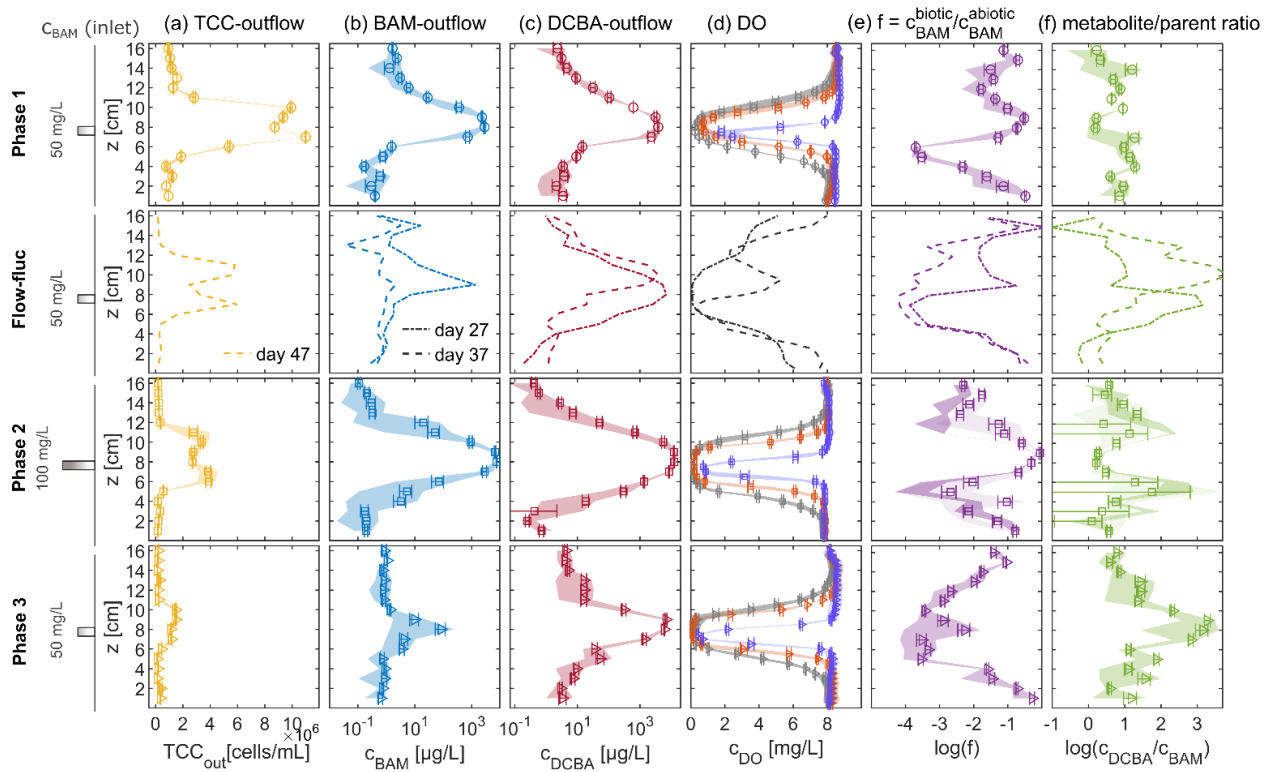


Figure 2.2. Vertical profiles of washed-out cell numbers, concentrations, and concentration ratios. Column (a): total number of washed-out cells; column (b): BAM concentrations; column (c): 2,6-DCBA concentrations; column (d): dissolved oxygen (DO) concentrations 2 cm from the inlet boundary (blue shade), in the middle of the tank (orange shade), and 2 cm from the outlet boundary (grey shade); column (e): residual BAM concentrations in the effluent relative to the expected concentration in an abiotic experiment $f = c_{BAM}^{biotic}/c_{BAM}^{abiotic}$, see eq 2.2; column (f): molar concentration ratios of 2,6-DCBA to BAM in the effluent in three experimental phases and on the flow fluctuation days. Colour shades represent the range of measurement values during the sampling periods. Data points with error bars represent the average values with standard errors during the quasi-steady state sampling periods. Dashed-dotted lines and dashed lines in the second row represent the data on the flow fluctuation days at the end of phase 1. DO profiles on the flow fluctuation days only represent the data measured along the outlet cross-section. Samples for concentration measurements were measured every three to five days from days 5 to 26, 66 to 135, and 140 to 169. Samples for TCC_{out} measurements were measured on days 17, 19, 47 (phase 1), 81, 83, 87 (phase 2), 155, and 159 (phase 3), respectively.

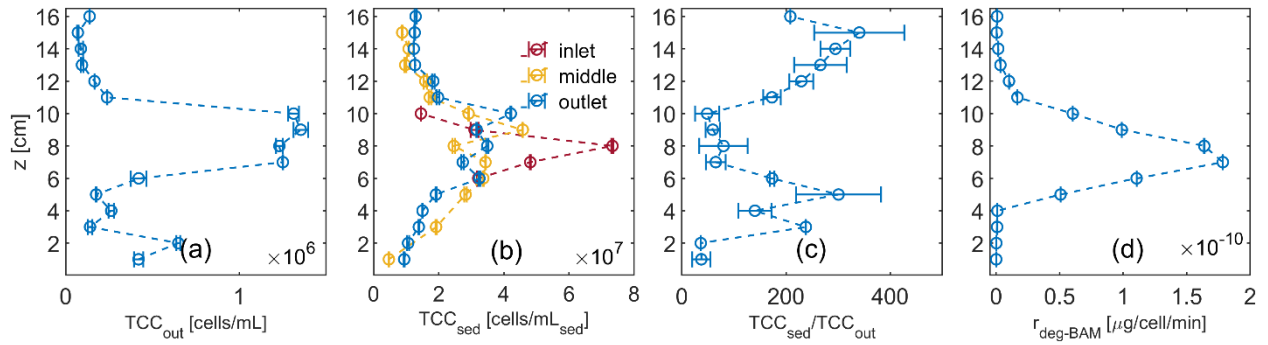


Figure 2.3. Vertical profiles of (a) total cell number of washed-out bacteria (TCC_{out}), (b) total cell number of bacteria attached to the sediments (TCC_{sed}) on the last sampling day of phase 3 (day 170) with 50 mg/L inlet concentration, (c) ratio of the cell number on sediments to the washed-out cell number per unit of bulk volume, (d) specific BAM degradation rate per cell $r_{deg-BAM}$ on day 170. In panel (b), red, yellow, and blue circles represent the measurements of TCC_{sed} at 2 cm distance from the inlet boundary, in the middle, and at 2 cm distance from the outlet boundary of the tank, respectively. Error bars in panel (a)–(b) represent the measurement errors (standard deviation); uncertainties in panel (c)–(d) were calculated based on Gauss’ error propagation law by using the standard deviations of TCC_{sed} values at different locations.

To better understand bacterial adaptation in the different zones of the BAM plume, we calculated the ratio of the number of sediment-attached bacteria to the washed-out bacterial cell number per unit of bulk volume (TCC_{sed}/TCC_{out}) at the end of phase 3 with 50 mg/L BAM inlet concentration (Figure 2.3). When calculating the ratio TCC_{sed}/TCC_{out} , the number of washed-out (suspended) bacterial cells per unit of water volume ($\text{cells L}_{liquid}^{-1}$) was transformed into the number of bacterial cells per unit of bulk volume ($\text{cells L}_{bulk}^{-1} = \text{cells L}_{sed}^{-1}$) by multiplication with the porosity of 0.45. The number of bacteria attached to the sediment was 13–220 times higher than the number of washed-out bacterial cells. In the center of the plume ($z = 7\text{--}10$ cm), where there was no substrate (BAM) limitation, the ratio of attached to suspended cells (TCC_{sed}/TCC_{out}) was the smallest. With the widening of the plume, this ratio increased. This trend of the TCC_{sed}/TCC_{out} ratio (Figure 2.3c) mirrors the observations in many microcosm^{28, 57} and field studies^{58–62} in which a low TCC_{sed}/TCC_{out} ratio occurs at high substrate concentrations, whereas a high TCC_{sed}/TCC_{out} ratio, albeit with overall lower absolute cell numbers, is typical of substrate-limited oligotrophic conditions.^{58, 63} This behavior can be explained by growth-mediated biomass transport.^{24, 28} When a certain density of the biomass in micro-colonies is reached, additional cells resulting from biomass growth are released into the mobile phase and can thus be washed out. In this framework, the increased

$TCC_{\text{sed}}/TCC_{\text{out}}$ ratio at smaller substrate concentrations indicates slower microbial growth at lower concentrations. We divided the BAM-mass consumed per time by the cell number of the attached bacteria to obtain the specific BAM-degradation rate per cell $r_{\text{deg-BAM}}$. In general, we observed a decreased $r_{\text{deg-BAM}}$ with decreasing BAM concentration which was consistent with the observed trend in the fraction f of transformed BAM in phase 3 (Figure 2.2e, fourth row).

Adaptation of *Aminobacter* sp. MSH1 and Change of the Biodegradation Efficiency when Exposed to Different Concentrations.

In phase 1 of the experiment, when we introduced 50 mg/L BAM through the central port, biodegradation of BAM started immediately after inoculation, and the system stayed at quasi-steady state from day 5 to day 26. The relatively high number of washed-out cells (Figure 2.2a, first row) indicated that bacteria were in the planktonic adaptation stage after inoculation, but not well adapted to attach to sediments. In addition, a fraction of these washed-out cells may be attributed to leftovers of the inoculation (cells did not initially attach to sediments). Interestingly, the spatial distribution of the biodegradation activity was not yet symmetric, with a smaller f -value at the lower than at the upper fringe of the plume (Figure 2.2e, first row). This observation indicates that the inoculation-induced activity of bacteria was still different in the two replicate parts of the tank, even after three weeks of operation. This may be attributed to the non-symmetric distribution of microbial activity, possibly in combination with slight variations in flow and/or bacterial adaptation.

At the end of phase 1, inadvertent partial “clogging” occurred shortly in the outlet ports on day 27 and day 35, which provided an opportunity to investigate the response of the system to a flow fluctuation. The plume of BAM slightly shifted upwards along with the fluctuation of 2,6-DCBA (Figure 2.2) and DO (Figure S1). More BAM was degraded as indicated by decreased BAM concentrations (Figure 2.2b, second row) and a decreased f -value (Figure 2.2e, second row). After the clogging was removed, the previous flow regime re-established, and the plume went back to its original position. The BAM concentrations remained at lower levels in conjunction with a smaller number of washed-out bacterial cells by the end of the first period (day 47). We speculate that the enhanced degradation of BAM could be driven by a better spread of the bacterial biomass.^{23, 28, 31} Specifically, when the plume center slightly moved upwards—as indicated by the shift of the conservative tracer metolachlor (Figure S2)—it reached the previous plume fringes where biomass hot spots were located. In addition, a shift of the BAM plume induced a shift in the distribution of biomass, leading to a buildup of cells

at new locations (as depicted in Figure 2.2a second row, the hot-spot fringe shifted upwards from $z = 10$ cm to $z = 11$ cm). Thus, the flow fluctuation (i.e., reduction of the flow rate or redirection of the plume due to the clogging) led to an unintended priming which stimulated a more even distribution of biodegradation activity throughout the spatial profile.

In phase 2, we increased the BAM concentration in the central inlet port to 100 mg/L, establishing a quasi-steady state after two weeks. Even though the increased inlet concentration would be expected to induce a higher growth rate of attached biomass, the numbers of washed-out cells were lower than in phase 1 and during the flow fluctuation period. This indicates that bacteria might not have well adapted until phase 2. Under the assumption that washed-out cell numbers represented cell growth, we calculated the carbon assimilation rate by dividing the amount of consumed carbon of BAM and 2,6-DCBA to the amount of carbon of the washed-out biomass (Table S1). The calculated carbon assimilation rate of $17 \pm 10\%$ indicates that carbon was primarily utilized for cell respiration rather than cell growth (carbon assimilation for biomass synthesis). Further, a widening of the BAM plume was observed when 100 mg/L BAM solution was fed through the central inlet port, due to a depletion of oxygen over a larger width of the plume center. Consequently, the plume fringes where bacteria were particularly enriched (Figure 2.3b) widened, from the locations at $z = 7$ cm and $z = 11$ cm to the location at $z = 6$ cm and $z = 11$ cm. In addition, the degradation activity became spatially more symmetric, as seen in the profiles of f -values and metabolite-to-parent compound ratio (Figure 2.2e, f, third row). This observation indicates that a more symmetric distribution of biomass in the system had developed with the spread of the contaminant plume.

In phase 3 (the final phase), we decreased the inlet BAM concentration from 100 mg/L back down to 50 mg/L. The remaining BAM concentration decreased within 20 hours after the switch, and up to an averaged BAM degradation efficiency of $99 \pm 2\%$ was reached in the sampling period (day 140 to day 169). The calculated carbon assimilation rate was $7 \pm 1\%$. The remaining BAM concentrations were generally smaller (Figure 2.4b), and the vertical distribution of the activity in the tank was more symmetric than in phase 1, even though the inlet concentration was the same (Figure 2.2e, fourth row). At the outlet ports at $z = 9$ – 12 cm, the f -values were about two orders of magnitude lower, and the isotope fractionation was generally 5–7‰ higher (Figure 2.4). This line of evidence (BAM concentration, f - values, and isotope value profiles) suggests that the combined effect of the inadvertent flow fluctuation and increased substrate concentration injection (priming) yielded an increased degradation

capacity/activity of attached cells and led to a higher degradation of BAM compared to phase 1, at identical BAM inlet concentrations (50 mg/L). It also suggests that once a new quasi-steady state related to substrate concentration and flow velocity²⁸ had been reached, a decrease in inlet concentrations between phase 2 and phase 3 did not drive an immediate decrease in bacterial activity. Instead, it persisted for a considerable time (weeks to months).^{12, 24, 63} Specifically, the zones of the highest attached cell numbers on the sediment in phase 3 ($z = 6, 9, \text{ and } 10 \text{ cm}$, Figure 2.2a, fourth row) were wider than the zone covered by the ports of the highest washed-out cell numbers in the initial operational phase 1 ($z = 7 \text{ and } 10 \text{ cm}$ at 50 mg/L BAM inlet concentration, Figure 2.2a, first row). This implies the persistence of biomass, established during the high-concentration phase 2, even after the BAM inlet concentration had decreased. Hence, although the plume width narrowed when the BAM inlet concentration was reduced from 100 mg/L (phase 2) back to 50 mg/L (phase 3), the observed elevated degradation in phase 3 indicated that the attached biomass distribution and activity likely remained similar as in phase 2 with 100 mg/L BAM inlet concentration. This result contrasts with the observation in phase 1 (large washed-out cell number with overall low degradation capacity) and the widely observed loss (more than 90%) of initially adhered *Aminobacter* sp. MSH1 bacteria and the simultaneous decrease in BAM degradation efficiency within the first weeks after inoculation in many sand-filter experiments without priming.^{13, 64}

Carbon Isotope Fractionation Revealed Underlying Limitations for Biodegradation over Three Experimental Phases.

To further elucidate the change of the microbial system in response to concentration changes, we analyzed the isotope fractionation profile along the outlet cross-section and against the fraction f (Figure 2.4). As recently demonstrated by Sun et al.,⁴⁹ isotope fractionation induced by dispersion, diffusion, and adsorption is negligible in the tank system so that changes in isotope values can directly be related to degradation and mass transfer into the cell interior.

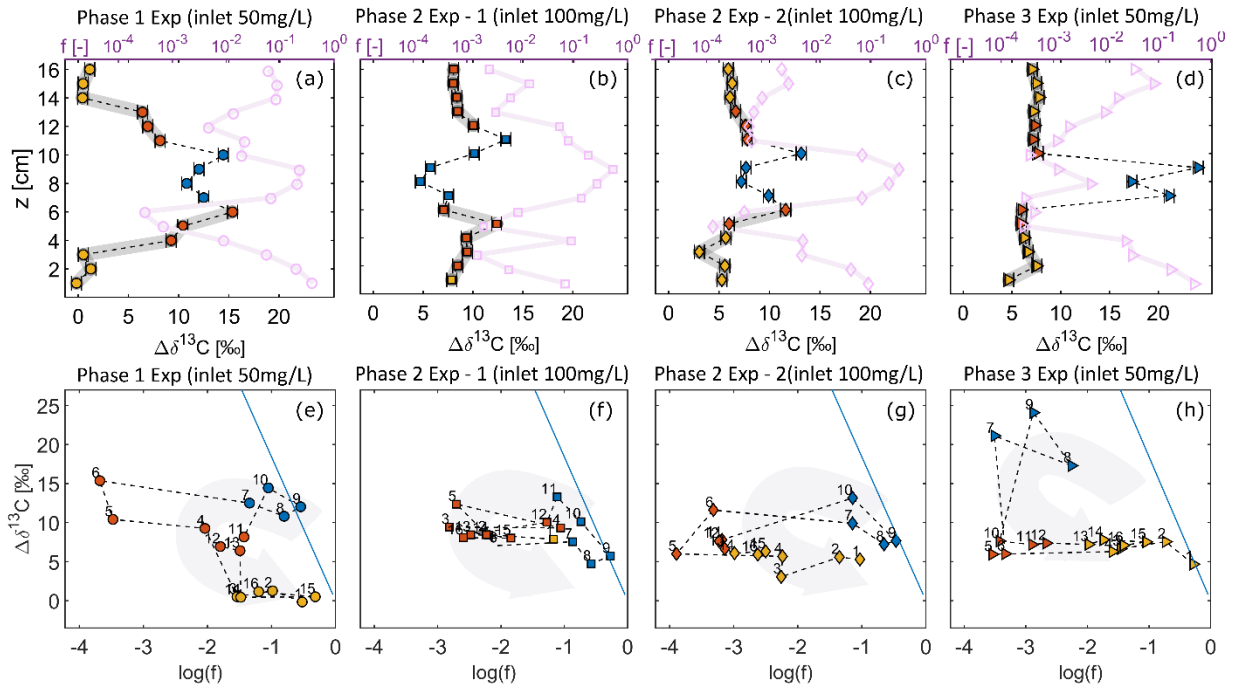


Figure 2.4 Observable isotope fractionation in the three experimental phases with BAM inlet concentrations of 50, 100, and 50 mg/L through the central inlet port. Panels (a)–(d): vertical profiles of carbon isotope values $\Delta\delta^{13}\text{C}$ (data with error bars) and mean values of the fraction f of residual BAM concentration ($f = c_{\text{BAM}}^{\text{biotic}}/c_{\text{BAM}}^{\text{abiotic}}$, purple data points); panels (e)–(h): carbon isotope values $\Delta\delta^{13}\text{C}$ vs. the fraction f —a typical representation of data under the assumption of the Rayleigh relation (eq 2.1). For comparison, blue solid lines represent the predicted Rayleigh relation between f and isotope values in the absence of mass-transfer limitation. Data points were labeled with the vertical outlet sampling position $z = 1$ –16 cm. Isotope data points with gray shadow in the upper panels (a)–(d) represent the isotope values strongly constrained by mass-transfer limitation (red points) or by both mass-transfer limitation and slowdown of enzyme reaction rate (yellow data points). Blue data points represent isotope fractionation close to the Rayleigh relation. Dashed lines connect data points from adjacent ports as a guide. Error bars represent ± 0.5 ‰ uncertainty of carbon isotope measurements.

The isotope fractionation profile along the outlet cross-section showed a general trend similar to the one observed and accurately simulated by Sun et al.⁴⁰. At high BAM concentrations (from the center of the plume to the plume fringes, blue data points in Figure 2.4a–c, e–g), isotope fractionation increased with decreasing remaining BAM concentrations and decreasing f -values. These trends follow Rayleigh behavior and indicate that degradation was only limited by the availability of the electron acceptor (i.e., DO). At the plume fringes, where electron donors and acceptors mixed most efficiently, isotope values were highest, corresponding to a small f -value and a high concentration ratio of 2,6-DCBA to BAM (Figure

2.2e, f). At lower BAM concentrations (from the plume fringes towards the upper and lower boundaries of the tank, red data points in Figure 2.4), the smaller extent of isotope fractionation (compared to the isotope fractionation that the Rayleigh equation would predict with the given f -values) revealed that mass transfer became limiting, so that observed isotope fractionation was strongly masked (“threshold region”). At locations where BAM concentrations were even lower (0.1–3 $\mu\text{g/L}$, in the uppermost and lowermost regions, yellow data points in Figure 2.4), changes in isotope values remained small relative to the isotope values in the threshold region. Beyond this general trend of isotope fractionation that was already observed by Sun et al.,⁴⁰ the design of our experiment in three phases enabled us to follow the relationship between isotope fractionation and the f -value over time (Figure 2.4e–h) and to explore whether it can elucidate the limitations of BAM degradation at low concentrations (e.g., mass-transfer limitation, or limitation by physiological adaptation) in response to the perturbations imposed.

In phase 1, we did not observe any isotope fractionation at the upper and lower boundaries of the tank (yellow dots in Figure 2.4a, e, at $z = 1, 2, 3, 14, 15, 16$ cm). A potential explanation is that bacteria were in the planktonic adaptation stage after inoculation, and neither the cell population nor the degradation activity was yet well established throughout the tank. Therefore, in the first sampling days, the associated turnover was limited, despite favorable thermodynamic conditions. Since we collected integrated samples over a longer time period, the original isotope ratio of non-degraded samples (BAM molecules having experienced no biodegradation) at the beginning of the sampling period may have diluted the isotope fractionation induced by biodegradation at the later stage of the sampling period. Thus, isotope fractionation may not have been discernible in the final time-integrated samples. This is consistent with our conclusion that the bottleneck of biodegradation in this experimental phase was the adaptation and establishment of the strain *Aminobacter* sp. MSH1 throughout the tank. Furthermore, even though the f -values in the upper region are approximately two orders of magnitude higher than the ones in the lower region, the difference of the observed isotope fractionation in the upper and lower regions is only 1–2 per mil (Figure 2.4a, e). As discussed in more detail below, this again is likely due to the effect of masking where similar changes in isotope values are observed irrespective of f -values.

In the first sampling period of phase 2, when the BAM inlet concentration in the central port had just been increased to 100 mg/L, the degradation hot spots where the isotope fractionation was highest were at the ports of $z = 5$ and 11 cm. In contrast, during the second

sampling period, when the bacteria had already adapted to the change of the higher inlet concentration, the biodegradation efficiency had increased, and the plume became narrower, as indicated by the smaller f -values and higher isotope fractionation at the hot spots at $z = 6$ and 10 cm. The corresponding experimental data of this phase has recently been analyzed in detail via a numerical reactive transport model.⁴⁰ The current study goes further and enables us to explore bacterial adaptation beyond this snapshot in time by following the change of biodegradation activity in the tank system over time.

In phase 3, after the BAM concentration in the central inlet port had been decreased to 50 mg/L, isotope values in the plume center (blue data points, Figure 2.4h) deviated from the theoretical trend of the Rayleigh relation (blue solid line, Figure 2.4h) and the constant isotope values in the low concentrations throughout the upper and lower regions of the tank (red and yellow data points, Figure 2.4h) revealed that biodegradation was limited by mass transfer throughout the tank, even in the plume center, which is an effect of the large biomass buildup during phase 2. The observation follows the trend observed during the second sampling period of phase 2 where the f -values at ports $z = 1-5$ cm and $z = 11-16$ cm increased towards the upper and lower boundaries, indicating a decreased biodegradation rate and a potential physiological limitation (see also Sun et al.⁴⁰). With sufficient biomass, the biodegradation efficiency of the system increased to the degree that it became limited by diffusion into the cells. Under these conditions, the changes in isotope values remained equally small at the upper and the lower plume region, whereas f -values increased with decreasing concentration, indicating a smaller extent of degradation (yellow dots). This zone of reduced degradation at $z = 1-4, 13-16$ cm was closer to the plume center compared to phases 1 and 2, which indicates a wider spread of a physiological adaptation (less active metabolism) in response to the mass-transfer limitation of substrate supply. In line with this observation, Figure 2.3d shows a much lower specific BAM degradation rate per cell at the upper and lower boundaries of the tank. Thus, although the overall biodegradation efficiency was enhanced, the degradation activity was limited by a physiological adaptation of the microorganisms to the low substrate concentration. (Note: degradation in the stimulated system, phase 3, was more efficient compared to the initial phase 1 when in the BAM inlet concentration was also 50 mg/L BAM). The higher biomass density at the onset of phase 3 (a legacy of the 100 mg/L injection during phase 2) drove the concentration drop in the breakthrough profiles. We hypothesize that this caused the bacteria to adapt to the low concentrations via a reduction in the cell-specific degradation activity, thus down-regulating their maintenance energy requirements. To this end

we reason that keeping a higher internal activity would mean high maintenance-energy requirements. This would be difficult to sustain at low substrate turnover because of strong mass-transfer limitation as indicated by close to zero fractionation. We speculate that such physiological limitations (e.g., downregulation of functional genes, or reduced activity of catabolic enzymes) resulted in lower bacterial activity which prevented complete degradation of BAM. This physiological limitation of *Aminobacter* sp. MSH1, which results in reduced BAM degrading ability at low BAM concentration, has also been observed by Sekhar et al.¹⁹, who explained it by reduced production of the amidase BbdA that converts BAM to 2,6-DCBA due to physiological adaptation.

2.3.4 Summary

Extensive research has been conducted that targets the classical priming effect of labile organic matter on the degradation/mineralization rate of recalcitrant organic matter.⁶⁵⁻⁶⁸ However, few studies have focused on the priming effect during biodegradation of organic contaminants.⁶⁹ In this study, we observed a priming effect on biodegradation when we introduced intermediate changes in environmental conditions (such as a temporary increase of the substrate concentration and a temporary, transient flow condition) in a flow-through sediment system. The elevated degradation efficiency continued over weeks after returning to the low inlet concentration, suggesting that such priming has the potential to establish a sustainable high degradation efficiency over a relatively long time (weeks or months). Exposing bacteria to elevated concentrations of the target compound and changing the flow regime is, therefore, a potential strategy to improve the degradation of organic contaminants in water treatment plants or *in-situ* remediation. To translate this into technologies for real water treatment facilities, future investigations may focus on pilot sand-filter experiments that introduce such intermediate disturbances during the back-flushing stage, or that focus on the influence of multiple carbon sources on such a priming effect.

Furthermore, the observed stimulated degradation activity after priming and temporal flow fluctuation also indicates that intermediate concentration/flow fluctuations can be a potential trigger that enriches biomass and stimulates the spread of the bacteria. For a conceptual assessment of *in-situ* biodegradation at contaminated sites, priming effects or intermediate system disturbances should therefore be considered.

Finally, isotope analysis over a range of different quasi-steady-state concentrations under different loading conditions suggested that mass transfer became increasingly limiting the more the system was stimulated and adapted over time. Hence, even under stimulated conditions with a sufficient supply of nutrients and other potential growth-limiting compounds (e.g., oxygen), mass-transfer limitation of the substrate, both macroscopically (by dispersion) and microscopically (by mass transfer between the bulk phase and the bacterial interior), will ultimately become a bottleneck for degradation. In response, physiological limitation may factor in when the concentrations are extremely low. Hence, the combined analysis of isotope fractionation and substrate concentrations in comparison to abiotic behavior has the potential to identify the underlying limiting factors during biodegradation in lab and in field applications.

References

1. Schwarzenbach, R. P.; Escher, B. I.; Fenner, K.; Hofstetter, T. B.; Johnson, C. A.; Von Gunten, U.; Wehrli, B., The challenge of micropollutants in aquatic systems. *Science* **2006**, *313* (5790), 1072-1077.
2. Tang, F. H.; Lenzen, M.; McBratney, A.; Maggi, F., Risk of pesticide pollution at the global scale. *Nat. Geosci.* **2021**, *14* (4), 206-210.
3. Bedient, P. B.; Rifai, H. S.; Newell, C. J., *Groundwater Contamination: Transport and Remediation*. Prentice-Hall International, Inc.: 1994.
4. Clausen, L.; Larsen, F.; Albrechtsen, H.-J., Sorption of the herbicide dichlobenil and the metabolite 2, 6-dichlorobenzamide on soils and aquifer sediments. *Environ. Sci. Technol.* **2004**, *38* (17), 4510-4518.
5. EU, E. C., Drinking Water Directive (COUNCIL DIRECTIVE 98/83/EC). Official Journal of the European Communities: 1998.
6. Ellegaard-Jensen, L.; Horemans, B.; Raes, B.; Aamand, J.; Hansen, L. H., Groundwater contamination with 2,6-dichlorobenzamide (BAM) and perspectives for its microbial removal. *Appl. Microbiol. Biotechnol.* **2017**, *101* (13), 5235-5245.
7. Vandermaesen, J.; Horemans, B.; Degryse, J.; Boonen, J.; Walravens, E.; Springael, D., Mineralization of the common groundwater pollutant 2,6-dichlorobenzamide (BAM) and its metabolite 2,6-dichlorobenzoic acid (2,6-DCBA) in sand filter units of drinking water treatment plants. *Environ. Sci. Technol.* **2016**, *50* (18), 10114-22.
8. Pukkila, V.; Kontro, M. H., Dichlobenil and 2,6-dichlorobenzamide (BAM) dissipation in topsoil and deposits from groundwater environment within the boreal region in southern Finland. *Environ. Sci. Pollut. Res.* **2014**, *21* (3), 2289-2297.
9. Sorensen, S. R.; Holtze, M. S.; Simonsen, A.; Aamand, J., Degradation and mineralization of nanomolar concentrations of the herbicide dichlobenil and its persistent metabolite 2,6-dichlorobenzamide by *Aminobacter* spp. isolated from dichlobenil-treated soils. *Appl. Environ. Microbiol.* **2007**, *73* (2), 399-406.

10. Zhang, S.; Mao, G.; Crittenden, J.; Liu, X.; Du, H., Groundwater remediation from the past to the future: A bibliometric analysis. *Water Res.* **2017**, *119*, 114-125.
11. Cycoń, M.; Mroziak, A.; Piotrowska-Seget, Z., Bioaugmentation as a strategy for the remediation of pesticide-polluted soil: A review. *Chemosphere* **2017**, *172*, 52-71.
12. Meckenstock, R. U.; Elsner, M.; Griebler, C.; Lueders, T.; Stumpp, C.; Aamand, J.; Agathos, S. N.; Albrechtsen, H. J.; Bastiaens, L.; Bjerg, P. L.; Boon, N.; Dejonghe, W.; Huang, W. E.; Schmidt, S. I.; Smolders, E.; Sorensen, S. R.; Springael, D.; van Breukelen, B. M., Biodegradation: Updating the concepts of control for microbial cleanup in contaminated aquifers. *Environ. Sci. Technol.* **2015**, *49* (12), 7073-81.
13. Albers, C. N.; Feld, L.; Ellegaard-Jensen, L.; Aamand, J., Degradation of trace concentrations of the persistent groundwater pollutant 2,6-dichlorobenzamide (BAM) in bioaugmented rapid sand filters. *Water Res.* **2015**, *83*, 61-70.
14. Ellegaard-Jensen, L.; Albers, C. N.; Aamand, J., Protozoa graze on the 2, 6-dichlorobenzamide (BAM)-degrading bacterium *Aminobacter* sp. MSH1 introduced into waterworks sand filters. *Appl. Microbiol. Biotechnol.* **2016**, *100* (20), 8965-8973.
15. Schultz-Jensen, N.; Knudsen, B. E.; Frkova, Z.; Aamand, J.; Johansen, T.; Thykaer, J.; Sorensen, S. R., Large-scale bioreactor production of the herbicide-degrading *Aminobacter* sp. strain MSH1. *Appl. Microbiol. Biotechnol.* **2014**, *98* (5), 2335-44.
16. Horemans, B.; Raes, B.; Vandermaesen, J.; Simanjuntak, Y.; Brocatus, H.; T'Syen, J.; Degryse, J.; Boonen, J.; Wittebol, J.; Lapanje, A.; Sorensen, S. R.; Springael, D., Biocarriers improve bioaugmentation efficiency of a rapid sand filter for the treatment of 2,6-dichlorobenzamide-contaminated drinking water. *Environ. Sci. Technol.* **2017**, *51* (3), 1616-1625.
17. Kjaergaard Nielsen, T.; Horemans, B.; Lood, C.; T'Syen, J.; van Noort, V.; Lavigne, R.; Ellegaard-Jensen, L.; Hylling, O.; Aamand, J.; Springael, D., Analyses of the complete genome sequence of 2, 6-dichlorobenzamide (BAM) degrader *Aminobacter* sp. MSH1 suggests a polyploid chromosome, phylogenetic reassignment, and functions of (un) stable plasmids. *bioRxiv* **2021**.
18. Sjöholm, O. R.; Nybroe, O.; Aamand, J.; Sorensen, J., 2,6-Dichlorobenzamide (BAM) herbicide mineralisation by *Aminobacter* sp. MSH1 during starvation depends on a subpopulation of intact cells maintaining vital membrane functions. *Environ. Pollut.* **2010**, *158* (12), 3618-25.
19. Sekhar, A.; Horemans, B.; Aamand, J.; Sorensen, S. R.; Vanhaecke, L.; Bussche, J. V.; Hofkens, J.; Springael, D., Surface colonization and activity of the 2,6-dichlorobenzamide (BAM) degrading *Aminobacter* sp. strain MSH1 at macro- and micropollutant BAM concentrations. *Environ. Sci. Technol.* **2016**, *50* (18), 10123-33.
20. Thullner, M.; Kampara, M.; Richnow, H. H.; Harms, H.; Wick, L. Y., Impact of bioavailability restrictions on microbially induced stable isotope fractionation. 1. Theoretical calculation. *Environ. Sci. Technol.* **2008**, *42* (17), 6544-6551.
21. Bosma, T. N. P.; Middeldorp, P. J. M.; Schraa, G.; Zehnder, A. J. B., Mass transfer limitation of biotransformation: quantifying bioavailability. *Environ. Sci. Technol.* **1997**, *31* (1), 248-252.
22. Kundu, K.; Marozava, S.; Ehrl, B.; Merl-Pham, J.; Griebler, C.; Elsner, M., Defining lower limits of biodegradation: atrazine degradation regulated by mass transfer and maintenance demand in *Arthrobacter aurescens* TC1. *ISME J.* **2019**, *13* (9), 2236-2251.

23. Eckert, D.; Kürzinger, P.; Bauer, R.; Griebler, C.; Cirpka, O. A., Fringe-controlled biodegradation under dynamic conditions: Quasi 2-D flow-through experiments and reactive-transport modeling. *J. Contam. Hydrol.* **2015**, *172*, 100-111.
24. Mellage, A.; Eckert, D.; Grosbacher, M.; Inan, A. Z.; Cirpka, O. A.; Griebler, C., Dynamics of suspended and attached aerobic toluene degraders in small-scale flow-through sediment systems under growth and starvation conditions. *Environ. Sci. Technol.* **2015**, *49* (12), 7161-9.
25. Torstensson, L., Microbial decomposition of herbicides in the soil. *Outlook Agric.* **1988**, *17* (3), 120-124.
26. Greenwood, P. F.; Wibrow, S.; George, S. J.; Tibbett, M., Hydrocarbon biodegradation and soil microbial community response to repeated oil exposure. *Org. Geochem.* **2009**, *40* (3), 293-300.
27. Kundu, K.; Weber, N.; Griebler, C.; Elsner, M., Phenotypic heterogeneity as key factor for growth and survival under oligotrophic conditions. *Environ. Microbiol.* **2020**, *22* (8), 3339-3356.
28. Grosbacher, M.; Eckert, D.; Cirpka, O. A.; Griebler, C., Contaminant concentration versus flow velocity: Drivers of biodegradation and microbial growth in groundwater model systems. *Biodegradation* **2018**, *29* (3), 211-232.
29. Prommer, H.; Barry, D. A.; Davis, G. B., Modelling of physical and reactive processes during biodegradation of a hydrocarbon plume under transient groundwater flow conditions. *J. Contam. Hydrol.* **2002**, *59* (1), 113-131.
30. Cirpka, O. A.; Attinger, S., Effective dispersion in heterogeneous media under random transient flow conditions. *Water Resour. Res.* **2003**, *39* (9).
31. Rodríguez-Escales, P.; Fernández-García, D.; Drechsel, J.; Folch, A.; Sanchez-Vila, X., Improving degradation of emerging organic compounds by applying chaotic advection in Managed Aquifer Recharge in randomly heterogeneous porous media. *Water Resour. Res.* **2017**, *53* (5), 4376-4392.
32. Kuntze, K.; Eisenmann, H.; Richnow, H.-H.; Fischer, A., Compound-specific stable isotope analysis (CSIA) for evaluating degradation of organic pollutants: An overview of field case studies. In *Anaerobic Utilization of Hydrocarbons, Oils, and Lipids*, Boll, M., Ed. Springer, Cham.: 2019; pp 323-360.
33. Meckenstock, R. U.; Morasch, B.; Griebler, C.; Richnow, H. H., Stable isotope fractionation analysis as a tool to monitor biodegradation in contaminated aquifers. *J. Contam. Hydrol.* **2004**, *75* (3-4), 215-55.
34. Schmidt, T. C.; Zwank, L.; Elsner, M.; Berg, M.; Meckenstock, R. U.; Haderlein, S. B., Compound-specific stable isotope analysis of organic contaminants in natural environments: a critical review of the state of the art, prospects, and future challenges. *Anal. Bioanal. Chem.* **2004**, *378* (2), 283-300.
35. Wu, L.; Verma, D.; Bondgaard, M.; Mølle, A.; Vogt, C.; Subudhi, S.; Richnow, H. H., Carbon and hydrogen isotope analysis of parathion for characterizing its natural attenuation by hydrolysis at a contaminated site. *Water Res.* **2018**, *143*, 146-154.

36. Richnow, H. H.; Annweiler, E.; Michaelis, W.; Meckenstock, R. U., Microbial in situ degradation of aromatic hydrocarbons in a contaminated aquifer monitored by carbon isotope fractionation. *J. Contam. Hydrol.* **2003**, *65* (1-2), 101-120.
37. Rayleigh, L., Theoretical considerations respecting the separation of gases by diffusion and similar processes. *London, Edinburgh Dublin Philos. Mag. J. Sci.* **1896**, *42* (259), 493-498.
38. Hoefs, J., *Stable Isotope Geochemistry*. Springer Verlag: Chicago, 1987.
39. Thullner, M.; Fischer, A.; Richnow, H.-H.; Wick, L. Y., Influence of mass transfer on stable isotope fractionation. *Appl. Microbiol. Biotechnol.* **2013**, *97* (2), 441-452.
40. Sun, F.; Mellage, A.; Gharasoo, M.; Melsbach, A.; Cao, X.; Zimmermann, R.; Griebler, C.; Thullner, M.; Cirpka, O. A.; Elsner, M., Mass-transfer-limited biodegradation at low concentrations—evidence from reactive transport modeling of isotope profiles in a bench-scale aquifer. *Environ. Sci. Technol.* **2021**, *55* (11), 7386-7397.
41. Ehrl, B. N.; Kundu, K.; Gharasoo, M.; Marozava, S.; Elsner, M., Rate-limiting mass transfer in micropollutant degradation revealed by isotope fractionation in chemostat. *Environ. Sci. Technol.* **2019**, *53* (3), 1197-1205.
42. Reinnicke, S.; Simonsen, A.; Sorensen, S. R.; Aamand, J.; Elsner, M., C and N isotope fractionation during biodegradation of the pesticide metabolite 2,6-dichlorobenzamide (BAM): potential for environmental assessments. *Environ. Sci. Technol.* **2012**, *46* (3), 1447-54.
43. Meyer, A. H.; Penning, H.; Elsner, M., C and N Isotope Fractionation Suggests Similar Mechanisms of Microbial Atrazine Transformation Despite Involvement of Different Enzymes (AtzA and TrzN). *Environ. Sci. Technol.* **2009**, *43* (21), 8079-8085.
44. Schurner, H. K.; Maier, M. P.; Eckert, D.; Brejcha, R.; Neumann, C. C.; Stumpp, C.; Cirpka, O. A.; Elsner, M., Compound-specific stable isotope fractionation of pesticides and pharmaceuticals in a mesoscale aquifer model. *Environ. Sci. Technol.* **2016**, *50* (11), 5729-39.
45. Lihl, C.; Heckel, B.; Grzybkowska, A.; Dybala-Defratyka, A.; Ponsin, V.; Torrentó, C.; Hunkeler, D.; Elsner, M., Compound-specific chlorine isotope fractionation in biodegradation of atrazine. *Environmental Science: Processes & Impacts* **2020**, *22* (3), 792-801.
46. Kampara, M.; Thullner, M.; Richnow, H. H.; Harms, H.; Wick, L. Y., Impact of bioavailability restrictions on microbially induced stable isotope fractionation. 2. Experimental evidence. *Environ. Sci. Technol.* **2008**, *42* (17), 6552-6558.
47. Kampara, M.; Thullner, M.; Harms, H.; Wick, L. Y., Impact of cell density on microbially induced stable isotope fractionation. *Applied microbiology and biotechnology* **2009**, *81* (5), 977-985.
48. Bauer, R. D.; Maloszewski, P.; Zhang, Y.; Meckenstock, R. U.; Griebler, C., Mixing-controlled biodegradation in a toluene plume--Results from two-dimensional laboratory experiments. *J. Contam. Hydrol.* **2008**, *96* (1-4), 150-68.
49. Sun, F.; Peters, J.; Thullner, M.; Cirpka, O. A.; Elsner, M., Magnitude of diffusion- and transverse dispersion-induced isotope fractionation of organic compounds in aqueous systems. *Environ. Sci. Technol.* **2021**, *55* (8), 4772-4782.

50. Jensen, G. G.; Bjorklund, E.; Simonsen, A.; Halling-Sorensen, B., Determination of 2,6-dichlorobenzamide and its degradation products in water samples using solid-phase extraction followed by liquid chromatography-tandem mass spectrometry. *J. Chromatogr. A* **2009**, *1216* (27), 5199-206.
51. Bayer, A.; Drexel, R.; Weber, N.; Griebler, C., Quantification of aquatic sediment prokaryotes—A multiple-steps optimization testing sands from pristine and contaminated aquifers. *Limnologica* **2016**, *56*, 6-13.
52. Pilloni, G.; von Netzer, F.; Engel, M.; Lueders, T., Electron acceptor-dependent identification of key anaerobic toluene degraders at a tar-oil-contaminated aquifer by Pyro-SIP. *FEMS Microbiol. Ecol.* **2011**, *78* (1), 165-75.
53. Tuxen, N.; Albrechtsen, H. J.; Bjerg, P. L., Identification of a reactive degradation zone at a landfill leachate plume fringe using high resolution sampling and incubation techniques. *J. Contam. Hydrol.* **2006**, *85* (3-4), 179-94.
54. Anneser, B.; Einsiedl, F.; Meckenstock, R. U.; Richters, L.; Wisotzky, F.; Griebler, C., High-resolution monitoring of biogeochemical gradients in a tar oil-contaminated aquifer. *Appl. Geochem.* **2008**, *23* (6), 1715-1730.
55. Thullner, M.; Mauclaire, L.; Schroth, M. H.; Kinzelbach, W.; Zeyer, J., Interaction between water flow and spatial distribution of microbial growth in a two-dimensional flow field in saturated porous media. *J. Contam. Hydrol.* **2002**, *58* (3-4), 169-89.
56. Horemans, B.; Vandermaesen, J.; Sekhar, A.; Rombouts, C.; Hofkens, J.; Vanhaecke, L.; Springael, D., Aminobacter sp. MSH1 invades sand filter community biofilms while retaining 2,6-dichlorobenzamide degradation functionality under C- and N-limiting conditions. *FEMS Microbiol. Ecol.* **2017**, *93* (6).
57. Bengtsson, G., Growth and metabolic flexibility in groundwater bacteria. *Microb. Ecol.* **1989**, *18* (3), 235-248.
58. Griebler, C.; Mindl, B.; Slezak, D.; Geiger-Kaiser, M., Distribution patterns of attached and suspended bacteria in pristine and contaminated shallow aquifers studied with an in situ sediment exposure microcosm. *Aquat. Microb. Ecol.* **2002**, *28* (2), 117-129.
59. Griebler, C.; Mindl, B.; Slezak, D., Combining DAPI and SYBR Green II for the enumeration of total bacterial numbers in aquatic sediments. *Int. Rev. Hydrobiol.* **2001**, *86* (4-5), 453-465.
60. Harvey, R. W.; Smith, R. L.; George, L., Effect of organic contamination upon microbial distributions and heterotrophic uptake in a Cape Cod, Mass., aquifer. *Appl. Environ. Microbiol.* **1984**, *48* (6), 1197-202.
61. Harvey, R. W.; George, L. H., Growth determinations for unattached bacteria in a contaminated aquifer. *Appl. Environ. Microbiol.* **1987**, *53* (12), 2992-2996.
62. Godsy, E. M. Methanogenic biodegradation of creosote-derived contaminants in natural and simulated ground water ecosystems. Stanford University, 1993.
63. Herzyk, A.; Fillinger, L.; Larentis, M.; Qiu, S.; Maloszewski, P.; Hunniger, M.; Schmidt, S. I.; Stumpp, C.; Marozava, S.; Knappett, P. S. K.; Elsner, M.; Meckenstock, R.; Lueders, T.; Griebler, C., Response and recovery of a pristine groundwater ecosystem impacted by toluene contamination - A meso-scale indoor aquifer experiment. *J. Contam. Hydrol.* **2017**, *207*, 17-30.

64. Albers, C. N.; Jacobsen, O. S.; Aamand, J., Using 2,6-dichlorobenzamide (BAM) degrading *Aminobacter* sp. MSH1 in flow through biofilters--initial adhesion and BAM degradation potentials. *Appl. Microbiol. Biotechnol.* **2014**, *98* (2), 957-67.
65. Guenet, B.; Danger, M.; Abbadie, L.; Lacroix, G., Priming effect: bridging the gap between terrestrial and aquatic ecology. *Ecology* **2010**, *91* (10), 2850-2861.
66. Bengtsson, M. M.; Attermeyer, K.; Catalán, N., Interactive effects on organic matter processing from soils to the ocean: are priming effects relevant in aquatic ecosystems? *Hydrobiologia* **2018**, *822* (1), 1-17.
67. Hofmann, R.; Griebler, C., DOM and bacterial growth efficiency in oligotrophic groundwater: absence of priming and co-limitation by organic carbon and phosphorus. *Aquat. Microb. Ecol.* **2018**, *81* (1), 55-71.
68. Kuzyakov, Y.; Friedel, J. K.; Stahr, K., Review of mechanisms and quantification of priming effects. *Soil Biology and Biochemistry* **2000**, *32* (11), 1485-1498.
69. Joner, E. J.; Hirmann, D.; Szolar, O. H.; Todorovic, D.; Leyval, C.; Loibner, A. P., Priming effects on PAH degradation and ecotoxicity during a phytoremediation experiment. *Environ. Pollut.* **2004**, *128* (3), 429-435.

Supporting Information for

Response of BAM-degradation activity to concentration and flow changes in a bench-scale sediment tank

Supplementary Table of Contents

Chemicals	116
Medium Preparation and Bacteria Cultivation	116
Set-up of the Quasi-Two-dimensional Flow-through Sediment Tank Experiment.....	117
Sample Preparation and Solid-Phase Extraction (SPE)	117
Table S0 SPE steps	118
BAM and 2,6-DCBA Concentration Measurements on LC-MS/MS	118
Carbon Isotope Measurements on GC-IRMS.....	118
T-RFLP Analysis	119
Additional Supporting Tables and Figures.....	120
Table S1. Overall mass balance of the entire system.	120
Figure S1. Metolachlor (conservative tracer) concentration profile changing with time..	120
Figure S2. Dissolved oxygen (DO) profiles	121
Figure S3. Abiotic BAM concentration profile under 50 mg/L BAM inlet concentration condition.	121
Figure S4. T-RFLP DNA fingerprint from the washed-out cells at different outlet positions	121
References	122

Chemicals

The chemicals used in this study are: 2,6-dichlorobenzamide (Sigma Aldrich, Germany), 2,6-dichlorobenzamide-3,4,5-d₃, 98.4%-d₃ (Alfa Chemistry, Ronkonkoma, NY), 2,6-dichlorobenzoic acid (Sigma Aldrich, Germany), and metolachlor (Chemos GmbH & Co. KG, Germany).

Medium Preparation and Bacteria Cultivation

The recipe of the growth medium for *Aminobacter* sp. Strain MSH1 was adapted from the optimized mineral salt medium MSNC_{opt} developed by Schultz-Jensen et al.¹ and is described in Sun et al.² Briefly, the medium was prepared in 990 mL MilliQ water, with Na₂HPO₄ (6 g/L), KH₂PO₄ (3 g/L), MgSO₄ × 7H₂O (0.2 g/L), CaCl₂ × 2H₂O (0.01 g/L). The pH of the medium was adjusted to 7.0 with hydrochloric acid before autoclaving (121 °C for 20 min). After autoclaving and cooling, 10 mL of trace element stock solution (with H₃BO₃ (39 mg/L), MnSO₄ × H₂O (84.5 mg/L), CuSO₄ × 5H₂O (125 mg/L), ZnCl₂ (69 mg/L), CoCl₂ × 6H₂O (119.5 mg/L), and Na₂MoO₄ × H₂O (121 mg/L)) was filtered through 0.22 μM syringe filters (Merck KGaA, Germany) and added to the medium solution. To prepare the anoxic BAM solution injected at the central inlet port of the tank, BAM (powder) was added to the medium and stirred vigorously for 24 h to facilitate dissolution. The medium was flushed with N₂ gas for 4 h to remove the dissolved oxygen. The oxic medium solution was injected at the inlet ports except for the central one, which was flushed with air for 2 h. All chemicals for the medium preparation were from Sigma Aldrich, Germany.

The BAM degrader—*Aminobacter* sp. Strain MSH1 was obtained from the Department of Geochemistry, the Geological Survey of Denmark and Greenland (GEUS), Denmark. The bacteria cultivation steps are described in Sun et al.² Briefly, precultures were prepared in 200 mL medium solution in 1 L shaker flask with added glucose (400g/L, 2 mL, autoclaved) as carbon source. A BAM solution (500 mg/L, 4 mL) was filtered through 0.22 μM syringe filters (Merck KGaA, Germany) and added to the preculture to ensure the BAM-degrading ability of bacteria. The incubation was performed in an orbital shaker at 130 rpm at 20 °C. When the optical density (OD) reached one, the preculture was centrifuged in four 50 mL centrifuge tubes at 4000 rpm for 5 min. Then cells were resuspended and washed in 10 mL medium solution (without glucose or BAM) three times. After resuspending the washed bacterial cell pellets in

2 L medium solution (without glucose or BAM), the culture was ready for inoculation to the tank.

Set-up of the Quasi-Two-dimensional Flow-through Sediment Tank Experiment

The setup of the quasi-two-dimensional flow-through sediment tank was adapted from Bauer et al.³ and is described in Sun et al.^{2,4} Briefly, two glass plates made up the front and back sides of the tank, with a Teflon spacer as the bottom and sidewalls. Two aluminum rims at either side of the chamber held the glass plates and Teflon spacer together. The tank is a quasi-two-dimensional system with inner dimensions of 95 cm × 18 cm × 1 cm (L × H × W). Sixteen ports were equally spaced (with 1.0 cm distance) at the inlet (left side) and outlet (right side) boundary of the tank. The tank was sterilized with 12 g/L NaOH solution and rinsed with autoclaved ultra-pure MilliQ water and wet packed with uniform quartz sands (0.8–1.2 mm diameter). Peristaltic pumps (Ismatec, Germany) were connected between the inlet ports of the tank and BAM/medium solution bottles, and between the outlet ports of the tank and the sampling vials via stainless steel capillaries and tygon pump-tubes.

Sample Preparation and Solid-Phase Extraction (SPE)

We conducted filtration and solid phase extraction to clean and separate the analytes before concentration and isotope measurements. For carbon isotope measurements, water samples were filtered through 0.2 µm PES filter (Nalgene Thermo Scientific, Germany) and cumulatively collected every day until enough sample volume (1–2 L) was collected. For concentration measurements, water samples (1 mL) were filtered through 0.22 µm syringe filters (Merck KGaA, Germany) and the pH was adjusted to pH 1.7 with HCl; the internal standard 2,6-dichlorobenzamide-3,4,5-d₃ was spiked into the samples before SPE. We adapted the SPE method from Torrentó et al.⁵ and Jensen et al.⁶ The SPE cartridges (PP SPE cartridges with PE frit, 20 µm pore size, Sigma Aldrich, Germany) were self-packed with hydrophobic polymer-based sorbent Bakerbond SDB-1 (J.T. Baker, USA). The SPE steps for isotope samples and concentration samples are described in Sun et al.² and are briefly listed in the table below.

Table S0 SPE steps

	Cartridges	Sorbents	Conditioning	Loading	Washing	Drying	Concentrating
Isotope samples	6 mL	0.2 g	3 mL EtOAc 2×3 mL MeOH 2×3 mL MilliQ	0.2–2 L	2×3 mL MilliQ	120 min	3 ml EtOAc
Concentration samples	1 mL	0.05g	1 mL EtOAc 2×1 mL MeOH 2×1 mL MilliQ	1 mL	2×1 mL MilliQ	60 min	1 ml MeCN

BAM and 2,6-DCBA Concentration Measurements on LC-MS/MS

The method of the concentration measurements on LC-MS/MS was adapted from Jensen et al.⁶ Briefly, the LC-MS/MS system consisted of an Agilent 1100 HPLC system (Agilent Technologies Inc, USA) coupled to a QTrap 4000 mass spectrometer (MS) equipped with electrospray ionization (ESI) (Sciex, USA) interface. Chromatographic separation was performed on a Kinetex® C18 column (2.6 µm, 10 nm, 100 × 2.1 mm i.d., Phenomenex, USA) guarded by a precolumn. The column oven temperature was maintained at 40 °C. The mobile phase was composed of solvents A (water/ammonium acetate (5 mM), pH of 2.4 adjusted by formic acid), and solvent B (acetonitrile). The separation was achieved by applying a gradient flow of 300 µL/min as follows: 0–5 min, 90% A; 5–9 min, 90%–10% A; 9–10 min, 10%–90% A; 10–15 min, 90% A. The injection volume was 10 µL. Detailed method description and parameters of target analytes on the MS are as same as described by Sun et al.²

Carbon Isotope Measurements on GC-IRMS

Carbon isotope measurements were performed on TRACE GC Ultra gas chromatograph (Thermo Fisher Scientific, Italy) coupled with a Finnigan MAT 253 isotope ratio mass spectrometer (IRMS). A Finnigan GC Combustion III interface (Thermo Fisher Scientific, Germany) was used to connect GC to IRMS. Compound separation was conducted on a DB-5 analytical column (30 m, 0.25 mm i.d., 0.5 µm film, Agilent Technologies, Germany) in the GC. The carrier gas was Helium (1.4 mL/L, grade 5.0). For high concentration samples, a Thermo injector in the split/split-less injection mode was used; for low concentration samples, on-column injection mode was set up using a programmable Optic 3 injector (system) with liquid N₂-cryofocusing (ATAS GL, distributed by Axel Semrau, Germany). The GC oven temperature program in the split/split-less injection mode started at 80 °C; temperature increased to 280 °C at a ramp rate of 15 °C/min, and held for 7 min. The GC oven temperature program in the on-column injection mode started at 35 °C holding for 30 s; the temperature

increased to 80 °C at a ramp rate of 5 °C/min. Then the temperature increased from 80 °C to 280 °C at a ramp rate of 15 °C/min. International reference standards Vienna PeeDee Belemnite (V-PDB) were used to determine the carbon isotope values $\delta^{13}\text{C}$ [‰] of the samples. The carbon isotope values $\delta^{13}\text{C}$ of the samples were calculated in relation to a lab reference gas (CO_2 , RM8562, RM8563). Further analytical details are as same as described in Sun et al.^{2,4}

T-RFLP Analysis

T-RFLP analysis of bacterial 16S rRNA genes was performed according to the previous protocol of Piloni et al. 2011.⁷ 16S rRNA genes were amplified using FAM-labeled primer pairs Ba27f (5'-FAM-aga gtt tga tcm tgg ctc ag-3') and 907r (5'-ccg tca att cct ttg agt tt-3'). The PCR thermal profile consisted of 25 cycles of denaturation step (30s, at 94 °C), an annealing step (30s, at 52 °C) and an extension step (60s, at 70 °C). The PCR reactions were performed in a total volume of 50 μL , including 1 \times PCR buffer, 1.5 mM MgCl_2 , 0.1 mM dNTPs, 1.25 U Taq polymerase (All from Fermentas, Germany), 0.2 $\mu\text{g}/\mu\text{L}$ BSA (Roche, Switzerland), 0.5 μM of each primer (Biomers, Germany), and 1 μL of template DNA. Amplicons were then purified with MinElute® PCR purification kit (Qiagen, Germany) according to the manufacturer's instruction. Purified amplicons were then restricted using MspI (HpaII, cleavage site 5'-ccgg-3') (Thermo Fisher Scientific, Germany) and resolved by capillary electrophoresis on a 3730 DNA Analyzer (Applied Biosystems, USA). All samples were performed in duplicates. Afterwards, electropherograms were analyzed by the software GeneMapper 4.0 (Applied Biosystems, USA) as previously reported.⁸ The data was then further denoised and analyzed with T-REX software.⁹ Software parameters were selected as reported in Mueller et al.¹⁰ The T-RFLP DNA fingerprint from the washed-out cells at different outlet position in phase 2 is shown in Figure S4.

Additional Supporting Tables and Figures

Table S1. Overall mass balance of the entire system calculated by the average values during the sampling days over the three different operational phases defined by different feed concentrations through the central inlet port. Data from the flow disturbance was excluded for the first 50 mg/L inlet concentration experiment.

	BAM_{total}^{inlet} [$\mu\text{mol/day}$]	BAM_{total}^{outlet} [$\mu\text{mol/day}$]	$DCBA_{total}^{outlet}$ [$\mu\text{mol/day}$]	$DO_{consumed}^{outlet}$ [$\mu\text{mol/day}$]	<i>Carbon in Biomass</i> [$\mu\text{mol/day}$]	<i>Biodegradation</i> Efficiency [%]	<i>Carbon-Assimilation</i> Ratio [%]
Phase 1	17.1	2.3 \pm 0.5	3.4 \pm 0.4	59.6 \pm 8.6	41 \pm 5	87 \pm 3	52 \pm 8*
Phase 2	34.1	6.2 \pm 1.5	14.8 \pm 2.6	85.3 \pm 3.8	15 \pm 3	86 \pm 3	17 \pm 10
Phase 3	17.1	0.04 \pm 0.05	5.0 \pm 1.2	72.4 \pm 5.1	6 \pm 1	99 \pm 2	7 \pm 1

*The calculated carbon-assimilation ratio based on washed-out cell number in phase 1 may not represent the true value due to the adaptation of bacteria in phase 1.

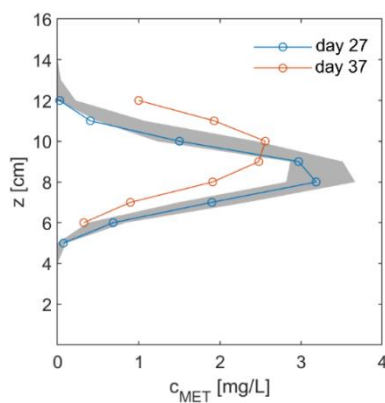


Figure S1. Metolachlor (conservative tracer) concentration profile changing with time under the first 50 mg/L BAM inlet concentration condition (phase 1). Grey shade represents the concentration range in the quasi-steady state period. Blue and orange data points represent the metolachlor concentration profiles on the flow fluctuation days.

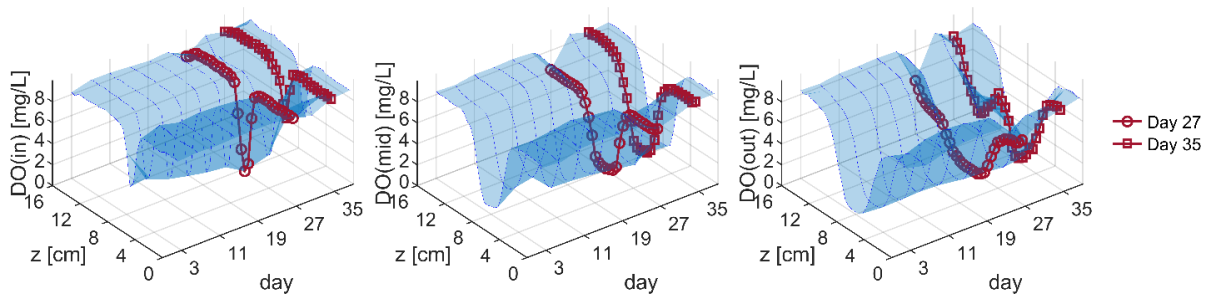


Figure S2. Dissolved oxygen (DO) profiles at the inlet, in the middle, and at the outlet of the tank, changing with time under the first 50 mg/L BAM inlet concentration condition (phase 1). Red data points represent the DO profiles on the flow fluctuation days.

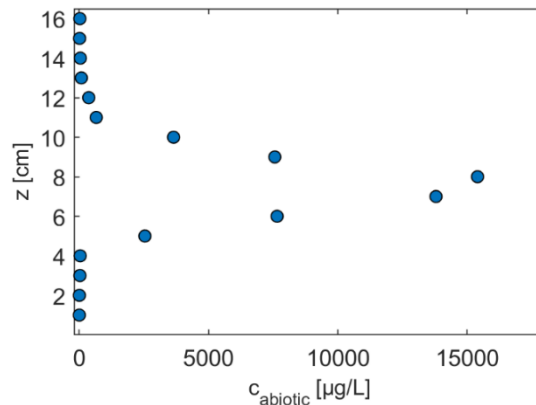


Figure S3. Abiotic BAM concentration profile under the 50 mg/L BAM inlet concentration condition.

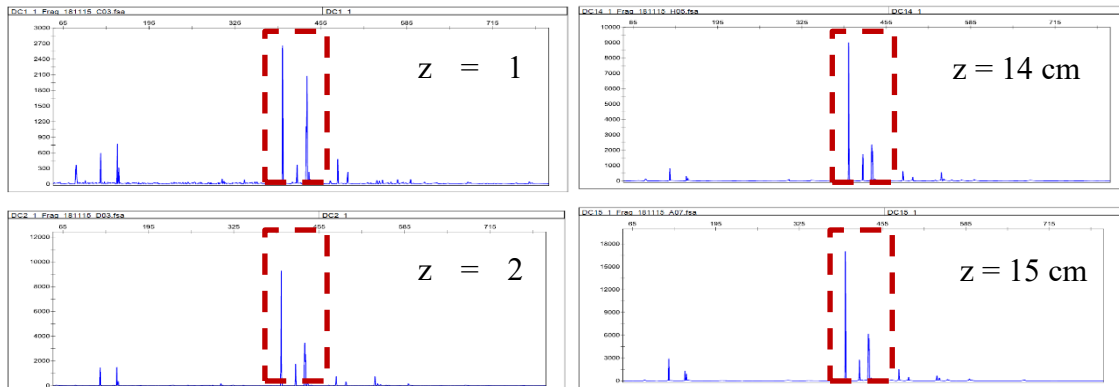


Figure S4. T-RFLP DNA fingerprint from the washed-out cells at different outlet positions in phase 2 (with BAM inlet concentration of 100 mg/L). The DNA fingerprint of strain *Aminobacter* sp. MSH1 (accession number DQ401867.1) was framed in the dashed-line rectangle.

References

1. Schultz-Jensen, N.; Knudsen, B. E.; Frkova, Z.; Aamand, J.; Johansen, T.; Thykaer, J.; Sorensen, S. R. Large-scale bioreactor production of the herbicide-degrading *Aminobacter* sp. strain MSH1. *Appl. Microbiol. Biotechnol.* **2014**, *98* (5), 2335-44.
2. Sun, F.; Mellage, A.; Gharasoo, M.; Melsbach, A.; Cao, X.; Zimmermann, R.; Griebler, C.; Thullner, M.; Cirpka, O. A.; Elsner, M. Mass-transfer-limited biodegradation at low concentrations—evidence from reactive transport modeling of isotope profiles in a bench-scale aquifer. *Environ. Sci. Technol.* **2021**, *55* (11), 7386-7397.
3. Bauer, R. D.; Maloszewski, P.; Zhang, Y.; Meckenstock, R. U.; Griebler, C. Mixing-controlled biodegradation in a toluene plume--Results from two-dimensional laboratory experiments. *J. Contam. Hydrol.* **2008**, *96* (1-4), 150-68.
4. Sun, F.; Peters, J.; Thullner, M.; Cirpka, O. A.; Elsner, M. Magnitude of diffusion- and transverse dispersion-induced isotope fractionation of organic compounds in aqueous systems. *Environ. Sci. Technol.* **2021**, *55* (8), 4772-4782.
5. Torrentó, C.; Bakkour, R.; Ryabenko, E.; Ponsin, V.; Prasuhn, V.; Hofstetter, T. B.; Elsner, M.; Hunkeler, D. Fate of four herbicides in an irrigated field cropped with corn: lysimeter experiments. *Procedia Earth Planet. Sci.* **2015**, *13*, 158-161.
6. Jensen, G. G.; Bjorklund, E.; Simonsen, A.; Halling-Sorensen, B. Determination of 2,6-dichlorobenzamide and its degradation products in water samples using solid-phase extraction followed by liquid chromatography-tandem mass spectrometry. *J. Chromatogr. A* **2009**, *1216* (27), 5199-206.
7. Pilloni, G.; von Netzer, F.; Engel, M.; Lueders, T. Electron acceptor-dependent identification of key anaerobic toluene degraders at a tar-oil-contaminated aquifer by Pyro-SIP. *FEMS Microbiol. Ecol.* **2011**, *78* (1), 165-75.
8. Winderl, C.; Anneser, B.; Griebler, C.; Meckenstock, R. U.; Lueders, T. Depth-resolved quantification of anaerobic toluene degraders and aquifer microbial community patterns in distinct redox zones of a tar oil contaminant plume. *Appl. Environ. Microbiol.* **2008**, *74* (3), 792-801.
9. Culman, S. W.; Bukowski, R.; Gauch, H. G.; Cadillo-Quiroz, H.; Buckley, D. H. T-REX: software for the processing and analysis of T-RFLP data. *BMC Bioinf.* **2009**, *10*, 171.
10. Mueller, M.; Pander, J.; Wild, R.; Lueders, T.; Geist, J. The effects of stream substratum texture on interstitial conditions and bacterial biofilms: Methodological strategies. *Limnologia* **2013**, *43* (2), 106-113.

3. Conclusions and Outlook

This thesis systematically explores the insight from isotope fractionation on the limitations of micropollutant biodegradation in a bench-scale aquifer as a model system for natural groundwater sediments. It illuminates the necessity of considering mass-transfer limitation in isotope data interpretation and biodegradation evaluation in the field. Furthermore, it sheds light on the application of priming strategies for optimizing bioremediation approaches.

The diffusion and dispersion experiments with organic compounds at natural isotopic abundances in the aqueous phase and flow-through sediment system showed that the isotope fractionation induced by diffusion and transverse dispersion is weak to negligible, with changes in carbon and nitrogen isotope values within $\pm 0.5\%$ and $\pm 1\%$, respectively. Therefore, based on the data in this study and the literature data for chlorinated solvent and gasoline contaminants at natural isotopic abundance,¹ this study suggests that maximum $\pm 1\%$ potential additional uncertainty could be added to current instrumental uncertainties on carbon or nitrogen isotope measurements for more accurate field data evaluation. This can significantly simplify the analysis of biodegradation from isotope fractionation measurements in the field. In addition, the observed weak-to-negligible mass dependence of the diffusion-induced isotope fractionation of organic compounds at natural abundance challenges the well-entrenched mass-dependence concept based on the Enskog diffusion theory.² Furthermore, to explain the weak mass dependence of diffusion of organic compounds at natural isotopic abundance, I proposed the following aspects which have not been considered by the conventional diffusion models based on the collision theory: (i) the isotopologue masses of polyatomic molecules are affected by isotopes of multiple elements, (ii) molecular vibrations or rotations may minimize the mass dependence of diffusion, and (iii) solute-solvents interaction (e.g., H-bonds) can further minimize collision effects. To further verify the hypothesis, future studies should undertake molecular dynamic simulations^{3,4} of isotope fractionations of organic compounds at natural isotopic abundance during diffusion in the aqueous phase. The estimation of the potential energy of each bound, angle, and dihedral in each solute molecule by the molecular model might further shed light on the influence of the above-mentioned factors on the aqueous-phase diffusion. Hence, the widely applied transport simulations⁵⁻⁸ by coupling the transverse-dispersion expression of Chiogna et al.⁹ with the Enskog/Woch diffusion equation to estimate transverse-dispersion-induced isotope fractionation would significantly overestimate the

isotope effect of transverse dispersion for organic compounds at natural isotopic abundances. This study, therefore, calls the attention of the researchers to choose the diffusion and transverse dispersion models more carefully when estimating the transverse-dispersion induced isotope fractionation.

Taking the conclusion from section 2.1 that diffusion and dispersion did not induce significant isotope fractionation, section 2.2 explored the limitations of micropollutant biodegradation in a bench-scale aquifer by analyzing the relation between isotope fractionation and concentrations. The drastic decrease in carbon and nitrogen isotope fractionation when substrate concentration decreased to a threshold range perfectly fit the reactive transport model and gave direct evidence of substrate mass-transfer limitation. This study indicates that mass-transfer limitation through the cell membrane is the main bottleneck for biodegradation; without considering mass-transfer limitation, the extent of *in-situ* biodegradation at low concentrations based on isotopic evidence would be underestimated. The typical interpretation of isotope ratio in geochemistry usually interprets the decreased isotope fractionation at low concentrations as the result of decreased degradation rate,¹⁰ isotopic interference from dilution or dispersion,^{11, 12} or other physical/chemical heterogeneity of the system,^{13, 14} and ignores the potential masking effect due to mass-transfer limitation. Even though the applicability of the Rayleigh equation in the mixing-controlled aquifer has been questioned, mass-transfer limitation has only been considered as a result of the heterogeneity of the system.¹⁵ This thesis highlights that besides all the above-mentioned factors, mass-transfer limitation through the bacterial cell membrane is an important factor that masks isotope fractionation, not only in heterogeneous systems but also in homogeneous systems. Thereby, this study significantly adds to the interpretation of isotope fractionation in geochemistry and creates new avenues to evaluate the bottlenecks of biotransformation/biodegradation in groundwater. In order to better integrate the results from this study into field applications, studies on how extra carbon sources influence the mass transfer of the target substrate and how mixed bacteria communities affect the uptake of the substrate might need further investigation in bench-scale aquifers and field sites. At the field scale, microbial community dynamics may interact with the environment physically, and chemically.^{16, 17} In addition, degradation pathways of different bacteria may vary and induce different isotope effects¹⁸⁻²⁰—some bacteria might show significantly small fractionation even at higher concentrations during biodegradation.²¹ Thus, future work is needed to explore whether the combined approach with CSIA and concentration analysis in

conjunction with numerical modeling can be applied to pinpoint mass-transfer limitation in natural systems with mixed microbial community. In addition, even though previous studies shown the physiological adaptation of bacteria under stress (e.g., at low substrate concentration) by analyzing the proteomic and fatty acid composition of bacteria in batch and chemostat experiments,^{22, 23} future work on the analysis of proteomics and fatty acids composition of bacteria in a larger scale flow-through sediment system may help to characterize the physiological response of the bacteria and identify mass-transfer limitation through the bacterial cell membrane in the field-like case.

Finally, in an attempt to increase the biodegradation capacity/efficiency of a bioaugmented system, especially under low concentration conditions, in section 2.3, I implemented intermediate disturbance as a priming strategy in a bacteria-inoculated flow-through sediment tank. After the priming and a temporal flow fluctuation, high degradation efficiency was reached in the relative long-term run, suggesting that this strategy has the potential to increase degradation capacity and extend the efficient degradation time. Therefore, introducing such intermediate disturbance may potentially enhance biomass distribution and re-active degradation activity of the inoculated bacteria in the sand filters in drinking water treatment plants (such as during the back-flushing stage). However, the flow rate in the flow-through sediment tank in this study was slower than that in the real sand filter systems in drinking water treatment plants, which may result in a lower cell detachment rate.²⁴ Hence, priming studies in pilot sand filter systems are still necessary. The observed stimulated degradation activity after priming also implies that when evaluating biodegradation in the field, intermediate concentration/flow fluctuation caused by the varying flow field may potentially facilitate mixing the redox conditions and stimulate the spread of the bacteria, thus further promote biodegradation. In addition, combined analysis of isotope fractionation and remaining substrate concentrations has the potential to identify the underlying limiting factors (e.g., mass-transfer limitation, physiological limitation) during biodegradation in the lab and field sites. A better understanding of the potential limitations during biodegradation would help us to find more specific and hybrid solutions (e.g., adding surfactants, extra carbon sources, or nutrients) in order to overcome the biodegradation bottlenecks and eliminate contaminant concentrations to a lower level.

In sum, I explored the limitations of biodegradation of organic micropollutants by applying CSIA in a bench-scale aquifer mimicking natural groundwater sediments. The finding that

mass-transfer limitation masked isotope fractionation at low concentrations has challenged the general assumption that the absence of isotope fractionation represents the absence of degradation in the field. By implementing a priming strategy (increasing and decreasing source concentration), the enhanced biomass distribution and higher biomass density were beneficial for the long-term performance of the bioaugmented system, thus, further enhanced the biodegradation in the relatively long run. But even with the indications from this thesis, there are still knowledge gaps that warrant further research. For example, further microbiological and molecular biology studies on the mechanisms of transformation or correlation between mass-transfer limitation and physiological limitation under oligotrophic conditions in flow-through sediment systems are needed in order to resolve the general mass-transfer limitation to eliminate contaminant concentration to zero in the field. The influence of multi-carbon sources and mixed bacteria communities on the identification of mass-transfer limitation by applying CSIA still needs further investigation. In addition, a field-scale reactive transport model which considers mass-transfer limitation through the bacterial cell membrane would further validate the findings in this thesis. Finally, the findings from the sediment tank experiment with priming and flow disturbance should be of significant interest for improving biodegradation/remediation strategies in drinking water treatment plants (e.g., in sand filter systems) and at field sites.

References

1. Wanner, P.; Hunkeler, D. Carbon and chlorine isotopologue fractionation of chlorinated hydrocarbons during diffusion in water and low permeability sediments. *Geochim. Cosmochim. Acta* **2015**, *157*, 198-212.
2. Tyrrell, H. J. V.; Harris, K. *Diffusion in Liquids: A theoretical and Experimental Study*. Butterworth-Heinemann: 2013.
3. Wanner, P.; Hunkeler, D. Molecular dynamic simulations of carbon and chlorine isotopologue fractionation of chlorohydrocarbons during diffusion in liquid water. *Environ. Sci. Technol. Lett.* **2019**, *6* (11), 681-685.
4. Bourg, I. C.; Richter, F. M.; Christensen, J. N.; Sposito, G. Isotopic mass dependence of metal cation diffusion coefficients in liquid water. *Geochim. Cosmochim. Acta* **2010**, *74* (8), 2249-2256.
5. Rolle, M.; Chiogna, G.; Bauer, R.; Griebler, C.; Grathwohl, P. Isotopic fractionation by transverse dispersion: Flow-through microcosms and reactive transport modeling study. *Environ. Sci. Technol.* **2010**, *44* (16), 6167-6173.
6. Rolle, M.; Jin, B. Normal and inverse diffusive isotope fractionation of deuterated toluene and benzene in aqueous systems. *Environ. Sci. Technol. Lett.* **2017**, *4* (7), 298-304.
7. Van Breukelen, B. M.; Rolle, M. Transverse hydrodynamic dispersion effects on isotope signals in groundwater chlorinated solvents' plumes. *Environ. Sci. Technol.* **2012**, *46* (14), 7700-8.
8. Xu, S.; Sherwood Lollar, B.; Sleep, B. E. Rethinking aqueous phase diffusion related isotope fractionation: Contrasting theoretical effects with observations at the field scale. *Sci. Total Environ.* **2017**, *607-608*, 1085-1095.
9. Chiogna, G.; Eberhardt, C.; Grathwohl, P.; Cirpka, O. A.; Rolle, M. Evidence of compound-dependent hydrodynamic and mechanical transverse dispersion by multitracer laboratory experiments. *Environ. Sci. Technol.* **2010**, *44* (2), 688-693.
10. Wanner, P.; Parker, B. L.; Chapman, S. W.; Aravena, R.; Hunkeler, D. Quantification of degradation of chlorinated hydrocarbons in saturated low permeability sediments using compound-specific isotope analysis. *Environ. Sci. Technol.* **2016**, *50* (11), 5622-30.
11. Prommer, H.; Anneser, B.; Rolle, M.; Einsiedl, F.; Griebler, C. Biogeochemical and isotopic gradients in a BTEX/PAH contaminant plume: Model-based interpretation of a high-resolution field data set. *Environ. Sci. Technol.* **2009**, *43* (21), 8206-8212.
12. Wenk, C. B.; Frame, C. H.; Koba, K.; Casciotti, K. L.; Veronesi, M.; Niemann, H.; Schubert, C. J.; Yoshida, N.; Toyoda, S.; Makabe, A.; Zopfi, J.; Lehmann, M. F. Differential N₂O dynamics in two oxygen-deficient lake basins revealed by stable isotope and isotopomer distributions. *Limnol. Oceanogr.* **2016**, *61* (5), 1735-1749.
13. Abe, Y.; Hunkeler, D. Does the Rayleigh equation apply to evaluate field isotope data in contaminant hydrogeology? *Environ. Sci. Technol.* **2006**, *40* (5), 1588-1596.
14. Thullner, M.; Centler, F.; Richnow, H.-H.; Fischer, A. Quantification of organic pollutant degradation in contaminated aquifers using compound specific stable isotope analysis – Review of recent developments. *Org. Geochem.* **2012**, *42* (12), 1440-1460.
15. Chen, S.; Zhang, K.; Jha, R. K.; Chen, C.; Yu, H.; Liu, Y.; Ma, L. Isotope fractionation in atrazine degradation reveals rate-limiting, energy-dependent transport across the cell membrane of gram-negative rhizobium sp. CX-Z. *Environ. Pollut.* **2019**, *248*, 857-864.
16. Thullner, M.; Regnier, P. Microbial controls on the biogeochemical dynamics in the subsurface. *Rev. Mineral. Geochem.* **2019**, *85* (1), 265-302.
17. Griebler, C.; Lueders, T. Microbial biodiversity in groundwater ecosystems. *Freshwater Biol.* **2009**, *54* (4), 649-677.

18. Elsner, M.; Zwank, L.; Hunkeler, D.; Schwarzenbach, R. P. A new concept linking observable stable isotope fractionation to transformation pathways of organic pollutants. *Environ. Sci. Technol.* **2005**, *39* (18), 6896-916.
19. Lihl, C.; Heckel, B.; Grzybkowska, A.; Dybala-Defratyka, A.; Ponsin, V.; Torrentó, C.; Hunkeler, D.; Elsner, M. Compound-specific chlorine isotope fractionation in biodegradation of atrazine. *Environmental Science: Processes & Impacts* **2020**, *22* (3), 792-801.
20. Mancini, S. A.; Devine, C. E.; Elsner, M.; Nandi, M. E.; Ulrich, A. C.; Edwards, E. A.; Sherwood Lollar, B. Isotopic evidence suggests different initial reaction mechanisms for anaerobic benzene biodegradation. *Environmental science & technology* **2008**, *42* (22), 8290-8296.
21. Meyer, A. H.; Penning, H.; Elsner, M. C and N Isotope Fractionation Suggests Similar Mechanisms of Microbial Atrazine Transformation Despite Involvement of Different Enzymes (AtzA and TrzN). *Environ. Sci. Technol.* **2009**, *43* (21), 8079-8085.
22. Kundu, K.; Marozava, S.; Ehrl, B.; Merl-Pham, J.; Griebler, C.; Elsner, M. Defining lower limits of biodegradation: atrazine degradation regulated by mass transfer and maintenance demand in *Arthrobacter aurescens* TC1. *ISME J.* **2019**, *13* (9), 2236-2251.
23. Wunderlich, A.; Heipieper, H. J.; Elsner, M.; Einsiedl, F. Solvent stress-induced changes in membrane fatty acid composition of denitrifying bacteria reduce the extent of nitrogen stable isotope fractionation during denitrification. *Geochim. Cosmochim. Acta* **2018**, *239*, 275-283.
24. Ellegaard-Jensen, L.; Schostag, M. D.; Nikbakht Fini, M.; Badawi, N.; Gobbi, A.; Aamand, J.; Hansen, L. H. Bioaugmented sand filter columns provide stable removal of pesticide residue from membrane retentate. *Front. water.* **2020**, *2* (55), 603567.

Acknowledgements

Pursuing a Ph.D. is a long, challenging journey. I am so lucky to meet a group of lovely people who offered me a great deal of support and assistance.

The first person I want to thank is my supervisor—Prof. Dr. Martin Elsner. Thank you for offering me this great opportunity to explore such an interdisciplinary project that opened windows for me to peer at various science subjects. Your supervision and support helped me to overcome many obstacles in my path to this destination. The discussions with you constantly motivated and inspired me. Thank you so much for always encouraging me when I doubt myself. You are the best mentor, not only leading me in the world of chemistry and science but also in my life.

Thanks to the members of my thesis committee—Prof. Dr. Olaf A. Cirpka and Dr. Martin Thullner. Olaf, thank you so much for offering me great opportunities to go to Tübingen for the modeling training, supervising me and giving me insightful advice on my projects. Your professional knowledge and great passion for science really inspired me. I really learned a lot by working with you, not only about modeling, but also critical thinking of research questions. Martin, thank you very much for being a member of my thesis committee. Whenever I have questions, you always replied to me in detail. Your advice has strongly supported my projects and has resulted in great papers and a better thesis. I also want to thank Prof. Dr. Christian Griebler. Thank you for teaching me how to set up the tank system step by step. It was challenging to run the system for years. However, you always stood by me and offered me great help nicely. Thanks also to Prof. Dr. Christine Stumpp, you always kept your door open to me and gave me as much help and support as you can. Your advice on tracer tests greatly supported my work! Thanks to Prof. Dr. Florian Einsiedl, and Prof. Dr. Wolfgang Eisenreich for serving as my defense committee.

Thanks to my amazing collaborators. Dr. Adrian Mellage, thank you for helping me with the modeling and sensitivity analysis. You are an excellent scientist and the best collaborator. Working with you was always a happy experience. Zhe Wang, thank you for the T-RFLP analysis. Your expertise in microbiology always brought new angles forward to look at my work. My thanks also go to Xin Cao and Ralf Zimmermann for their assistance on LC-MS/MS measurements.

Thanks to the nice fellow members in IGOE. Mehdi, thank you for giving me detailed advice on modeling and offering me help whenever I met difficulties. Sviatlana, you are like a sister to me. You always kindly shared your knowledge of microbiology and lab experiences with me, wiped away my tears in the labs, took me out for hiking during the pandemic, etc. Thank you for everything! Lauren, thank you for your endless support and encouragement. And thanks a lot for nicely checking the language of this thesis. I also want to thank Kankana, who gave me many hugs and advice in my work and life; Thanks to Benno, Tina, Aileen, Benni, and Christina who always generously helped me with the troubleshooting on the GC-IRMS; Thanks to Oleksii and Gabriel for sharing me research experiences and cheering me up; Thanks to Susi, Petra, Ramona, and Sigrid for their technical support. Moving labs during the Ph.D. was not easy. Rani, thanks a lot for building up a warm group and pleasant working environment in Garching. Thanks for advising me in my work and life. Your expertise in analytical chemistry strongly supported my work. Furthermore, I am grateful to work with the best group members and officemates, David and Chris. Thanks for offering me help and encouragement. Working with you was a nice experience, especially during the pandemic.

My thanks also go to my lovely friends, He, Lu, Bauli, Zhe, and Kirsa. Thanks for helping me and cheering me up all the time in the lab or out of it. Thank you to Kirsa Bätzel for nicely translating the abstract into German. I also want to thank my lunch group members (Sviatlana, Lauren, Armin, He, Anna, Clemens, and Luzie). We shared not only fabulous food but also happiness and sorrows, laboratory success and failures.

Moreover, I want to thank my parents. Thank you for always supporting me and being by my side, though thousands of miles apart. Your endless love and tremendous support keep me going forward.

Last but not least, thanks to Kai. Meeting you at HMGU was the best thing that happened to me in Munich. Thank you for your company on those working weekends. Exploring and seeing a bigger world with you brought me a lot of joy and force during my Ph.D.

List of prior publications

Publications

1. **Sun, F.**; Mellage, A.; Wang, Z.; Bakkour, R.; Griebler, C.; Thullner, M.; Cirpka, A. O.; Elsner, M. Response of BAM-degradation activity to concentration and flow changes in a bench-scale sediment tank. *Environ. Sci. Technol.* **2021**, *in preparation*.
2. **Sun, F.**; Mellage, A.; Gharasoo, M.; Melsbach, A.; Cao, X.; Zimmermann, R.; Griebler, C.; Thullner, M.; Cirpka, A. O.; Elsner, M. Mass-Transfer-Limited Biodegradation at Low Concentrations—Evidence from Reactive Transport Modeling of Isotope Profiles in a Bench-Scale Aquifer. *Environ. Sci. Technol.* **2021**, *55* (11), 7386-7397.
3. **Sun, F.**; Peters, J.; Thullner, M.; Cirpka, O. A.; Elsner, M. Magnitude of Diffusion- and Transverse Dispersion-Induced Isotope Fractionation of Organic Compounds in Aqueous Systems. *Environ. Sci. Technol.* **2021**, *55* (8), 4772-4782.
4. Tatomir, A.; De Vriendt, K.; Zhou, D.; Gao, H.; Duschl, F.; **Sun, F.**; Licha, T.; Sauter, M. Kinetic Interface Sensitive Tracers: Experimental Validation in a Two-Phase Flow Column Experiment. A Proof of Concept. *Water Resour. Res.* **2018**, *54* (12), 10,223-10,241.
5. Holzbecher, E.; **Sun, F.** Modeling a Nozzle in a Borehole. COMSOL Conf., Cambridge. 2014

Presentations & Abstracts

1. **Sun, F.**; Melsbach, A.; Wang, Z.; Bakkour, R.; Gharasoo, M. G.; Mellage, A.; Griebler, C.; Thullner, M.; Cirpka, O. A.; Elsner, M. *Response of BAM-degradation activity to concentration and flow changes in a bench-scale sediment tank*. Presented in AGU Fall Meeting, San Francisco, US, Dec. 2019; pp H12E-07. Oral presentation.
2. **Sun, F.**; Melsbach, A.; Wang, Z.; Bakkour, R.; Gharasoo, M.; Griebler, C.; Thullner, M.; Cirpka, O. A.; Elsner, M. *Bioavailability as bottleneck for biodegradation of organic micro-pollutants in groundwater? –Evidence from compound-specific isotope analysis in two-dimensional tank experiment*. Presented in EGU, Vienna, Austria, Apr. 2019. Oral presentation.
3. **Sun, F.**; Cirpka, O. A.; Elsner, M; etc. *Compound-specific stable- isotope analysis for investigating bioavailability limitation of micro-pollutants in 2D flow through tank experiments*. Presented at ASI 2018 -Jahrestagung der Arbeitsgemeinschaft Stable Isotope, Raitenhaslach, Germany, Mar. 2018; Oral presentation.
4. **Sun, F.**; Maier, F.; Tatomir, A.; etc. *Numerical simulation of kinetic interface sensitive tracers in laboratory column experiments with COMSOL Multiphysics*. Presented at COMSOL Conference, Munich, Germany, Oct. 2016; Oral presentation.

Fengchao Sun

Lehrstuhl für Analytische Chemie und Wasserchemie, Fakultät für Chemie.

Technische Universität München

AUSBILDUNG

- Promotion, Technische Universität München, München, Deutschland** 07/2016 –
im Arbeitskreis von Prof. Dr. Martin Elsner, Lehrstuhl für Analytische
Chemie und Wasserchemie, Fakultät für Chemie.
*Thema: Insights from isotope fractionation on limitations of micropollutant
biodegradation—Evaluating mass-transfer limitation and biodegradation in a
bench-scale aquifer*
- M.Sc. in Hydrogeologie und Umweltgeowissenschaften,** 10/2013 – 03/2016
Georg-August-Universität Göttingen, Göttingen, Deutschland
Fakultät für Geowissenschaften und Geographie
*Thema: Kinetic Interface Sensitive (KIS) Tracers Development —From Lab
Column Experiment to Multi-Phase Flow Modeling*
- B.Sc. in Hydrologie und Wasserresourcentechnik,** 09/2009 – 06/2013
China Universität für Geowissenschaften (Wuhan), Wuhan, China
Fakultät für Umweltstudien
Thema: Adsorption and Desorption of Lindane on Clay Minerals

FORSCHUNGSERFAHRUNGEN

- Studentische Hilfskraft** 01/2016 – 06/2016
Georg-August-Universität Göttingen, Göttingen, Deutschland
Fakultät für Geowissenschaften und Geographie
- Studentische Hilfskraft** 01/2015 – 06/2015
Georg-August-Universität Göttingen, Göttingen, Deutschland
Fakultät für Geowissenschaften und Geographie